



*Midwest Pooled Fund Research Program
Fiscal Years 2019-2022 (Year 29)
Research Project Number TPF-5(193) Supplement #141
NDOT Sponsoring Agency Code RFPF-19-AGT-1*

EVALUATION OF FLARE RATES FOR APPROACH GUARDRAIL TRANSITIONS – PHASE I

Submitted by

Ryan F. Bickhaus, M.S.M.E.
Former Graduate Research Assistant

Jennifer D. Rasmussen, Ph.D., P.E.
Former Research Associate Professor

Robert W. Bielenberg, M.S.M.E.
Research Engineer

Scott K. Rosenbaugh, M.S.C.E.
Research Engineer

Ronald K. Faller, Ph.D., P.E.
Research Professor & MwRSF Director

John D. Reid, Ph.D.
Professor Emeritus

MIDWEST ROADSIDE SAFETY FACILITY

Nebraska Transportation Center
University of Nebraska-Lincoln

Main Office

Prem S. Paul Research Center at Whittier School
Room 130, 2200 Vine Street
Lincoln, Nebraska 68583-0853
(402) 472-0965

Outdoor Test Site

4630 N.W. 36th Street
Lincoln, Nebraska 68524

Submitted to

MIDWEST POOLED FUND PROGRAM

Nebraska Department of Transportation
1500 Nebraska Highway 2
Lincoln, Nebraska 68502

MwRSF Research Report No. TRP-03-439a-22

November 22, 2022

TECHNICAL REPORT DOCUMENTATION PAGE

1. Report No. TRP-03-439a-22	2. Government Accession No.	3. Recipient's Catalog No.	
4. Title and Subtitle Evaluation of Flare Rates for Approach Guardrail Transitions – Phase I		5. Report Date November 22, 2022	
		6. Performing Organization Code	
7. Author(s) Bickhaus, R.F., Rasmussen, J.D., Bielenberg, R.W., Rosenbaugh, S.K., Faller, R.K., and Reid, J.D.		8. Performing Organization Report No. TRP-03-439a-22	
9. Performing Organization Name and Address Midwest Roadside Safety Facility (MwRSF) Nebraska Transportation Center University of Nebraska-Lincoln Main Office: Prem S. Paul Research Center at Whittier School Room 130, 2200 Vine Street Lincoln, Nebraska 68583-0853		10. Work Unit No.	
		11. Contract TPF-5(193) Supplement #141	
12. Sponsoring Organization Name and Address Midwest Pooled Fund Program Nebraska Department of Transportation 1500 Nebraska Highway 2 Lincoln, Nebraska 68502		13. Type of Report and Period Covered Final Report: 2018 – 2022	
		14. Sponsoring Agency Code RFPF-19-AGT-1	
15. Supplementary Notes Prepared in cooperation with U.S. Department of Transportation, Federal Highway Administration.			
16. Abstract <p>The objective of this research study was to use computer simulation to identify the critical flare rate for flaring approach guardrail transitions (AGTs) away from the primary roadway. Installing an AGT with a flared configuration results in a reduction of the length of need (LON) as well as an increase in the clear zone area in front of the barrier, which would reduce both installation cost and accident frequency. The research focused on the determination of the maximum allowable flare rate that could safely be utilized with 31-in. (787-mm) tall three-beam AGTs without concrete curbs that utilize the Midwest Guardrail System (MGS) upstream of the transition. The Phase I research consisted of a literature review, development and validation of a tangent AGT LS-DYNA model, LS-DYNA simulation of multiple AGT flare rates from 10:1 to 25:1 with respect to the roadway, and the determination of the critical flare rate and critical impact points (CIPs) for full-scale testing.</p> <p>The simulation study identified the 15:1 (3.81 degrees from roadway) and 12.5:1 (4.57 degrees from roadway) flare rates as the critical flare rates that exhibited significant LON reduction while maintaining acceptable <i>Manual for Assessing Safety Hardware</i> (MASH 2016) safety performance criteria. Further simulation identified CIPs. In comparisons between the critical flare rates at the CIPs, the 15:1 flare rate exhibited improved vehicle stability and occupant risk criteria and should have a greater potential to pass MASH 2016 criteria, compared to the 12.5:1 flare rate. As a result, with sponsor feedback, the 15:1 flare rate was selected as the critical flare rate for full-scale crash testing.</p>			
17. Key Words Highway Safety, Crash Test, Roadside Appurtenances, Compliance Test, MASH 2016, Test Level 3, Approach Guardrail Transition, AGT, Flare, Flared Guardrail, Computer Simulation		18. Distribution Statement No restrictions. This document is available through the National Technical Information Service. 5285 Port Royal Road Springfield, VA 22161	
19. Security Class (of this report) Unclassified	20. Security Classification (of this page) Unclassified	21. No. of Pages 169	22. Price

DISCLAIMER STATEMENT

This material is based upon work supported by the Federal Highway Administration, U.S. Department of Transportation and the Midwest Pooled Fund Program under TPF-5(193) Supplement # 141. The contents of this report reflect the views and opinions of the authors who are responsible for the facts and the accuracy of the data presented herein. The contents do not necessarily reflect the official views or policies of the University of Nebraska-Lincoln, state highway departments participating in the Midwest Pooled Fund Program, nor the Federal Highway Administration, U.S. Department of Transportation. This report does not constitute a standard, specification, or regulation. Trade or manufacturers' names, which may appear in this report, are cited only because they are considered essential to the objectives of the report. The United States (U.S.) government and the State of Nebraska do not endorse products or manufacturers.

ACKNOWLEDGEMENTS

The authors wish to acknowledge the sources of contribution to this project. The work was sponsored by the Midwest Pooled Fund Program, funded by the California Department of Transportation, Florida Department of Transportation, Georgia Department of Transportation, Hawaii Department of Transportation, Illinois Department of Transportation, Indiana Department of Transportation, Iowa Department of Transportation, Kansas Department of Transportation, Kentucky Department of Transportation, Minnesota Department of Transportation, Missouri Department of Transportation, Nebraska Department of Transportation, New Jersey Department of Transportation, North Carolina Department of Transportation, Ohio Department of Transportation, South Carolina Department of Transportation, South Dakota Department of Transportation, Utah Department of Transportation, Virginia Department of Transportation, Wisconsin Department of Transportation, and Wyoming Department of Transportation.

This work was completed utilizing the Holland Computing Center of the University of Nebraska, which receives support from the Nebraska Research Initiative. Acknowledgement is also given to the following individuals who contributed to the completion of this research project.

Midwest Roadside Safety Facility

J.C. Holloway, M.S.C.E., Research Engineer & Assistant Director –Physical Testing Division
K.A. Lechtenberg, M.S.M.E., Research Engineer
C.S. Stolle, Ph.D., Research Assistant Professor
J.S. Steelman, Ph.D., P.E., Associate Professor
M. Asadollahi Pajouh, Ph.D., P.E., Research Assistant Professor
B.J. Perry, M.E.M.E., Research Engineer
A.T. Russell, B.S.B.A., Testing and Maintenance Technician II
E.W. Krier, B.S., Engineering Testing Technician II
D.S. Charroin, Engineering Testing Technician II
R.M. Novak, Engineering Testing Technician II
S.M. Tighe, Engineering Testing Technician I
T.C. Donahoo, Engineering Testing Technician I
J.T. Jones, Engineering Testing Technician I
E.L. Urbank, B.A., Research Communication Specialist
Z.Z. Jabr, Engineering Technician
Undergraduate and Graduate Research Assistants

California Department of Transportation

Bob Meline, Chief, Roadside Safety Research Branch
David Whitesel, P.E., Transportation Engineer
John Jewell, P.E., Senior Transportation Engineer,
Specialist

Florida Department of Transportation

Derwood C. Sheppard, Jr., P.E., Design Standards
Publication Manager, Roadway Design Engineer

Georgia Department of Transportation

Christopher Rudd, P.E., State Design Policy Engineer
Frank Flanders IV, P.E., Assistant State Design Policy
Engineer

Hawaii Department of Transportation

James Fu, P.E., State Bridge Engineer
Dean Takiguchi, P.E., Engineer, Bridge Design Section
Kimberly Okamura, Engineer, Bridge Design Section

Illinois Department of Transportation

Filiberto Sotelo, P.E., Engineering Policy Unit Chief
Martha Brown, P.E., Safety Evaluation Unit Chief

Indiana Department of Transportation

Katherine Smutzer, P.E., Standards Engineer
Elizabeth Phillips, P.E., Highway Design Director

Iowa Department of Transportation

Chris Poole, P.E., Roadside Safety Engineer
Daniel Harness, P.E., Transportation Engineer Specialist
Stuart Nielsen, P.E., Transportation Engineer
Administrator, Design

Kansas Department of Transportation

Ron Seitz, P.E., Director of Design
Scott King, P.E., Road Design Bureau Chief
Brian Kierath Jr., Engineering Associate III, Bureau of
Road Design

Kentucky Department of Transportation

Jason J. Siwula, P.E., Assistant State Highway Engineer
Kevin Martin, P.E., Transportation Engineer Specialist
Gary Newton, Engineering Tech III, Design Standards

Minnesota Department of Transportation

Michael Elle, P.E., Design Standards Engineer
Michelle Moser, P.E., Assistant Design Standards Engineer

Missouri Department of Transportation

Sarah Kleinschmit, P.E., Policy and Innovations Engineer

Nebraska Department of Transportation

Phil TenHulzen, P.E., Design Standards Engineer
Jim Knott, P.E., Construction Engineer
Mick Syslo, P.E., State Roadway Design Engineer
Brandon Varilek, P.E., Materials and Research Engineer &
Division Head
Mark Fischer, P.E., PMP, Research Program Manager
Lieska Halsey, Research Project Manager
Angela Andersen, Research Coordinator
David T. Hansen, Internal Research Coordinator
Jodi Gibson, Former Research Coordinator

New Jersey Department of Transportation

Hung Tang, P.E., Principal Engineer, Transportation
Joseph Warren, Assistant Engineer, Transportation

North Carolina Department of Transportation

Neil Mastin, P.E., Manager, Transportation Program
Management – Research and Development
D. D. “Bucky” Galloway, P.E., CPM, Field Operations
Engineer
Brian Mayhew, P.E., State Traffic Safety Engineer
Joel Howerton, P.E., Plans and Standards Engineer

Ohio Department of Transportation

Don Fisher, P.E., Roadway Standards Engineer

South Carolina Department of Transportation

J. Adam Hixon, P.E., Design Standards Associate
Mark H. Anthony, P.E., Letting Preparation Engineer
Henry Cross, P.E., Design Standards Engineer
Jason Hall, P.E., Engineer

South Dakota Department of Transportation

David Huft, P.E., Research Engineer
Randy Brown, P.E., Standards Engineer

Utah Department of Transportation

Shawn Debenham, Traffic and Safety Specialist
Glenn Blackwelder, Operations Engineer

Virginia Department of Transportation

Charles Patterson, P.E., Standards/Special Design Section
Manager
Andrew Zickler, P.E., Complex Bridge Design and ABC
Support Program Manager

Wisconsin Department of Transportation

Erik Emerson, P.E., Standards Development Engineer
Rodney Taylor, P.E., Roadway Design Standards Unit
Supervisor

Wyoming Department of Transportation

William Wilson, P.E., Architectural and Highway
Standards Engineer

Federal Highway Administration

David Mraz, Division Bridge Engineer, Nebraska Division
Office

TABLE OF CONTENTS

DISCLAIMER STATEMENT	ii
ACKNOWLEDGEMENTS	ii
LIST OF FIGURES	vi
LIST OF TABLES	ix
1 INTRODUCTION	1
1.1 Background	1
1.2 Research Objective	2
1.3 Scope	2
2 LITERATURE REVIEW	3
2.1 Approach Guardrail Transitions	3
2.1.1 MASH Iowa Transition	3
2.1.2 Texas Transition – Without Curb	6
2.1.3 Texas MASH TL-2 Transition	8
2.1.3.1 Test No. 420021-4	9
2.1.3.2 Test No. 420021-6	9
2.1.3.3 Test No. 420021-7	9
2.1.4 W-Beam with Channel Rubrail	11
2.1.5 California Transition	13
2.1.5.1 Test No. 516	15
2.1.5.2 Test No. 517	15
2.1.5.3 Test No. 519	15
2.1.5.4 Test No. 518	16
2.1.5.5 Test No. 514	16
2.1.6 Standardized Transition Buttress	19
2.1.6.1 Test No. AGTB-1	21
2.1.6.2 Test No. AGTB-2	21
2.1.7 34-in. (864-mm) AGT Buttress	22
2.1.7.1 Test No. 34AGT-1	24
2.1.7.2 Test No. 34AGT-2	24
2.1.8 MGS Stiffness Transition	25
2.1.8.1 Test no. MWTSP-1	27
2.1.8.2 Test no. MWTSP-2	27
2.1.8.3 Test no. MWTSP-3	27
2.1.9 MGS Stiffness Transition with Curb	29
2.1.9.1 Test no. MWTC-1	31
2.1.9.2 Test no. MWTC-2	31
2.1.9.3 Test no. MWTC-3	31
2.1.10 TXDOT T131RC Bridge Rail Transition	33
2.1.10.1 Test No. 490022-6	35

2.1.10.2 Test No. 490022-8	35
2.1.11 Florida Transition.....	36
2.1.12 TTI Stacked W-Beam	38
2.2 Short Radius Guardrail System.....	40
2.2.1.1 Test No. 467114-3	43
2.2.1.2 Test No. 467114-4	43
2.2.1.3 Test No. 467114-5	43
2.2.1.4 Test No. 467114-6	43
2.2.1.5 Test No. 467114-7	43
2.3 Flare Rate Study.....	45
2.3.1.1 Test No. FR-1.....	47
2.3.1.2 Test No. FR-2.....	47
2.3.1.3 Test No. FR-3.....	47
2.3.1.4 Test No. FR-4.....	47
2.3.1.5 Test No. FR-5.....	48
3 CRITICAL APPROACH GUARDRAIL TRANSITION SELECTION	50
4 LENGTH OF NEED ANALYSIS	52
4.1 LON Calculation.....	52
4.2 Discussion.....	59
5 AGT BASELINE COMPUTER SIMULATION	61
5.1 Tangent AGT Model Details	61
5.2 Tangent AGT LS-DYNA Baseline Simulations.....	64
6 FLARED AGT COMPUTER SIMULATION	71
6.1 Flared AGT Model Details	71
6.2 Evaluation Criteria.....	72
6.3 Determination of Critical Flare Rates	74
6.3.1 Silverado Flare Rate Analysis.....	75
6.3.2 Ram Flare Rate Analysis	77
6.3.3 Critical Flare Rate Selection	81
6.4 Critical Impact Point (CIP) Studies	83
6.4.1 2270P CIP Study.....	83
6.4.2 1100C CIP Study	92
6.4.3 Critical Flare CIP Comparison.....	97
7 SUMMARY, CONCLUSIONS, AND RECOMMENDATIONS	103
8 REFERENCES	105
9 APPENDICES	108
Appendix A. AGT LS-DYNA Model Parts.....	109
Appendix B. V&V of Silverado and Tangent AGT Simulation	113
Appendix C. V&V of Ram and Tangent AGT Simulation.....	132
Appendix D. 2270P CIP Study Simulation Sequential Images	151
Appendix E. 1100C CIP Study Simulation Sequential Images	162

LIST OF FIGURES

Figure 1. AGT Installation [1]	1
Figure 2. MASH Iowa Transition Installation Layout [8]	5
Figure 3. Sequential Photographs for Test No. 2214T-1 [8]	6
Figure 4. Texas Transition – Without Curb Installation Layout [9]	7
Figure 5. Sequential Photographs for Test No. 490022-4 [9].....	8
Figure 6. Texas MASH TL-2 Transition Layout [10]	9
Figure 7. Sequential Photographs for Test No. 420021-4 [10].....	10
Figure 8. Sequential Photographs for Test No. 420021-6 [10].....	10
Figure 9. Sequential Photographs for Test No. 420021-7 [10].....	10
Figure 10. W-Beam with Channel Rubrail Transition Installation Layout [11].....	12
Figure 11. Sequential Photographs for Test No. 476460-1-3 [11]	13
Figure 12. California Transition Layout – Design 3 [12]	14
Figure 13. Sequential Photographs for Test No. 514 [12]	17
Figure 14. Sequential Photographs for Test No. 516 [12]	17
Figure 15. Sequential Photographs for Test No. 517 [12]	18
Figure 16. Sequential Photographs for Test No. 518 [12]	18
Figure 17. Sequential Photographs for Test No. 519 [12]	19
Figure 18. Standardized Transition Buttress Test Installation Layout [1].....	20
Figure 19. Sequential Photographs for Test No. AGTB-1 [1].....	22
Figure 20. Sequential Photographs for Test No. AGTB-2 [1].....	22
Figure 21. 34-in. (864-mm) AGT Buttress Test Installation Layout [13]	23
Figure 22. Sequential Photographs for Test No. 34AGT-1 [13].....	24
Figure 23. Sequential Photographs for Test No. 34AGT-2 [13].....	24
Figure 24. MGS Stiffness Transition Test Installation Layout [14]	26
Figure 25. Sequential Photographs for Test No. MWTSP-1 [14].....	28
Figure 26. Sequential Photographs for Test No. MWTSP-2 [14].....	28
Figure 27. Sequential Photographs for Test No. MWTSP-3 [14].....	28
Figure 28. MGS Stiffness Transition with Curb Test Installation Layout [15]	30
Figure 29. Sequential Photographs for Test No. MWTC-1 [15]	32
Figure 30. Sequential Photographs for Test No. MWTC-2 [15]	32
Figure 31. Sequential Photographs for Test No. MWTC-3 [15]	32
Figure 32. TXDOT T131RC Bridge Rail Transition Test Installation Layout [16].....	34
Figure 33. Sequential Photographs for Test No. 490022-6 [16].....	35
Figure 34. Sequential Photographs for Test No. 490022-8 [16].....	35
Figure 35. Florida Transition Test Installation Layout [17]	37
Figure 36. Sequential Photographs for Test No. 0385-1 [17].....	38
Figure 37. TTI Stacked W-Beam Test Installation Layout [18].....	39
Figure 38. Sequential Photographs for Test No. 604581-1 [18].....	40
Figure 39. MASH TL-3 Short Radius Guardrail Test Installation – Test No. 467114-7 [19].....	42
Figure 40. Sequential Photographs for Test No. 467114-3 [19].....	44
Figure 41. Sequential Photographs for Test No. 467114-4 [19].....	44
Figure 42. Sequential Photographs for Test No. 467114-5 [19].....	45
Figure 43. Sequential Photographs for Test No. 467114-6 [19].....	45
Figure 44. Sequential Photographs for Test No. 467114-7 [19].....	45
Figure 45. MGS – Flare Rates, 13:1 (4.4 degrees from roadway) Flared Test Installation [2]	46

Figure 46. Sequential Photographs for Test No. FR-1 [2].....	48
Figure 47. Sequential Photographs for Test No. FR-2 [2].....	49
Figure 48. Sequential Photographs for Test No. FR-3 [2].....	49
Figure 49. Sequential Photographs for Test No. FR-4 [2].....	49
Figure 50. Sequential Photographs for Test No. FR-5 [2].....	49
Figure 51. LON Layout [20].....	52
Figure 52. Flared AGT LON Diagram	55
Figure 53. Hybrid Flare AGT LON Diagram	57
Figure 54. Comparison of Hybrid vs. Pure Flared AGT Configurations.....	58
Figure 55. AGTB-2 Guardrail Installation.....	63
Figure 56. Finite Element Model of AGTB-2 Guardrail Installation	63
Figure 57. Full-Scale Crash Test No. AGTB-2 (Top) and Silverado Simulation (Bottom) [22].....	65
Figure 58. Test No. AGTB-2 (Left) vs. Silverado Simulation (Right) Sequential Photographs [22].....	66
Figure 59. Full-Scale Crash Test No. AGTB-2 (Top) and Ram Simulation (Bottom) [22].....	69
Figure 60. Test No. AGTB-2 (Left) vs. Ram Simulation (Right) Sequential Photographs [22].....	70
Figure 61. Location of Flare Initiation Point	71
Figure 62. Modeled Flared Installations	71
Figure 63. Post No. 20 Deflection Measurement.....	72
Figure 64. Critical Pocketing Angle [14].....	73
Figure 65. Tire-Buttress Overlap Measurement	73
Figure 66. Deformed 2270P Tire Model Comparison	74
Figure 67. Flared Simulation Impact Point Shift, Tangent vs. 10:1 Flare Rate.....	75
Figure 68. Flared Silverado Longitudinal Occupant Risk	76
Figure 69. Flared AGT Comparison of Silverado Tire-Buttress Overlap	77
Figure 70. Flare Rate Study Sequential Photographs, Ram Vehicle Model	79
Figure 71. Flared Ram Longitudinal Occupant Risk	80
Figure 72. Flared AGT Comparison of Ram Tire-Buttress Overlap	81
Figure 73. Flared AGT Longitudinal Occupant Risk	82
Figure 74. Flared AGT Lateral Occupant Risk.....	82
Figure 75. 2270P CIP Study Impact Locations	84
Figure 76. Fender-Buttress Penetration – 15:1 Flare Rate at US3 Impact Location	84
Figure 77. Ram Vehicle Model Right-Front Suspension Joints	85
Figure 78. 2270P CIP Study Longitudinal Occupant Risk.....	88
Figure 79. Post No. 20 Deflection	89
Figure 80. Euler Roll Angular Displacement – 15:1 (Left); 12.5:1 (Right)	89
Figure 81. Tire-Buttress Overlap	90
Figure 82. 15:1 2270P CIP Location	91
Figure 83. 12.5:1 2270P CIP Location	91
Figure 84. 1100C CIP Impact Point Locations.....	92
Figure 85. 15:1 1100C CIP Study Longitudinal Occupant Risk	94
Figure 86. 12.5:1 1100C CIP Study Longitudinal Occupant Risk	95
Figure 87. 1100C Right-Front Tire-Buttress Overlap.....	95
Figure 88. 15:1 1100C CIP Location (DS1)	97
Figure 89. 12.5:1 1100C CIP Location (DS1)	97

Figure 90. Comparison of Change in Velocity	98
Figure 91. Tire-Buttress Overlap Comparison.....	98
Figure 92. Vehicle Orientation at Exit: Tangent, 15:1, 12.5:1	99
Figure 93. 2270P Vehicle Trajectory and Exit Box.....	100
Figure 94. 1100C Vehicle Trajectory and Exit Box	101
Figure D-1. 15:1 DS4 Simulation (Left) vs. 15:1 DS3 Simulation (Right) Sequential Images	152
Figure D-2. 15:1 DS2 Simulation (Left) vs. 15:1 DS1 Simulation (Right) Sequential Images	153
Figure D-3. 15:1 X Simulation (Left) vs. 15:1 US1 Simulation (Right) Sequential Images.....	154
Figure D-4. 15:1 US2 Simulation (Left) vs. 15:1 US3 Simulation (Right) Sequential Images	155
Figure D-5. 15:1 US4 Simulation Sequential Images.....	156
Figure D-6. 12.5:1 DS4 Simulation (Left) vs. 12.5:1 DS3 Simulation (Right) Sequential Images	157
Figure D-7. 12.5:1 DS2 Simulation (Left) vs. 12.5:1 DS1 Simulation (Right) Sequential Images	158
Figure D-8. 12.5:1 X Simulation (Left) vs. 12.5:1 US1 Simulation (Right) Sequential Images	159
Figure D-9. 12.5:1 US2 Simulation (Left) vs. 12.5:1 US3 Simulation (Right) Sequential Images	160
Figure D-10. 12.5:1 US4 Simulation Sequential Images.....	161
Figure E-1. 15:1 DS3 Simulation (Left) vs. 15:1 DS2 Simulation (Right) Sequential Images...	163
Figure E-2. 15:1 DS1 Simulation (Left) vs. 15:1 X Simulation (Right) Sequential Images	164
Figure E-3. 15:1 US1 Simulation Sequential Images	165
Figure E-4. 12.5:1 DS2 Simulation (Left) vs. 12.5:1 DS1 Simulation (Right) Sequential Images	166
Figure E-5. 12.5:1 X Simulation (Left) vs. 12.5:1 US1 Simulation (Right) Sequential Images	167
Figure E-6. 12.5:1 US2 Simulation Sequential Images	168

LIST OF TABLES

Table 1. Summary of Reviewed Crash Test Data.....	4
Table 2. Summary of Crash Test Data for MASH Iowa Transition	6
Table 3. Summary of Crash Test Data for Texas Transition – Without Curb	8
Table 4. Summary of Crash Test Data for Texas MASH TL-2 Transition	10
Table 5. Summary of Crash Test Data for W-Beam with Channel Rubrail	13
Table 6. Summary of Crash Test Data for California Transition	16
Table 7. Summary of Crash Test Data for Standardized Transition Buttress.....	21
Table 8. Summary of Crash Test Data for 34-in. (864-mm) AGT Buttress	24
Table 9. Summary of Crash Test Data for MGS Stiffness Transition	28
Table 10. Summary of Crash Test Data for MGS Stiffness Transition with Curb.....	32
Table 11. Summary of Crash Test Data for TXDOT T131RC Bridge Rail Transition.....	35
Table 12. Summary of Crash Test Data for Florida Transition	38
Table 13. Summary of Crash Test Data for TTI Stacked W-Beam.....	40
Table 14. Summary of Crash Test Data for MASH TL-3 Short Radius Guardrail	44
Table 15. Summary of Crash Test Data for MGS – Flare Rates	48
Table 16. LON Calculation Variables	53
Table 17. Studied Flare Rates	53
Table 18. Calculated Flared AGT LON.....	54
Table 19. Calculated Hybrid Flared AGT LON	56
Table 20. Summary of Flare Rate vs. Impact Severity	60
Table 21. Summary of Test No. AGTB-2 and Silverado Simulation Results	64
Table 22. Summary of Crash Test No. AGTB-2 and Ram Simulation Results.....	68
Table 23. Critical Flare Rate Study Impact Locations.....	75
Table 24. Summary of Flared Simulation Results with Silverado Vehicle Model.....	76
Table 25. Summary of Flared Simulation Results with Ram Vehicle Model	78
Table 26. Summary of 2270P CIP Study Impact Locations.....	84
Table 27. Summary of 2270P Ram 15:1 Flared AGT CIP Study.....	86
Table 28. Summary of 2270P Ram 12.5:1 Flared AGT CIP Study.....	87
Table 29. Summary of 1100C CIP Study Impact Locations	92
Table 30. Summary of 1100C 15:1 Flared AGT CIP Study.....	93
Table 31. Summary of 1100C 12.5:1 Flared AGT CIP Study.....	94
Table 32. 1100C Simulation Post No. 20 Deflections	96
Table 33. Exit Conditions	99
Table 34. Summary of 12.5:1 vs. 15:1 Flared AGT Evaluation Criteria.....	102
Table A-1. Summary of AGT Model Parts and LS-DYNA Parameters.....	110
Table A-2. Summary of AGT Model Parts and LS-DYNA Parameters, Cont.....	111
Table A-3. Summary of AGT Model Parts and LS-DYNA Parameters, Cont.....	112

1 INTRODUCTION

1.1 Background

Approach guardrail transitions (AGTs) are commonly used to safeguard rigid hazards, including bridge railings and concrete parapets. A typical AGT is shown in Figure 1 [1]. AGT installations provide a safe transition in lateral stiffness between semi-rigid guardrail and rigid bridge rail installations. Oftentimes intersecting roadways or other roadside obstacles create space constraints that limit the ability to install an AGT within the desired area. Thus, a need exists to minimize the length of AGTs tangent to the roadway.



Figure 1. AGT Installation [1]

Installing an AGT with a flare away from the roadway would reduce the system length along the primary roadway, as the guardrail would intercept the vehicle runout path closer to the hazard, when compared to a tangent installation. Additionally, the flared AGT configuration would result in a greater lateral offset between the guardrail and the traveled roadway. Thus, the flared AGT configuration would move the hazard posed by impacts with the guardrail farther away from the traveled road, and increase the area for the driver to regain control of the vehicle. As a result, flared AGT installations would reduce both accident frequency and the overall installation maintenance and material costs.

Previously, guidance for flaring the Midwest Guardrail System (MGS) away from the roadway was established in accordance with NCHRP Report 350 Test Level 3 (TL-3) criteria [2, 3]. Due to the need to reduce guardrail length adjacent to the rigid parapet, initiating the flare in the transition region is more desirable as it would provide a greater reduction in barrier length along the primary road than flaring the W-beam section of guardrail at the upstream end of the transition. Unfortunately, minimal research and full-scale crash testing has been conducted on flared AGTs.

Previous flare rate studies raised several concerns for flared AGTs. Flaring a guardrail system away from the roadway increases the vehicle impact angle with the barrier installation, which increases the chance for pocketing and wheel snag. The increased impact angle also results in larger loads imparted to the barrier system, which could lead to component failure or rail rupture. Thus, a need exists to evaluate and establish guidance for flaring AGT installations under the *Manual for Assessing Safety Hardware, Second Edition* (MASH 2016) criteria [4].

1.2 Research Objective

The objective of this research study was to identify the critical flare rate for flaring AGTs away from the primary roadway. The research focused on the determination of the maximum allowable flare rate that could safely be applied to 31-in. (787-mm) tall three-beam AGTs without concrete curbs that utilize MGS upstream of the transition. Additionally, the standardized buttress was targeted for use at the downstream end of the AGT, because it included chamfers intended to mitigate tire snag [1].

1.3 Scope

The proposed research began with a literature review of existing AGTs, short radius guardrail systems, and flare rate studies that could be used when determining the critical flared transition design. Next, a model of a 31-in. (787-mm) tall tangent AGT without concrete curb was developed in LS-DYNA [5] and validated. This validated model was modified to incorporate a flare away from the roadway and was used to evaluate five transition flare rates from 10:1 to 25:1 to determine the critical flare rate and CIPs for full-scale testing.

2 LITERATURE REVIEW

A literature search was performed on existing AGTs, short radius guardrail systems, and flare rate studies to select a critical AGT design for use in the flared AGT study, as well as to provide initial information regarding vehicle behavior during impacts with AGTs and flared guardrail installations. System parameters and results, including dynamic deflection, impact point, post spacing, post size, post embedment depth, guardrail composition, downstream barrier, and MASH compliance, were recorded for each system. A summary of the crash test data for each reviewed full-scale test is shown in Table 1.

2.1 Approach Guardrail Transitions

AGTs are guardrail installations placed upstream of a rigid barrier to provide a safe transition in lateral stiffness from a semi-rigid guardrail installation to a rigid barrier installation. AGTs accomplish the transition in lateral stiffness by utilizing combinations of decreased post spacing, increased post size, increased embedment depth, and nesting or increased rail thickness in the transition region. Twelve different AGT systems were reviewed during this literature search, with primary consideration being given to *Manual for Assessing Safety Hardware* (MASH 2009) [6] and MASH 2016 tested installations. However, relevant NCHRP Report 350 [3] and NCHRP Report 230 [7] tested installations were also included. Metrics such as test designation number, impact conditions, lateral and longitudinal occupant impact velocities (OIVs), lateral and longitudinal occupant ridedown accelerations (ORAs), dynamic system deflection, and test result were recorded for each test.

2.1.1 MASH Iowa Transition

In 2006, the Midwest Roadside Safety Facility (MwRSF) conducted a research project to develop a MASH TL-3 compliant AGT [8]. The AGT test installation in test no. 2214T-1 was 80.7 ft (24.6 m) long and was constructed of 17 guardrail posts, which supported the 12-gauge (2.7-mm) W-beam and nested 12-gauge (2.7-mm) thrie-beam guardrail sections. The nested thrie-beam had a top rail mounting height of 31 in. (787 mm) and was attached to a 12-ft (3.66-m) long New Jersey safety shape end section with a connector plate. The W6x9 steel posts within the transition region, post nos. 12 through 17, were spaced 18¾ in. (476 mm) on center and embedded at a depth of 49 in. (1,245 mm). A 4-in. (102-mm) tall x 15-ft (4.6-m) long concrete curb was installed within the transition region at the base of post nos. 10 through 17. The test installation layout is shown in Figure 2.

Table 1. Summary of Reviewed Crash Test Data

Test Series	Test Number	Test Designation	Test Vehicle Weight lb (kg)	Impact Speed mph (km/h)	Impact Angle degrees	OIV		ORA		Dynamic Deflection in. (mm)	Pass/Fail	Reference #
						ft/s (m/s)		g's				
						Longitudinal	Lateral	Longitudinal	Lateral			
MASH Iowa Transition	2214T-1	3-21	5,083 (2,306)	60.3 (97.0)	24.8	-24.43 (-7.45)	-24.96 (-7.61)	-12.72	-8.71	11.4 (290)	Pass	[8]
Texas Transition - Without Curb	490022-4	3-21	5,002 (2,269)	62.6 (100.7)	23.9	16.4 (5.0)	27.6 (8.4)	14.4	9.0	5.9 (150)	Fail	[9]
Texas MASH TL-2 Transition	420021-4	2-21	5,089 (2,308)	43.7 (70.3)	25.8	18.4 (5.6)	19.7 (6.0)	5.9	8.0	5.7 (145)	Pass	[10]
	420021-6	2-20	2,418 (1,097)	43.5 (70.0)	26.4	29.5 (9.0)	14.1 (4.3)	9.0	5.9	14.4 (366)	Pass	
	420021-7	2-20	2,416 (1,096)	43.5 (70.0)	24.4	19.7 (6.0)	24.6 (7.5)	11.9	3.8	3.4 (86)	Pass	
W-Beam with Channel Rubrail	476460-1-3	3-21	5,029 (2,281)	62.8 (101.1)	25.7	16.4 (5.0)	28.5 (8.7)	-8.1	16.4	3.8 (97)	Pass	[11]
California Transition	514	4-22	17,661 (8,011)	46.9 (75.5)	16.0	N/A	N/A	N/A	N/A	N/A	Pass	[12]
	516	4-21	4,328 (1,963)	62.4 (100.5)	25.0	34.84 (10.62)	24.25 (7.39)	-8.11	-10.51	13.0 (330)	Fail	
	517	4-21	4,409 (2,000)	62.4 (100.5)	26.0	N/A	N/A	N/A	N/A	7.5 (190)	Fail	
	518	4-21	4,400 (1,996)	62.1 (99.9)	25.0	29.04 (8.85)	22.24 (6.78)	-5.61	-10.82	9.4 (240)	Pass	
	519	4-21	4,352 (1,974)	62.1 (100.0)	25.5	26.12 (7.96)	25.13 (7.66)	-4.26	-4.26	3.1 (80)	Pass	
Standardized Transition Buttress	AGTB-1	3-21	5,039 (2,286)	61.9 (99.6)	24.4	-22.70 (-6.92)	27.68 (8.44)	-30.03	9.96	6.0 (152)	Fail	[11]
	AGTB-2	3-21	4,998 (2,267)	62.7 (100.8)	25.4	-20.28 (-6.18)	-24.61 (-7.50)	-7.06	-10.40	5.4 (136)	Pass	
34-in. (864-mm) AGT Buttress	34AGT-1	3-21	5,024 (2,279)	62.2 (100.1)	24.8	-20.18 (-6.15)	25.92 (7.90)	-10.77	8.85	7.8 (198)	Pass	[13]
	34AGT-2	3-20	2,420 (1,098)	62.1 (99.9)	25.5	-22.65 (-6.90)	32.71 (9.97)	-10.84	14.70	2.7 (69)	Pass	
MGS Stiffness Transition	MWTSP-1	3-21	5,009 (2,272)	61.5 (99.0)	24.7	-18.62 (-5.68)	-16.49 (-5.03)	-24.82	-7.01	47.2 (1,199)	Fail	[14]
	MWTSP-2	3-21	4,993 (2,265)	61.2 (98.5)	26.3	-21.21 (-6.46)	-16.91 (-5.15)	-12.03	-9.87	32.8 (833)	Pass	
	MWTSP-3	3-20	2,394 (1,086)	61.0 (98.2)	25.7	-25.62 (-7.81)	-18.61 (-5.67)	-13.70	-6.74	18.5 (470)	Pass	
MGS Stiffness Transition with Curb	MWTC-1	3-20	2,457 (1,114)	62.9 (101.2)	25.0	-32.56 (-9.92)	17.59 (5.36)	-22.25	-8.51	N/A	Fail	[15]
	MWTC-2	3-20	2,410 (1,093)	61.3 (98.7)	25.6	-23.04 (-7.02)	24.14 (7.36)	-16.58	12.45	14.4 (366)	Pass	
	MWTC-3	3-21	4,969 (2,254)	61.0 (98.1)	24.4	-17.46 (-5.32)	17.79 (5.42)	-12.29	9.18	23.9 (607)	Pass	
TXDOT T131RC Bridge Rail Transition	490022-6	3-20	2,423 (1,099)	61.5 (99.0)	25.6	21.0 (6.4)	27.6 (8.4)	6.1	6.3	7.4 (188)	Pass	[16]
	490022-8	3-21	5,015 (2,275)	62.7 (100.9)	25.1	18.4 (5.6)	23.6 (7.2)	6.6	9.4	8.4 (213)	Pass	
Florida Transition	0385-1	30*	4,500 (2,041)	63.0 (101.4)	24.0	30.1 (9.2)	-26.2 (-8.0)	-7.1	34.8	6.0 (152)	Pass	[17]
TTI Stacked W-Beam	604581-1	3-21	5,005 (2,270)	64.0 (103.0)	25.0	19.4 (5.9)	29.9 (9.1)	5.6	15.0	4.0 (102)	Fail	[18]
MASH TL-3 Short Radius Guardrail	467114-3	3-33	5,041 (2,287)	62.8 (101.1)	14.4	28.5 (8.7)	5.9 (1.8)	8.2	10.0	300.0 (7,620)	Pass	[19]
	467114-4	3-32	2,424 (1,100)	62.1 (99.9)	14.8	36.4 (11.1)	3.6 (1.1)	12.0	6.2	195.6 (4,968)	Pass	
	467114-5	3-31	5,023 (2,278)	63.5 (102.2)	0.2	9.2 (2.8)	10.5 (3.2)	5.4	4.5	34.1 (866)	Pass	
	467114-6	3-35	5,016 (2,275)	62.6 (100.7)	25.1	25.3 (7.7)	23.3 (7.1)	10.8	10.0	21.1 (536)	Fail	
	467114-7	3-35	5,014 (2,274)	64.5 (103.8)	25.2	25.3 (7.7)	26.2 (8.0)	7.5	8.5	14.3 (363)	Pass	
MGS – Flare Rates	FR-1	3-11	4,467 (2,026)	63.9 (102.9)	30.6	21.36 (6.51)	13.52 (4.12)	8.08	10.41	66.3 (1,684)	Pass	[2]
	FR-2	3-11	4,460 (2,023)	63.1 (101.6)	34.0	24.18 (7.37)	13.55 (4.13)	9.92	7.16	75.8 (1,925)	Pass	
	FR-3	3-10	1,970 (894)	63.5 (102.2)	28.7	21.82 (6.65)	17.78 (5.42)	8.20	9.70	36.4 (925)	Pass	
	FR-4	3-11	4,441 (2,014)	65.0 (104.7)	36.8	26.25 (8.00)	13.32 (4.06)	7.15	6.35	75.6 (1,919)	Pass	
	FR-5	3-10	2,002 (908)	59.4 (99.5)	31.8	-22.51 (-6.86)	-16.04 (-4.89)	-9.27	-7.98	35.7 (908)	Pass	

* - NCHRP Report 230; N/A – Not Applicable

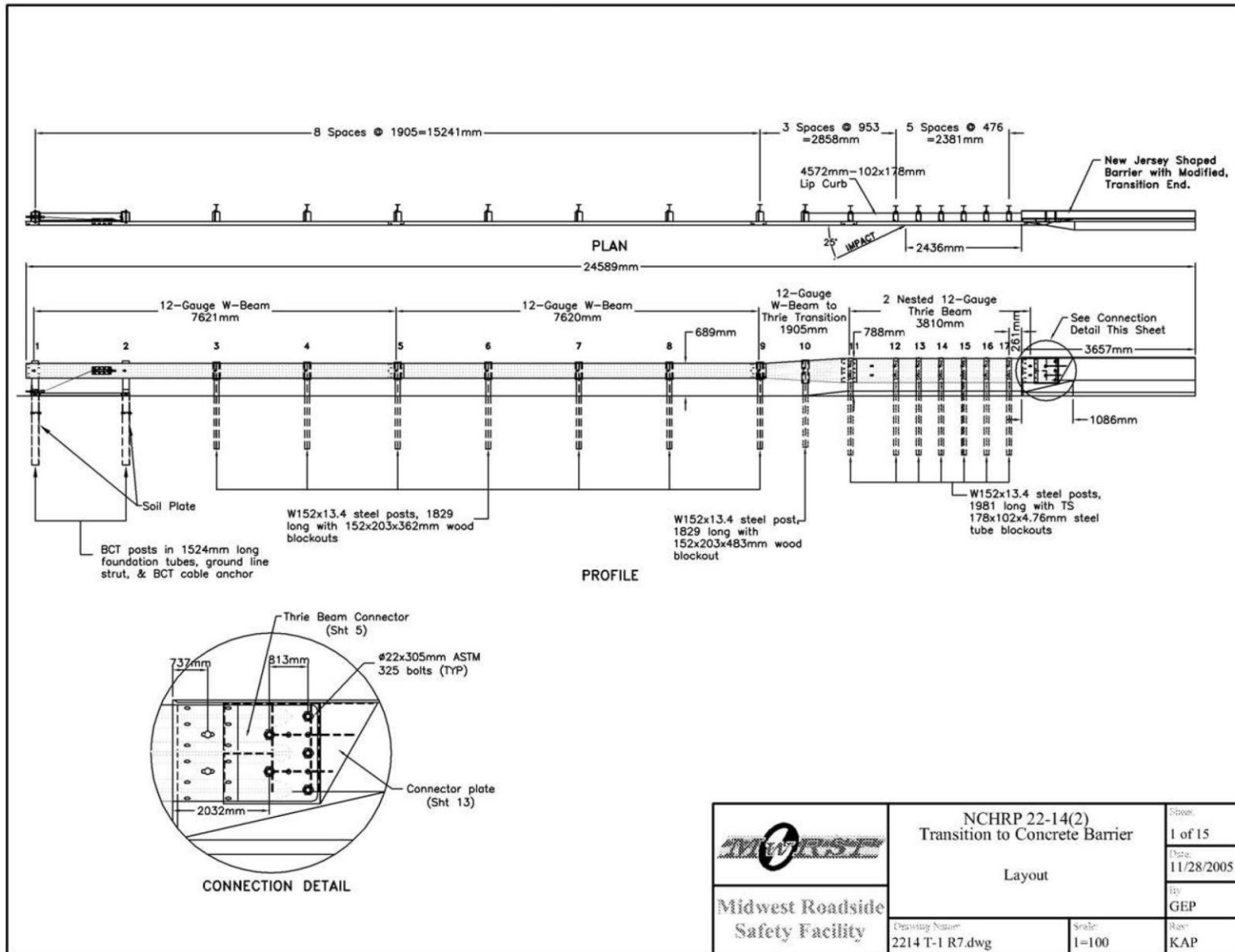


Figure 2. MASH Iowa Transition Installation Layout [8]

 Midwest Roadside Safety Facility	NCHRP 22-14(2) Transition to Concrete Barrier Layout		Sheet: 1 of 15
	Drawing Name: 2214 T-1 R7.dwg		Date: 11/28/2005
		Scale: 1=100	By: GEP
			Rev: KAP

In test no. 2214T-1, the 5,083-lb (2,306-kg) pickup truck impacted the AGT system at a speed of 60.3 mph (97.0 km/h) and at an angle of 24.8 degrees, 7 ft – 11⁷/₈ in. (2.4 m) upstream from the upstream end of the concrete barrier. The barrier system successfully contained and redirected the vehicle with a maximum lateral dynamic deflection of 11.4 in. (289 mm) located at the centerline of post no. 15. Barrier damage was minimal, consisting of contact marks and deformed thrie-beam guardrail. Post nos. 12 through 17 rotated backward slightly and minor contact marks were found on the bottom toe of the concrete barrier. The vehicle was redirected with moderate damage and met all occupant risk criteria. Test no. 2214T-1 was determined to be acceptable according to the Update to NCHRP Report 350 (MASH 2009) TL-3 safety performance criteria for test designation no. 3-21. The crash test data for test no. 2214T-1 is summarized in Table 2, and sequential photographs are presented in Figure 3.

Table 2. Summary of Crash Test Data for MASH Iowa Transition

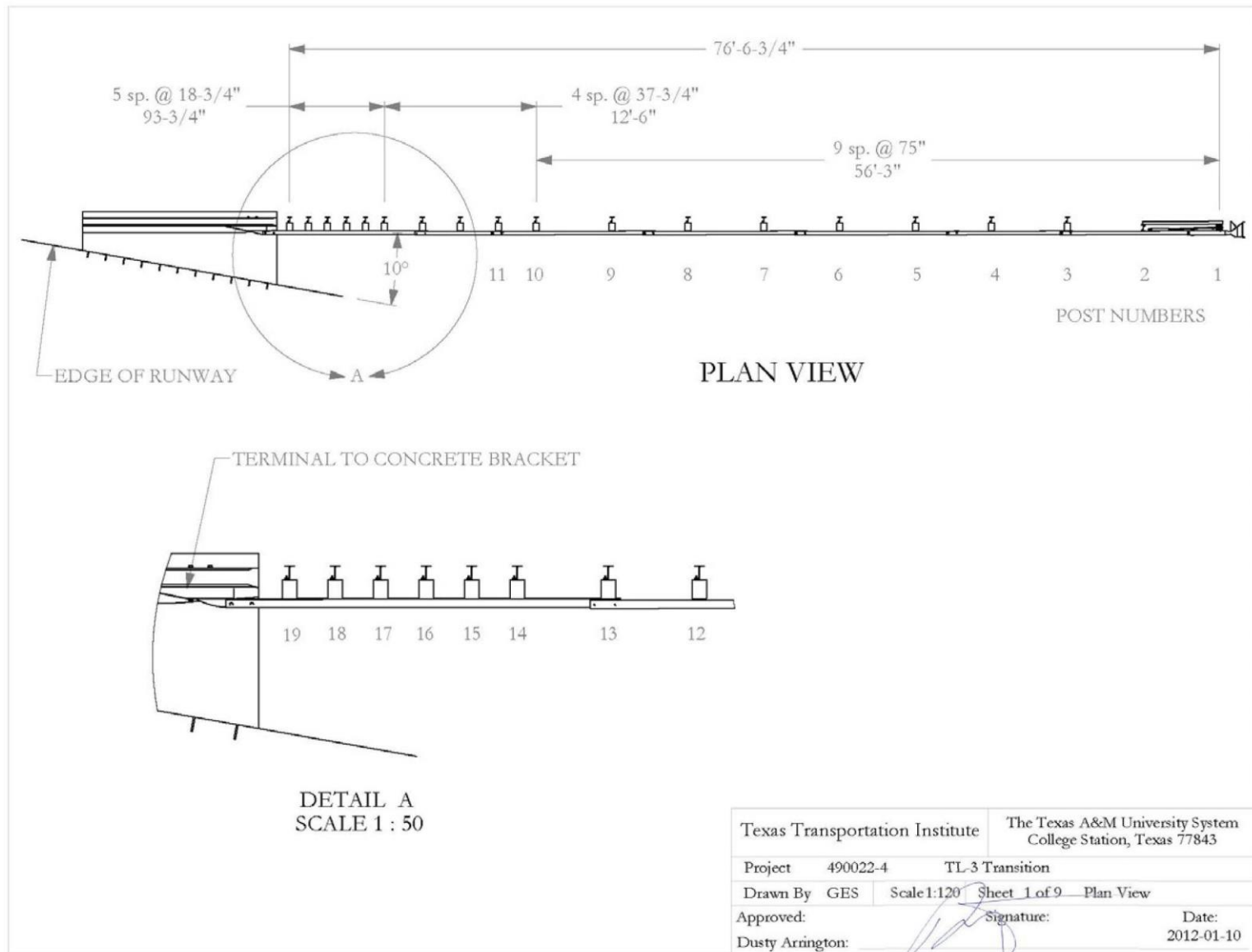
Test Number	Test Desig.	Test Vehicle lb (kg)	Impact Speed mph (km/h)	Impact Angle degrees	OIV ft/s (m/s)		ORA g's		Dynamic Defl. in. (mm)	Pass/Fail
					Long.	Lateral	Long.	Lateral		
2214T-1	3-21	5,083 (2,306)	60.3 (97.0)	24.8	-24.43 (-7.45)	-24.96 (-7.61)	-12.72	-8.71	11.4 (290)	Pass



Figure 3. Sequential Photographs for Test No. 2214T-1 [8]

2.1.2 Texas Transition – Without Curb

In 2013, the Texas A&M Transportation Institute (TTI) completed a research project to develop a MASH TL-3 compliant AGT [9]. The AGT test installation in test no. 490022-4 was 92 ft – 6³/₄ in. (28.2 m) long and was constructed of 19 guardrail posts, which supported the 12-gauge (2.7-mm) W-beam and nested 12-gauge (2.7-mm) thrie-beam guardrail sections. The nested thrie-beam section was connected to a 16-ft (4.9-m) long x 36-in. (914-mm) tall concrete single slope traffic rail with a 1/4-in. (6-mm) thick adapter plate and a 10-gauge (3.4-mm) thrie-beam terminal connector. The guardrail was installed with a top mounting height of 31 in. (787 mm). The W6x8.5 steel posts within the transition region, post nos. 14 through 19, were spaced 18³/₄ in. (476 mm) on center and embedded at a depth of 52 in. (1,321 mm). The test installation layout is shown in Figure 4.



T:\2011-2012\490022 TRDOT\4 TL-3 Transition\Drafting\TL-3 Installation

Figure 4. Texas Transition – Without Curb Installation Layout [9]

In test no. 490022-4, the 5,002-lb (2,269-kg) pickup truck impacted the AGT system at a speed of 62.6 mph (100.7 km/h) and at an angle of 23.9 degrees, 89 in. (2.3 m) upstream from the upstream end of the concrete parapet. The barrier system successfully contained and redirected the vehicle with a maximum lateral dynamic deflection of 5.9 in. (150 mm). Post nos. 13 through 19 deflected backward and contact marks were found on the upstream face of the concrete parapet. The vehicle’s right-front tire and wheel contacted the concrete parapet during the impact and disengaged from the vehicle. The vehicle rolled onto its right side as it exited the transition. While the vehicle was successfully contained and redirected by the test installation, it did not meet all occupant risk criteria due to vehicle rollover. Test no. 490022-4 was determined to be unacceptable according to the MASH TL-3 safety performance criteria for test designation no. 3-21. The crash test data for test no. 490022-4 is summarized in Table 3 and sequential photographs are presented in Figure 5.

Table 3. Summary of Crash Test Data for Texas Transition – Without Curb

Test Number	Test Desig.	Test Vehicle lb (kg)	Impact Speed mph (km/h)	Impact Angle degrees	OIV ft/s (m/s)		ORA g’s		Dynamic Defl. in. (mm)	Pass/Fail
					Long.	Lateral	Long.	Lateral		
490022-4	3-21	5,002 (2,269)	62.6 (100.7)	23.9	16.4 (5.0)	27.6 (8.4)	14.4	9.0	5.9 (150)	Fail



Figure 5. Sequential Photographs for Test No. 490022-4 [9]

2.1.3 Texas MASH TL-2 Transition

In 2011, TTI completed a research project to develop a MASH Test Level 2 (TL-2) compliant AGT [10]. The AGT test installation in test nos. 420021-4, 420021-6, and 420021-7 was 55 ft – 6½ in. (16.9 m) long and was constructed of 11 guardrail posts, which supported the 12-gauge (2.7-mm) W-beam and 10-gauge (3.4-mm) thrie-beam guardrail sections. The 10-gauge (3.4-mm) thrie-beam section was twisted onto the sloped traffic face of a 36-in. (914-mm) tall concrete single slope traffic rail and attached using a 10-gauge (3.4-mm) thrie-beam terminal connector. The guardrail was installed with a top mounting height of 31 in. (787 mm). The W6x8.5 steel posts within the transition region, post nos. 8 through 11, were spaced 37.5 in. (953 mm) on center and embedded at a depth of 40 in. (1,016 mm). The test installation layout is shown in Figure 6 and the crash test data for test nos. 420021-4, 420021-6, and 420021-7 is summarized in Table 4. Sequential photographs are presented in Figures 7 through 9.

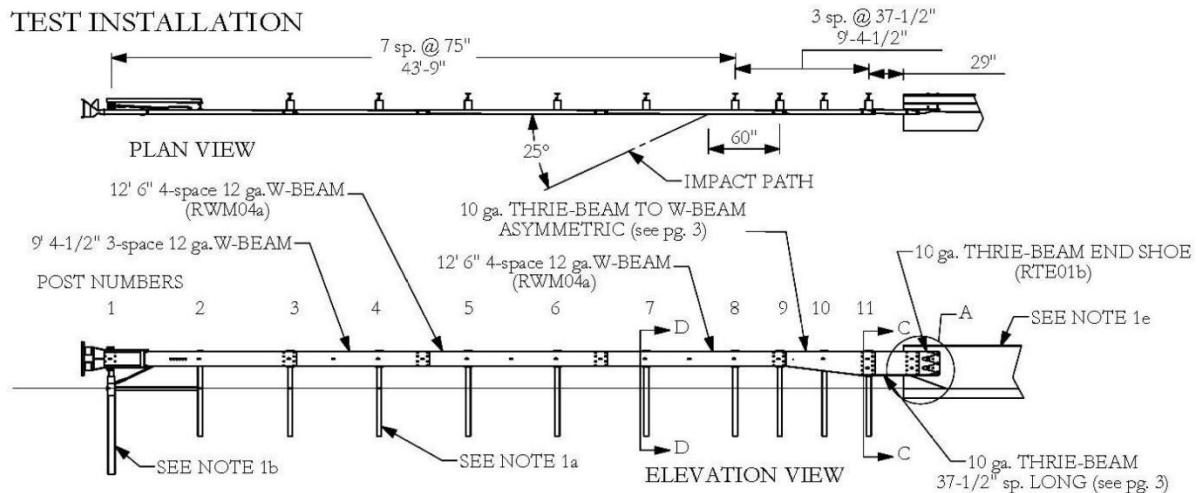


Figure 6. Texas MASH TL-2 Transition Layout [10]

2.1.3.1 Test No. 420021-4

The 5,089-lb (2,308-kg) pickup truck impacted the AGT system at a speed of 43.7 mph (70.3 km/h) and at an angle of 25.8 degrees, 55 in. (1.4 m) upstream from the upstream end of the concrete parapet. The barrier system successfully contained and redirected the vehicle with a maximum lateral dynamic deflection of 5.7 in. (145 mm). Post nos. 9 through 11 deflected backward and minor contact marks were found at the base of the concrete parapet. The test installation met all occupant risk criteria and test no. 420021-4 was determined to be acceptable according to the MASH TL-2 safety performance criteria for test designation no. 2-21.

2.1.3.2 Test No. 420021-6

In test no. 420021-6, the 2,418-lb (1,097-kg) small car impacted the upstream end of the transition at a speed of 43.5 mph (70.0 km/h) and at an angle of 26.4 degrees, 175 in. (4.4 m) upstream from the upstream end of the concrete parapet. The barrier system successfully contained and redirected the vehicle with a maximum lateral dynamic deflection of 14.4 in. (366 mm). Post nos. 7 through 10 deflected backward and moderate guardrail deformation was observed. The test installation met all occupant risk criteria and test no. 420021-6 was determined to be acceptable according to the MASH TL-2 safety performance criteria for test designation no. 2-20.

2.1.3.3 Test No. 420021-7

The 2,416-lb (1,096-kg) small car impacted the AGT system at a speed of 43.5 mph (70.0 km/h) and at an angle of 24.4 degrees, 54 in. (1.4 m) upstream from the upstream end of the concrete parapet. The barrier system successfully contained and redirected the vehicle with a maximum lateral dynamic deflection of 3.4 in. (86 mm). The vehicle's left-front wheel contacted the traffic face of post no. 11, and post nos. 8 through 11 deflected backward. The test installation met all occupant risk criteria and test no. 420021-6 was determined to be acceptable according to the MASH TL-2 safety performance criteria for test designation no. 2-20.

Table 4. Summary of Crash Test Data for Texas MASH TL-2 Transition

Test Number	Test Desig.	Test Vehicle lb (kg)	Impact Speed mph (km/h)	Impact Angle degrees	OIV ft/s (m/s)		ORA g's		Dynamic Defl. in. (mm)	Pass/Fail
					Long.	Lateral	Long.	Lateral		
420021-4	2-21	5,089 (2,308)	43.7 (70.3)	25.8	18.4 (5.6)	19.7 (6.0)	5.9	8.0	5.7 (145)	Pass
420021-6	2-20	2,418 (1,097)	43.5 (70.0)	26.4	29.5 (9.0)	14.1 (4.3)	9.0	5.9	14.4 (366)	Pass
420021-7	2-20	2,416 (1,096)	43.5 (70.0)	24.4	19.7 (6.0)	24.6 (7.5)	11.9	3.8	3.4 (86)	Pass



Figure 7. Sequential Photographs for Test No. 420021-4 [10]

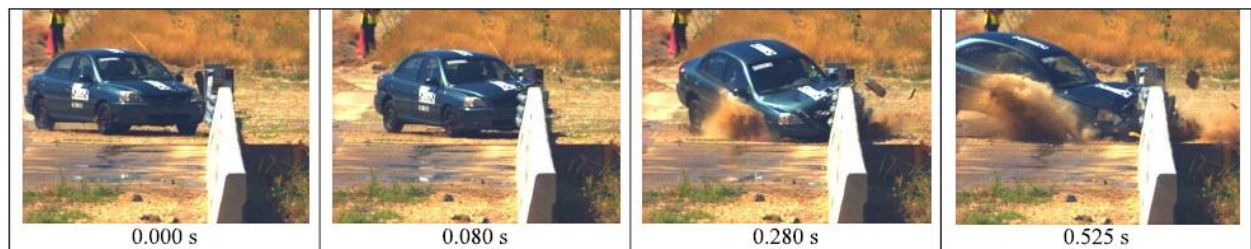


Figure 8. Sequential Photographs for Test No. 420021-6 [10]



Figure 9. Sequential Photographs for Test No. 420021-7 [10]

2.1.4 W-Beam with Channel Rubrail

In 2010, TTI completed a research project to develop a MASH TL-3 compliant W-beam AGT [11]. The AGT test installation in test no. 476460-1-3 was 86 ft (26.2 m) long and was constructed of 19 guardrail posts, which supported the 12-gauge (2.7-mm) W-beam and nested 12-gauge (2.7-mm) W-beam guardrail sections. In addition, the transition incorporated a “flared back” C6x8.2 rubrail. The nested W-beam guardrail was attached to the traffic face of a 16-ft 5-in. (5.0-m) long x 42-in. (1,067-mm) tall F-shape concrete parapet with a 10-gauge (3.4-mm) terminal connector welded to a steel plate. The W-beam guardrail and C6x8.2 rubrail were installed with a top mounting height of 31 in. (787 mm) and 16 in. (406 mm), respectively. The W6x8.5 steel posts within the transition region, post nos. 16 through 19, were spaced 18¾ in. (476 mm) on center and embedded at a depth of 52 in. (1,321 mm). The test installation layout is shown in Figure 10.

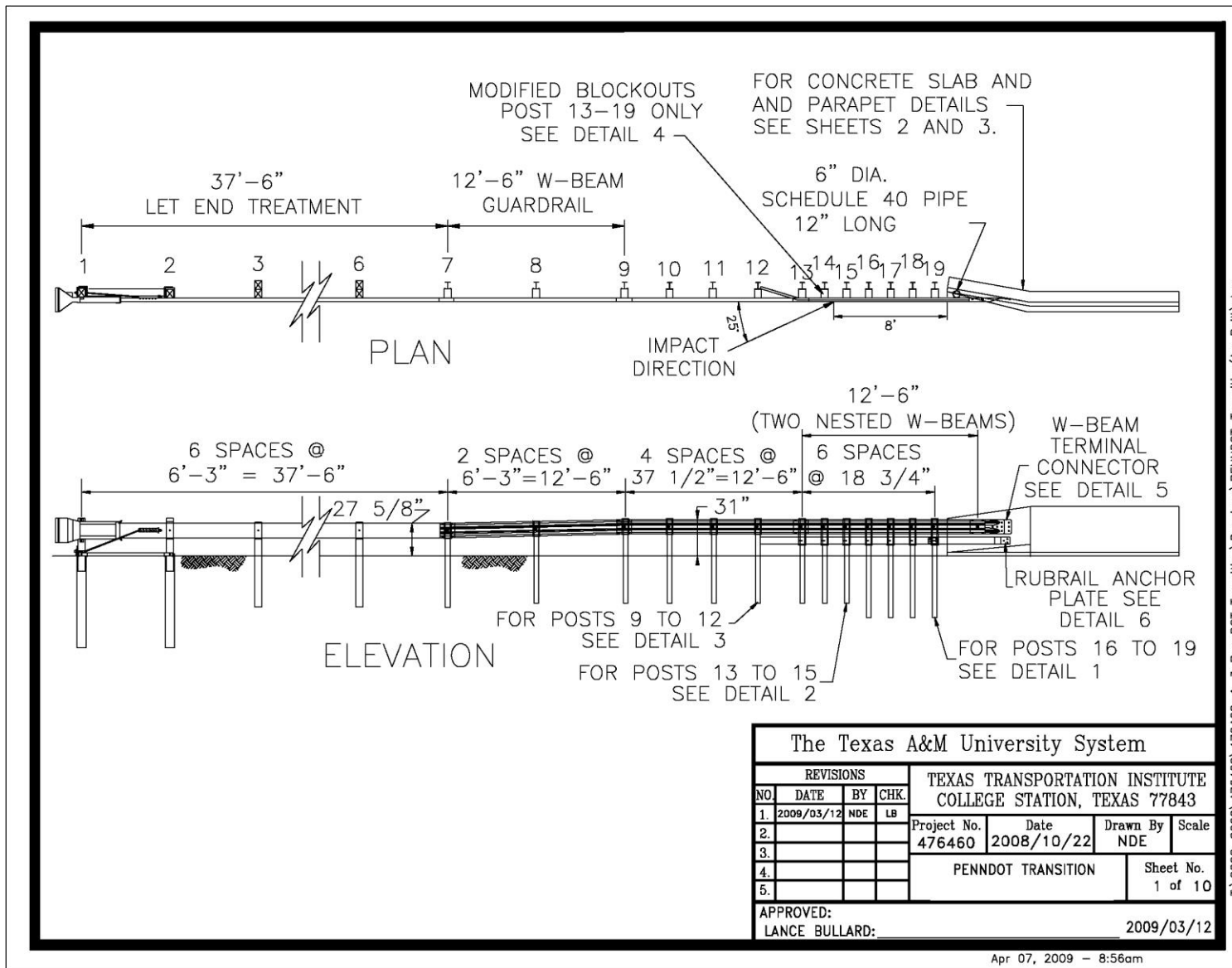


Figure 10. W-Beam with Channel Rubrail Transition Installation Layout [11]

In test no. 476460-1-3, the 5,029-lb (2,281-kg) pickup truck impacted the AGT system at a speed of 62.8 mph (101.1 km/h) and at an angle of 25.7 degrees, 103 in. (2.6 m) upstream from the upstream end of the concrete parapet. The barrier system successfully contained and redirected the vehicle with a maximum lateral dynamic deflection of 3.8 in. (97 mm). Deformation of both the nested W-beam and the rubrail were observed and post nos. 12 through 19 deflected backward. The test installation met all occupant risk criteria and test no. 476460-1-3 was determined to be acceptable according to the MASH TL-3 safety performance criteria for test designation no. 3-21. The crash test data for test no. 476460-1-3 is summarized in Table 5 and sequential photographs are presented in Figure 11.

Table 5. Summary of Crash Test Data for W-Beam with Channel Rubrail

Test Number	Test Desig.	Test Vehicle lb (kg)	Impact Speed mph (km/h)	Impact Angle degrees	OIV ft/s (m/s)		ORA g's		Dynamic Defl. in. (mm)	Pass/Fail
					Long.	Lateral	Long.	Lateral		
476460-1-3	3-21	5,029 (2,281)	62.8 (101.1)	25.7	16.4 (5.0)	28.5 (8.7)	-8.1	16.4	3.8 (97)	Pass

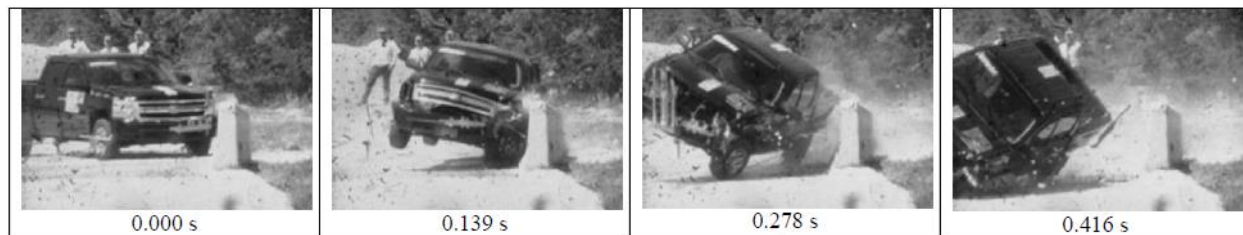


Figure 11. Sequential Photographs for Test No. 476460-1-3 [11]

2.1.5 California Transition

In 2002, the California Department of Transportation (CALTRANS) conducted a research project to develop a bridge rail transition design to NCHRP Report 350 Test Level 4 (TL-4) criteria [12]. Three AGT designs were tested during the CALTRANS study due to the failure of the system to meet NCHRP Report 350 criteria in test nos. 516 and 517. All three designs were 68 ft – 4 in. (20.8 m) long and transitioned between a W-beam guardrail with a top rail height of 28 in. (711 mm) and a 31.9-in. (810-mm) tall concrete bridge rail. All guardrail sections in the first design were 12-gauge (2.7-mm) galvanized steel. The thrie-beam guardrail closest to the concrete bridge rail was supported by three 9.8-in. x 9.8-in (250-mm x 250-mm) Douglas Fir posts with an embedment depth of 40 in. (1,016 mm) and a post spacing of 37.5 in. (953 mm). After the failure of the first design, the guardrail section thicknesses and post embedment depths were increased in the second design, but the installation remained unsuccessful. The third design included additional post and rail updates, and was tested successfully in test nos. 514, 518, and 519. The test installation layout of the successfully tested transition (Design 3) is shown in Figure 12. The crash test data for test nos. 514 and 516 through 519 is summarized in Table 6 and sequential photographs are presented in Figures 13 through 17.

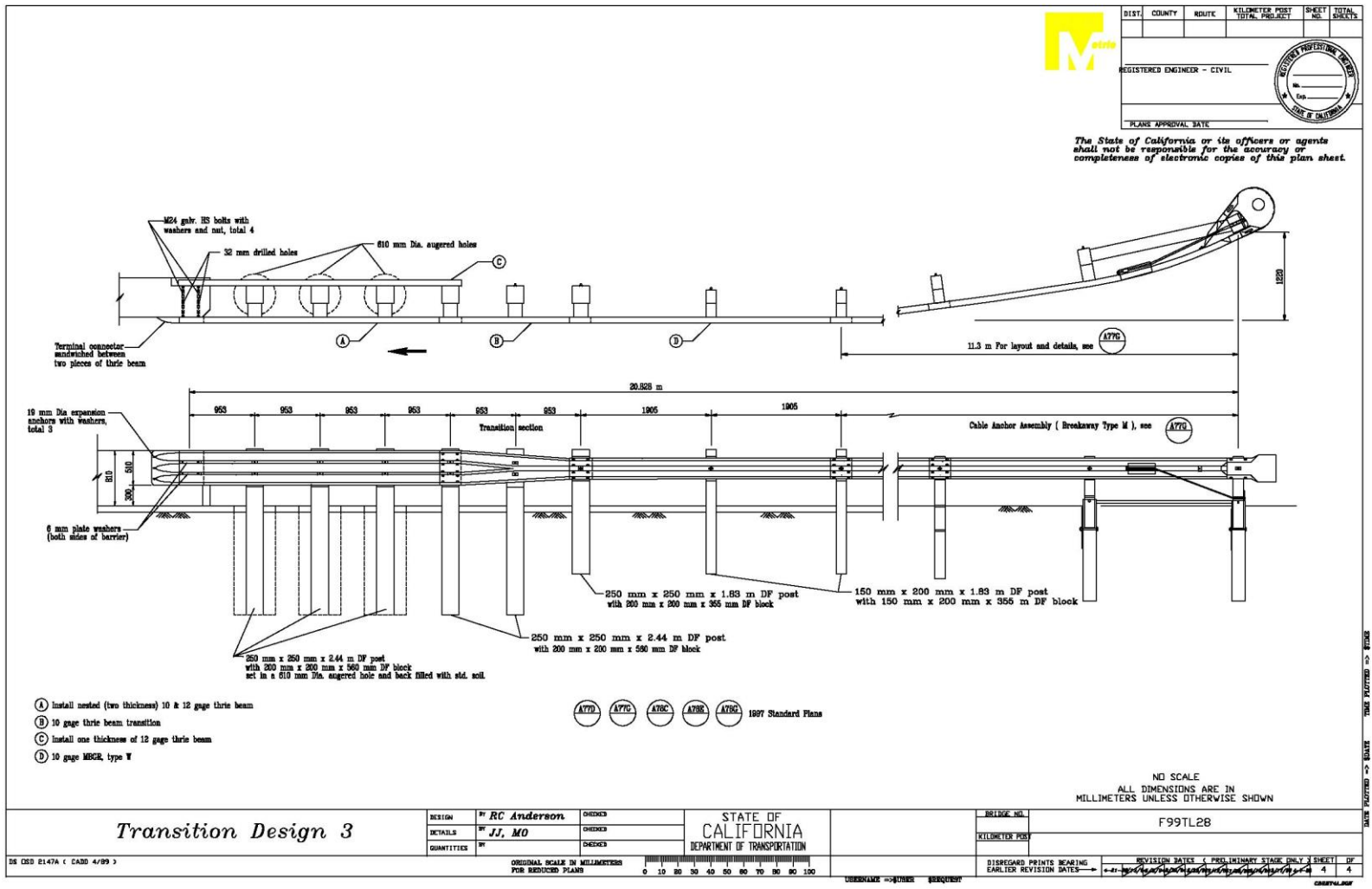


Figure 12. California Transition Layout – Design 3 [12]

2.1.5.1 Test No. 516

In test no. 516, the 4,328-lb (1,963-kg) pickup truck impacted the first AGT test installation at a speed of 62.4 mph (100.5 km/h) and at an angle of 25.0 degrees. The impact location was approximately 81 in. (2.1 m) upstream from the bridge rail, which was located between post nos. 13 and 14, the second and third posts upstream of the concrete bridge rail. The test installation successfully contained and redirected the test vehicle with a maximum dynamic deflection of 13 in. (330 mm). Damage to the barrier system was moderate and consisted of deflected posts, deformed guardrail, and a deformed metal box spacer. During the test, the barrier pocketed severely and the vehicle snagged on the upstream face of the concrete parapet. The vehicle snag led to excessive deformation of the passenger side floor pan. Test no 516 did not satisfy all occupant risk criteria and was determined to be unacceptable according to the NCHRP Report 350 TL-4 safety performance criteria for test designation no. 4-21.

2.1.5.2 Test No. 517

Due to the failure in test no. 516, the first design was updated to minimize vehicle snagging and pocketing. Design 2 increased the thickness of the W-to-thrie transition section from 12-gauge (2.7 mm) to 10-gauge (3.4 mm), nested the thrie-beam section in front of the barrier, added an additional thrie-beam section to the back of the posts, directly attached the thrie-beam to the concrete bridge rail, and increased the post embedment depth from 40 in. (1,016 mm) to 52 in. (1,321 mm).

The 4,409-lb (2,000-kg) pickup truck impacted the second AGT test installation at a speed of 62.4 mph (100.5 km/h) and at an angle of 26.0 degrees. The impact occurred at post no. 13, the third post upstream of the concrete bridge rail, which was approximately 106 in. (2.7 m) upstream from the upstream end of the concrete parapet. The test installation experienced minor damage while it contained and redirected the test vehicle with a maximum dynamic deflection of 7.5 in. (190 mm). After losing contact with the barrier, the vehicle underwent rollover, which prevented the acceptance of test no. 517. Test no. 517 did not satisfy all occupant risk criteria and was determined to be unacceptable according to the NCHRP Report 350 TL-4 safety criteria for test designation no. 4-21.

2.1.5.3 Test No. 519

Due to the failure of the test no. 517, Design 2 was updated to resolve the excessive system deflections. Design 3 increased the thickness of the W-beam section adjacent to the W-to-thrie transition section and one of the nested thrie-beam rail sections from 12-gauge (2.7 mm) to 10-gauge (3.4 mm) and increased the post size and embedment depth of the five posts closest to the bridge rail to 9.8 in. x 9.8 in. (250 mm x 250 mm) and 64 in. (1,630 mm), respectively.

In test no. 519, the 4,352-lb (1,974-kg) pickup truck impacted the third AGT test installation at a speed of 62.1 mph (100.0 km/h) and at an angle of 25.5 degrees. The impact occurred at post no. 13, the third post upstream of the concrete bridge rail, which was approximately 106 in. (2.7 m) upstream from the upstream end of the concrete parapet. The vehicle was adequately contained and redirected by the test installation with a maximum deflection of 3.1 in. (80 mm). Damage to the barrier system was minimal and consisted of minor post deflections, wood blockout damage, and contact marks. Test no. 519 satisfied all occupant risk criteria and was

determined to be acceptable according to the NCHRP Report 350 TL-4 safety criteria for test designation no. 4-21.

2.1.5.4 Test No. 518

The 4,400-lb (1,996-kg) pickup truck impacted the Design 3 test installation at a speed of 62.1 mph (99.9 km/h) and at an angle of 25.0 degrees. The test vehicle impacted the upstream end of the stiffness transition 218.5 in. (5.5 m) upstream from the upstream end of the concrete parapet and was safely contained and redirected. The maximum dynamic deflection of the test installation was 9.4 in. (240 mm). Damage to the barrier system was minimal and consisted of deflected posts, wood blackout damage, contact marks, and rail deformation. All occupant risk criteria were satisfied and test no. 518 was determined to be acceptable according to the NCHRP Report 350 TL-4 safety criteria for test designation no. 4-21.

2.1.5.5 Test No. 514

The 17,661-lb (8,011-kg) single unit truck (SUT) impacted the Design 3 test installation at a speed of 46.9 mph (75.5 km/h) and at an angle of 16.0 degrees. The impact location was approximately 87 in. (2.2 m) upstream from the bridge rail, which was located midway between post nos. 13 and 14, the second and third posts upstream of the concrete bridge rail. The test vehicle was contained and redirected by the test installation. Damage to the system was moderate, and included deflected posts, contact marks, and tearing of the outer thrie-beam guardrail. Test no. 514 satisfied all occupant risk criteria and was determined to be acceptable according to the NCHRP Report 350 TL-4 safety performance criteria for test designation no. 4-22.

Table 6. Summary of Crash Test Data for California Transition

Test Number	Test Desig.	Test Vehicle lb (kg)	Impact Speed mph (km/h)	Impact Angle degrees	OIV ft/s (m/s)		ORA g's		Dynamic Defl. in. (mm)	Pass/Fail
					Long.	Lateral	Long.	Lateral		
514	4-22	17,661 (8,011)	46.9 (75.5)	16.0	N/A	N/A	N/A	N/A	N/A	Pass
516	4-21	4,328 (1,963)	62.4 (100.5)	25.0	34.84 (10.62)	24.25 (7.39)	-8.11	-10.51	13 (330)	Fail
517	4-21	4,409 (2,000)	62.4 (100.5)	26.0	N/A	N/A	N/A	N/A	7.5 (190)	Fail
518	4-21	4,400 (1,996)	62.1 (99.9)	25.0	29.04 (8.85)	22.24 (6.78)	-5.61	-10.82	9.4 (240)	Pass
519	4-21	4,352 (1,974)	62.1 (100.0)	25.5	26.12 (7.96)	25.13 (7.66)	-4.26	-4.26	3.1 (80)	Pass

N/A – Not Applicable

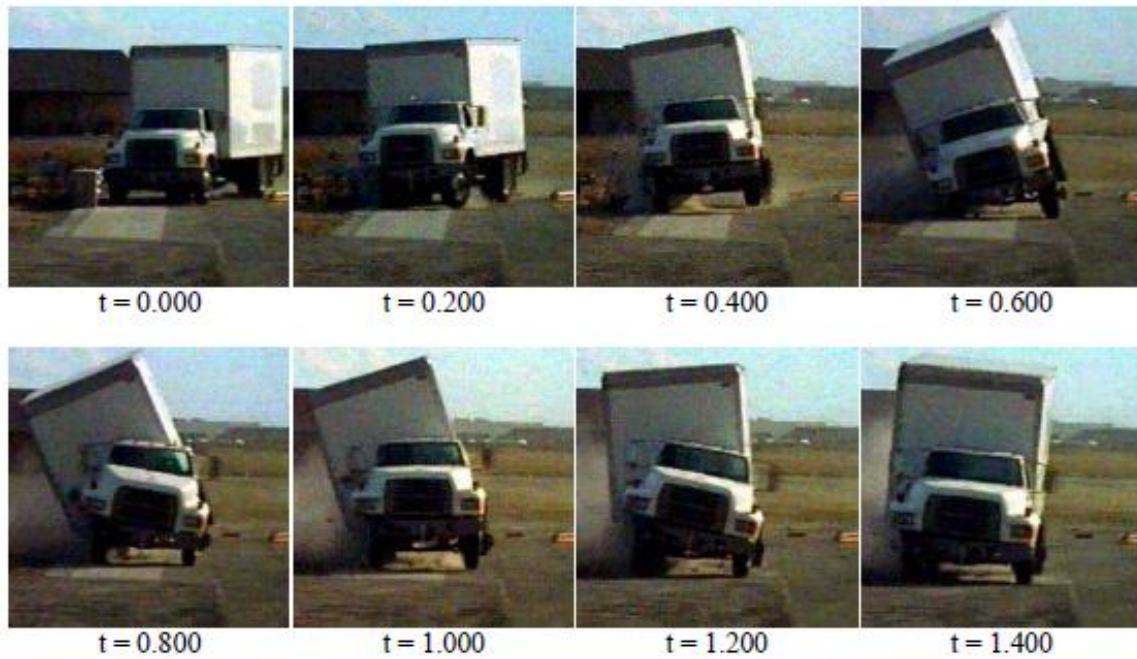


Figure 13. Sequential Photographs for Test No. 514 [12]



Figure 14. Sequential Photographs for Test No. 516 [12]

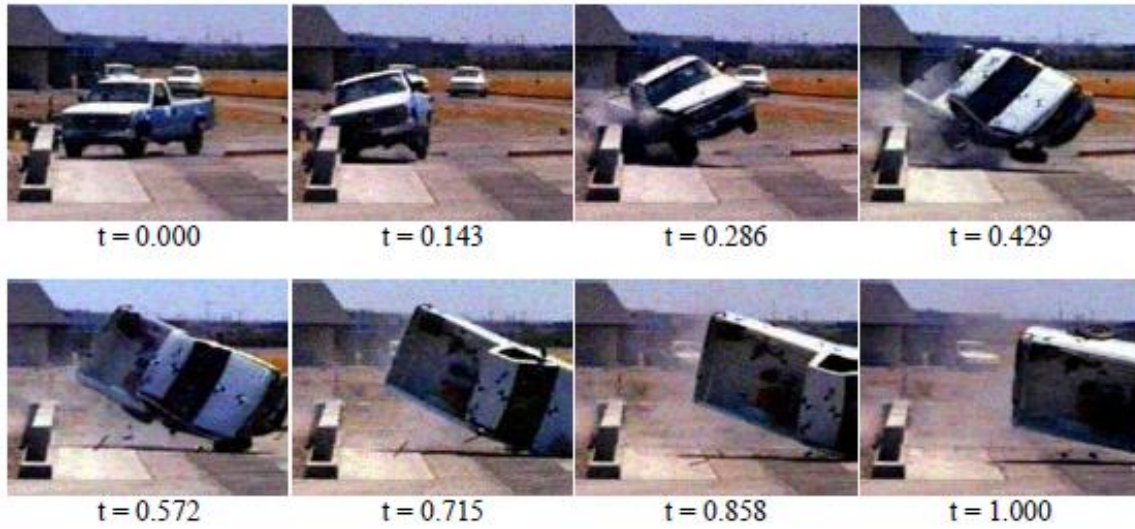


Figure 15. Sequential Photographs for Test No. 517 [12]

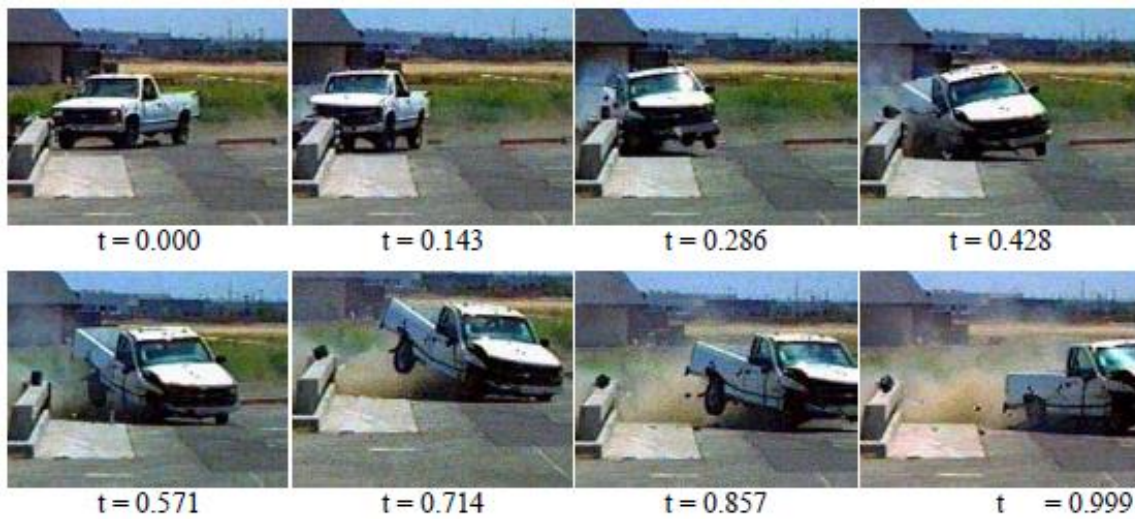


Figure 16. Sequential Photographs for Test No. 518 [12]

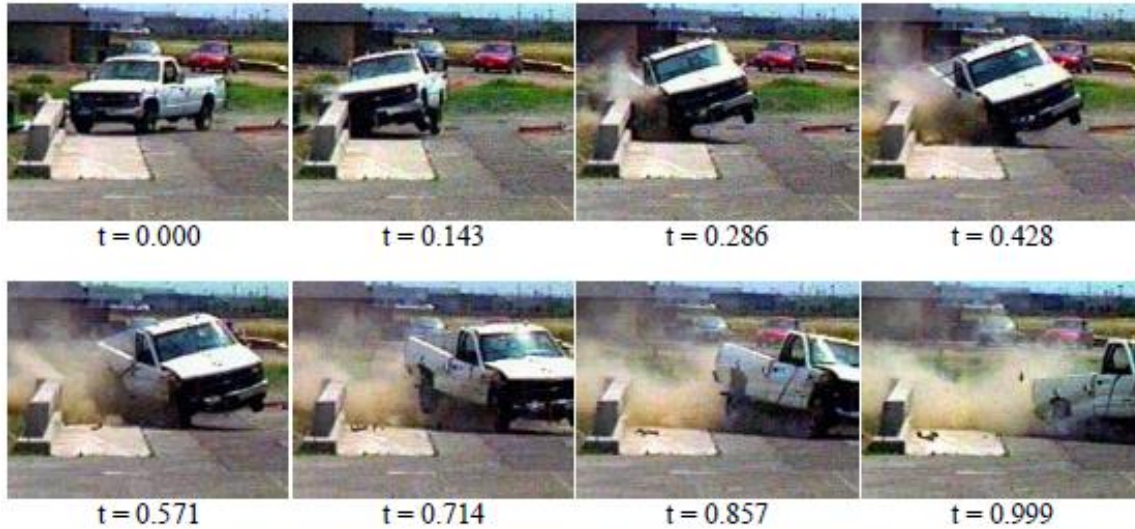


Figure 17. Sequential Photographs for Test No. 519 [12]

2.1.6 Standardized Transition Buttress

In 2020, MwRSF completed a research project to develop a MASH TL-3 compliant AGT with a standardized concrete buttress [1]. The AGT test installations in test nos. AGTB-1 and AGTB-2 were approximately 81 ft – 8¼ in. (24.9 m) long, and consisted of 21 guardrail posts, which supported the 12-gauge (2.7-mm) W-beam and nested 12-gauge (2.7-mm) thrie-beam guardrail sections. The nested thrie-beam guardrail was attached to the traffic face of a vertical concrete buttress with a 12-gauge (2.7-mm) terminal connector and a 10-gauge (3.4-mm) terminal connector in test nos. AGTB-1 and AGTB-2, respectively. The vertical concrete buttress was 84 in. (2,134 mm) long x 36 in. (914 mm) tall and had a longitudinal chamfer on the lower upstream front face to reduce wheel snagging. The guardrail was installed with a top mounting height of 31 in. (787 mm) in both tests. The W6x8.5 steel posts within the transition region, post nos. 16 through 21, were spaced 18¾ in. (476 mm) on center and embedded at a depth of 49 in. (1,245 mm). The Standardized Transition Buttress test installation layout is shown in Figure 18 and the crash test data for test nos. AGTB-1 and AGTB-2 is summarized in Table 7. Sequential photographs are presented in Figures 19 and 20.

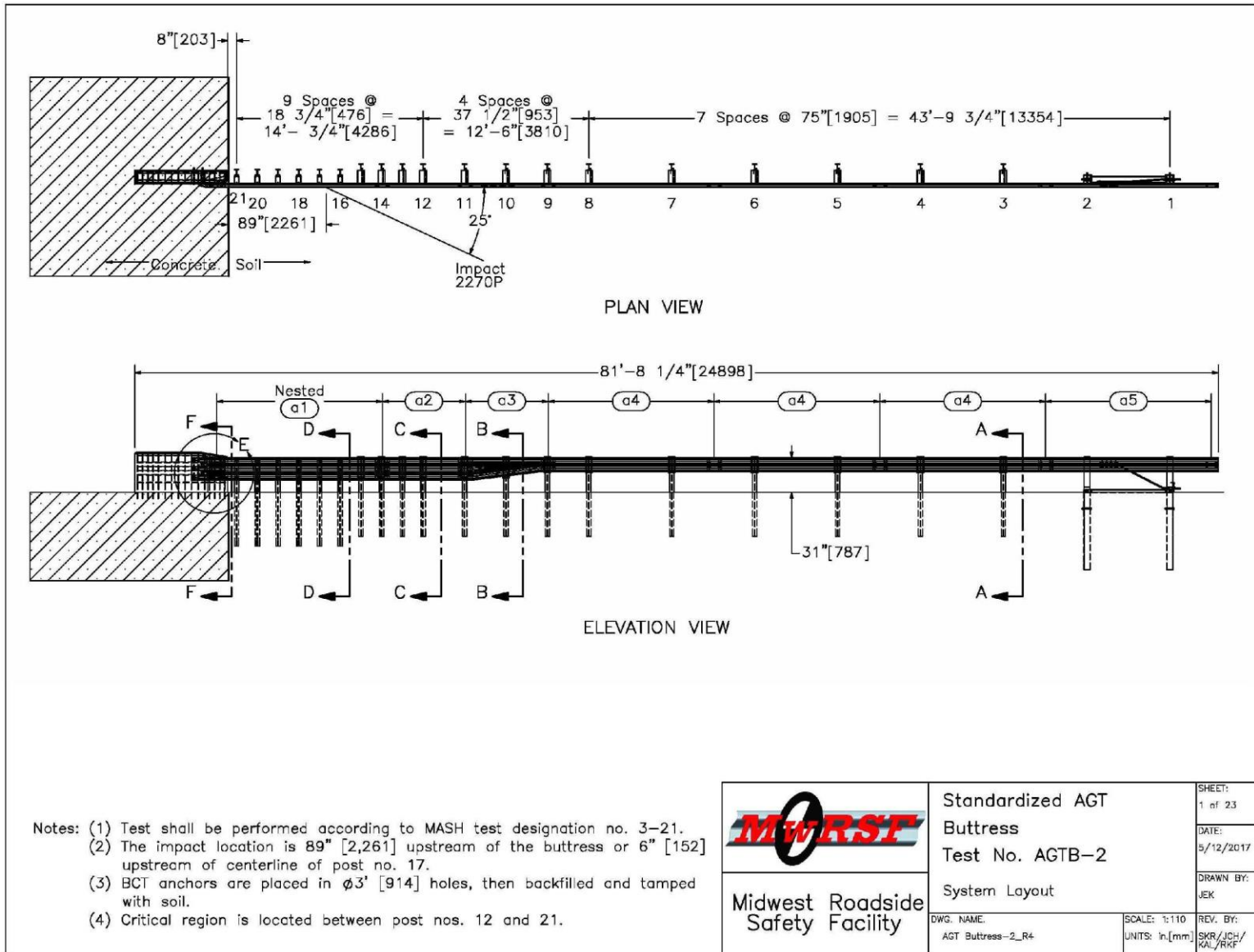


Figure 18. Standardized Transition Buttress Test Installation Layout [1]

2.1.6.1 Test No. AGTB-1

The 5,039-lb (2,286-kg) pickup truck impacted the AGT system at a speed of 61.9 mph (99.6 km/h) and at an angle of 24.4 degrees. The impact location was 80½ in. (2.0 m) upstream from the upstream end of the concrete parapet. The barrier system successfully contained and redirected the vehicle with a maximum lateral dynamic deflection of 6.0 in. (153 mm) located at post no. 19. Damage to the test installation was minimal, primarily consisting of contact marks and minor guardrail deformation. While the vehicle was successfully contained and redirected by the test installation, excessive accelerations that exceeded the acceptable ORA limit occurred due to floorboard buckling during the test. Test no. AGTB-1 was determined to be unacceptable according to the MASH TL-3 safety performance criteria for test designation no. 3-21.

2.1.6.2 Test No. AGTB-2

Test no. AGTB-2 was conducted under the same impact conditions as test no. AGTB-1, but with slight changes to the geometry of the rigid buttress. The height and lateral offset of the buttress lower chamfer were increased and the slope of the chamfer was decreased from 3:1 to 4:1 to reduce the amount of vehicle tire snag on the buttress. The 4,998-lb (2,267-kg) pickup truck impacted the AGT system at a speed of 62.7 mph (100.8 km/h) and at an angle of 25.4 degrees. The impact location was 86 in. (2.2 m) upstream from the upstream end of the concrete parapet. The barrier system successfully contained and redirected the vehicle with a maximum lateral dynamic deflection of 5.4 in. (136 mm) located at post no. 19. Damage to the test installation was minimal, primarily consisting of contact marks and minor guardrail deformation. The test installation met all occupant risk criteria and test no. AGTB-2 was determined to be acceptable according to the MASH TL-3 safety performance criteria for test designation no. 3-21.

Table 7. Summary of Crash Test Data for Standardized Transition Buttress

Test Number	Test Desig.	Test Vehicle lb (kg)	Impact Speed mph (km/h)	Impact Angle degrees	OIV ft/s (m/s)		ORA g's		Dynamic Defl. in. (mm)	Pass/Fail
					Long.	Lateral	Long.	Lateral		
AGTB-1	3-21	5,039 (2,286)	61.9 (99.6)	24.4	-22.70 (-6.92)	27.68 (8.44)	-30.03	9.96	6.0 (152)	Fail
AGTB-2	3-21	4,998 (2,267)	62.7 (100.8)	25.4	-20.28 (-6.18)	-24.61 (-7.50)	-7.06	-10.40	5.4 (136)	Pass

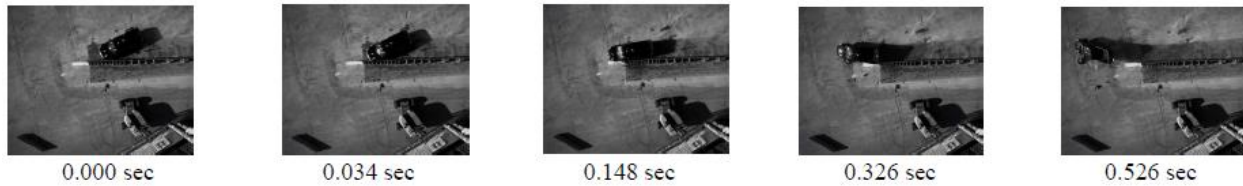


Figure 19. Sequential Photographs for Test No. AGTB-1 [1]

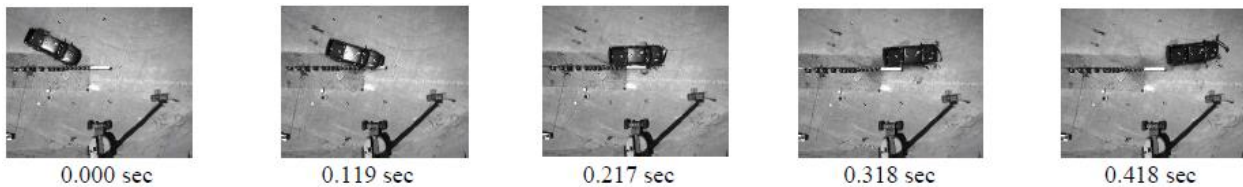


Figure 20. Sequential Photographs for Test No. AGTB-2 [1]

2.1.7 34-in. (864-mm) AGT Buttress

In 2019, MwRSF completed a research project to develop a MASH TL-3 compliant AGT with a 34-in. (864-mm) tall standardized concrete buttress [13]. The AGT test installation in test nos. 34AGT-1 and 34AGT-2 was 87 ft – 11¼ in. (26.8 m) long and consisted of 19 guardrail posts, which supported the 12-gauge (2.7-mm) W-beam and nested 12-gauge (2.7-mm) thrie-beam guardrail sections. The nested thrie-beam guardrail was attached to the traffic face of an 84-in. (2,134-mm) long x 39-in. (991-mm) tall vertical concrete buttress with a 10-gauge (3.4-mm) thrie-beam terminal connector. The W-beam guardrail was installed with a top mounting height of 31 in. (787 mm), which transitioned to a top mounting height of 34 in. (864 mm) over the 10-gauge (3.4-mm) symmetrical W-to-thrie transition section. The remaining length of thrie-beam guardrail maintained a 34 in. (864 mm) top mounting height. The W6x15 steel posts within the transition region, post nos. 17 through 19, were spaced 37½ in. (953 mm) on center and were embedded at a depth of 52 in. (1,321 mm). The test installation layout is shown in Figure 21 and the crash test data for test nos. 34AGT-1 and 34AGT-2 is summarized in Table 8. Sequential photographs are presented in Figures 22 and 23.

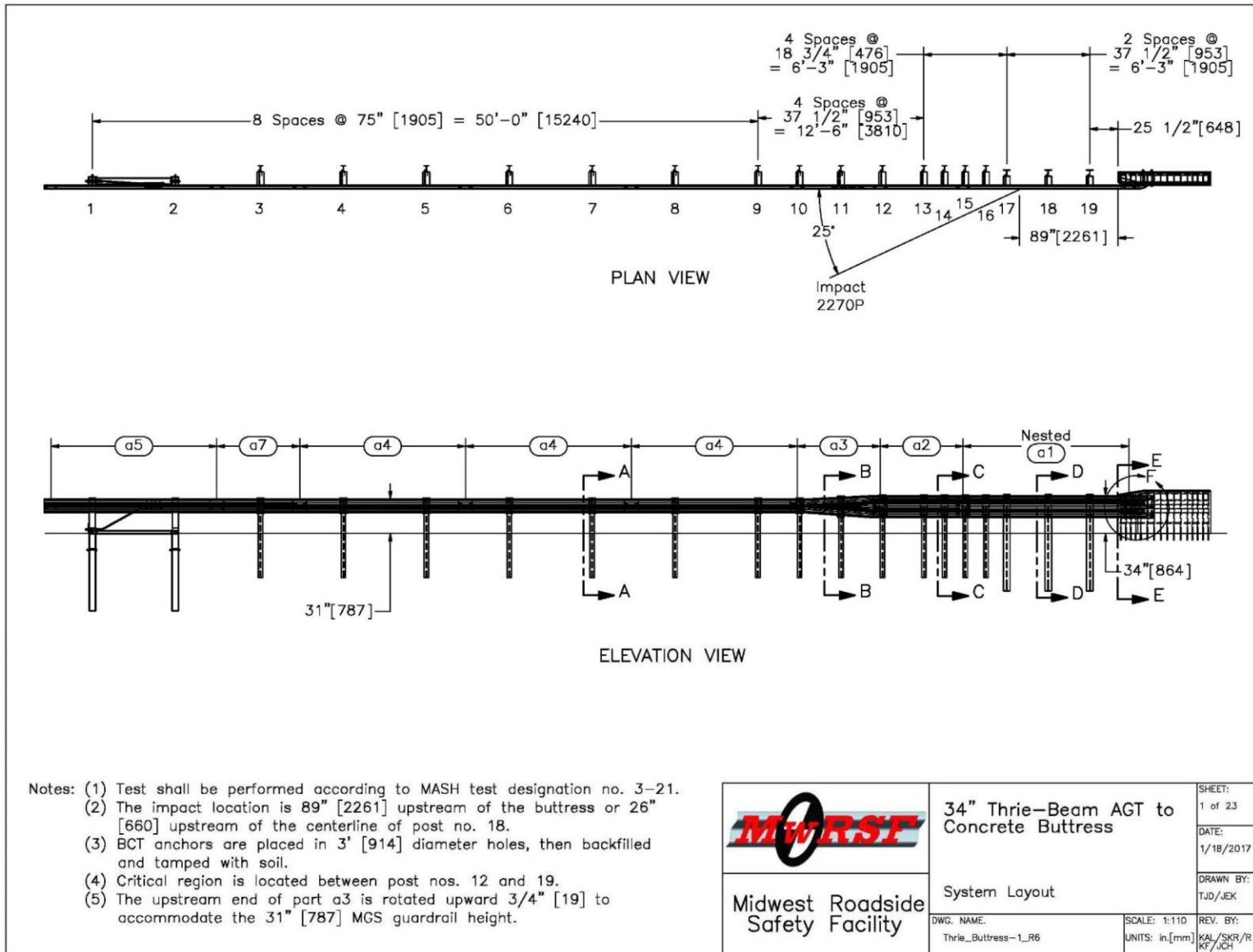


Figure 21. 34-in. (864-mm) AGT Buttress Test Installation Layout [13]

2.1.7.1 Test No. 34AGT-1

The 5,024-lb (2,279-kg) pickup truck impacted the AGT system at a speed of 62.2 mph (100.1 km/h) and at an angle of 24.8 degrees. The impact occurred 90½ in. (2.3 m) upstream from the upstream end of the concrete buttress. The barrier system successfully contained and redirected the vehicle with a maximum lateral dynamic deflection of 7.8 in. (198 mm) located at post no. 19. Damage to the test installation was moderate, primarily consisting of rail and post deformation, contact marks, concrete gouging, and concrete cracking. The test installation met all occupant risk criteria and test no. 34AGT-1 was determined to be acceptable according to the MASH TL-3 safety performance criteria for test designation no. 3-21.

2.1.7.2 Test No. 34AGT-2

In test no. 34AGT-2, the 2,420-lb (1,098-kg) small car impacted the AGT system at a speed of 62.1 mph (99.9 km/h) and at an angle of 25.5 degrees. The impact location was 65 in. (1.7 m) upstream from the upstream end of the concrete buttress. The barrier system successfully contained and redirected the vehicle with a maximum lateral dynamic deflection of 2.7 in. (69 mm) located at post no. 19. Damage to the test installation was minimal, and primarily consisted of rail and post deformation, contact marks, and concrete gouging. The test installation met all occupant risk criteria and test no. 34AGT-2 was determined to be acceptable according to the MASH TL-3 criteria for test designation no. 3-20.

Table 8. Summary of Crash Test Data for 34-in. (864-mm) AGT Buttress

Test Number	Test Desig.	Test Vehicle lb (kg)	Impact Speed mph (km/h)	Impact Angle degrees	OIV ft/s (m/s)		ORA g's		Dynamic Defl. in. (mm)	Pass/Fail
					Long.	Lateral	Long.	Lateral		
34AGT-1	3-21	5,024 (2,279)	62.2 (100.1)	24.8	-20.18 (-6.15)	25.92 (7.90)	-10.77	8.85	7.8 (198)	Pass
34AGT-2	3-20	2,420 (1,098)	62.1 (99.9)	25.5	-22.65 (-6.90)	32.71 (9.97)	-10.84	14.70	2.7 (69)	Pass

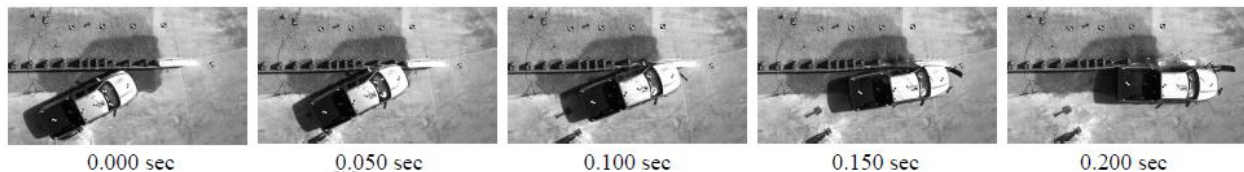


Figure 22. Sequential Photographs for Test No. 34AGT-1 [13]

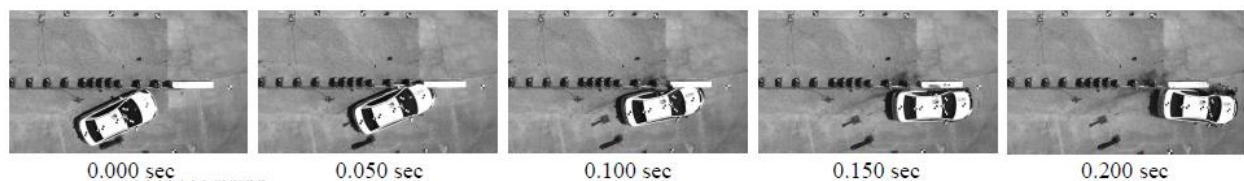


Figure 23. Sequential Photographs for Test No. 34AGT-2 [13]

2.1.8 MGS Stiffness Transition

In 2010, MwRSF conducted a research project to develop a MASH TL-3 compliant AGT that connects to the MGS [14]. Test nos. MWTSP-1 through MWTSP-3 were conducted to evaluate the upstream end of a stiffness transition for the propensity of vehicle pocketing and wheel snag. The test installation for test nos. MWTSP-1 through MWTSP-3 was 87 ft – 6 in. (26.7 m) long and consisted of five major structural components as shown in Figure 24: (1) standard 12-gauge (2.66-mm) W-beam rail attached to a simulated anchorage device, (2) asymmetrical 10-gauge (3.42-mm) W-to-thrie transition element, (3) standard 12-gauge (2.66-mm) thrie-beam guardrail, (4) nested 12-gauge (2.66-mm) thrie-beam guardrail, and (5) a thrie-beam-and-channel bridge railing system. All guardrail had a top mounting height of 31 in. (787 mm). Post nos. nos. 1 and 2 were timber posts in steel foundation tubes, and functioned as part of an anchorage system used to develop the required tensile capacity of a tangent guardrail terminal. Post nos. 3 through 15 were W6x9 steel posts embedded 40 in. (1,016 mm) and post nos. 16 through 18 were W6x15 steel posts embedded 55½ in. (1,400 mm). Bridge post nos. 19 through 21 were W6x20 steel posts rigidly attached to the concrete tarmac. The crash test data for test nos. MWTSP-1 through MWTSP-3 is summarized in Table 9 and sequential photographs are presented in Figures 25 through 27.

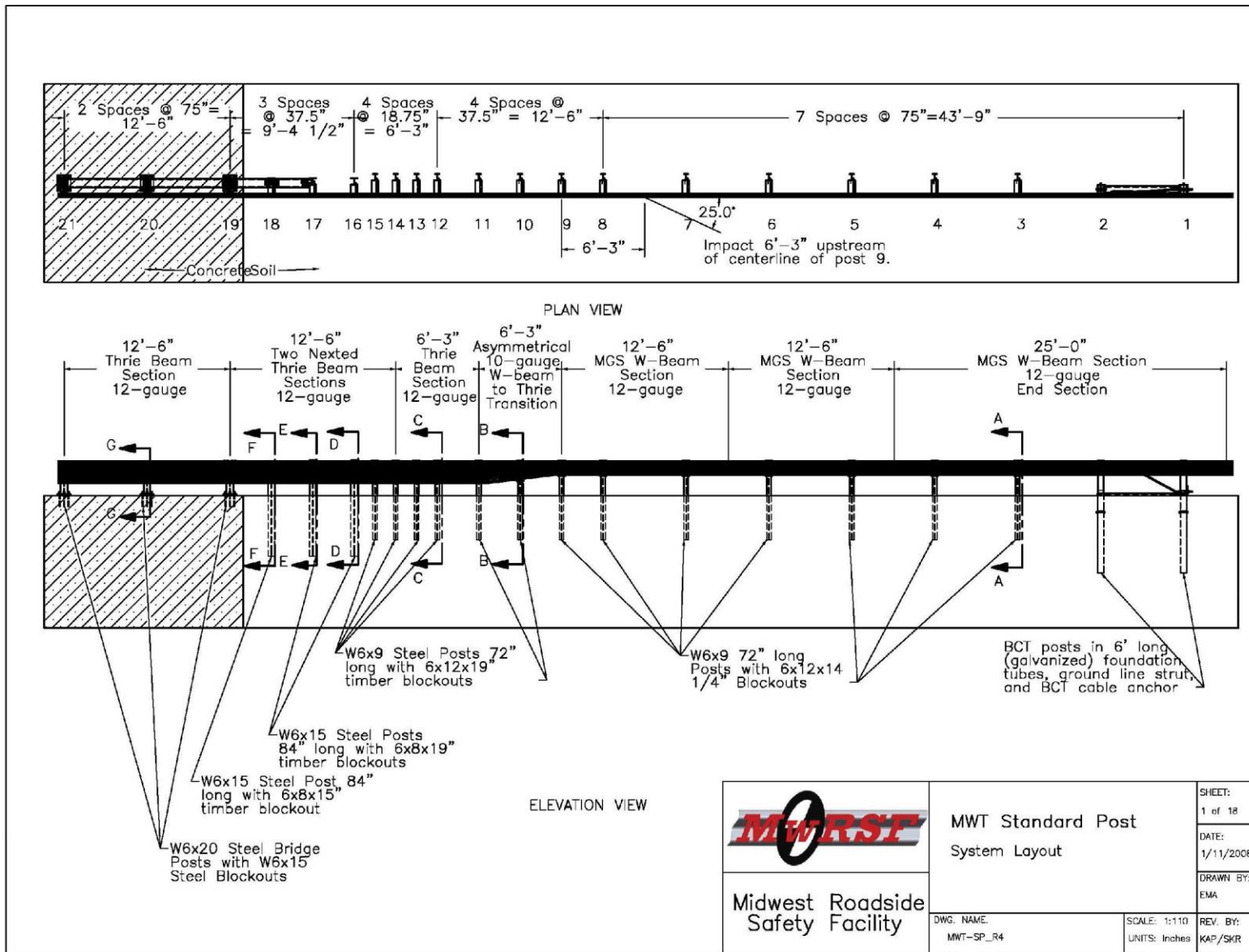


Figure 24. MGS Stiffness Transition Test Installation Layout [14]

2.1.8.1 Test no. MWTSP-1

The 5,009-lb (2,272-kg) pickup truck impacted the upstream end of the stiffness transition at a speed of 61.5 mph (99.0 km/h) and at an angle of 24.7 degrees. The impact location was 71 in. (1,803 mm) upstream from post no. 9. The test installation successfully contained the vehicle, but it enabled the vehicle to pocket and failed to redirect the vehicle. Damage to the system was moderate and primarily consisted of rail and post deformations, fractured wooden posts and blockouts, and contact marks. During the test, post no. 1 fractured prematurely due to material defects, which prevented the anchorage from developing its full capacity and enabled the vehicle to pocket. As a result, test no. MWTSP-1 failed to meet the occupant risk criteria and was determined to be unacceptable according to the MASH TL-3 safety performance criteria for test designation no. 3-21.

2.1.8.2 Test no. MWTSP-2

Test no. MWTSP-2 was conducted to retest the system tested in test no. MWTSP-1 under the same impact conditions, but with a wooden anchor post free from defects. The 4,993-lb (2,265-kg) pickup truck impacted the upstream end of the stiffness transition at a speed of 61.2 mph (98.5 km/h) and at an angle of 26.3 degrees. The impact occurred 74½ in. (1,892 mm) upstream from post no. 9. The AGT safely contained and redirected the vehicle with a maximum dynamic deflection of 32.8 in. (833 mm) at post no. 11. Damage to the test installation was moderate and primarily consisted of rail and post deformations, contact marks, and fractured wooden blockouts. Test no. MWTSP-2 met all occupant risk criteria and was determined to be acceptable according to the MASH TL-3 safety performance criteria for test designation no. 3-21.

2.1.8.3 Test no. MWTSP-3

The 2,394-lb (1,086-kg) small car impacted the upstream end of the stiffness transition at a speed of 61.0 mph (98.2 km/h) and at an angle of 25.7 degrees. The impact location was 93¾ in. (2.4 m) upstream from post no. 9. The test installation successfully contained the vehicle with a maximum dynamic deflection of 18.5 in. (470 mm) at post no. 11. Damage to the barrier was moderate and consisted of deformed guardrail and posts, fractured wooden blockouts, and contact marks on the guardrail. Wheel snag on the guardrail posts occurred during the impact, but test no. MWTSP-3 satisfied all occupant risk criteria and was determined to be acceptable according to the MASH TL-3 safety performance criteria for test designation no. 3-20.

Table 9. Summary of Crash Test Data for MGS Stiffness Transition

Test Number	Test Desig.	Test Vehicle lb (kg)	Impact Speed mph (km/h)	Impact Angle degrees	OIV ft/s (m/s)		ORA g's		Dynamic Defl. in. (mm)	Pass/Fail
					Long.	Lateral	Long.	Lateral		
MWTSP-1	3-21	5,009 (2,272)	61.5 (99.0)	24.7	-18.62 (-5.68)	-16.49 (-5.03)	-24.82	-7.01	47.2 (1,199)	Fail
MWTSP-2	3-21	4,993 (2,265)	61.2 (98.5)	26.3	-21.21 (-6.46)	-16.91 (-5.15)	-12.03	-9.87	32.8 (833)	Pass
MWTSP-3	3-20	2,394 (1,086)	61.0 (98.2)	25.7	-25.62 (-7.81)	-18.61 (-5.67)	-13.70	-6.74	18.5 (470)	Pass

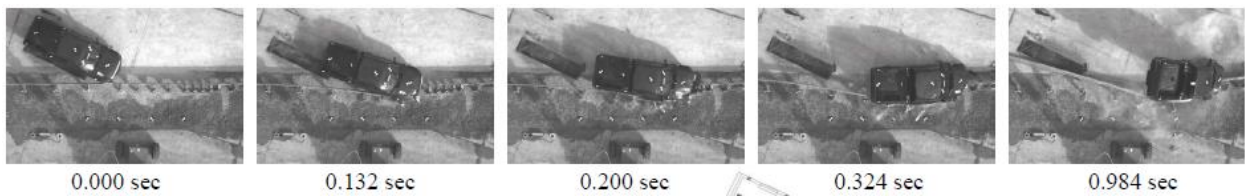


Figure 25. Sequential Photographs for Test No. MWTSP-1 [14]

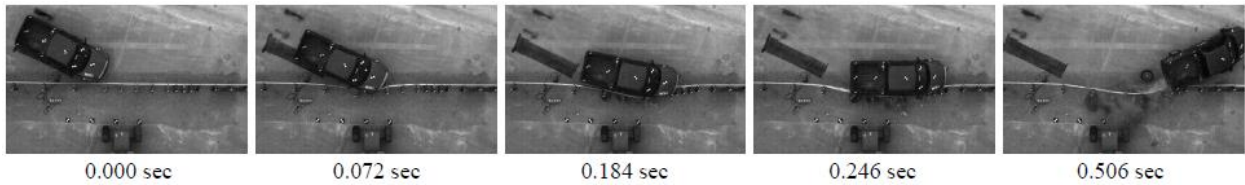


Figure 26. Sequential Photographs for Test No. MWTSP-2 [14]

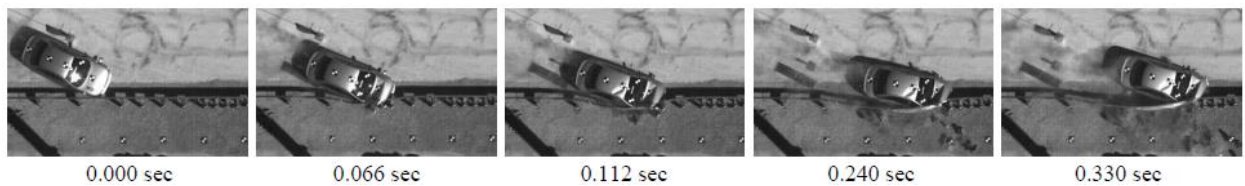


Figure 27. Sequential Photographs for Test No. MWTSP-3 [14]

2.1.9 MGS Stiffness Transition with Curb

In 2014, MwRSF conducted a research project to develop a MASH TL-3 compliant AGT that connects to the MGS and incorporates a 4-in. (102-mm) tall concrete curb [15]. Test nos. MWTC-1 through MWTC-3 were conducted to evaluate the propensity of vehicle pocketing and wheel snag at the upstream end of the stiffness transition. The test installation was 87 ft – 6 in. (26.7 m) long and consisted of five major structural components as shown in Figure 28: (1) standard 12-gauge (2.66-mm) W-beam rail attached to a simulated anchorage device, (2) asymmetrical 10-gauge (3.42-mm) W-to-thrie transition element, (3) standard 12-gauge (2.66-mm) thrie-beam guardrail, (4) nested 12-gauge (2.66-mm) thrie-beam guardrail, and (5) a thrie-beam-and-channel bridge railing system. All guardrail had a top mounting height of 31 in. (787 mm). Post nos. nos. 1 and 2 were BCT posts in steel foundation tubes, and functioned as part of an anchorage system. Post nos. 3 through 15 were W6x8.5 steel posts embedded 40 in. (1,016 mm) and post nos. 16 through 18 were W6x15 steel posts embedded 55 $\frac{1}{8}$ in. (1,400 mm). Bridge post nos. 19 through 21 were W6x20 steel posts rigidly attached to the concrete tarmac. The crash test data for test nos. MWTC-1 through MWTC-3 is summarized in Table 10 and sequential photographs are presented in Figures 29 through 31.

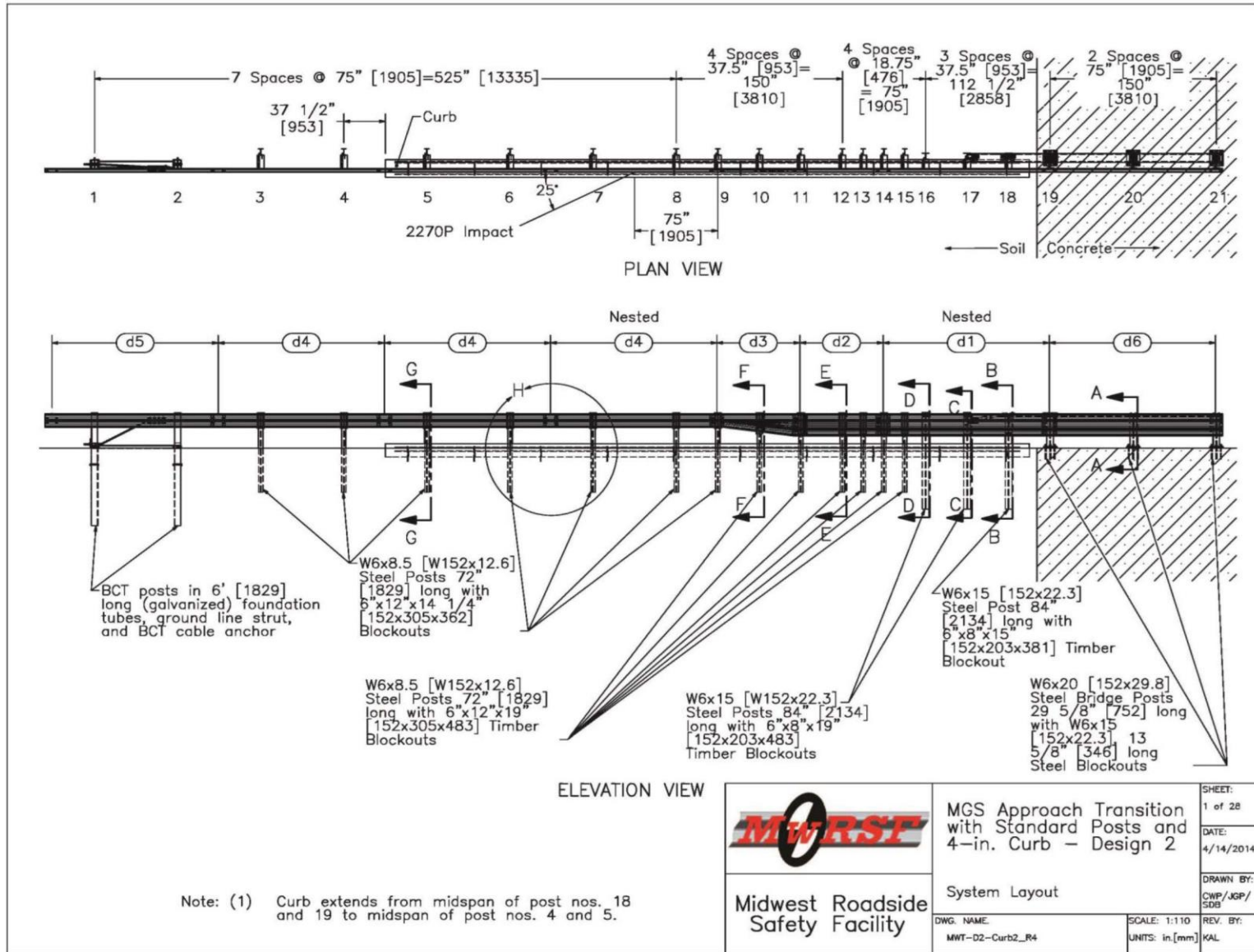


Figure 28. MGS Stiffness Transition with Curb Test Installation Layout [15]

2.1.9.1 Test no. MWTC-1

The 2,457-lb (1,114-kg) small car impacted the upstream end of the stiffness transition at a speed of 62.9 mph (101.2 km/h) and at an angle of 25.0 degrees. The impact location was 14¾ in. (375 mm) downstream from post no. 7. The test installation failed to redirect the test vehicle and experienced severe damage. Damage to the system consisted of deformed rail and posts, fractured wooden blockouts, contact marks, and ruptured W-beam rail. During the test, the small car penetrated under the W-beam rail, which resulted in rail rupture and severe vehicle snag on the barrier. Test no. MWTC-1 exceeded the acceptable longitudinal ORA values and was determined to be unacceptable according to the MASH TL-3 safety performance criteria for test designation no. 3-20.

2.1.9.2 Test no. MWTC-2

Following the failure of test no. MWTC-1, an additional W-beam rail section was nested with the existing W-beam section upstream of the W-to-thrie transition section to reinforce the area that experienced rail rupture. Test no. MWTC-2 was conducted to retest the AGT test installation with the addition of a 12 ft – 6 in. (3.8-m) long nested W-beam section prior to the W-to-thrie transition segment. In test no. MWTC-2, the 2,410-lb (1,093-kg) small car impacted the upstream end of the stiffness transition at a speed of 61.3 mph (98.7 km/h) and at an angle of 25.6 degrees. The impact occurred 11¼ in. (286 mm) downstream from post no. 7. The test installation adequately contained the test vehicle with a maximum dynamic deflection of 14.4 in. (366 mm) at post no. 9. Damage to the barrier was moderate, consisting of deformed rail and posts, fractured wooden blockouts, and contact marks. Test no. MWTC-2 satisfied all occupant risk criteria and was determined to be acceptable according to the MASH TL-3 safety performance criteria for test designation no. 3-20.

2.1.9.3 Test no. MWTC-3

The 4,969-lb (2,254-kg) pickup truck impacted the upstream end of the stiffness transition at a speed of 61.0 mph (98.2 km/h) and at an angle of 24.4 degrees. The impact location was 75 in. (1,905 mm) upstream from post no. 9. The test installation adequately contained and redirected the test vehicle with a maximum dynamic deflection of 23.9 in. (607 mm). Damage to the barrier was moderate and consisted of deformed rail and steel posts, fractured wooden posts, gouged wooden blockouts, and contact marks. Test no. MWTC-3 satisfied all occupant risk criteria and was determined to be acceptable according to the MASH TL-3 safety performance criteria for test designation no. 3-21.

Table 10. Summary of Crash Test Data for MGS Stiffness Transition with Curb

Test Number	Test Desig.	Test Vehicle lb (kg)	Impact Speed mph (km/h)	Impact Angle degrees	OIV ft/s (m/s)		ORA g's		Dynamic Defl. in. (mm)	Pass/Fail
					Long.	Lateral	Long.	Lateral		
MWTC-1	3-20	2,457 (1,114)	62.9 (101.2)	25.0	-32.56 (-9.92)	17.59 (5.36)	-22.25	-8.51	N/A	Fail
MWTC-2	3-20	2,410 (1,093)	61.3 (98.7)	25.6	-23.04 (-7.02)	24.14 (7.36)	-16.58	12.45	14.4 (366)	Pass
MWTC-3	3-21	4,969 (2,254)	61.0 (98.1)	24.4	-17.46 (-5.32)	17.79 (5.42)	-12.29	9.18	23.9 (607)	Pass

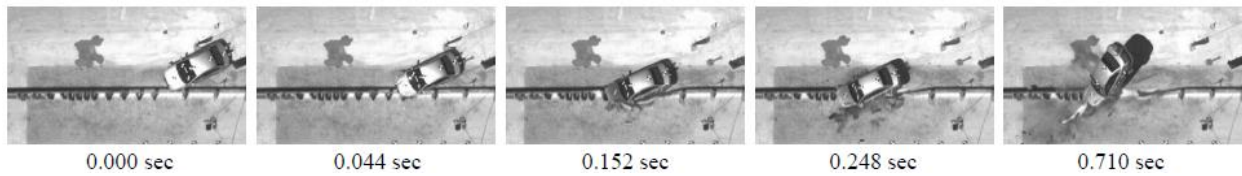


Figure 29. Sequential Photographs for Test No. MWTC-1 [15]



Figure 30. Sequential Photographs for Test No. MWTC-2 [15]

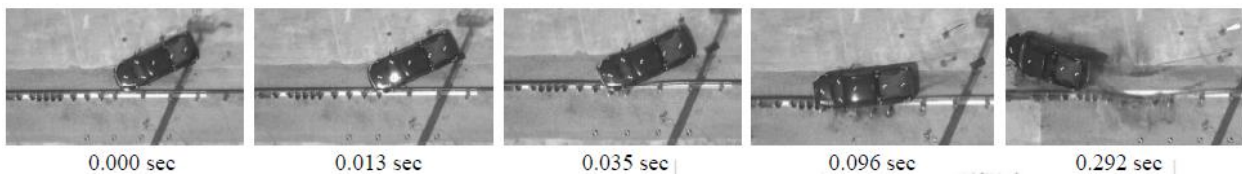
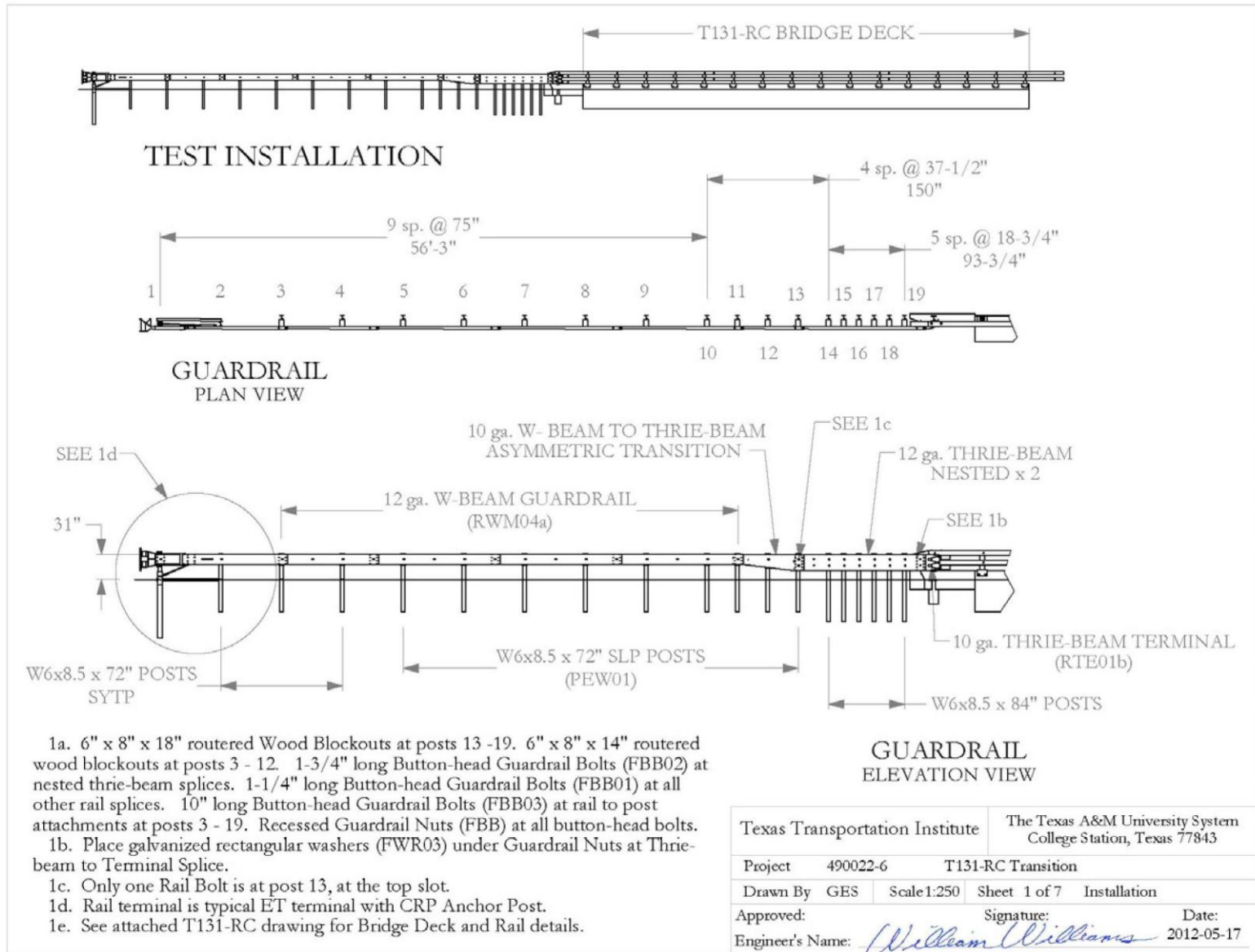


Figure 31. Sequential Photographs for Test No. MWTC-3 [15]

2.1.10 TXDOT T131RC Bridge Rail Transition

In 2013, TTI designed and crash tested an AGT design for the Texas Department of Transportation (TxDOT) T131RC bridge rail according to MASH TL-3 safety performance criteria [16]. The test installation for test nos. 490022-6 and 490022-8 was 79 ft – 6¾ in. (24.3 m) long and was constructed with 19 guardrail posts, which supported the 12-gauge (2.7-mm) W-beam and 12-gauge (2.7-mm) nested thrie-beam guardrail sections. All guardrail sections had a top mounting height of 31 in. (787 mm). Post nos. 14 through 19 supported the nested thrie-beam section of guardrail and were W6x8.5 steel posts spaced at 18¾ in. (476 mm) on center with an embedment depth of 53 in. (1,346 mm). The downstream end of the AGT was attached to a T131RC bridge rail that was anchored on top of a 12-in. (305-mm) wide x 11-in. (279-mm) tall concrete curb. The test installation layout is shown in Figure 32 and the crash test data for test nos. 490022-6 and 490022-8 is summarized in Table 11. Sequential photographs are presented in Figures 33 and 34.



T:\2011-2012\490022 TXDOT\6&8 T131RC Transition\Drafting\2012-05-17 rev\490022-6 Drawing

Figure 32. TXDOT T131RC Bridge Rail Transition Test Installation Layout [16]

2.1.10.1 Test No. 490022-6

The 2,423-lb (1,099-kg) small car impacted the AGT test installation at a speed of 61.5 mph (99.0 km/h) and at an angle of 25.6 degrees. The impact occurred 31.6 in. (803 mm) upstream from the upstream end of the concrete curb. The test installation adequately contained and redirected the test vehicle with a maximum dynamic deflection of 7.4 in. (188 mm). Damage to the test installation was minimal, consisting of contact marks, concrete curb cracking, and rail deformation. Test no. 490022-6 met all occupant risk criteria and was determined to be acceptable according to the MASH TL-3 safety performance criteria for test designation no. 3-20.

2.1.10.2 Test No. 490022-8

The 5,015-lb (2,275-kg) pickup truck impacted the AGT test installation at a speed of 62.7 mph (100.9 km/h) and at an angle of 25.1 degrees. The impact location was 57½ in. (1,461 mm) upstream from the upstream end of the concrete curb. The test article contained and redirected the test vehicle with a maximum dynamic deflection of 8.4 in. (213 mm). Damage to the test installation was moderate and included post and rail deformation, concrete curb cracking, and contact marks. Test no. 490022-8 satisfied all occupant risk criteria and was determined to be acceptable according to the MASH TL-3 safety performance criteria for test designation no. 3-21.

Table 11. Summary of Crash Test Data for TXDOT T131RC Bridge Rail Transition

Test Number	Test Desig.	Test Vehicle lb (kg)	Impact Speed mph (km/h)	Impact Angle degrees	OIV ft/s (m/s)		ORA g's		Dynamic Defl. in. (mm)	Pass/Fail
					Long.	Lateral	Long.	Lateral		
490022-6	3-20	2,423 (1,099)	61.5 (99.0)	25.6	21.0 (6.4)	27.6 (8.4)	6.1	6.3	7.4 (188)	Pass
490022-8	3-21	5,015 (2,275)	62.7 (100.9)	25.1	18.4 (5.6)	23.6 (7.2)	6.6	9.4	8.4 (213)	Pass



Figure 33. Sequential Photographs for Test No. 490022-6 [16]



Figure 34. Sequential Photographs for Test No. 490022-8 [16]

2.1.11 Florida Transition

In 1989, TTI crash tested and evaluated the performance of an AGT connected to a bridge traffic rail wing post [17]. The test no. 0385-1 installation overall length was 62-ft 6-in. (19.1 m) and incorporated a parabolic curve over the upstream 37-ft 6-in. (11.4 m) of the test installation as well as a 33.33:1 flare rate initiated at the downstream end of the transition. The test installation was constructed of 16 6-in. x 8-in. (152-mm x 203-mm) timber posts with blockouts, which supported the W-beam guardrail. The six farthest downstream posts had a post spacing of 18¾ in. (476 mm) on center and were embedded at a depth of 50 in. (1,270 mm). The downstream end of the AGT test installation was anchored to a 32-in. (813-mm) tall rigid concrete wing post barrier. The test installation is shown in Figure 35. The crash test data for test no. 0385-1 is summarized in Table 12 and sequential photographs are presented in Figure 36.

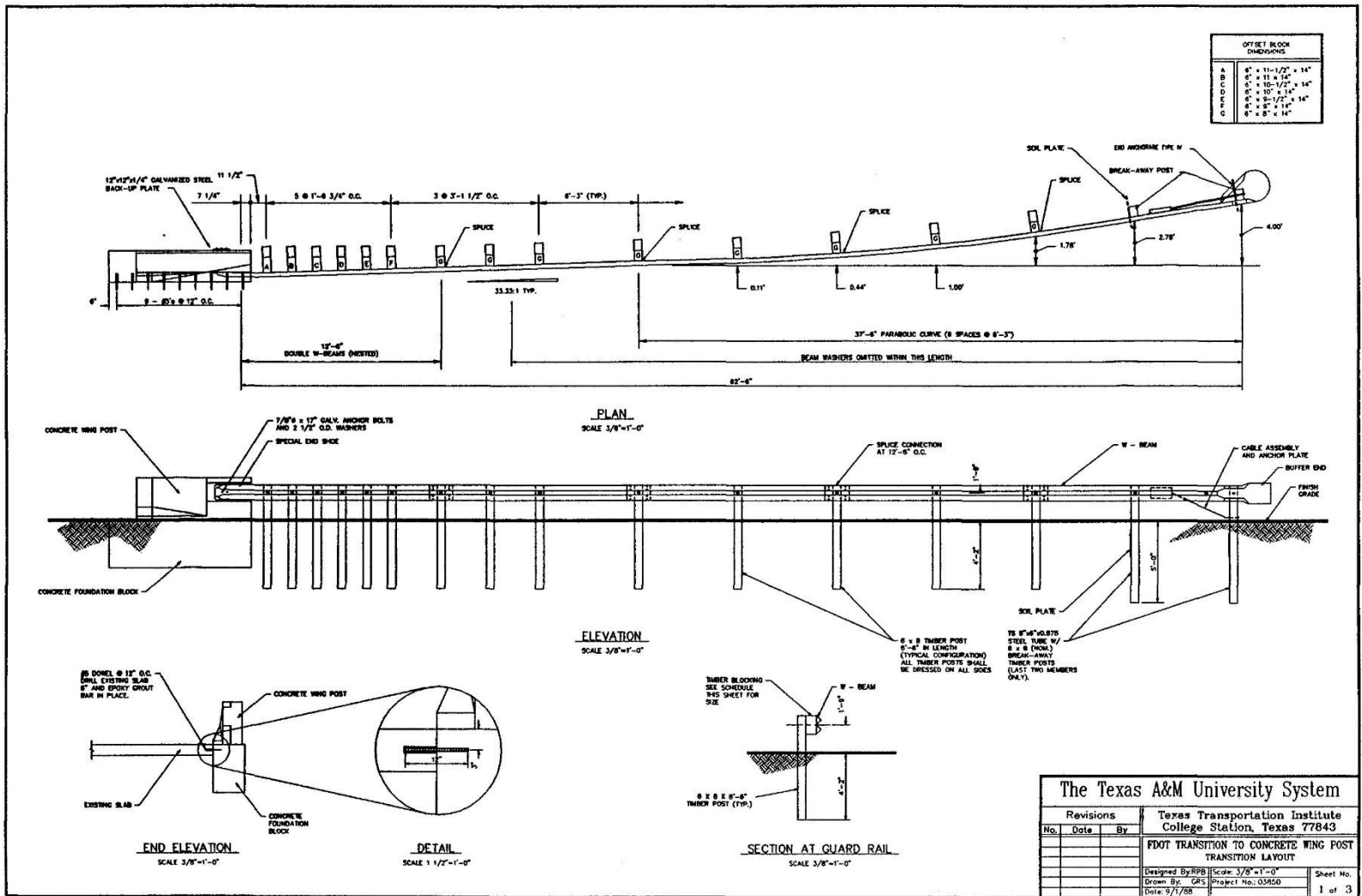


Figure 35. Florida Transition Test Installation Layout [17]

In test no. 0385-1, the 4,500-lb (2,041-kg) passenger car impacted the AGT test installation at a speed of 63.0 mph (101.4 km/h) and at an angle of 24.0 degrees. The impact location was 108 in. (2.7 m) upstream from the upstream end of the rigid concrete wing post barrier. The test installation successfully contained and redirected the test vehicle with a maximum dynamic deflection of 6.0 in. (152 mm). The test installation had minimal damage following the test, which consisted of rail deformation and contact marks. The ORA values were -7.1 g (longitudinal) and 34.8 g (lateral), and were noted as “not applicable” for the test under the safety criteria in NCHRP Report 230. Test no. 0385-1 was determined to satisfy the occupant risk criteria and was judged to be in compliance with the safety performance criteria set forth in NCHRP Report 230 Test 30.

Table 12. Summary of Crash Test Data for Florida Transition

Test Number	Test Desig.	Test Vehicle lb (kg)	Impact Speed mph (km/h)	Impact Angle degrees	OIV ft/s (m/s)		ORA g's		Dynamic Defl. in. (mm)	Pass/Fail
					Long.	Lateral	Long.	Lateral		
0385-1	30	4,500 (2,041)	63.0 (101.4)	24.0	30.1 (9.2)	-26.2 (-8.0)	-7.1	34.8	6.0 (152)	Pass

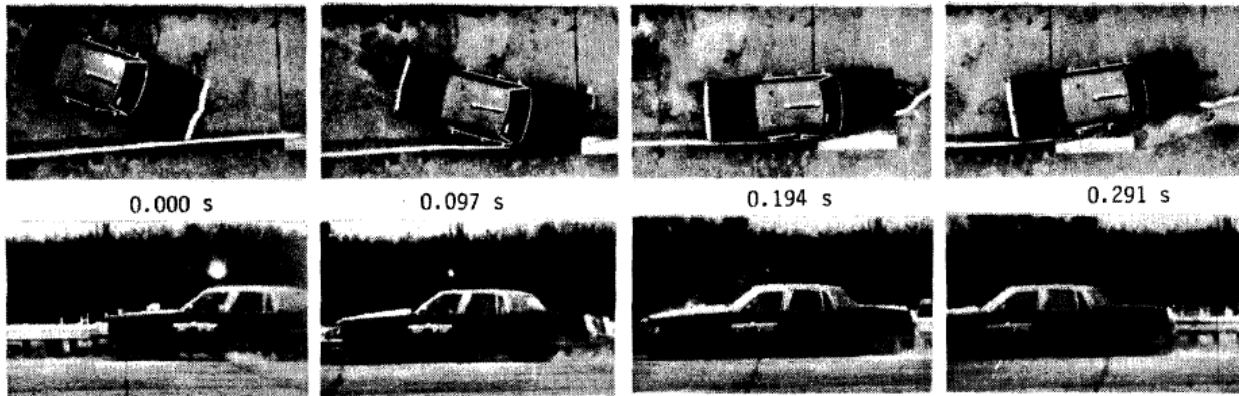


Figure 36. Sequential Photographs for Test No. 0385-1 [17]

2.1.12 TTI Stacked W-Beam

In 2016, TTI investigated the crashworthiness of a stacked W-beam AGT design for use with a 31-in. (787-mm) guardrail system [18]. The test no. 604581-1 AGT test installation had an overall length of 100 ft – 8 in. (30.7 m). The barrier system was constructed with 18 guardrail posts, which supported the 12-gauge (2.7-mm) W-beam guardrail and nested 12-gauge (2.7-mm) W-beam rubrail. The W-beam guardrail was installed with a top rail height of 31 in. (787 mm). The W-beam rubrail spanned from post nos. 13 to 18 and was installed below the W-beam guardrail with a centerline rail height of 10⁷/₈ in. (276 mm). Post nos. 3 through 16 and post nos. 17 and 18 were W6x8.5 and W8x13 steel posts, respectively. Post nos. 2 through 11, post nos. 11 through 15, and post nos. 15 through 18 were spaced at 75 in. (1,905 mm), 37¹/₂ in. (953 mm), and 18³/₄ in. (476 mm), respectively. The downstream end of the test installation was anchored to a 32-in. (813-mm) tall F-shape concrete parapet. The test installation is shown in Figure 37.

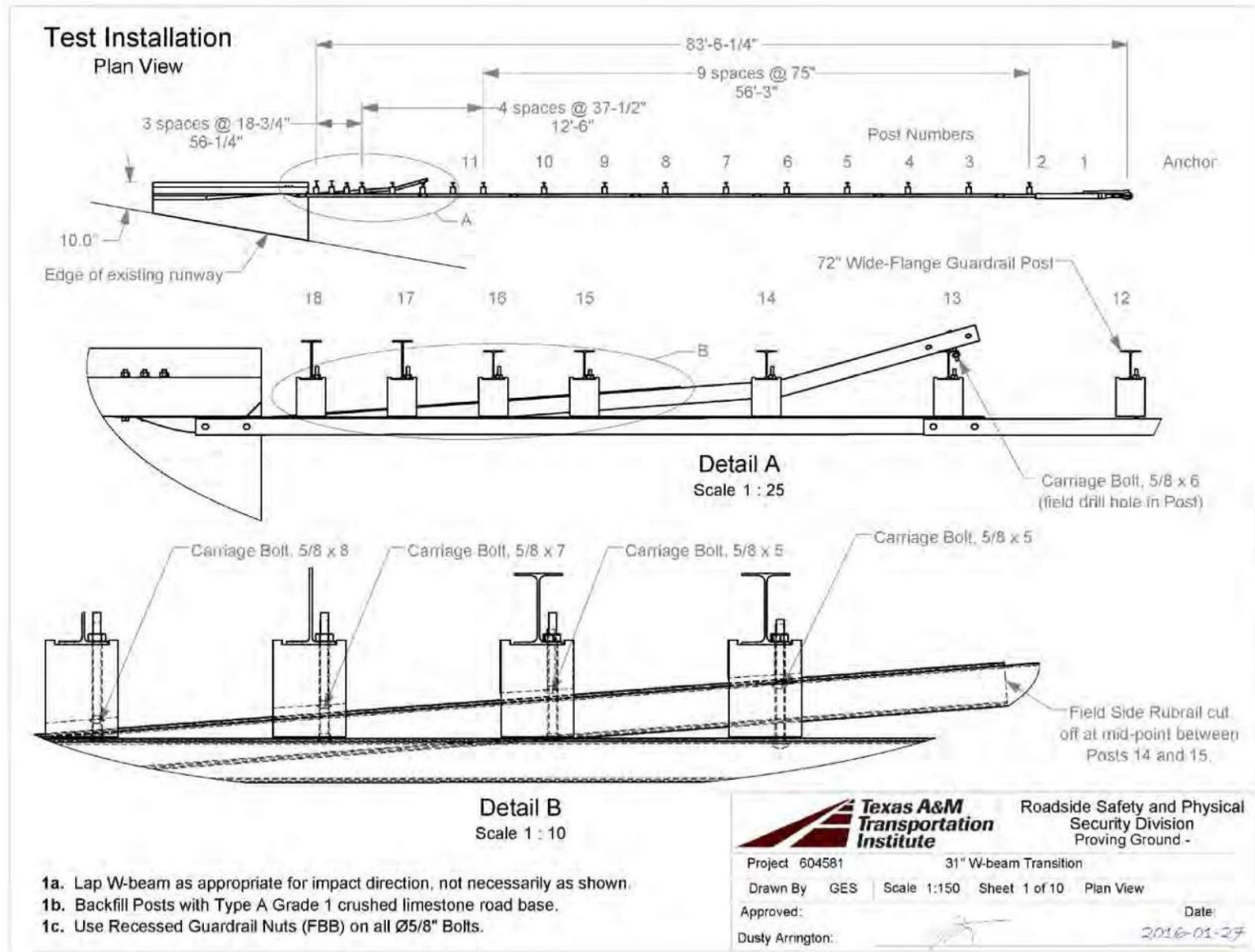


Figure 37. TTI Stacked W-Beam Test Installation Layout [18]

In test no. 604581-1, the 5,005-lb (2,270-kg) pickup truck impacted the AGT test installation at a speed of 64.0 mph (103.0 km/h) and at an angle of 25.0 degrees. The impact location was 76 in. (1.9 m) upstream from the upstream end of the concrete parapet. The test installation successfully contained and redirected the test vehicle with a maximum dynamic deflection of 4.0 in. (102 mm). The AGT test installation experienced minimal damage, which included post and guardrail deformations and contact marks. After exiting the barrier system, the test vehicle rolled onto its right side and came to rest. Test no. 604581-1 satisfied the occupant risk values but was determined to be unacceptable according to the MASH TL-3 safety criteria for test designation no. 3-21 due to vehicle rollover. The crash test data for test no. 604581-1 is summarized in Table 13 and sequential photographs are presented in Figure 38.

Table 13. Summary of Crash Test Data for TTI Stacked W-Beam

Test Number	Test Desig.	Test Vehicle lb (kg)	Impact Speed mph (km/h)	Impact Angle degrees	OIV ft/s (m/s)		ORA g's		Dynamic Defl. in. (mm)	Pass/Fail
					Long.	Lateral	Long.	Lateral		
604581-1	3-21	5,005 (2,270)	64.0 (103.0)	25.0	19.4 (5.9)	29.9 (9.1)	5.6	15.0	4.0 (102)	Fail



Figure 38. Sequential Photographs for Test No. 604581-1 [18]

2.2 Short Radius Guardrail System

Short radius guardrail systems are utilized when space constraints prevent the installation of a tangent guardrail system with the proper length, transition, and end treatment along the primary roadway. Short radius systems utilize a section of curved guardrail with runs of longitudinal guardrail along both the primary and secondary roadways. Oftentimes short radius guardrail systems are installed upstream from a rigid bridge rail and require a stiffness transition. In 2015, TTI developed and crash tested an optimized short radius guardrail design that transitioned to a rigid concrete parapet and incorporated a 4-degree flare away from the primary roadway [19].

Test nos. 467114-3 through 467114-7 were conducted to evaluate the crashworthiness of the optimized short radius guardrail design. The short radius test installation for test nos. 467114-3 through 467114-6 had a total length of 58 ft – 10 in. (17.9 m) with an 18-ft 9-in. (5.7-m) long section along the secondary road and a 27-ft 7¼-in. (8.4-m) long section along the primary

roadway. The length of guardrail along the primary roadway transitioned to a 32-in. (813-mm) tall vertical concrete parapet and incorporated a 4-degree flare away from the primary roadway. The guardrail sections were 12-gauge (2.7-mm) thrie-beam guardrail with a top rail height of 31 in. (787 mm) and were supported by 16 guardrail posts. Post nos. 1 through 7, 7 through 11, and 11 through 16 were spaced at 75 in. (1,905 mm), 37½ in. (953 mm), and 18¾ in. (476 mm), respectively. Post nos. 2 through 8 were modified timber posts and post nos. 9 through 16 were W6x8.5 steel posts. Along the primary roadway, post nos. 9 and 10 and post nos. 11 through 16 were embedded at depths of 40 in. (1,016 mm) and 52 in. (1,321 mm), respectively. An anchor cable spanned the curved guardrail section from post nos. 4 to 7 and four 700-lb (318-kg) sand barrels were placed behind the guardrail. The system was modified for test no. 467114-7 by adding an additional W6x8.5 steel post between post no. 10 and the concrete parapet. The test no. 467114-7 installation layout is shown in Figure 39. The crash test data for test nos. 467114-3 through 467114-7 is summarized in Table 14 and sequential photographs are presented in Figures 40 through 44.

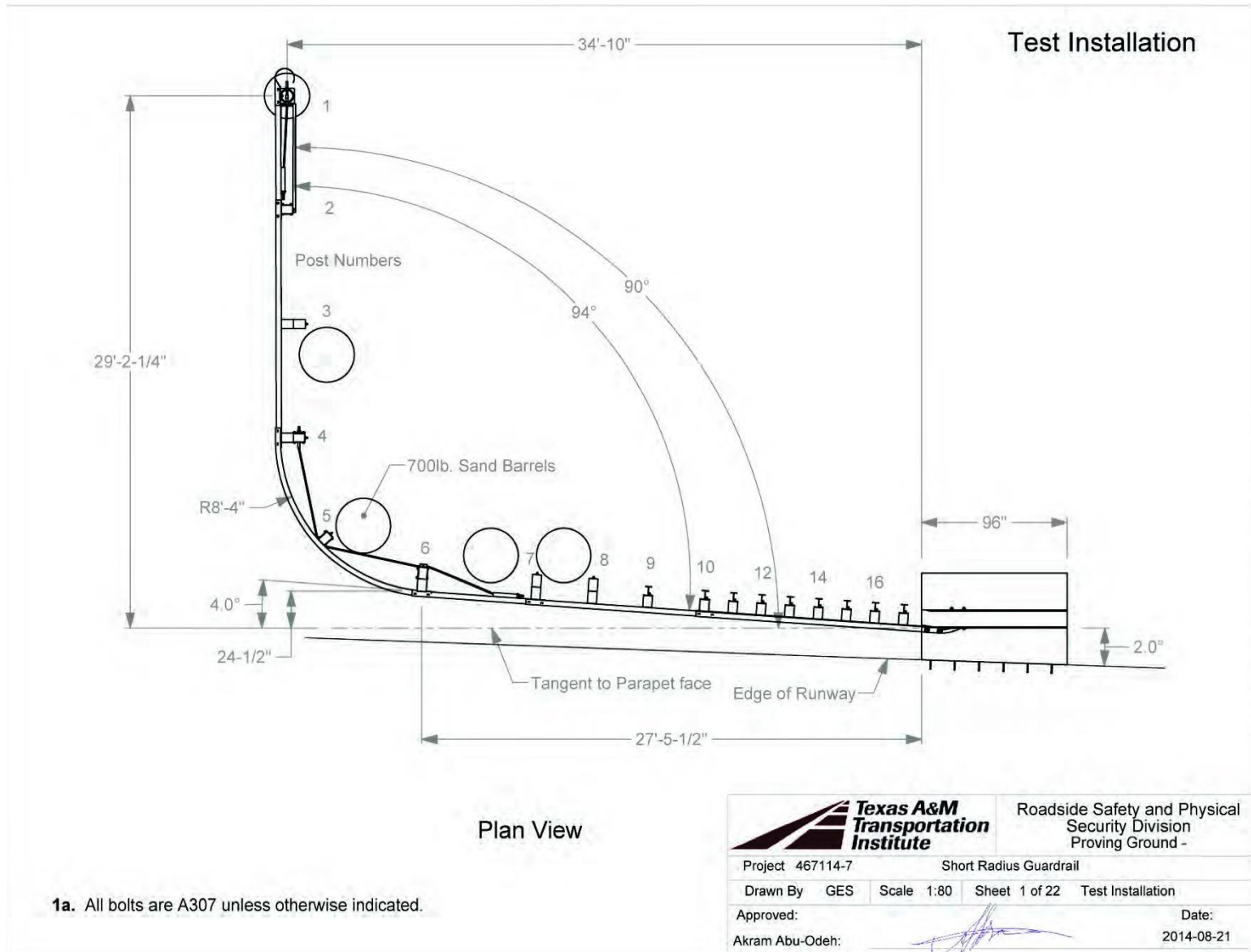


Figure 39. MASH TL-3 Short Radius Guardrail Test Installation – Test No. 467114-7 [19]

2.2.1.1 Test No. 467114-3

In test no 467114-3, the 5,041-lb (2,287-kg) pickup truck impacted the short radius test installation at a speed of 62.8 mph (101.1 km/h) and at an angle of 14.4 degrees, at the nose of the radius. The test installation successfully contained the test vehicle with a maximum dynamic deflection of 25 ft (7.6 m) relative to the primary roadway. Damage to the test installation was severe and consisted of fractured posts and deformed and torn guardrail. The test vehicle remained upright and all occupant risk criteria were met. Test no. 467114-3 was determined to be acceptable according to the MASH TL-3 safety performance criteria for test designation no. 3-33.

2.2.1.2 Test No. 467114-4

The 2,424-lb (1,100-kg) small car impacted the short radius test installation at a speed of 62.1 mph (99.9 km/h) and at an angle of 14.8 degrees, at the nose of the radius. The test installation successfully contained the test vehicle and brought it to a controlled stop with a maximum dynamic deflection of 16.3 ft (5.0 m) relative to the primary roadway. Damage to the test installation was moderate. The damage consisted of deflected and fractured posts and deformed guardrail. Test no. 467114-4 successfully met all occupant risk criteria and was determined to be acceptable according to the MASH TL-3 safety performance criteria for test designation no. 3-32.

2.2.1.3 Test No. 467114-5

The 5,023-lb (2,278-kg) pickup truck impacted the short radius test installation at a speed of 63.5 mph (102.2 km/h) and at an angle of 0.2 degrees, at the nose of the radius. The test installation successfully contained and redirected the test vehicle with a maximum dynamic deflection of 34.1 in. (866 mm). The test installation experienced moderate damage that included fractured and deflected posts, deformed guardrail, and contact marks. Test no. 467114-5 met all occupant risk criteria and was determined to be acceptable according to the MASH TL-3 safety performance criteria for test designation no. 3-31.

2.2.1.4 Test No. 467114-6

In test no. 467114-6, the 5,016-lb (2,275-kg) pickup truck impacted post no. 9 of the short radius test installation, which was approximately 193¼ in. (4.9 m) upstream from the upstream end of the concrete parapet. The impact occurred at a speed of 62.6 mph (100.7 km/h) and at an angle of 25.1 degrees. The test installation successfully contained and redirected the test vehicle with a maximum dynamic deflection of 21.1 in. (536 mm). Damage to the test installation was moderate. Damage consisted of deformed posts, deformed guardrail, and contact marks. After exiting the barrier system, the vehicle rolled three complete revolutions before coming to rest. Due to vehicle rollover, test no. 467114-6 was determined to be unacceptable according to the MASH TL-3 safety performance criteria for test designation no. 3-35.

2.2.1.5 Test No. 467114-7

Following the failure of test no. 467114-6, the test installation was modified to include an additional post between post no. 10 and the parapet. Test no. 467114-7 was conducted to re-evaluate MASH test designation no. 3-35. The 5,014-lb (2,274-kg) pickup truck impacted post no. 9 of the short radius test installation, which was approximately 177¾ in. (4.5 m) upstream from

the upstream end of the concrete parapet. The impact occurred at a speed of 64.5 mph (103.8 km/h) and at an angle of 25.2 degrees. The test installation adequately contained and redirected the test vehicle with a maximum dynamic deflection of 14.3 in. (363 mm). Damage to the test installation was moderate and included post and rail deformations. The vehicle remained upright during and after the test and successfully met all occupant risk criteria. Test no. 467114-7 was determined to be acceptable according to the MASH TL-3 safety performance criteria for test designation no. 3-35.

Table 14. Summary of Crash Test Data for MASH TL-3 Short Radius Guardrail

Test Number	Test Desig.	Test Vehicle lb (kg)	Impact Speed mph (km/h)	Impact Angle degrees	OIV ft/s (m/s)		ORA g's		Dynamic Defl. in (mm)	Pass/Fail
					Long.	Lateral	Long.	Lateral		
467114-3	3-33	5,041 (2,287)	62.8 (101.1)	14.4	28.5 (8.7)	5.9 (1.8)	8.2	10.0	300 (7,620)	Pass
467114-4	3-32	2,424 (1,100)	62.1 (99.9)	14.8	36.4 (11.1)	3.6 (1.1)	12.0	6.2	195.6 (4,968)	Pass
467114-5	3-31	5,023 (2,278)	63.5 (102.2)	0.2	9.2 (2.8)	10.5 (3.2)	5.4	4.5	34.1 (866)	Pass
467114-6	3-35	5,016 (2,275)	62.6 (100.7)	25.1	25.3 (7.7)	23.3 (7.1)	10.8	10.0	21.1 (536)	Fail
467114-7	3-35	5,014 (2,274)	64.5 (103.8)	25.2	25.3 (7.7)	26.2 (8.0)	7.5	8.5	14.3 (363)	Pass



Figure 40. Sequential Photographs for Test No. 467114-3 [19]



Figure 41. Sequential Photographs for Test No. 467114-4 [19]



Figure 42. Sequential Photographs for Test No. 467114-5 [19]



Figure 43. Sequential Photographs for Test No. 467114-6 [19]



Figure 44. Sequential Photographs for Test No. 467114-7 [19]

2.3 Flare Rate Study

In 2008, MwRSF conducted an evaluation of the critical flare rates for the MGS [2]. Flaring a guardrail system provides the benefit of reductions in crash frequency, installation length, and construction and maintenance costs. However, flaring a guardrail installation increases the impact severity of a collision due to an increase in the impact angle relative to the guardrail installation. Although the test installation is not an AGT, this study provides valuable insight regarding the effects of flaring roadside barrier systems.

Test nos. FR-1 through FR-5 were conducted to determine the critical flare rates for the MGS. Three system layouts with flare rates of 13:1 (4.4 degrees from roadway), 7:1 (8.1 degrees from roadway), and 5:1 (11.3 degrees from roadway), were evaluated. The three designs were identical except for the flare rate of the system. The two farthest upstream and downstream posts in the systems were 5½-in. x 7½-in. (140-mm x 190-mm) timber anchorage posts. The remaining posts in the systems were W6x9 steel posts embedded at a depth of 40 in. (1,016 mm) with a post spacing of 75 in. (1,905 mm). The guardrail posts supported the 12-gauge (2.7-mm) W-beam guardrail, which was installed with a top rail height of 31 in. (787 mm). The test installation layout of the 13:1 (4.4 degrees from roadway) flare rate is shown in Figure 45. The crash test data for test nos. FR-1 through FR-5 is summarized in Table 15 and sequential photographs are presented in Figures 46 through 50.

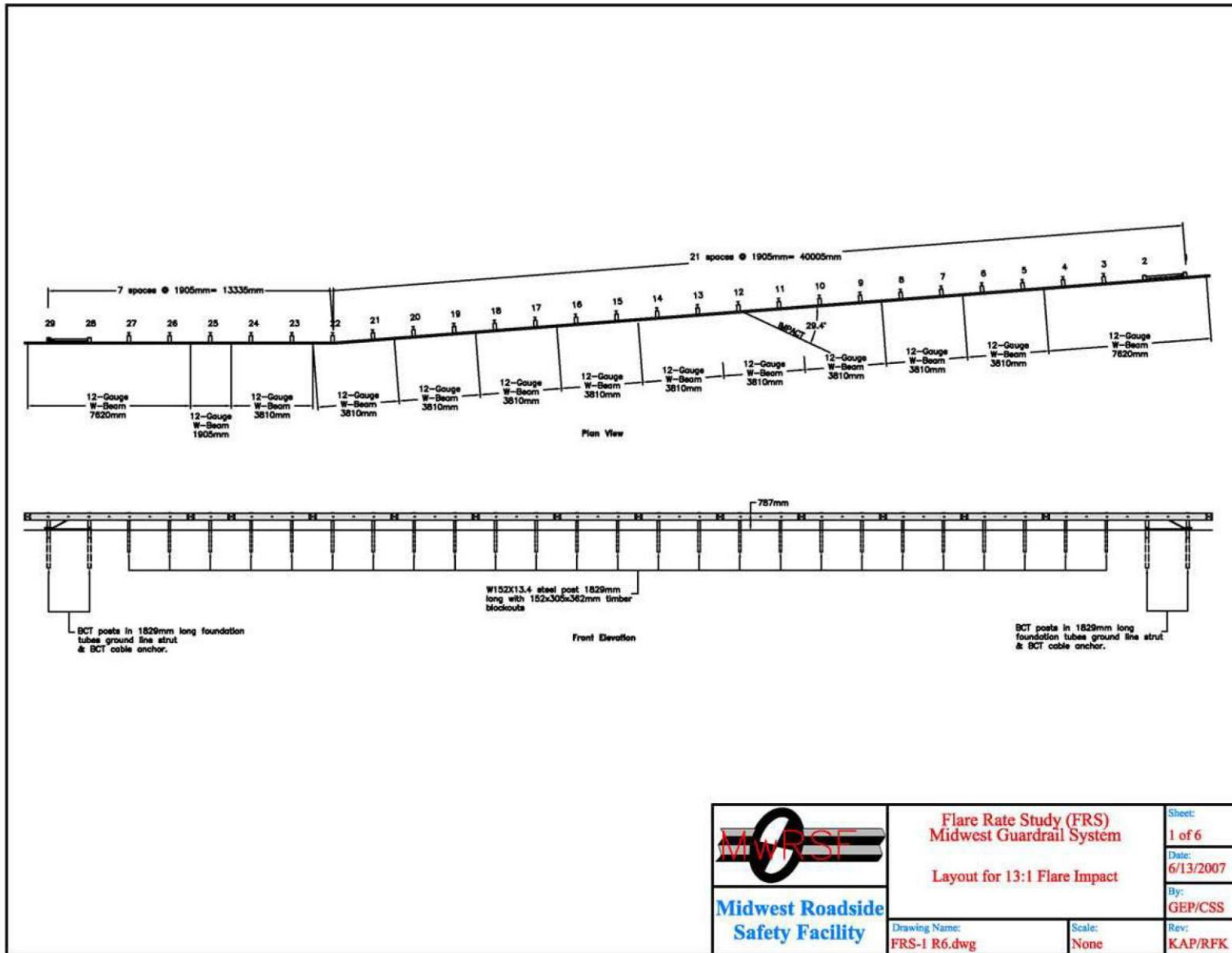


Figure 45. MGS – Flare Rates, 13:1 (4.4 degrees from roadway) Flared Test Installation [2]

2.3.1.1 Test No. FR-1

The 4,467-lb (2,026-kg) pickup truck impacted the 13:1 flared MGS test installation at a speed of 63.9 mph (102.9 km/h) and at an angle of 30.6 degrees relative to the guardrail (or 26.2 degrees relative to the roadway). The impact location was 16 ft – 3⁵/₈ in. (4.97 m) upstream from the centerline of the splice between post nos. 14 and 15. The test installation successfully contained and redirected the test vehicle with a maximum dynamic deflection of 66.3 in. (1,684 mm). Test installation damage was moderate and consisted of deformed posts and guardrail, disengaged blockouts, and contact marks. Test no. FR-1 met all occupant risk criteria and was determined to be acceptable according to the NCHRP Report 350 TL-3 safety performance criteria for test designation no. 3-11.

2.3.1.2 Test No. FR-2

The 4,460-lb (2,023-kg) pickup truck impacted the 7:1 flared MGS test installation at a speed of 63.1 mph (101.6 km/h) and at an angle of 34.0 degrees relative to the guardrail (or 25.9 degrees relative to the roadway). The impact occurred 17 ft – 1 in. (5.21 m) upstream from the centerline of the splice between post nos. 14 and 15. The test vehicle was adequately contained and redirected by the test installation with a maximum dynamic deflection of 75.8 in. (1,925 mm). Damage to the system was moderate and consisted of deformed posts and guardrail, disengaged blockouts, and contact marks. Test no. FR-2 satisfied all occupant risk criteria and was determined to be acceptable according to the NCHRP Report 350 TL-3 safety performance criteria for test designation no. 3-11.

2.3.1.3 Test No. FR-3

The 1,970-lb (894-kg) small car vehicle impacted the 7:1 flared MGS test installation at a speed of 63.5 mph (102.2 km/h) and at an angle of 28.7 degrees relative to the guardrail (or 20.6 degrees relative to the roadway). The impact occurred 5 ft – 10¹⁵/₁₆ in. (1.8 m) upstream from the centerline of the splice between post nos. 12 and 13. The MGS test installation successfully contained and redirected the test vehicle with a maximum dynamic deflection of 36.4 in. (925 mm). Barrier damage was moderate and consisted of deformed posts and guardrail, disengaged blockouts, and contact marks. The lateral and longitudinal OIV and ORA values were within the suggested limits. Test no. FR-3 satisfied all occupant risk criteria and was determined to be acceptable according to the NCHRP Report 350 TL-3 safety performance criteria for test designation no. 3-10.

2.3.1.4 Test No. FR-4

The 4,441-lb (2,014-kg) pickup truck impacted the 5:1 flared MGS test installation at a speed of 65.0 mph (104.7 km/h) and at an angle of 36.8 degrees relative to the guardrail (or 25.5 degrees relative to the roadway). The impact location was 15 ft – 7¹/₂ in. (4.76 m) upstream from the centerline of the splice between post nos. 14 and 15. The test vehicle was adequately contained and redirected by the test installation with a maximum dynamic deflection of 75.6 in. (1,919 mm). The MGS installation experienced moderate damage, which included deformed posts and guardrail, disengaged blockouts, and contact marks. Test no. FR-4 satisfied all occupant risk

criteria and was determined to be acceptable according to the NCHRP Report 350 TL-3 safety criteria for test designation no. 3-11.

2.3.1.5 Test No. FR-5

The 2,002-lb (908-kg) small car vehicle impacted the 5:1 flared MGS test installation at a speed of 59.4 mph (95.5 km/h) and at an angle of 31.8 degrees relative to the guardrail (or 20.5 degrees relative to the roadway). The impact occurred 4 ft – 6¼ in. (1.38 m) upstream from the centerline of the splice between post nos. 12 and 13. The MGS test installation adequately contained and redirected the test vehicle with a maximum dynamic deflection of 35.7 in. (908 mm). Damage to the barrier system was minimal and consisted of deformed posts and guardrail, disengaged blockouts, and contact marks. All occupant risk criteria were satisfied and test no. FR-5 was determined to be acceptable according to the NCHRP Report 350 TL-3 safety criteria for test designation no. 3-10.

Table 15. Summary of Crash Test Data for MGS – Flare Rates

Test Number	Test Desig.	Test Vehicle lb (kg)	Impact Speed mph (km/h)	Impact Angle degrees	OIV ft/s (m/s)		ORA g's		Dynamic Defl. in. (mm)	Pass/Fail
					Long.	Lateral	Long.	Lateral		
FR-1	3-11	4,467 (2,026)	63.9 (102.9)	30.6	21.36 (6.51)	13.52 (4.12)	8.08	10.41	66.3 (1,684)	Pass
FR-2	3-11	4,460 (2,023)	63.1 (101.6)	34.0	24.18 (7.37)	13.55 (4.13)	9.92	7.16	75.8 (1,925)	Pass
FR-3	3-10	1,970 (894)	63.5 (102.2)	28.7	21.82 (6.65)	17.78 (5.42)	8.20	9.70	36.4 (925)	Pass
FR-4	3-11	4,441 (2,014)	65.0 (104.7)	36.8	26.25 (8.00)	13.32 (4.06)	7.15	6.35	75.6 (1,919)	Pass
FR-5	3-10	2,002 (908)	59.4 (99.5)	31.8	-22.51 (-6.86)	-16.04 (-4.89)	-9.27	-7.98	35.7 (908)	Pass

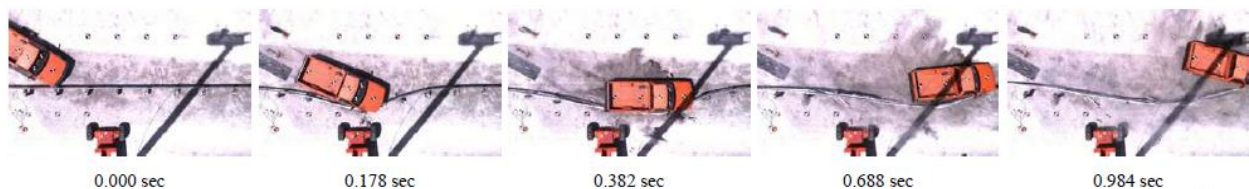


Figure 46. Sequential Photographs for Test No. FR-1 [2]



Figure 47. Sequential Photographs for Test No. FR-2 [2]



Figure 48. Sequential Photographs for Test No. FR-3 [2]



Figure 49. Sequential Photographs for Test No. FR-4 [2]

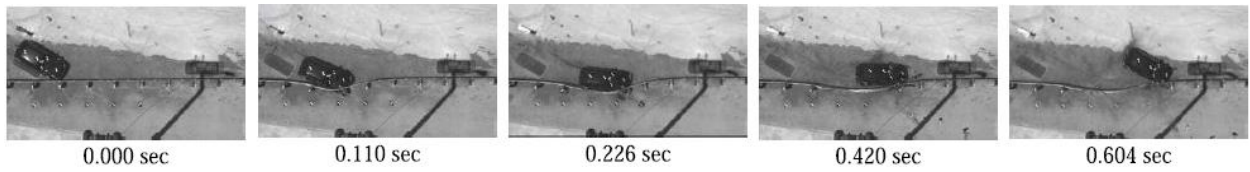


Figure 50. Sequential Photographs for Test No. FR-5 [2]

3 CRITICAL APPROACH GUARDRAIL TRANSITION SELECTION

State departments of transportation utilize a wide variety of three-beam AGTs that have various post sizes, spacings, and embedment depths. It was desired to select a critical AGT that was weaker and would deflect more than other AGTs, so that all crashworthy, tangent, three-beam AGTs could be used in the flared configuration. Several factors evaluated in the literature review were utilized to determine the critical AGT design, including dynamic deflection, impact point, post spacing, post size, post embedment depth, guardrail composition, downstream barrier, and safety performance. Previous testing of AGT installations has shown various examples of how slight alterations to an AGT can change the outcome of full-scale tests. Post embedment depth, buttress geometry, or the addition/removal of a curb can be attributed to the difference between a successful and an unsuccessful full-scale test.

For example, the tested Iowa Transition installation (Section 2.1.1) incorporated nested three-beam guardrail and 18¾-in. (476-mm) post spacing with a post embedment depth of 49 in. (1,245 mm) and the addition of a 4-in. (102-mm) tall concrete curb [8]. The test installation successfully met the MASH safety criteria for TL-3. In 2014, a similar transition, denoted the Texas Transition (Section 2.1.2), was evaluated which also utilized nested three-beam guardrail supported by posts spaced at 18¾ in. (476 mm), but had a post embedment depth of 52 in. (1,321 mm) and did not include the concrete curb [9]. During the full-scale test, the vehicle experienced excessive snag and underwent rollover, resulting in a failed test. In the Standardized Transition Buttress test (Section 2.1.6), the test installation again included nested three-beam guardrail and 18¾-in. (476-mm) post spacing with a post embedment depth of 49 in. (1,245 mm), but with the standardized transition buttress and no concrete curb [1]. The test installation successfully met the MASH safety criteria for TL-3.

Due to the sensitive nature of the three previous transition designs that incorporated nested three-beam guardrail supported by W6x9 or W6x8.5 steel posts spaced at 18¾ in. (476 mm), it was desired that the transition design selected as the critical transition design to model also include these design elements.

Both the Iowa Transition and the Standardized Transition Buttress test installations were identified as potential critical AGTs because they utilized 18¾-in. (476-mm) post spacing with standard 12-gauge (2.7-mm) W-beam and nested three-beam guardrail sections and successfully met MASH TL-3 safety performance criteria.

In both designs, the nested three-beam guardrail sections were mounted at a top rail height of 31 in. (787 mm). The guardrail was supported by W6x9 and W6x8.5 steel posts in the Iowa Transition installation and the Standardized Transition Buttress installation, respectively. The Iowa Transition and Standardized Transition Buttress installations were identified as potential critical AGTs due to the large dynamic deflections exhibited during full-scale testing and the small size of the guardrail posts when compared to other AGT installations. Both factors are critical to the crashworthiness of AGT installations due to the greater propensity for vehicle pocketing and snag on the rigid barrier. The systems were also desirable due to the use of a single standard post size of either W6x9 or W6x8.5 throughout the installation.

In addition to implementing the critical design components of the Iowa Transition, the Standardized Transition Buttress test installation for test no. AGTB-2 did not include a concrete

curb and incorporated a uniform top rail height of 31 in. (787 mm) and the standardized transition buttress. The standardized transition buttress design included chamfers on the upstream and top faces of the buttress, which minimized vehicle snag during impact with the installation and would produce the greatest likelihood of test success during impacts with a flared installation.

The AGT transition design discussed in Section 2.1.6 and previously full-scale crash tested in test no. AGTB-2 combined the critical design elements from the Iowa and Texas transitions with the newly developed standardized transition buttress. For this reason, it was selected as the critical transition design, as it was desired to select design that was weaker and would deflect more than other AGTs, so that all crashworthy, tangent, three-beam AGTs could be used in the flared configuration. Thus, the test no. AGTB-2 AGT design was utilized in the analysis and evaluation of the flared guardrail transition.

4 LENGTH OF NEED ANALYSIS

A barrier installation's length-of-need (LON), a parameter determined by the LON formulas found in the American Association of State Highway and Transportation Officials' (AASHTO's) *Roadside Design Guide* [20], specifies the minimum required length of a roadside barrier necessary to safeguard a hazard or area of concern. Oftentimes intersecting roadways or other roadside obstacles create longitudinal space constraints that limit the ability to install a tangent AGT with a proper LON. Installing an AGT with a flare away from the roadway would reduce the longitudinal length of the barrier required to meet LON guidelines. Unfortunately, no research or full-scale crash testing has been conducted on flared AGTs and the actual LON reduction of a flared installation is unknown. Thus, a LON study was conducted to quantify the LON reduction associated with various flare rates.

4.1 LON Calculation

The *Roadside Design Guide* outlines the method for calculating the necessary LON to safeguard a hazard. The parameter is dependent on site geometry, vehicle speed, and traffic volume, which are represented by the following variables: lateral area of concern (L_A), runout length (L_R), tangent transition length (L_1), barrier offset (L_2), and flare rate.

The lateral area of concern (L_A) is the lateral extent of the hazard being safeguarded, measured from the edge of the traveled roadway. The runout length (L_R) is the longitudinal distance along the roadway measured from the location that the vehicle departs the roadway to the beginning of the area of concern. The tangent transition length (L_1) is the length of guardrail that is parallel to the roadway measured from the upstream end of the rigid barrier to the beginning of the flared section. Barrier offset (L_2) is a measure of the distance between the guardrail installation and the edge of the traveled roadway. These variables as well as the required LON (X) and the lateral offset (Y) are illustrated in Figure 51.

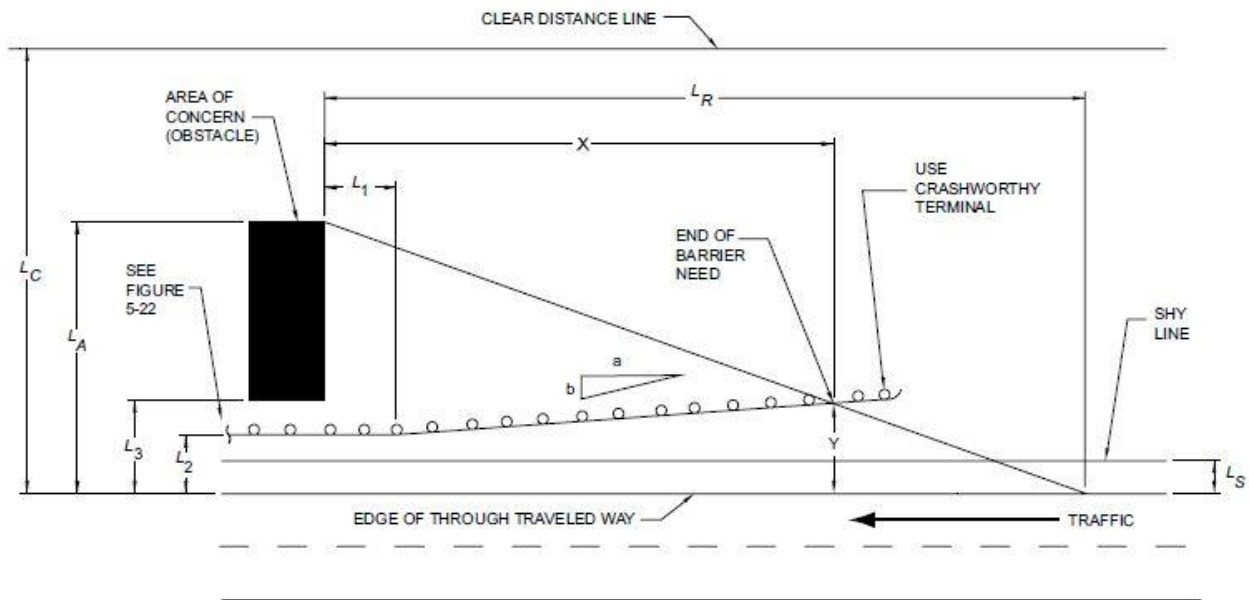


Figure 51. LON Layout [20]

The sample LON calculations for this study were performed for a roadway with a design speed of 70.0 mph (112.7 km/h) and a traffic volume of 5,000 to 10,000 vehicles per day that incorporated a barrier offset of 10 ft (3 m) and a lateral area of concern equal to 30 ft (9.1 m). The runout length (L_R) was selected from the Suggested Runout Lengths for Barrier Design tables in the *Roadside Design Guide* using the described roadway parameters [20]. Table 16 contains the selected variables for the LON calculations based on the described roadway.

Table 16. LON Calculation Variables

Variable		Value ft (m)
Lat. Area of Concern	L_A	30.0 (9.1)
Runout Length	L_R	330.0 (100.6)
Tangent Transition	L_1	0.0 (0.0)
Barrier Offset	L_2	10.0 (3.0)

Note that the tangent transition length (L_1) is equal to zero. Previous guidance in the *Roadside Design Guide* states that the tangent length of barrier (L_1) should be at least as long as the transition section to reduce the possibility of pocketing and increase the likelihood of a smooth redirection [20]. However, due to the objective of this research and the desire to maximize the reduction in barrier length, the flare was initiated at the upstream end of the rigid concrete buttress. Thus, the tangent transition length (L_1) was set equal to zero when calculating the flared installation LON. At the request of the sponsor, a brief LON analysis was also performed for a hybrid-flared configuration, in which the tangent transition length was set equal to 50 ft (15.2 m).

The study investigated five different flare rates, ranging from 25:1 (2.29 degrees from roadway) to 10:1 (5.71 degrees from roadway). This range of flare rates was selected because it was likely to provide a significant reduction in LON and was in the range of previously tested guardrail flare rates. A complete list of the studied flare rates and corresponding angles is provided in Table 17.

Table 17. Studied Flare Rates

Flare Rate	Flare Angle (degrees from roadway)
Tangent	0
25:1	2.29
20:1	2.86
15:1	3.81
12.5:1	4.57
10:1	5.71

Once the appropriate variables were selected, the LON and the lateral offset parameters were calculated for each of the flare rates using Equations 1 and 2:

$$\text{Length of Need: } X = \frac{L_A + (b/a)(L_1) - L_2}{(b/a) + (L_A/L_R)} \quad (1)$$

$$\text{Lateral Offset: } Y = L_A - \frac{L_A}{L_R} * X \quad (2)$$

where

X = Length of Need; ft (m)

Y = Lateral Offset; ft (m)

L_A = Lateral Area of Concern; ft (m)

L_R = Runout Length; ft (m)

L₁ = Tangent Transition Length; ft (m)

L₂ = Barrier Offset; ft (m)

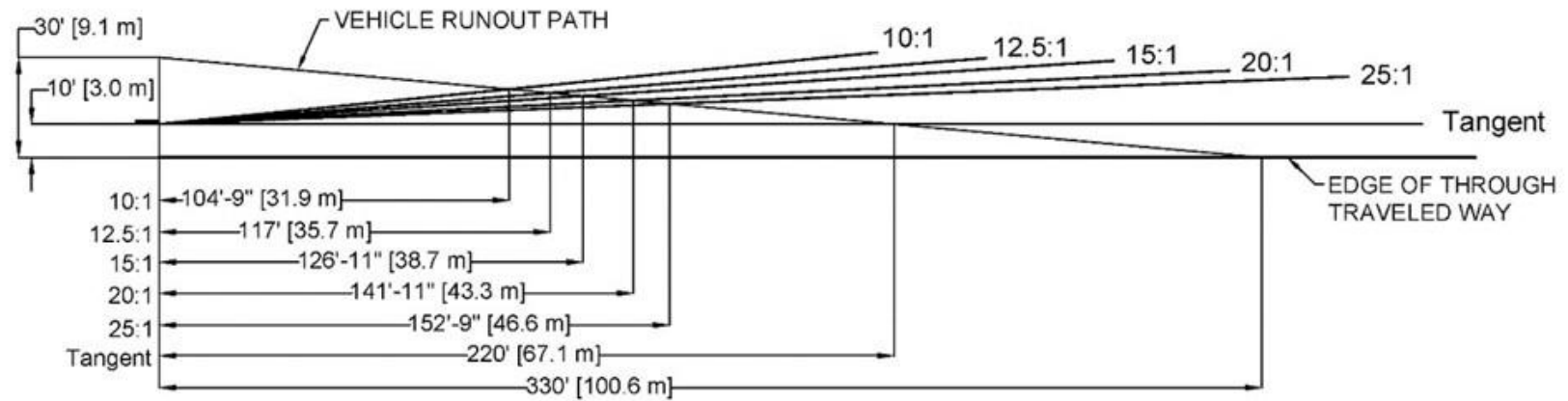
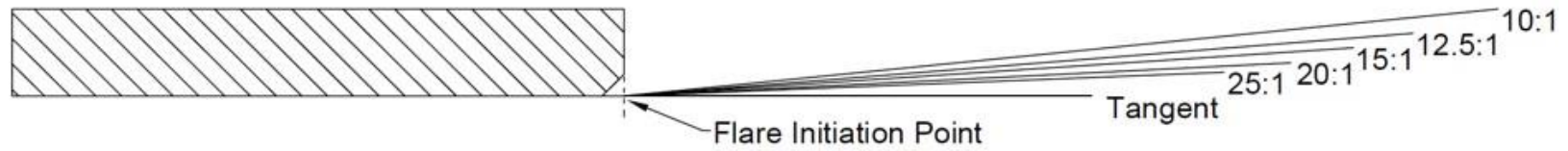
a = Longitudinal Component of Flare Rate; ft (m)

b = Lateral Component of Flare Rate; ft (m)

The calculated LON and lateral offset values for the tangent installation and each of the studied flare rates are summarized in Table 18. Additionally, Table 18 contains the reduction in LON, calculated as a percentage of the tangent LON, and the increase in lateral offset, calculated as a percentage of the tangent lateral offset. Figure 52 depicts each of the investigated flare rates with dimensioned LON values.

Table 18. Calculated Flared AGT LON

Flare Rate	Flare degrees	LON ft (m)	LON Reduction %	Lateral Offset ft (m)	Lateral Offset Increase %
Tangent	0	220.0 (67.1)	-	10.0 (3.0)	-
25:1	2.29	152.8 (46.6)	30.5	16.1 (4.9)	61.0
20:1	2.86	141.9 (43.3)	35.5	17.1 (5.2)	71.0
15:1	3.81	126.9 (38.7)	42.3	18.5 (5.6)	85.0
12.5:1	4.57	117.0 (35.7)	46.8	19.4 (5.9)	94.0
10:1	5.71	104.8 (31.9)	52.4	20.5 (6.2)	105.0



Lateral Area of Concern: 30.0 ft (9.1 m)
 Runout Length: 330.0 ft (100.6 m)
 Barrier Offset: 10.0 ft (3.0 m)

Parameters based on 70.0 mph (112.7 km/h) and 5,000 to 10,000 vehicles/day.

55

Figure 52. Flared AGT LON Diagram

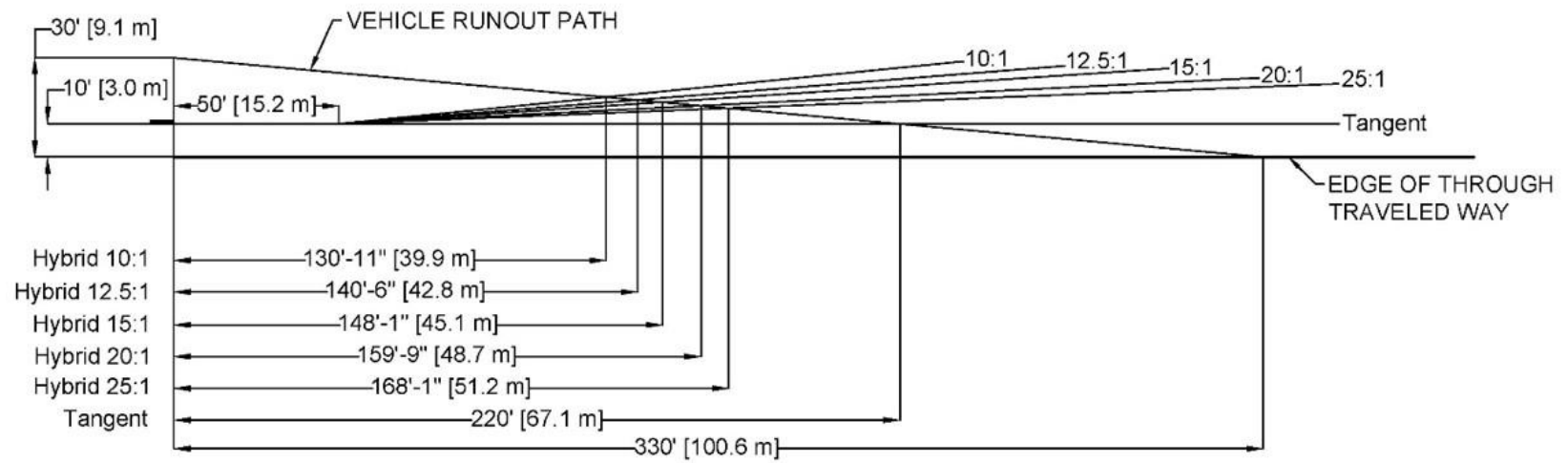
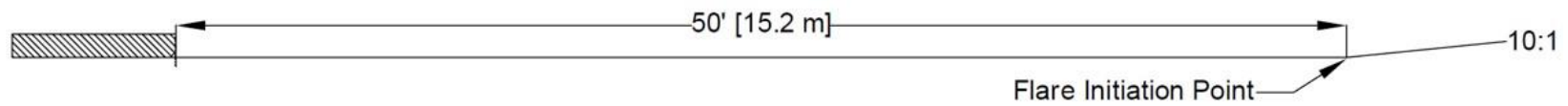
Additional hybrid flare rates were examined at the request of the sponsor to assess the benefit of flaring the AGT installation away from the roadway after a 50-ft (15.2-m) long section of tangent guardrail located upstream from the buttress. The analysis was performed using the LON equations outlined in the *Roadside Design Guide*. Table 19 contains a summary of the evaluated hybrid flare rates and Figure 53 depicts each of the investigated hybrid flare rates with dimensioned LON values.

Table 19. Calculated Hybrid Flared AGT LON

Flare Rate	Flare degrees	LON ft (m)	LON Reduction %	Lateral Offset ft (m)	Lateral Offset Increase %
Tangent	0	220.0 (67.1)	-	10.0 (3.0)	-
25:1	2.29	168.1 (51.2)	23.6	14.7 (4.5)	47
20:1	2.86	159.7 (48.7)	27.4	15.5 (4.7)	55
15:1	3.81	148.1 (45.1)	32.7	16.5 (5.0)	65
12.5:1	4.57	140.4 (42.8)	36.2	17.2 (5.2)	72
10:1	5.71	131.0 (39.9)	40.5	18.1 (5.5)	81

Installing the AGT with the hybrid flared configuration would likely reduce the propensity for vehicle snag on the upstream end of the rigid buttress due to the tangent section of guardrail located immediately upstream of the buttress. However, initiating the flare upstream of the W-to-thrie transition section could result in an additional pocketing and snag hazard due to the greater stiffness of the transition. Additionally, as previously noted, it is desirable to initiate the flare at the upstream end of the concrete buttress to maximize the LON reduction and the lateral offset from the traveled roadway.

A direct comparison between the pure 15:1 (3.81 degrees from roadway) and 12.5:1 (4.57 degrees from roadway) flare rates initiated at the buttress and the hybrid 15:1 and 12.5:1 flare rates initiated 50 ft upstream of the buttress is shown in Figure 54. Compared to the pure flared configuration, the hybrid flared configuration LON is increased 21 ft – 2 in. (6.5 m) at the 15:1 flare rate and 23 ft – 6in. (7.2 m) at the 12.5:1 flare rate.

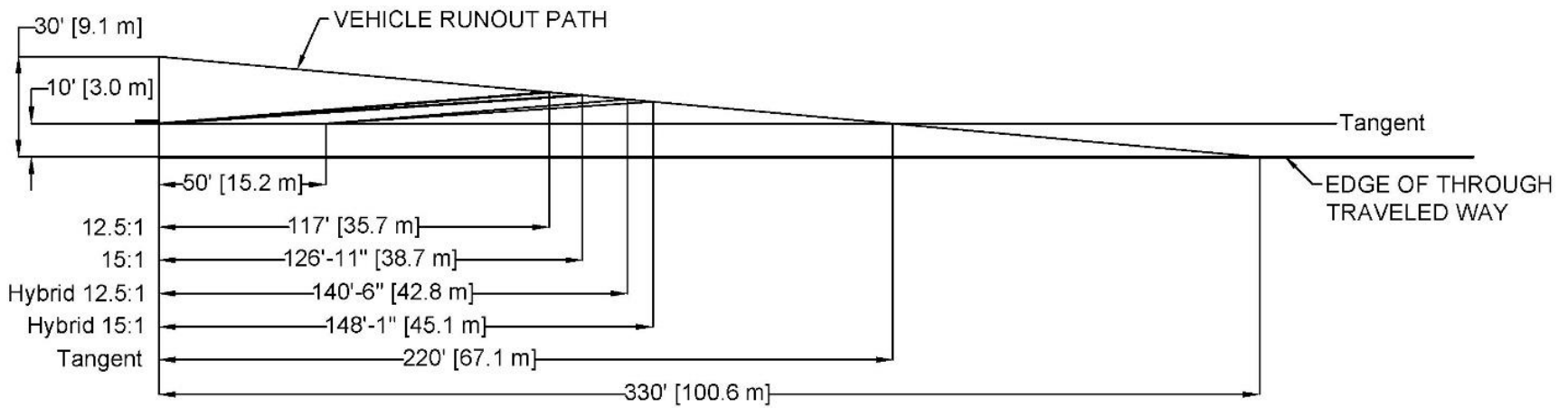


Lateral Area of Concern: 30.0 ft (9.1 m)
 Runout Length: 330.0 ft (100.6 m)
 Barrier Offset: 10.0 ft (3.0 m)

Parameters based on 70.0 mph (112.7 km/h) and 5,000 to 10,000 vehicles/day.

57

Figure 53. Hybrid Flare AGT LON Diagram



Lateral Area of Concern: 30.0 ft (9.1 m)
 Runout Length: 330.0 ft (100.6 m)
 Barrier Offset: 10.0 ft (3.0 m)

Parameters based on 70.0 mph (112.7 km/h) and 5,000 to 10,000 vehicles/day.

Figure 54. Comparison of Hybrid vs. Pure Flared AGT Configurations

4.2 Discussion

The motivation behind flaring AGTs away from the roadway has been that the reduction in installation length and the increase in available space in front of the barrier installation will improve both cost-effectiveness and roadside safety through the reduction of accident frequency. This study has shown that a barrier installed with a flare away from the roadway can lead to a significant reduction in LON.

The investigated pure flare rates (i.e. flare started at the buttress) ranged from 25:1 to 10:1, and reduced the LON by 67.2 ft (20.5 m) to 115.2 ft (35.1 m) (30.5 to 52.4 percent), when compared to the tangent barrier LON with the stated roadway design criteria. Additionally, the lateral offset of the barrier increased from 10 ft (3 m) with the tangent installation to 20.5 ft (6.2 m) with the steepest studied flare rate of 10:1. Even the modest 25:1 flare rate resulted in a 67.2 ft (20.5 m) reduction in LON and a lateral offset increase of 6.1 ft (1.9 m). Thus, an AGT installed with a flare away from the roadway will enable shorter barrier installations with more area in front of the barrier for the errant driver to regain control of the vehicle and avoid impact.

This study provided significant insight into the benefits associated with flaring an AGT installation. However, the LON values calculated with the equations outlined in the *Roadside Design Guide* are intended to provide an approximation for the LON of an AGT installation. The equations calculate simplified values, determining the distance from the upstream end of the rigid barrier to the intersection point of the guardrail and the vehicle runout path. Factors such as standard manufactured guardrail section lengths and guardrail end terminals were not included in the previous calculations and could result in the required system length being longer than the calculated LON approximations.

Despite the significant reduction in LON associated with the steepest flare rates, the benefit is not without consequence. Flaring a guardrail system away from the roadway increases the vehicle's effective impact angle with the barrier installation, which leads to larger system deflections and a greater chance for pocketing and wheel snag when compared to a tangent installation. Additionally, the higher impact angle results in a higher impact severity.

Impact severity is a parameter outlined in MASH 2016, which calculates the kinetic energy imparted laterally into the barrier as a function of the vehicle's impact angle [4]. The steepest investigated flare rate of 10:1 increased the impact angle from 25 degrees to 30.7 degrees, which corresponded to 46 percent increase in impact severity. A summary of the effect of flare rate on impact angle and impact severity for each of the studied flare rates is shown in Table 20.

Table 20. Summary of Flare Rate vs. Impact Severity

Flare Rate	Flare Angle degrees	Impact Angle degrees	Impact Severity kip-ft (kJ)	Percent Increase from Tangent %
Tangent	0	25	117.3 (159.0)	-
25:1	2.29	27.29	138.1 (187.2)	17.7
20:1	2.86	27.86	143.4 (194.4)	22.3
15:1	3.81	28.81	152.5 (206.8)	30.0
12.5:1	4.57	29.57	159.9 (216.8)	36.3
10:1	5.71	30.71	171.3 (232.2)	46.0

Flaring the AGT installation also results in larger loads imparted to the barrier system, which could lead to component failure or rail rupture. Thus, to determine the critical flare rate for flaring AGT installations, further investigations of vehicle behavior and barrier performance were needed.

5 AGT BASELINE COMPUTER SIMULATION

5.1 Tangent AGT Model Details

Computer simulation was used to initially evaluate the critical flare rate of the AGT installation that would provide the greatest reduction in LON while upholding MASH 2016 TL-3 safety performance criteria. A model of a tangent 81 ft – 8¼ in. (24.9-m) long AGT installation was validated against test no. AGTB-2, the critical AGT selected for this study, using the procedures for verification and validation (V&V) of computer simulations used for roadside safety applications, outlined in NCHRP Report W179 [21]. The physical AGTB-2 test installation and the modeled AGT guardrail installation are shown in Figures 55 and 56, respectively.

The modeled AGT installation was composed of 21 guardrail posts, W-beam guardrail, thrie-beam guardrail, a W-to-thrie transition section, and the standardized concrete buttress [22]. Post nos. 3 through 21 were steel guardrail posts and post nos. 1 and 2 were timber breakaway cable terminal (BCT) posts, which composed the upstream anchorage. The steel guardrail posts were modeled with fully integrated shell elements with a piecewise linear plasticity material formulation and the two BCT posts were modeled with fully integrated solid elements with a plastic kinematic material formulation.

In the initial model, the steel guardrail posts were modeled as W6x9 posts with a yield stress of 47 ksi (324 MPa). The post geometry and strength in the final model were changed to W6x8.5 with a yield stress of 56 ksi (386 MPa), which matched the post size and material certifications in test no. AGTB-2. The post spacing was 75 in. (1,905 mm), 37½ in. (953 mm), and 18¾ in. (476 mm) between post nos. 1 through 8, post nos. 8 through 12, and post nos. 12 through 21, respectively.

The soil for post nos. 3 through 21 was modeled with a rigid soil tube around the base of each post with a pair of soil springs attached to the top of the soil tube in the lateral and longitudinal directions. The soil tubes were pinned at their center of gravity, which allowed rotation. The springs simulated the reaction of the soil on the posts and were used for computational efficiency. The soil springs were assigned a loading curve that calibrated the soil resistance. Post nos. 1 and 2 were embedded into solid Drucker-Prager soil elements, which offered a more accurate representation of soil deformation.

W-beam guardrail with a top rail height of 31 in. (787 mm) composed the upstream portion of the AGT installation. The system transitioned from W-beam to standard thrie-beam guardrail with an asymmetrical W-to-thrie transition section, which maintained the 31-in. (787-mm) top rail height. All guardrail sections were modeled with fully integrated shell elements and a piecewise linear plasticity material formulation.

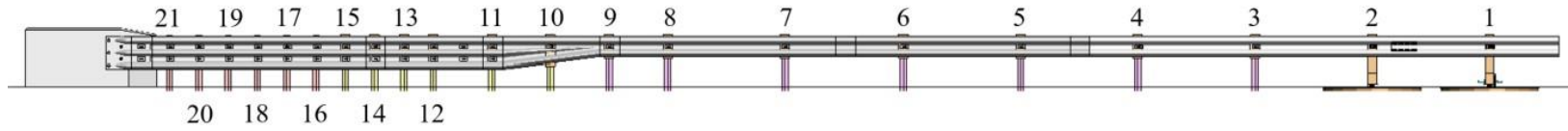
The W-beam and single thrie-beam guardrails were modeled as 12-gauge (2.7 mm), and the W-to-thrie transition section and thrie-beam terminal connector were modeled as 10-gauge (3.4 mm) thick shell elements. The nested section of 12-gauge (2.7-mm) thrie-beam guardrail was modeled with a single section of thrie-beam that had a thickness of 0.21 in. (5.34 mm). Other methods of modeling the nested guardrail section were explored, including a single section of thrie-beam with a thickness of 0.14 in. (3.43 mm) or two overlaid sections of thrie-beam with

thicknesses of 0.11 in. (2.67 mm), but these methods did not provide better dynamic system deflections.

The thrie-beam was anchored to the standardized concrete buttress located at the downstream end of the installation with merged rigid bodies at the bolt locations of the thrie-beam terminal connector. The standardized concrete buttress was modeled with rigid shell elements and included a dual taper design intended to minimize tire snag on the upstream face of the buttress. Appendix A contains a summary of the validated AGT model parts and LS-DYNA parameters.



Figure 55. AGTB-2 Guardrail Installation



63 Figure 56. Finite Element Model of AGTB-2 Guardrail Installation

5.2 Tangent AGT LS-DYNA Baseline Simulations

The model of the tangent AGT installation complete with the standardized transition buttress was validated with the results from full-scale test no. AGTB-2. In test no. AGTB-2, a 4,998-lb (2,267-kg) 2010 Dodge Ram 1500 pickup truck impacted the AGT test installation at a speed of 62.7 mph (100.8 km/h) and at an angle of 25.4 degrees. Test no. AGTB-2 met all safety performance criteria and was determined to be acceptable according to MASH 2016 test designation no. 3-21 [1].

Two different versions of the AGT model were compared to the full-scale crash test data using the NCHRP Report W179 V&V procedures [21]. The first AGT model supported the guardrail with W6x9 posts that had a yield stress of 47 ksi (324 MPa) and was impacted by the reduced-element, 2270P 2007 Chevrolet Silverado pickup truck model. This vehicle model was originally developed by the National Crash Analysis Center at George Washington University [23], and was later modified by researchers at MwRSF for use in roadside safety applications.

In the first validation of the AGT model, the 2270P Silverado vehicle model impacted the modeled AGT installation at a speed of 62.7 mph (100.8 km/h) and at an angle of 25 degrees, 89 in. (2,261 mm) upstream from the concrete buttress. The modeled AGT successfully contained and redirected the Silverado vehicle model with OIVs and ORAs that satisfied the MASH 2016 safety performance criteria, as shown in Table 21. However, when compared to the test no. AGTB-2 crash test data, the Silverado simulation exhibited greater longitudinal and lateral OIVs and ORAs and lower system deflections. A summary of the results from the Silverado simulation and full-scale test no. AGTB-2 is contained in Table 21 and the full V&V of the Silverado simulation is included in Appendix B. A comparison between the Silverado simulation and full-scale test no. AGTB-2 is depicted in Figure 57 at a time state of 100 ms after impact and sequential photographs are shown in Figure 58.

Table 21. Summary of Test No. AGTB-2 and Silverado Simulation Results

Evaluation Criteria		AGTB-2	Silverado Simulation	MASH Limits
OIV ft/s (m/s)	Longitudinal	-20.28 (-6.18)	-26.34 (-8.03)	±40
	Lateral	24.61 (7.50)	26.68 (8.13)	±40
ORA (g's)	Longitudinal	-7.06	-12.10	±20.49
	Lateral	10.40	11.00	±20.49
Maximum Angular Displacement degrees	Roll	21.3	29.1	±75
	Pitch	6.3	6.1	±75
	Yaw	39.6	39.4	not required
Post Max. Dynamic Deflection in. (mm)		5.35 (136)	4.96 (126)	NA
Length of Contact in. (mm)		159 (4,039)	120.79 (3,068)	NA



Figure 57. Full-Scale Crash Test No. AGTB-2 (Top) and Silverado Simulation (Bottom) [22]



0.000 sec



0.100 sec



0.200 sec



0.300 sec



0.400 sec



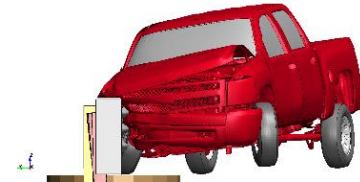
0.500 sec

AGT - 2275a Silverado (4x4) at 100 km/h @ 25 deg
Time = 0.000



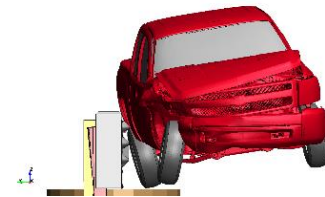
0.000 sec

AGT - 2275a Silverado (4x4) at 100 km/h @ 25 deg
Time = 0.100



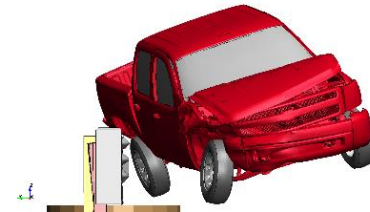
0.100 sec

AGT - 2275a Silverado (4x4) at 100 km/h @ 25 deg
Time = 0.200



0.200 sec

AGT - 2275a Silverado (4x4) at 100 km/h @ 25 deg
Time = 0.300



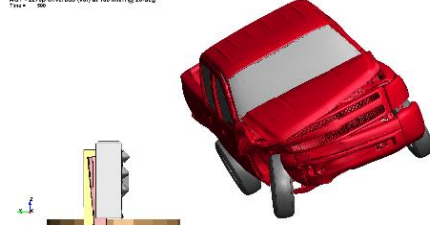
0.300 sec

AGT - 2275a Silverado (4x4) at 100 km/h @ 25 deg
Time = 0.400



0.400 sec

AGT - 2275a Silverado (4x4) at 100 km/h @ 25 deg
Time = 0.500



0.500 sec

Figure 58. Test No. AGTB-2 (Left) vs. Silverado Simulation (Right) Sequential Photographs [22]

The Silverado simulation would only pass the V&V procedure requirements with exceptions, as the Silverado simulation's longitudinal ORA, vehicle roll, and exit angle exceeded those of the full-scale test. The simulation overpredicted the longitudinal ORA by 5.0 g's (71 percent), which exceeded the V&V relative difference limit of either 4.0 g's or 20 percent. Additionally, the Silverado simulation did not meet the maximum roll or exit angle criteria, as the simulation overpredicted the roll by 7.9 degrees (37.0 percent) and the exit angle by 5.0 degrees (55.6 percent), which both exceeded the V&V angular relative difference limit of either 20 percent or 5 degrees.

Finally, the hourglass energy and added mass criteria required by the V&V procedures were not satisfied. The hourglass energy at the end of the simulation exceeded the total initial energy at the beginning of the run by more than 5 percent and exceeded the total internal energy at the end of the run by more than 10 percent. The right-front tire exhibited the highest amount of hourglass energy, which exceeded the total internal energy of the tire by more than 10 percent and did not meet the V&V criteria. The added mass of the steel transition blockouts exceeded the initial mass of the part by 19.96 percent, which did not satisfy the V&V criteria requirement of less than 10 percent. However, it is important to note that both the hourglass energy and added mass could be resolved at the cost of greater computational run time when compared to the current model.

Thus, the Silverado simulation would not meet the V&V criteria without additional modifications and/or exceptions. The Silverado vehicle model was geometrically different from the tested 2010 Dodge Ram vehicle and was expected to diverge from the full-scale test data. However, due to the magnitude of the discrepancies between the Silverado simulation and the full-scale test, the simulation only satisfied the V&V requirements with the noted exceptions.

During the development of the AGT model, researchers obtained a vehicle model of a 2018 Dodge Ram pickup truck. Previously, all simulations had used the reduced-element model of the 2007 Chevrolet Silverado. The Ram vehicle model was originally developed by the Center for Collision Safety and Analysis Team at George Mason University [24], and was modified by MwRSF personnel for use in roadside safety applications. It was believed that the Ram vehicle model would provide a much better correlation between the simulations and the full-scale test than the Silverado vehicle model due to vehicle geometry and vehicle deformation characteristics that were closer to the full-scale crash tested vehicle.

The second validation of the AGT model used the 2270P 2018 Dodge Ram vehicle model and included changes to the previously modeled AGT that was impacted by the Silverado vehicle model. In the Ram simulation, the thrie-beam post sections were changed from W6x9 to W6x8.5 and the yield stress of the transition posts was increased from 47 ksi (324 MPa) to 56 ksi (386 MPa) to match the material certifications for the guardrail posts from test no. AGTB-2. Additionally, the simulated impact with the Ram vehicle model included suspension failure in an effort to accurately represent test no. AGTB-2.

In the numerical simulation, the 2270P Ram vehicle model impacted the modeled AGT installation at a speed of 62.7 mph (100.8 km/h) and at an angle of 25 degrees, 89 in. (2,261 mm) upstream from the concrete buttress. The modeled AGT successfully contained and redirected the Ram vehicle model with OIVs and ORAs that satisfied the MASH 2016 safety performance criteria, as shown in Table 22. However, when compared to the test no. AGTB-2 crash test data, the Ram simulation exhibited greater longitudinal and lateral OIV values and longitudinal ORA

value. Additionally, the Ram simulation had lower system deflections and a lateral ORA value that was lower than test no. AGTB-2. A summary of the evaluated simulation and full-scale test no. AGTB-2 is contained in Table 22. The full V&V of the Ram simulation is included in Appendix C.

Table 22. Summary of Crash Test No. AGTB-2 and Ram Simulation Results

Evaluation Criteria		AGTB-2	Ram Simulation	MASH Limits
OIV ft/s (m/s)	Longitudinal	-20.28 (-6.18)	-20.84 (-6.35)	±40
	Lateral	24.61 (7.50)	27.04 (8.24)	±40
ORA (g's)	Longitudinal	-7.06	-7.75	±20.49
	Lateral	10.40	8.13	±20.49
Maximum Angular Displacement degrees	Roll	21.3	24.8	±75
	Pitch	6.3	6.3	±75
	Yaw	39.6	43.2	not required
Post Max. Dynamic Deflection in. (mm)		5.35 (136)	4.31 (109)	NA
Length of Contact in. (mm)		159 (4,039)	125 (3,165)	NA

The Ram simulation satisfied the V&V procedure requirements with exceptions. The modeled AGT installation exhibited fewer significantly bent posts than test no. AGTB-2. A threshold value of 1 in. (25 mm) was used to classify a post deflection as significant. Seven posts exhibited deflections greater than 1 in. (25 mm) in the full-scale test and only five posts experienced a deflection of this magnitude in the simulation. This resulted in a relative difference of 29 percent, which exceeded the 20 percent relative difference limit established in the V&V criteria. The difference between the numbers of deflected posts was likely caused by the behavior of the soil. The posts were installed at a post spacing of 18¾ in. (476 mm) within the impacted region. In the full-scale test, the close proximity resulted in the soil resistance being dependent on the loading of the adjacent posts. However, in the simulation, the soil for each post was modeled with independent soil springs that did not account for the loading of the surrounding soil. Due to this modeling simplification, the load imparted into the barrier by the impacting vehicle in the simulation resulted in localized deflections and fewer significantly deflected posts compared to the full-scale test.

The Ram vehicle model also exhibited an excessive exit angle of 14.1 degrees that was 5.1 degrees (57 percent) greater than the 9.0 degree exit angle in full-scale test no. AGTB-2, which exceeded the 20-percent or 5-degree limit of the V&V criteria. During the full-scale test, the vehicle's right-front wheel detached and slid under the vehicle, vacating the wheel well. This behavior was not recreated by the model, as the detached right-front wheel remained in the wheel well while the vehicle was in contact with the installation, likely contributing to the exit angle discrepancy.

Additionally, the simulation did not meet the hourglass energy and added mass requirements outlined in NCHRP Report W179 [21]. The excessive hourglass energy occurred in the impacting right-front inner rim of the vehicle model and the part with the most added mass was the set of steel transition blockouts located at post nos. 16 through 21. While the hourglass energy and added mass could be resolved, it would result in greater computational run time compared to the current model. Thus, exceptions were made for the excessive hourglass energy and added mass.

Despite the exceptions, the simulation successfully met the V&V criteria for dynamic deflection, OIV, ORA, roll, pitch, yaw, and exit velocity. Thus, the simulated AGT impact with the Ram vehicle model passed the validation criteria with the noted exceptions. A comparison between the Ram simulation and full-scale test no. AGTB-2 is depicted in Figure 59 at a time state of 100 ms after impact and sequential photographs are shown in Figure 60. Appendix A contains a summary of the validated AGT model parts and LS-DYNA parameters.

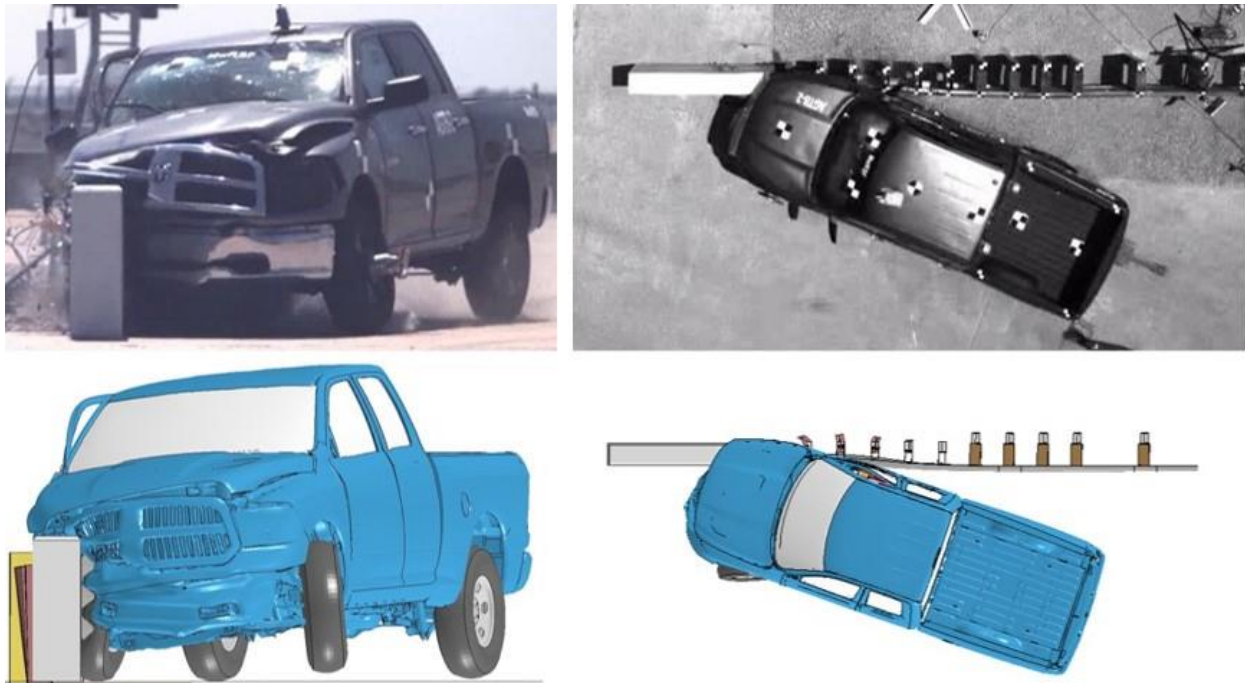


Figure 59. Full-Scale Crash Test No. AGTB-2 (Top) and Ram Simulation (Bottom) [22]

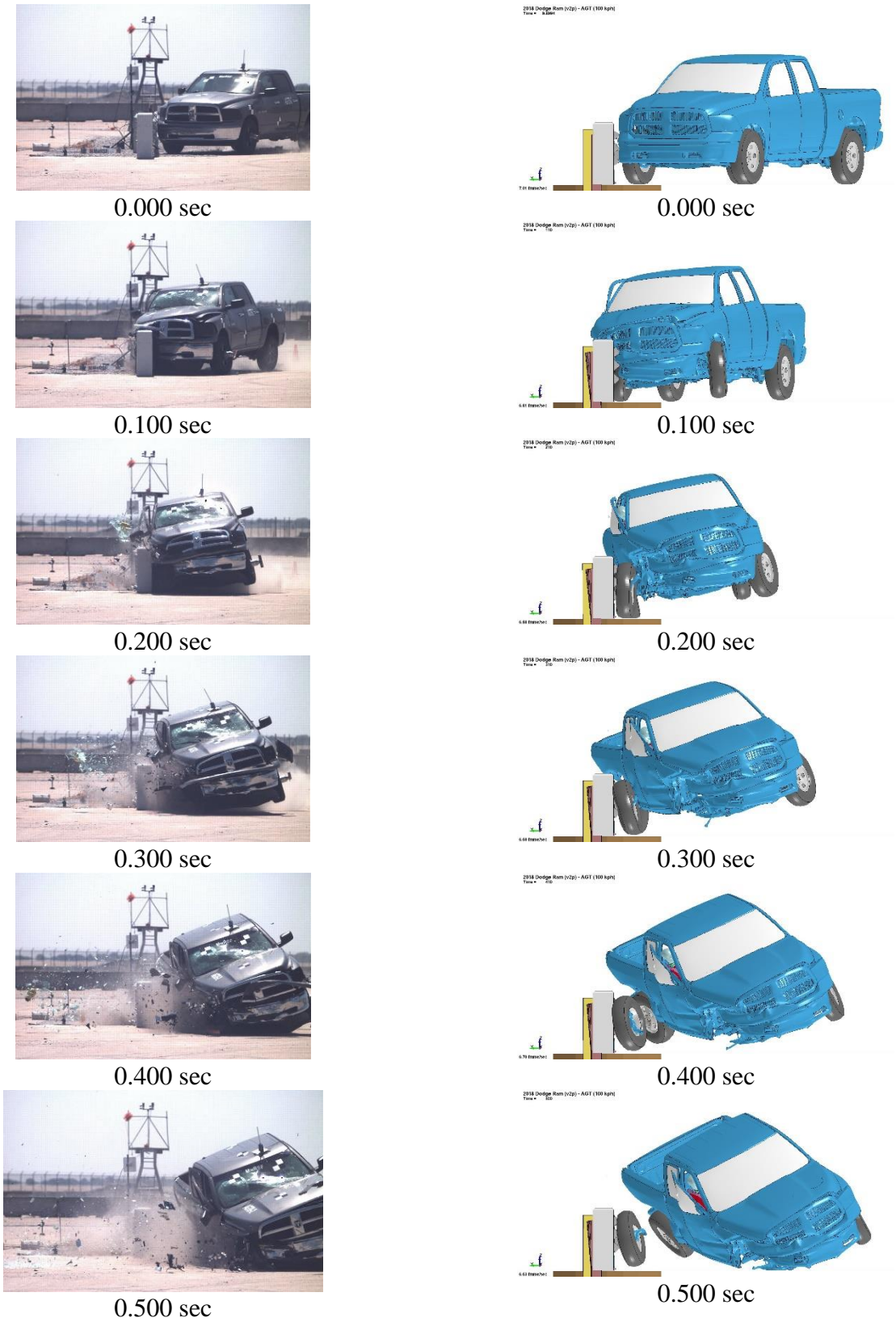


Figure 60. Test No. AGTB-2 (Left) vs. Ram Simulation (Right) Sequential Photographs [22]

6 FLARED AGT COMPUTER SIMULATION

6.1 Flared AGT Model Details

The model of the validated tangent installation was modified to incorporate a straight flare away from the roadway. Five different flare rates were investigated, ranging from 25:1 to 10:1. To maximize the LON reduction, the flare was initiated at the upstream end of the thrie-beam terminal connector, which was located approximately at the upstream end of the buttress, as shown in Figure 61. All posts and guardrail components were rotated around this point to the desired flare rate. The tangent installation and the five studied flare rates are illustrated in Figure 62.

A series of computer simulations was conducted to identify the critical flare rate for full-scale crash testing. The analysis primarily focused on MASH 2016 TL-3 impacts with the 2270P pickup truck due to the greater propensity for vehicle snag on the upstream face of the rigid buttress with the 2270P vehicle versus the 1100C vehicle. However, once the critical flare rates were identified, small car impacts at the downstream end of the transition were simulated to estimate the interaction between the small car and rigid buttress and identify the CIP.

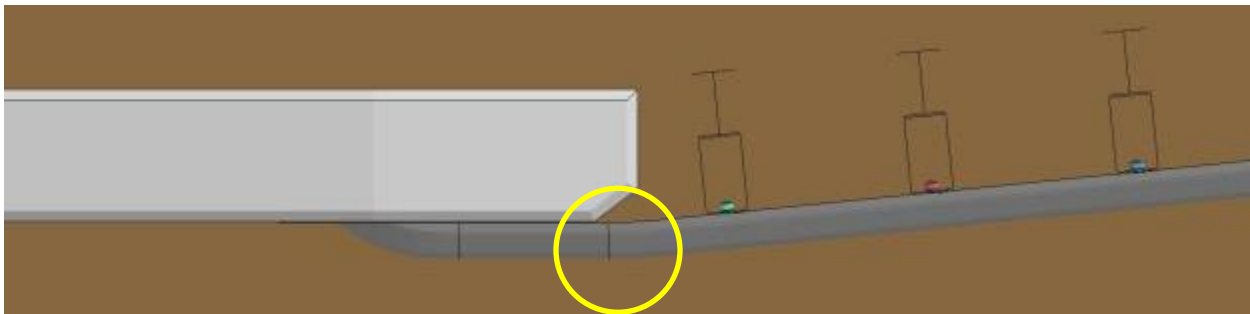


Figure 61. Location of Flare Initiation Point

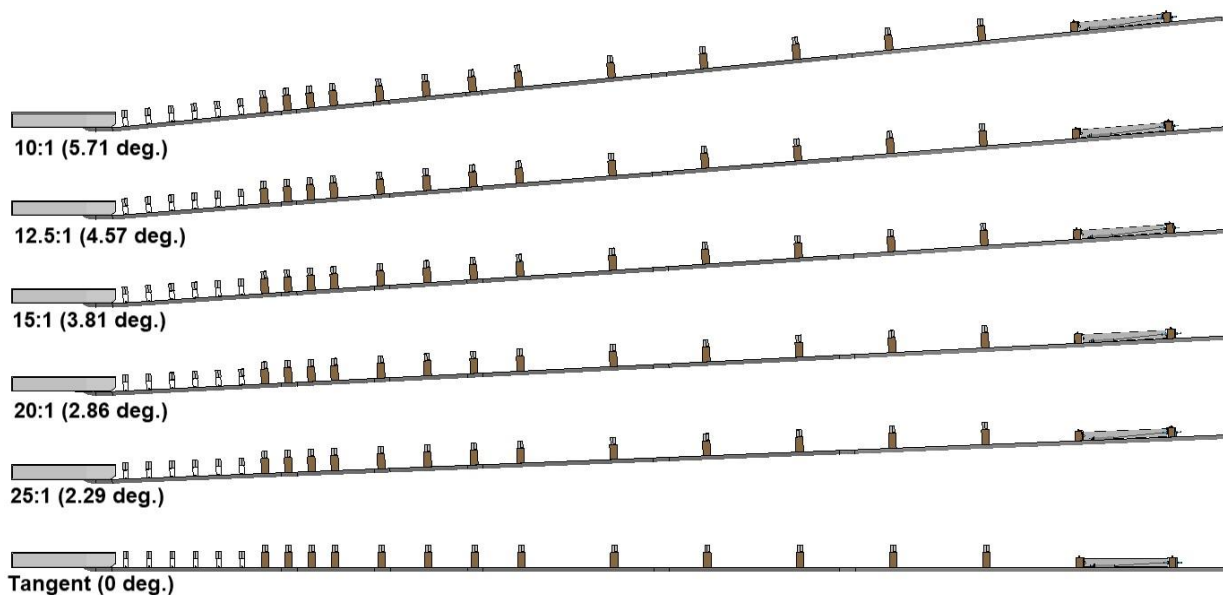


Figure 62. Modeled Flared Installations

6.2 Evaluation Criteria

Installing an AGT with a flare away from the roadway may result in excessive vehicle snag on the guardrail posts and/or the upstream face of the concrete buttress. Additionally, the flared AGT configuration increases the effective impact angle resulting in higher impact severity, larger system deflections, and greater loads imparted into the system when compared to a tangent installation. This contributes to a higher likelihood of excessive vehicle instabilities and accelerations. Criteria such as vehicle stability, occupant impact velocity, and occupant ridedown acceleration were evaluated for each simulation to assess the barrier's ability to safely contain and redirect the impacting vehicle.

Although not criteria with defined limits, post and guardrail deflections were measured for each simulation to quantify the increase in system deflection with flare rate, as greater system deflections could result in greater snag potential and larger exit angles. The post deflections were measured by tracking the displacement of a node on the top, back, center of each post, and the guardrail deflections were measured by tracking nodal displacements on the upper corrugation of the guardrail.

Additionally, during the CIP study, the deflections of the second post located upstream from the buttress (post no. 20) were measured relative to the flared guardrail in each of the simulations, as shown in Figure 63, and compared to evaluate the potential for excessive vehicle snag on the upstream end of the buttress. Large deflections of post no. 20 would expose the upstream face of the buttress and likely result in a greater propensity for vehicle interaction with the rigid buttress and larger occupant risk values.

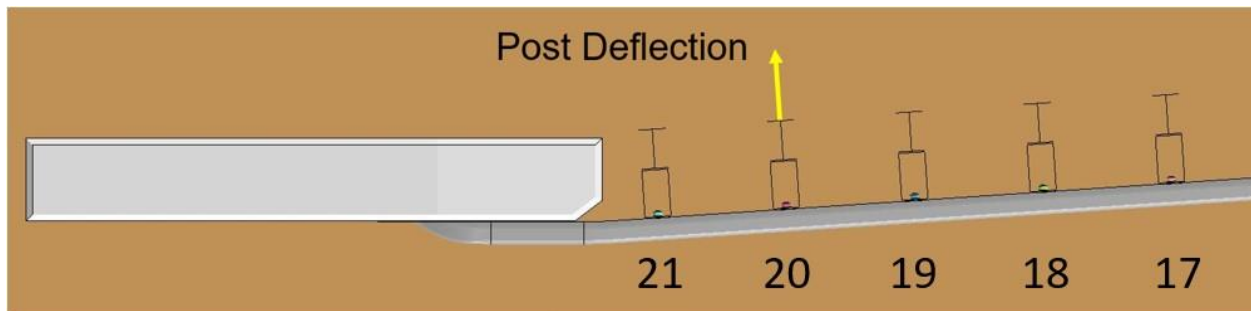


Figure 63. Post No. 20 Deflection Measurement

The larger system deflections that result from the increased effective impact angles of flared installations can create larger rail pocketing angles. The pocketing angle has been defined as the angle between the guardrail region just in front of the impacting vehicle and the downstream section of the rail, as shown in Figure 64 [14]. Large deflections and pocketing angles can affect the ability of the installation to perform as desired and may result in excessive occupant risk values. Previously, MwRSF reviewed many guardrail and AGT tests involving the 2000P vehicle, the standard pickup truck in NCHRP Report 350, and estimated the critical pocketing angle to be approximately 23 degrees [25]. However, it is believed that the larger 2270P vehicle of MASH 2016 is more stable than the 2000P vehicle and would have a critical pocketing angle closer to 30 degrees [14].

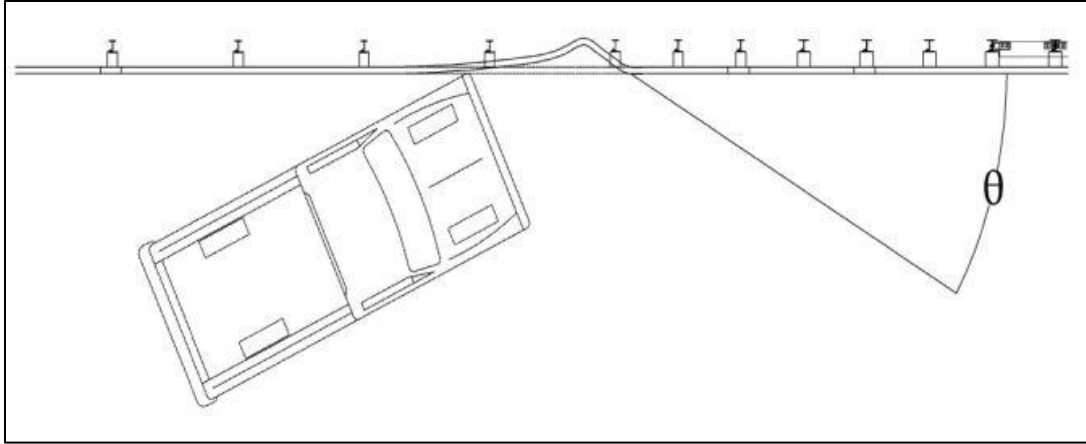


Figure 64. Critical Pocketing Angle [14]

Throughout the simulation study, the pocketing angles were measured to determine how much the pocketing angle changed for each flare rate when compared to the tangent system. Pocketing angles were measured and recorded by tracking the relative displacement of two nodes located on the center corrugation of the guardrail spaced at approximately 19-in. (483-mm) intervals.

The lateral overlap of the impacting tire across the upstream face of the standardized concrete buttress was measured with respect to the tangent roadway to gauge the propensity for wheel snag on the upstream face of the buttress. As illustrated in Figure 65, the lateral tire overlap was measured from the traffic face of the buttress to the tire node that extended the farthest laterally across the upstream face of the buttress. The measurement was recorded at the final plot state prior to the tire contacting the rigid buttress, or when the tire was approximately 26 in. (660 mm) upstream from the buttress. Note that the measurements were recorded from the saved plot states. Thus, variation of the longitudinal position of the tire measurement upstream from the buttress occurred due to the save frequency of the plot states (10 ms) and the deformed shape of the tire. In the simulations that modeled suspension failure, the wheel was detached at the time of measurement, but remained within the wheel well.

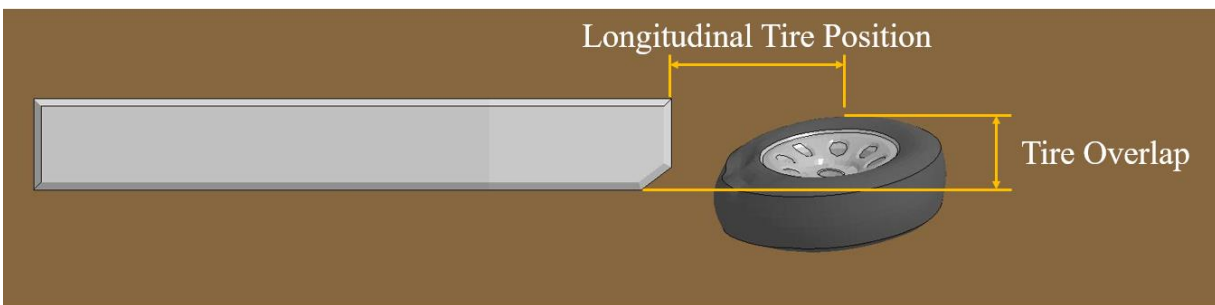


Figure 65. Tire-Buttress Overlap Measurement

It is important to note that the Ram vehicle model's tire is modeled differently than the Silverado vehicle model's tire and, as a result, exhibits significantly more deformation, as shown in Figure 66. The Silverado tire model is constructed with purely-elastic shell elements that model

the tire tread and sidewalls, while the Ram tire model is constructed with elastic-plastic shell elements that model the tire tread and sidewalls, and with plastically deformable beam elements that model the steel belts and body plies of the tire. Additionally, deflation of the tire is not modeled in either tire model. Thus, the deformed shapes of the modeled tires likely are not realistic, but can provide a general trend of how the tire overlap changes with respect to flare rate and impact point.

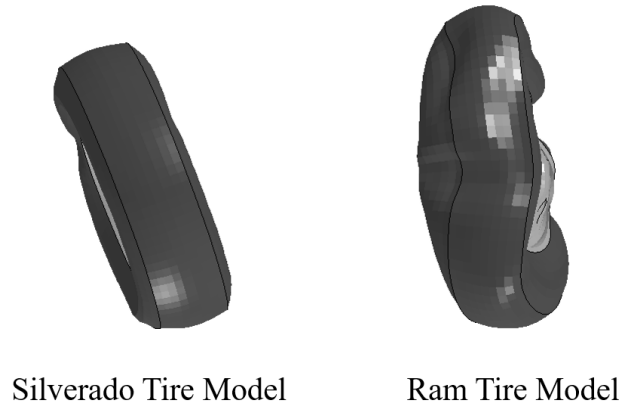


Figure 66. Deformed 2270P Tire Model Comparison

Vehicle stability was evaluated by measuring the roll, pitch, and yaw of the vehicle during the impact event. According to the criteria outlined in MASH 2016, maximum roll and pitch values should not exceed ± 75 degrees [4]. Occupant risk criteria, which includes longitudinal and lateral ORA as well as longitudinal and lateral OIV, were calculated at the center of gravity of the vehicle model. MASH 2016 states that the OIV values should fall below 40 ft/s (12.2 m/s) and that the ORA values should fall below the maximum value of 20.49 g's [4]. The occupant risk criteria and Euler angle data were recorded from the local accelerometer node at the model center of gravity. Other MASH 2016 evaluation criteria, such as occupant compartment crush, were not explicitly measured in the simulations.

6.3 Determination of Critical Flare Rates

Two series of LS-DYNA simulations were run with a 2270P vehicle model impacting the flared AGT installations. In the first series, the 2007 Chevrolet Silverado vehicle model was used to evaluate the various flare rates. Although the Silverado impact with the tangent installation was not successfully validated with the full-scale test, it was used during the initial flared study to examine the trends associated with flaring the AGT. Discrepancies between the Silverado simulation and full-scale test were considered during the flared simulation analysis. The second series of flared AGT simulations utilized the 2018 Dodge Ram vehicle model and included updates to the transition post dimensions and material properties.

The 2270P vehicle model remained in the same initial position, with the right-front corner of the bumper located approximately 93 in. (2,361 mm) upstream from the buttress and 6 in. (152 mm) laterally in front of the traffic-side face of the buttress, and the guardrail was adjusted as necessary for each of the preliminary flared simulations with the both the Silverado and Ram vehicle models. As a result, the traffic face of the guardrail moved farther from the front bumper of the vehicle and the impact point shifted downstream as the flare rate was increased, as illustrated

in Figure 67. The vehicle’s position was not adjusted to maintain a uniform vehicle impact point relative to the buttress for each investigated flare rate.

As shown in Table 23, the initial impact point for the tangent installation shifted approximately 19 in. (483 mm) downstream when the steepest flare rate was evaluated. Thus, it is likely that some variation in the vehicle’s interaction with the installation occurred due to the variation in impact point on the nested thrie-beam relative to the buttress. This concept is illustrated in Figure 67, which depicts the impact point’s longitudinal shift X between the tangent installation and the 10:1 flared installation.

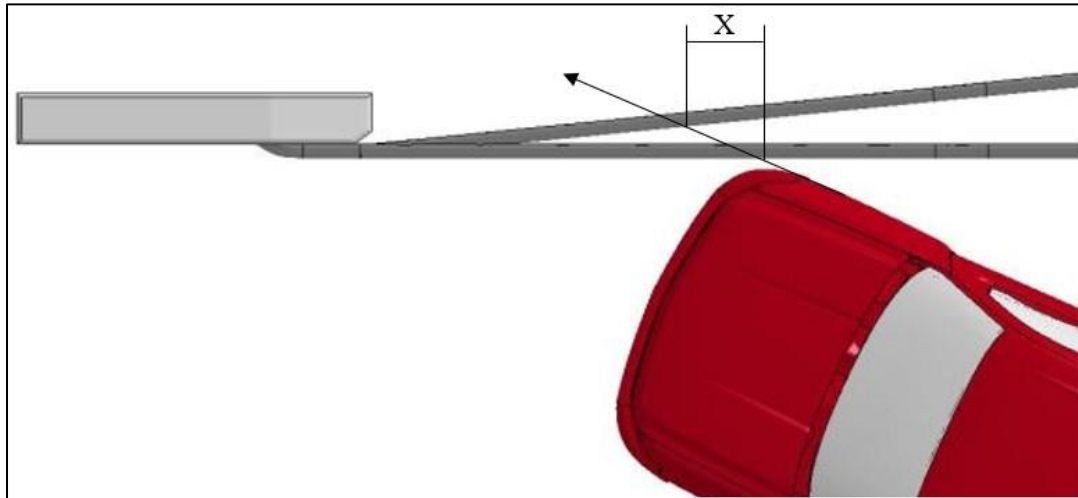


Figure 67. Flared Simulation Impact Point Shift, Tangent vs. 10:1 Flare Rate

Table 23. Critical Flare Rate Study Impact Locations

Flare Rate	Tangent	25:1	20:1	15:1	12.5:1	10:1
Impact Location* in. (mm)	89.0 (2,261)	80.2 (2,037)	77.1 (1,958)	75.1 (1,908)	74.2 (1,885)	70.2 (1,783)

*Impact location measured upstream from end of buttress tangent to flared guardrail

6.3.1 Silverado Flare Rate Analysis

In the initial series of flared AGT simulations, six simulations were run: the tangent installation and each of the five investigated flare rates. The simulations used the Silverado vehicle model and the AGT installation, which utilized W6x9 posts with a yield stress of 47 ksi (324 MPa). Parameters including Euler angles, occupant risk values, system deflections, pocketing angle, and tire-buttress overlap were evaluated for each of the simulations.

In the first series of flared AGT simulations, the reduced-element, 2270P Silverado vehicle model impacted each of the flared AGT installations at a speed of 62.7 mph (100.8 km/h). The effective impact angle relative to the transition system ranged from 25 degrees for the tangent installation to 30.7 degrees for the installation installed with a 10:1 flare. A summary of the results for the preliminary flared simulations is contained in Table 24.

Table 24. Summary of Flared Simulation Results with Silverado Vehicle Model

Evaluation Criteria		AGTB-2	Tangent	25:1	20:1	15:1	12.5:1	10:1	MASH 2016 Limits
OIV ft/s (m/s)	Longitudinal	-20.3 (-6.2)	-26.3 (-8.0)	-31.3 (-9.6)	-32.4 (-9.9)	-33.6 (-10.3)	-35.2 (-10.7)	-37.9 (-11.6)	±40 (12.2)
	Lateral	24.6 (7.5)	26.7 (8.1)	27.4 (8.4)	27.3 (8.3)	27.3 (8.3)	27.0 (8.2)	26.9 (8.2)	±40 (12.2)
ORA g's	Longitudinal	-7.1	-12.1	-14.2	-17.0	-18.1	-21.6	-24.3	±20.49
	Lateral	10.4	11.0	17.1	16.3	14.5	7.2	9.7	±20.49
Maximum Angular Displacement degrees	Roll	21.3	29.1	25.5	16.4	26.1	10.6	11.4	±75
	Pitch	6.3	6.1	8.4	4.8	6.5	4.4	7.6	±75
	Yaw	39.6	39.4	44.1	46.6	55.5	26.6	36.5	not required
Peak System Deflection in. (mm)		5.4 (136)	5.0 (126)	5.9 (150)	6.0 (153)	6.9 (175)	7.4 (189)	8.1 (206)	-
Peak Pocketing Angle degrees		-	7.1	12.3	13.5	16.2	18.3	21.4	-

The processed simulation results revealed clear trends in the evaluated parameters that correlated with the increasing flare rate. The lateral ORA reached a peak value of 17.1 g's at the 25:1 flare rate and then decreased as the flare rate increased, likely due to the vehicle having to yaw to a larger angle for tail-slap to occur. As illustrated in Figure 68, the longitudinal OIVs and ORAs increased as the flare rate became greater. The two steepest flare rates, 12.5:1 and 10:1, exhibited longitudinal ORA values of -21.6 g's and -24.3 g's, respectively, which exceeded the MASH 2016 limit of ±20.49 g's. However, the tangent simulation overpredicted the longitudinal ORA and longitudinal OIV by 5.0 g's and 6.1 ft/s (1.8 m/s), respectively, when compared to the full-scale test. Thus, it is possible that the longitudinal occupant risk values for the flared installations may also overpredict the physical test values.

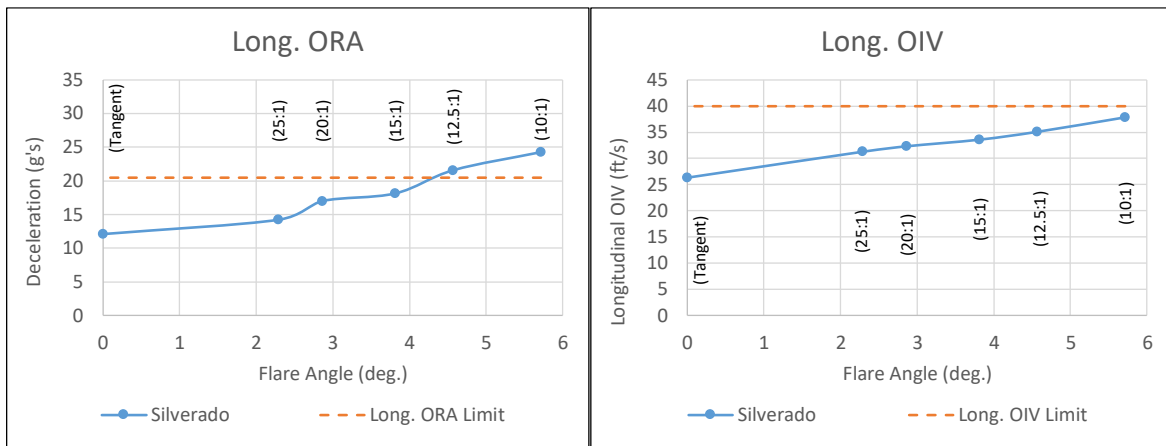


Figure 68. Flared Silverado Longitudinal Occupant Risk

The peak dynamic deflections and pocketing angles were presented in Table 24. The peak dynamic deflections ranged from 5.0 in. (126 mm) in the tangent simulation to 8.1 in. (206 mm) in the 10:1 flared simulation. The peak pocketing angles ranged from 7.1 degrees with the tangent simulation to 21.4 degrees with the 10:1 flared simulation. As shown in Figure 69, the measured tire-buttruss overlap exhibited the same increasing trend as the flare rate was increased.

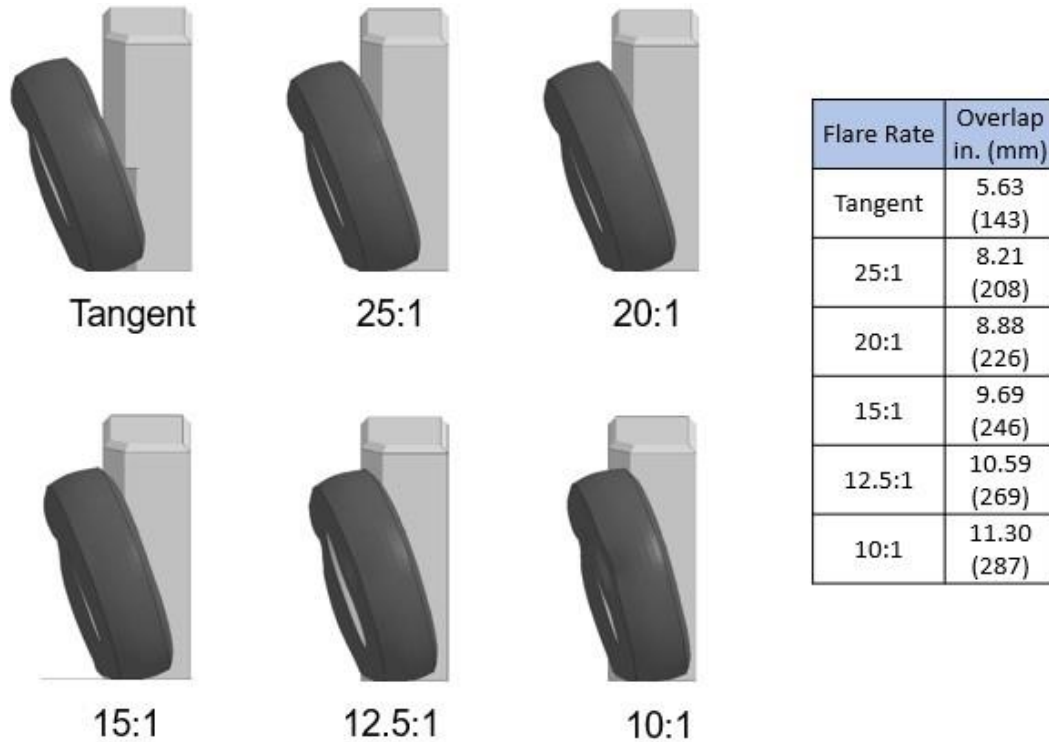


Figure 69. Flared AGT Comparison of Silverado Tire-Buttruss Overlap

Several shortcomings were present with the flared Silverado simulations. The baseline tangent model only met the V&V requirements with several exceptions, including the model overpredicting the longitudinal occupant risk values. As a result, it was believed that the flared simulations may also overpredict the longitudinal occupant risk criteria. Additionally, the Silverado vehicle model was geometrically different than the Ram vehicle used in full-scale crash testing, which could lead to additional discrepancies. Also, the disengagement of the vehicle’s right-front wheel was not modeled, and this may have contributed to the additional ridedown accelerations due to wheel snag. Although an additional model that included right-front wheel disengagement was modeled for the baseline tangent installation, it did not result in improved correlation and wheel detachment was not pursued further with the Silverado vehicle model.

6.3.2 Ram Flare Rate Analysis

The second series of flared AGT simulations utilized the 2018 Dodge Ram vehicle model and the validated AGT model complete with updates to the transition post dimensions and material properties, i.e., W6x8.5 post geometry with a 56-ksi (386-MPa) yield strength. The initial validation of the tangent AGT with the Ram vehicle model included suspension failure, which led

to the detachment of the right-front wheel. For consistency, suspension failure was not modeled during the flare rate study, but was considered in subsequent detailed simulations.

In the series of flared AGT simulations, the 2270P Ram vehicle model impacted each of the flared AGT installations at a speed of 62.1 mph (100 km/h) and did not include detachment of the right-front wheel. The effective impact angles relative to the transition system ranged from 25 degrees for the tangent installation to 30.7 degrees for the installation with a 10:1 flare.

The simulation with the 10:1 flared AGT did not run to the desired simulation completion time. During the simulation, the vehicle’s right-front fender and hood penetrated the non-traffic side of the buttress due to modeling simplifications. This resulted in model instabilities and early termination at 160 ms. Although the simulation did not run to completion, the OIV values were recorded from the impact, since the simulation ran past the t^* value of 99.1 ms. However, the simulation terminated prior to tail slap and, as a result, the ORA values may be inaccurate. A summary of the results for the Ram flared AGT simulations is contained in Table 25. Sequential images of the Ram flared AGT simulations and test no. AGTB-2 are shown in Figure 70.

Table 25. Summary of Flared Simulation Results with Ram Vehicle Model

Evaluation Criteria		AGTB-2	Tangent	25:1	20:1	15:1	12.5:1	10:1*	MASH 2016 Limits
OIV ft/s (m/s)	Longitudinal	-20.3 (-6.2)	-21.0 (-6.4)	-25.8 (-7.9)	-25.7 (-7.9)	-27.3 (-8.3)	-29.6 (-9.0)	-31.8 (-9.7)	±40 (12.2)
	Lateral	24.6 (7.5)	27.2 (8.3)	27.0 (8.2)	27.3 (8.3)	28.6 (8.7)	29.0 (8.8)	29.2 (8.9)	±40 (12.2)
ORA g’s	Longitudinal	-7.1	-6.4	-9.7	-9.5	-13.1	-11.7	-14.0	±20.49
	Lateral	10.4	8.2	12.0	12.0	11.0	12.8	12.3	±20.49
Maximum Angular Displacement Degrees	Roll	21.3	26.5	19.5	19.1	16.6	17.4	4.0	±75
	Pitch	6.3	7.2	7.3	7.5	5.0	8.1	-2.9	±75
	Yaw	39.6	42.7	48.4	46.7	47.8	57.3	14.2	not required
Peak System Deflection in. (mm)		5.4 (136)	4.5 (115)	6.5 (166)	7.3 (186)	7.2 (184)	9.4 (239)	10.1 (257)	-
Peak Pocketing Angle degrees		-	5.8	12.4	15.6	15.1	20.9	23.0	-

* Simulation terminated prematurely at $t = 160$ ms

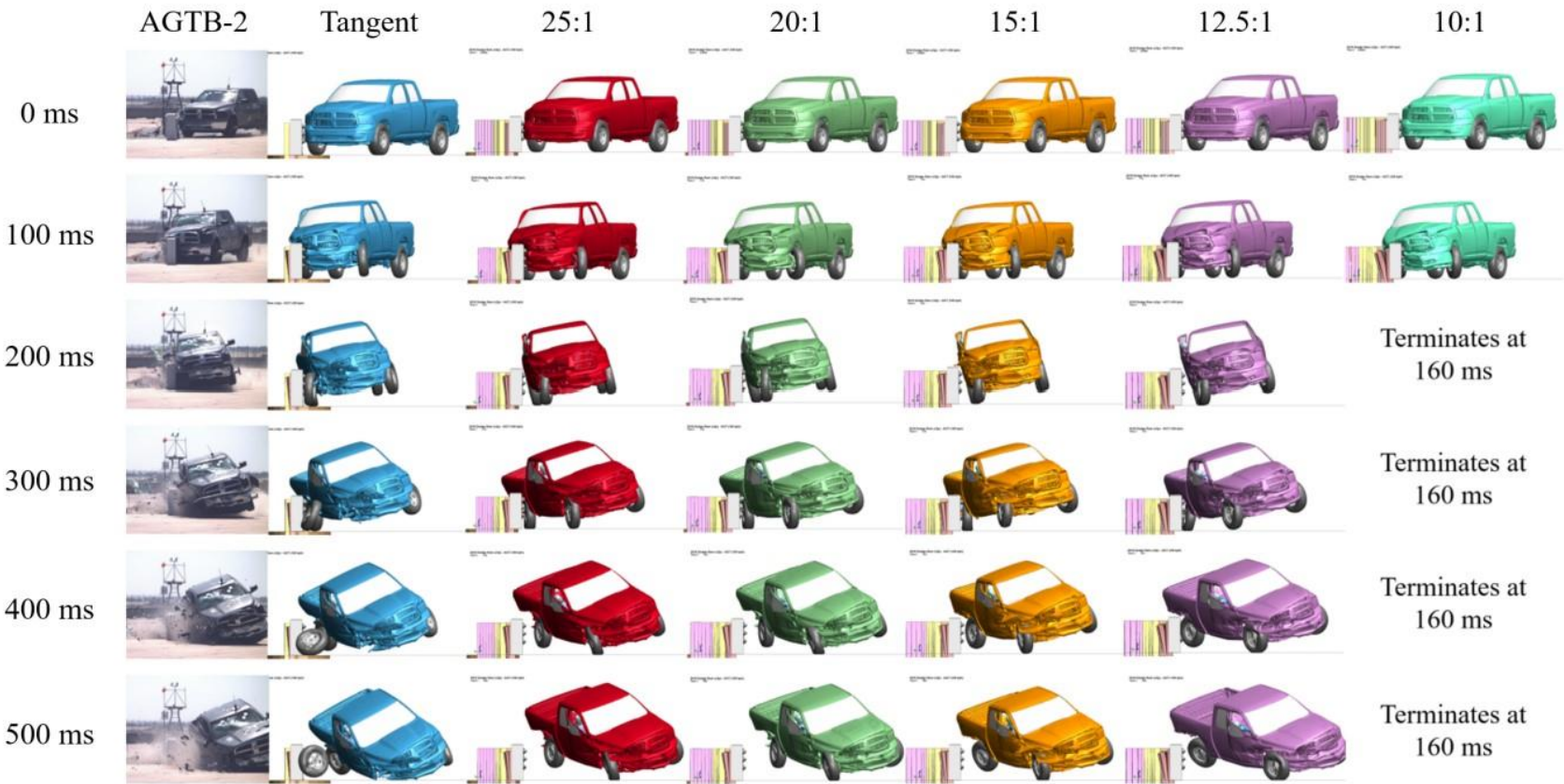


Figure 70. Flare Rate Study Sequential Photographs, Ram Vehicle Model

The processed simulation results revealed trends in the evaluated parameters that correlated with flare rate. As illustrated in Figure 71, the longitudinal OIVs and ORAs generally increased in magnitude as the flare rate became greater. The two steepest flare rates, 12.5:1 and 10:1, exhibited longitudinal ORA values of -11.7 g's and -14.0 g's, respectively, which did not exceed the MASH 2016 limit of ± 20.49 g's and did not reflect the larger longitudinal ORAs observed for the same flare rates with the Silverado vehicle model. The two steepest flare rates, 12.5:1 and 10:1, exhibited longitudinal OIV values of -29.6 ft/s (-9.0 m/s) and -31.8 ft/s (-9.7 m/s), respectively, which did not exceed the MASH 2016 limit of ± 40 ft/s (12.2 m/s).

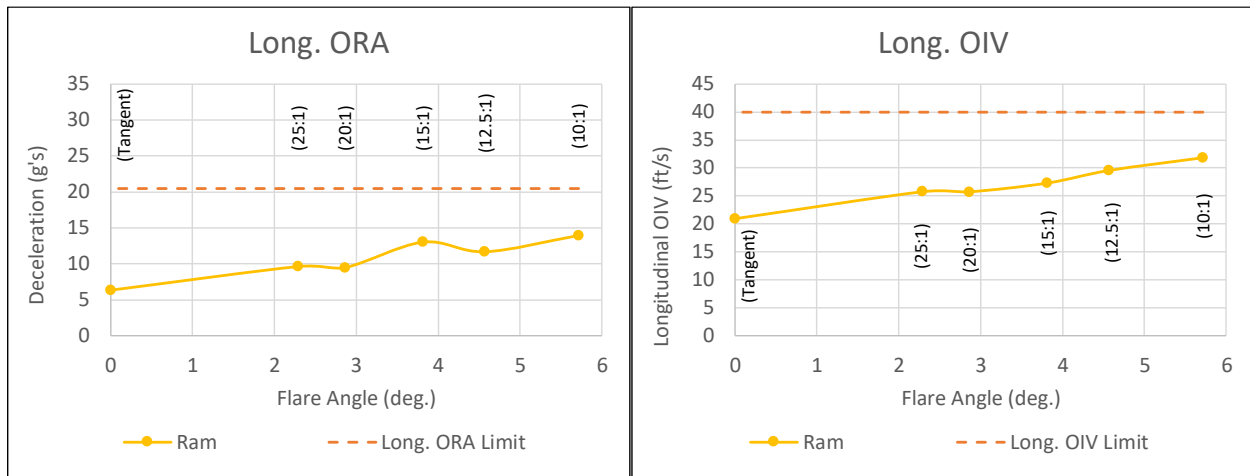


Figure 71. Flared Ram Longitudinal Occupant Risk

The peak dynamic deflections and pocketing angles, presented in Table 25, generally increased with the flare rate. The peak dynamic deflections ranged from 4.5 in. (115 mm) in the tangent simulation to 10.1 in. (257 mm) in the 10:1 flared simulation. The peak pocketing angles ranged from 5.8 degrees with the tangent simulation to 23.0 degrees with the 10:1 flared simulation. The lateral overlap of the impacting tire across the upstream face of the standardized concrete buttress was measured with respect to the tangent roadway to gauge the propensity for wheel snag. As shown in Figure 72, the measured tire-buttress overlap exhibited the same general increasing trend as the flare rate increased.

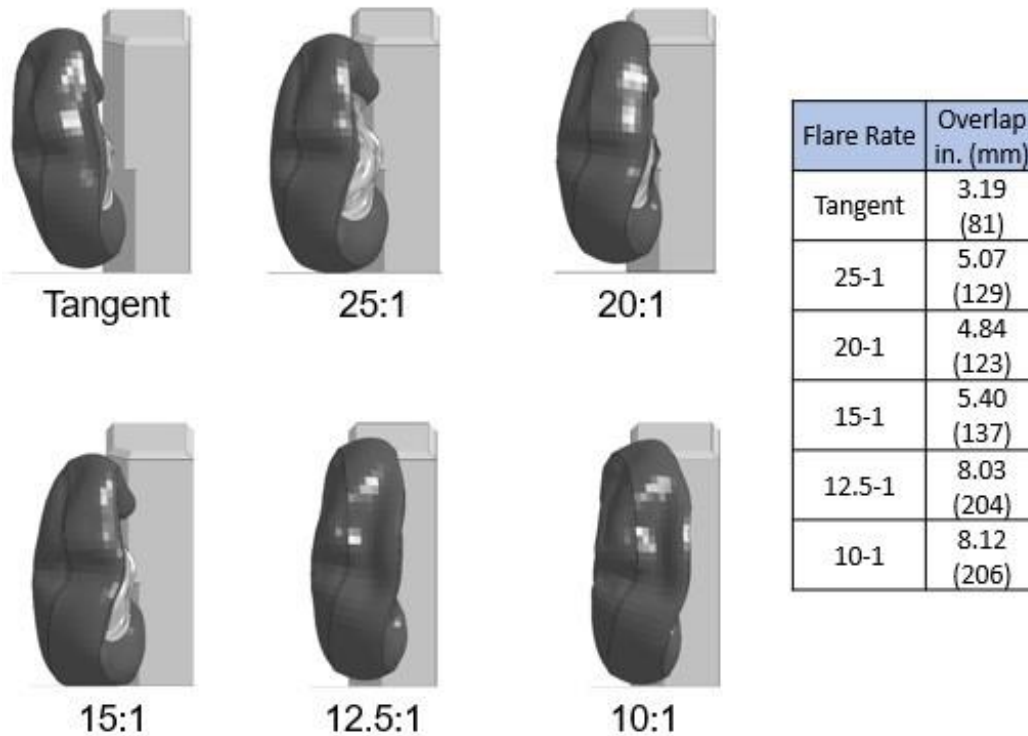


Figure 72. Flared AGT Comparison of Ram Tire-Buttress Overlap

The simulated Ram vehicle model impacts with the flared AGTs provided additional insight into the relationship between installation flare rate and crashworthiness. In general, the evaluation criteria values increased in magnitude as the flare rate increased. Thus, an increase in the flare rate also increases the likelihood of occupant injury and failure of the installation to meet MASH 2016 safety performance criteria. The data collected from the preliminary Ram simulations, in addition to the Silverado simulations, enabled the selection of critical AGT flare rates for further evaluation.

6.3.3 Critical Flare Rate Selection

The preliminary simulated impacts with the Dodge Ram and Chevrolet Silverado vehicle models exhibited clear trends indicating that an increase in the flare rate of the installation reduces the probability of satisfying evaluation criteria. An evaluation of the occupant risk factors coupled with the estimated LON reduction for each studied flare rate was performed to select two critical flare rates for further consideration.

The OIV and ORA values for the tangent installation and each of the flared installations are shown in Figures 73 and 74 for both the Silverado and Ram vehicle models. Note that the lateral occupant risk values were not a primary concern when determining the critical flare rate, as they remained relatively constant and did not exceed MASH 2016 limits at lower flare rates and decreased in magnitude at the larger flare rates. The 25:1, 20:1, and 15:1 flared installations successfully met the occupant risk criteria with both vehicle models. The 25:1 and 20:1 flared installations resulted in LON reductions of 67.2 ft (20.5 m) and 78.1 ft (23.8 m), respectively.

Although beneficial, the magnitudes of LON reduction for these two flare rates were significantly lower than the reductions associated with the steeper flare rates. Thus, the lowest two flare rates were not determined to be critical and were eliminated from further consideration.

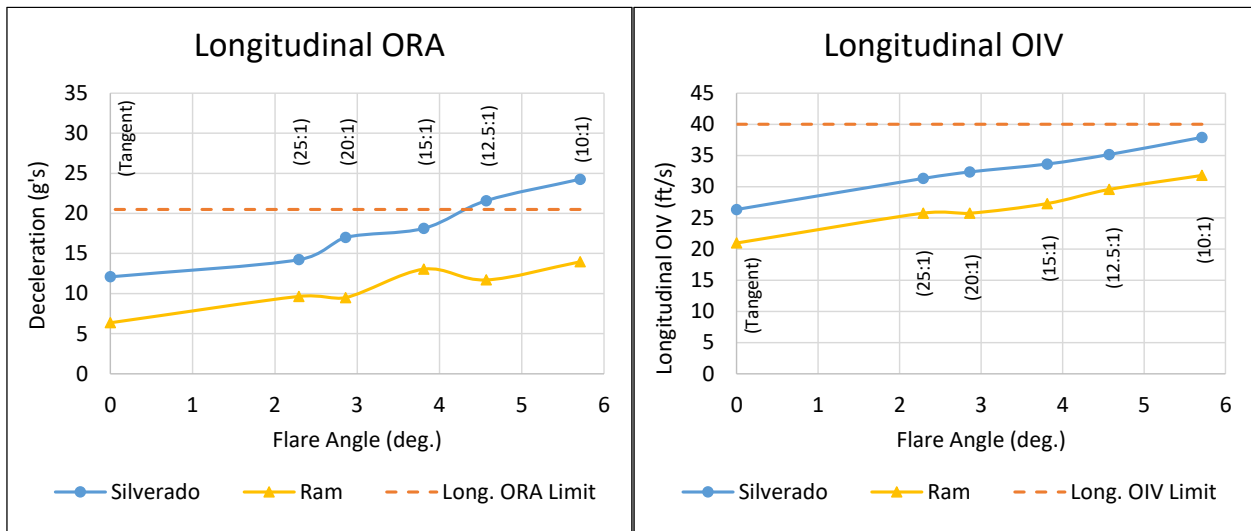


Figure 73. Flared AGT Longitudinal Occupant Risk

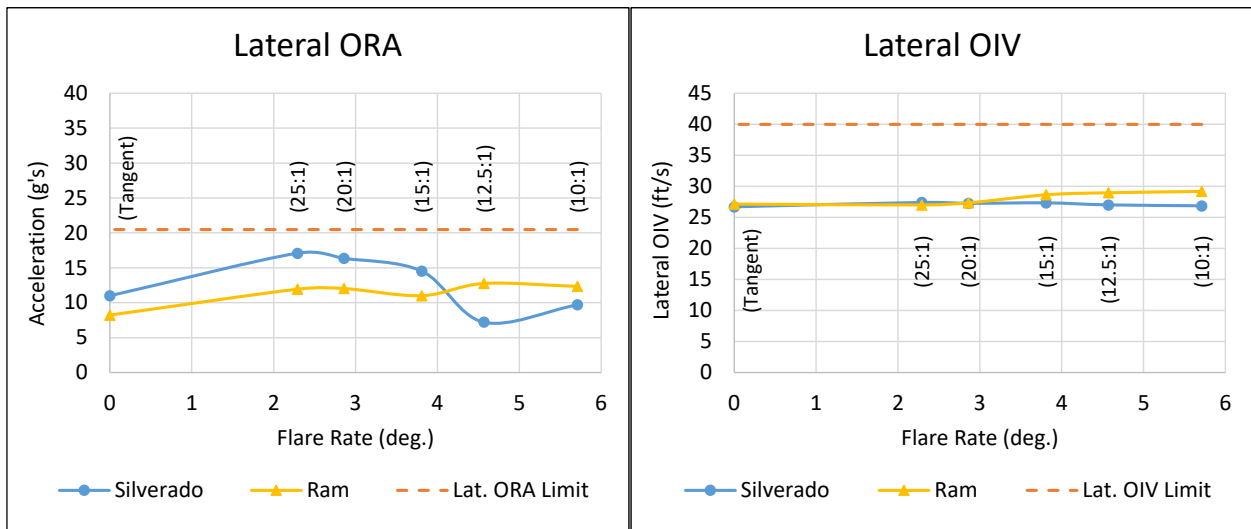


Figure 74. Flared AGT Lateral Occupant Risk

The 10:1 flared installation, when impacted with the Silverado vehicle model, exhibited a longitudinal ORA value that did not meet the MASH 2016 safety performance criteria. Although the occupant risk values in the Ram model did not exceed MASH 2016 safety performance criteria, they were larger than for other flare rates studied. As the steepest studied flare rate, the 10:1 flare rate offered the largest LON reduction of 115.2 ft (35.1 m). However, due to the excessive longitudinal ORA of -24.3 g's with the Silverado, coupled with the largest system deflections, tire overlaps with the buttress, pocketing angles, and longitudinal OIV values, the 10:1 flare rate had a low potential to satisfy MASH 2016 safety performance criteria.

The 15:1 and 12.5:1 flare rates exhibited the greatest balance between LON reduction and occupant risk. The 15:1 flare was the steepest flare rate that met the longitudinal occupant risk criteria with both the Silverado and Ram vehicle models. The 15:1 flare rate resulted in a LON reduction of 93.1 ft (28.4 m).

The 12.5:1 flare was also identified as a potential, more aggressive, critical flare rate. The 12.5:1 flare resulted in a 103.0-ft (31.4-m) reduction of the LON, or an approximately 10 ft (3 m) larger LON reduction than the 15:1 flared installation. Although the MASH 2016 longitudinal ORA criterion was exceeded in the Silverado simulation at the 12.5:1 flare rate by 1.1 g's, it is possible that this represents an overprediction of the physical value based on the tangent simulation with the Silverado vehicle, where the longitudinal ORA was overpredicted by 5.0 g's and the impacting tire remained attached throughout the impact event.

Thus, the 15:1 and the 12.5:1 flare rates were identified as the two critical flare rates. The occupant risk values for both flare rates exhibited a high probability of meeting MASH 2016 safety performance criteria while providing a substantial reduction in the LON of a guardrail installation.

6.4 Critical Impact Point (CIP) Studies

To further evaluate the performance of the 15:1 and 12.5:1 flare rates, CIP studies were performed with the 2270P (Ram) and 1100C (Yaris) vehicle models at the downstream end of the transition to identify the impact location, that would provide the most severe impact scenario. The 2270P CIP study utilized the same Ram vehicle model that was used to identify the critical flare rates, while a 2010 Toyota Yaris vehicle model, originally developed by the National Crash Analysis Center at the George Washington University, was used during the 1100C CIP study [26].

6.4.1 2270P CIP Study

The CIP study was conducted using the Ram vehicle model to identify the critical impact location for the 15:1 and 12.5:1 flared installations that would result in the greatest likelihood of test failure. Several factors were considered when selecting the installation CIP, including occupant risk, Euler angles, system deflections, and propensity for vehicle snag on the buttress.

In each simulation, the Ram vehicle model impacted the flared AGT installation at a speed of 62.1 mph (100 km/h) and at an angle of 25 degrees relative to the roadway. Eight impact points spaced at 9-in. (229-mm) intervals were selected in addition to the initial impact point, X, for each flare rate, resulting in nine impact locations along the AGT. Four impact points were selected downstream of the initial impact point (denoted DS1 through DS4) and four impact points were selected upstream (denoted US1 through US4), as shown in Figure 75. The impact locations relative to the buttress are summarized for the 15:1 and 12.5:1 flared installations in Table 26.

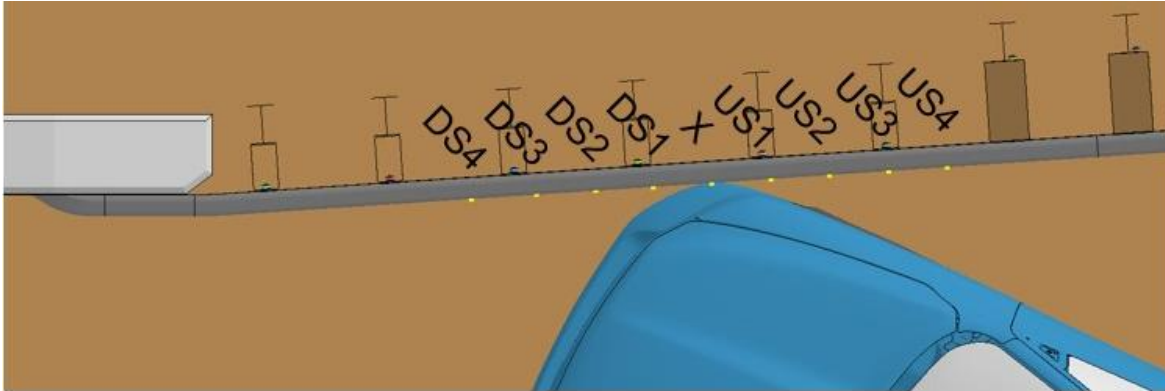


Figure 75. 2270P CIP Study Impact Locations

Table 26. Summary of 2270P CIP Study Impact Locations

Flare Rate	Impact Location in. (mm)								
	DS4	DS3	DS2	DS1	X	US1	US2	US3	US4
15:1	39 (991)	48 (1,219)	57 (1,448)	66 (1,676)	75 (1,905)	84 (2,134)	93 (2,362)	102 (2,591)	111 (2,819)
12.5:1	38 (965)	47 (1,194)	56 (1,422)	65 (1,651)	74 (1,880)	83 (2,108)	92 (2,337)	101 (2,565)	110 (2,794)

*Impact location measured upstream from end of buttress tangent to flared guardrail

In the initial series of 2270P CIP study simulations of the 15:1 and 12.5:1 flare rates, tire detachment was not modeled in order to estimate suspension joint failure times based on examining part forces and contact. Several simulations exhibited snagging on the buttress due to buttress modeling simplifications. As shown in Figure 76, a single element was initially used to simplify the chamfer on the top non-traffic-side edge of the buttress, which enabled the penetration of the right-front fender through the top of the buttress and resulted in model instabilities and early termination. Thus, complete analysis could not be performed on the initial series of CIP study simulations. However, each simulation ran long enough to measure the forces in the vehicle’s upper control arm, lower control arm, and steering arm joints during the initial impact with the AGT installation. The measured joint forces enabled the determination of the estimated failure time for the suspension components resulting in wheel detachment.

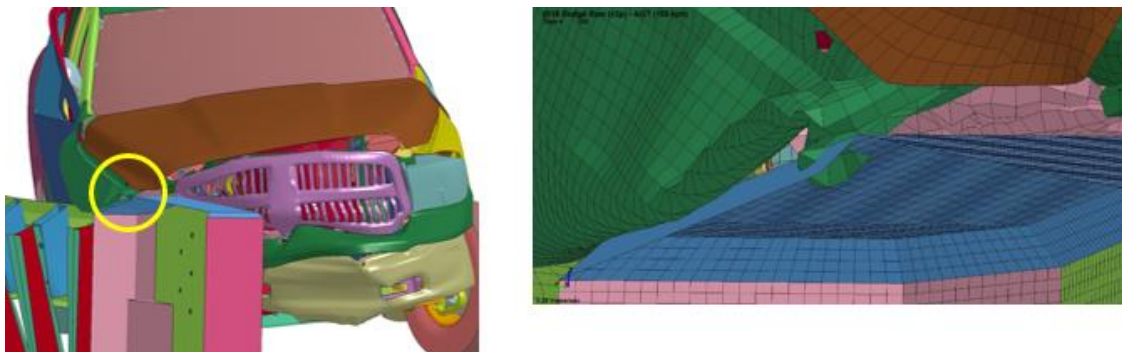


Figure 76. Fender-Buttress Penetration – 15:1 Flare Rate at US3 Impact Location

Suspension failure and wheel detachment were modeled by assigning a failure time to the upper control arm, lower control arm, and steering arm joints that connected the suspension to the right-front wheel. In the tangent AGT simulation, the lower control arm joint failed at 30 ms, the upper control arm joint failed at 35 ms, and the steering arm joint failed at 40 ms after the start of the simulation. To calibrate the suspension joint failure times of the flared AGT simulations, the upper control arm, lower control arm, and steering arm joint forces in all nine CIP simulations were averaged individually by part in time throughout the simulations. The averaged forces in each joint were then compared to the respective joint forces at failure measured during the tangent simulation.

For example, at $t = 35$ ms the lower control arm joint force was measured in each of the nine 15:1 CIP simulations and averaged. This averaged lower control arm joint force was then compared to the lower control arm joint force measured at the time of failure in the tangent simulation (30 ms after the start of the simulation). Failure times for each of the suspension joints were selected such that the joints would fail when each of the averaged joint forces of the flared simulations reached a magnitude approximately equal to the joint forces measured at failure during the tangent simulation (32.5 kN in the lower control arm joint, 42.7 kN in the upper control arm joint, and 20.4 kN in the steering arm joint).

The joint force study found that when the lower control arm joint failed at 40 ms, the upper control arm joint failed at 45 ms, and the steering arm joint failed at 50 ms after the start of the simulation, the suspension joint forces in the flared simulations were representative of the joint forces at the time of failure in the tangent simulation. This effectively shifted the tangent suspension failure times by 10 ms, which accounted for the greater distance between the flared installation and the impacting corner of the vehicle, when compared to impacts with the tangent installation. The Ram vehicle model front suspension components are shown in Figure 77.

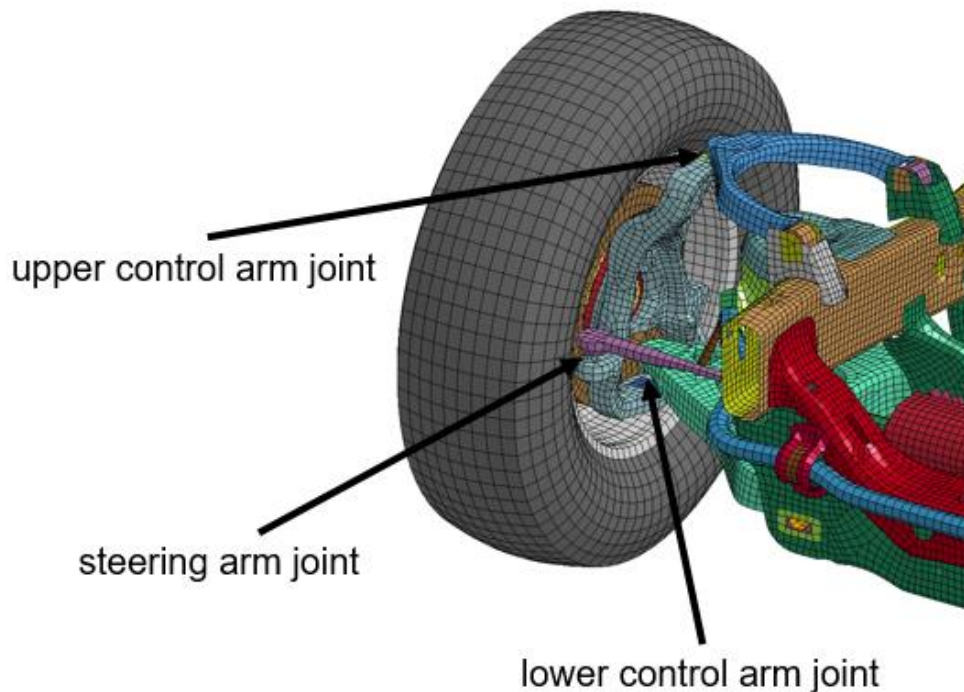


Figure 77. Ram Vehicle Model Right-Front Suspension Joints

To resolve the model instabilities, a refined buttress mesh with a smaller element size was added to the non-traffic-side of the buttress. The refined buttress mesh prevented the penetration of the vehicle hood and right-front fender, which eliminated the excessive, unrealistic buttress snag and enabled all simulations to run to completion except for one. The 12.5:1 flared simulation at impact point X had unresolvable errors and did not run to completion. Peak longitudinal occupant risk values were recorded from the impact, as the simulation ran past the t^* value of 97.3 ms, but the simulation terminated prior to tail slap and, as a result, the ORA values may be inaccurate.

In the second series of flared AGT CIP study simulations, the 2270P Ram vehicle model impacted each of the flared AGT installations at a speed of 62.1 mph (100 km/h). These simulations included the vehicle’s right-front suspension failure and wheel detachment at the failure time determined by the joint force study. The effective impact angles with respect to the guardrail system were 28.8 degrees with the 15:1 flared installation and 29.6 degrees with the installation installed with a 12.5:1 flare. Summaries of the results for the 15:1 and 12.5:1 flared CIP studies are contained in Tables 27 and 28, respectively, and sequential images are presented in Appendix D.

Table 27. Summary of 2270P Ram 15:1 Flared AGT CIP Study

Impact Location US from Buttress Tangent to Rail in. (mm)		39 (991)	48 (1,219)	57 (1,448)	66 (1,676)	75 (1,905)	84 (2,134)	93 (2,362)	102 (2,591)	111 (2,819)	MASH 2016 Limits
Evaluation Criteria		DS4	DS3	DS2	DS1	X	US1	US2	US3	US4	
OIV ft/s (m/s)	Long.	-23.0 (-7.0)	-25.7 (-7.8)	-26.3 (-8.0)	-27.0 (-8.2)	-27.3 (-8.3)	-27.8 (-8.5)	-26.0 (-7.92)	-24.4 (-7.5)	-23.1 (-7.1)	±40 (12.2)
	Lateral	27.0 (8.2)	28.6 (8.7)	29.0 (8.8)	30.0 (9.1)	28.3 (8.6)	25.9 (7.9)	25.2 (7.7)	24.9 (7.6)	24.7 (7.5)	±40 (12.2)
ORA g’s	Long.	-5.5	-4.7	-9.2	-13.5	-12.3	-14.6	-13.9	-14.4	-13.2	±20.49
	Lateral	6.7	7.0	8.0	7.6	10.8	13.6	14.8	13.0	12.7	±20.49
Maximum Angular Displacement degrees	Roll	-7.7	10.1	12.3	17.6	19.9	23.5	27.2	32.2	38.8	±75
	Pitch	6.0	7.0	4.5	6.1	5.6	8.3	8.8	10.3	10.4	±75
	Yaw	37.7	41.8	46.5	51.7	49.5	57.0	54.1	58.7	59.1	not required
Maximum Dynamic Deflection in. (mm)		1.4 (35)	2.4 (60)	3.6 (92)	5.0 (127)	6.5 (164)	9.2 (233)	10.7 (272)	11.7 (296)	12.3 (312)	N/A

Table 28. Summary of 2270P Ram 12.5:1 Flared AGT CIP Study

Impact Location US from Buttress Tangent to Rail in. (mm)		38 (965)	47 (1,194)	56 (1,422)	65 (1,651)	74 (1,880)	83 (2,108)	92 (2,337)	101 (2,565)	110 (2,794)	MASH 2016 Limits
Evaluation Criteria		DS4	DS3	DS2	DS1	X*	US1	US2	US3	US4	
OIV ft/s (m/s)	Long.	-23.7 (-7.2)	-25.3 (-7.7)	-26.4 (-8.0)	-27.8 (-8.5)	-29.7 (-9.1)	-28.3 (-8.6)	-27.8 (-8.5)	-25.3 (-7.7)	-24.1 (-7.4)	±40 (12.2)
	Lateral	27.2 (8.3)	29.3 (8.9)	30.3 (9.2)	30.5 (9.3)	29.5 (9.0)	27.5 (8.4)	25.4 (7.7)	24.9 (7.6)	24.9 (7.6)	±40 (12.2)
ORA g's	Long.	-5.0	-7.8	-10.2	-11.9	-12.3	-11.0	-16.0	-14.6	-13.0	±20.49
	Lateral	6.1	7.1	8.0	6.9	10.8	14.2	14.9	13.8	13.6	±20.49
Maximum Angular Displacement degrees	Roll	7.6	10.7	13.0	15.9	-6.0	25.6	30.3	32.8	39.0	±75
	Pitch	6.1	6.2	5.3	8.1	-4.0	8.3	9.9	8.9	9.3	±75
	Yaw	38.1	42.5	44.6	51.8	15.1	57.9	62.1	61.3	60.4	not require d
Maximum Dynamic Deflection in. (mm)		1.3 (34)	2.3 (57)	4.1 (103)	6.4 (162)	8.2 (207)	9.5 (242)	11.1 (283)	12.4 (314)	12.2 (310)	N/A

* Simulation at location X terminated prematurely at t = 160ms

For the 15:1 flare rate, the simulated impact at the US1 location resulted in the greatest longitudinal OIV and ORA values, with magnitudes of 14.6 g's and 27.8 ft/s (8.5 m/s), respectively. For the 12.5:1 flare rate, the greatest longitudinal ORA occurred at the US2 impact location with a magnitude of 16.1 g's and the greatest longitudinal OIV occurred at the X impact location with a magnitude of 29.7 ft/s (9.1 m/s). The vehicle roll, pitch, and yaw magnitudes were significantly lower for the downstream impact locations, when compared to the impact locations evaluated farther upstream. Additionally, for both flared installations, the greatest system dynamic deflections occurred at the two most upstream impact locations, US3 and US4.

Analysis of the CIP study results showed that the longitudinal occupant risk values and peak system deflections generally decreased as the impact point was shifted downstream, i.e., closer to the buttress. Due to the variable post spacing and rail section used in the AGT, the lateral stiffness of the installation decreased as the impact point shifted farther upstream from the rigid hazard. As a result, the upstream impact points generally produced larger system deflections, tire-buttress overlaps, and pocketing angles.

To select a CIP that would produce the greatest likelihood of test failure, three main parameters were considered: occupant risk, system deflection immediately upstream of the buttress, and vehicle angular displacements. The parameters were selected to gauge the propensity for vehicle snag on the upstream end of the rigid buttress and vehicle rollover, as well as to quantify the severity of the impact to the vehicle's occupants.

The longitudinal occupant risk values for the 15:1 flared and 12.5:1 flared CIP studies are shown in Figure 78. Due to the smaller magnitudes of occupant risk values exhibited by impact locations DS1 through DS4, impact points located downstream from the initial impact location were eliminated from CIP consideration. The largest longitudinal ORA and OIV values observed in the 15:1 flare CIP study were -14.6 g's and -27.8 ft/s (-8.5 m/s), respectively, and both measurements occurred at the US1 location. The location of the maximum longitudinal occupant risk values did not coincide in the 12.5:1 CIP study. The maximum longitudinal ORA of -16.0 g's occurred at the US2 location, and the maximum longitudinal OIV of -29.7 ft/s (-9.1 m/s) occurred at the initial impact point.

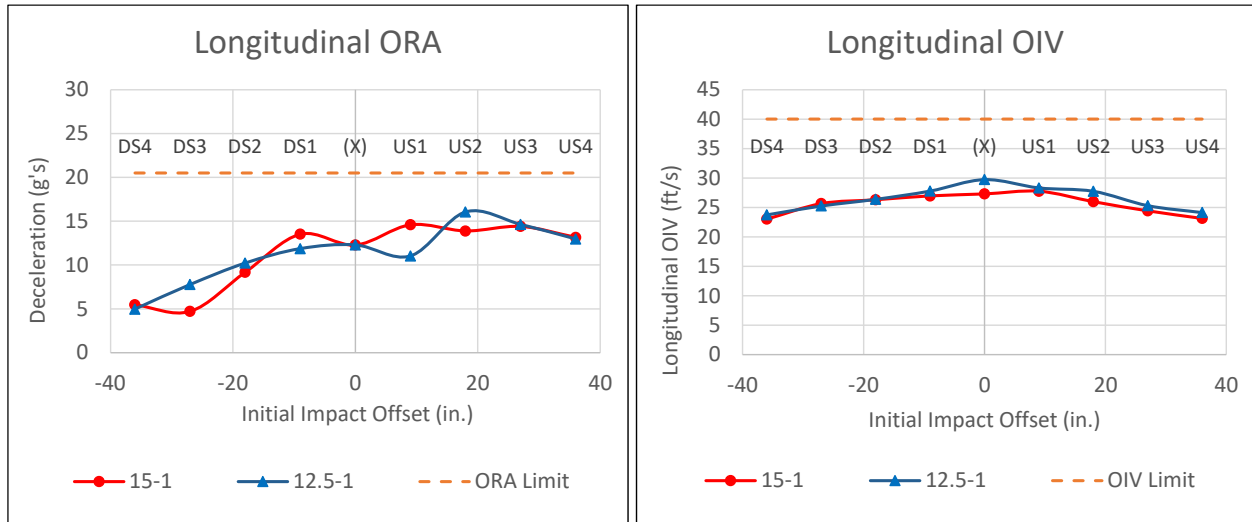


Figure 78. 2270P CIP Study Longitudinal Occupant Risk

The peak dynamic deflection of post no. 20 for each impact scenario is shown in Figure 79. Recall that post no. 20, shown in Figure 63, was adjacent to the parapet and was believed to be a good indicator of snag risk. The peak deflection of post no. 20 increased as the impact point shifted upstream. However, the post no. 20 deflections remained relatively constant after reaching the US1 impact location for the 15:1 flare CIP study and moderately increased from the initial impact location to the US3 impact location for the 12.5:1 flare CIP study.

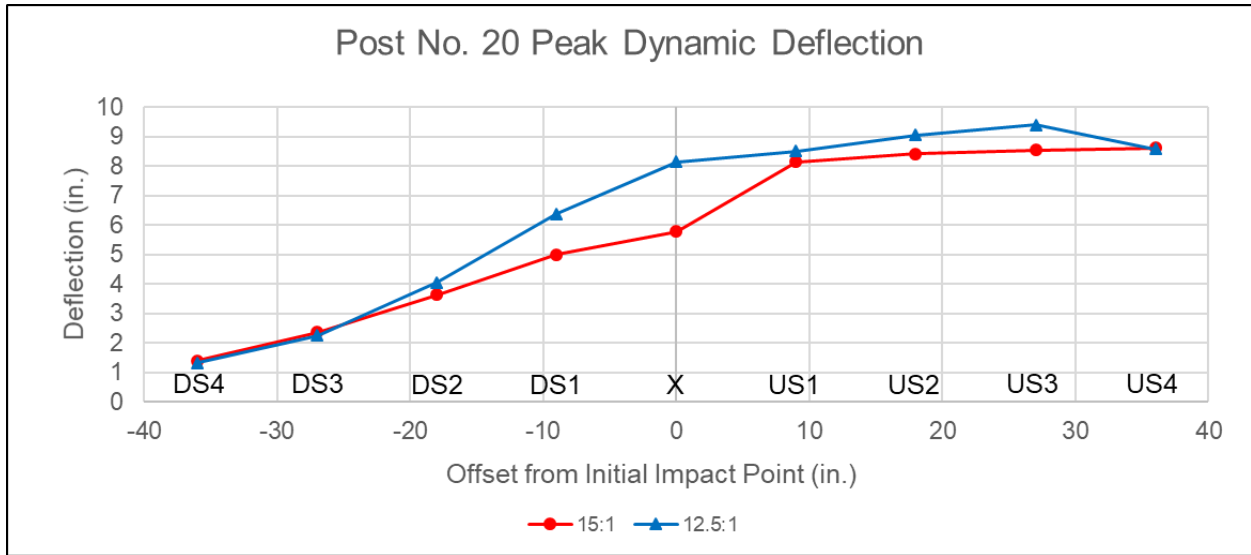


Figure 79. Post No. 20 Deflection

Vehicle stability was evaluated by measuring the roll, pitch, and yaw of the vehicle during the impact event. According to the criteria outlined in MASH 2016, maximum roll and pitch values should not exceed ± 75 degrees [4]. Extended simulation impact event run times of impact points US1 through US4 were conducted to allow proper time for the vehicle to exit the barrier and to evaluate the propensity for vehicle rollover. Plots of vehicle roll versus time are shown in Figure 80.

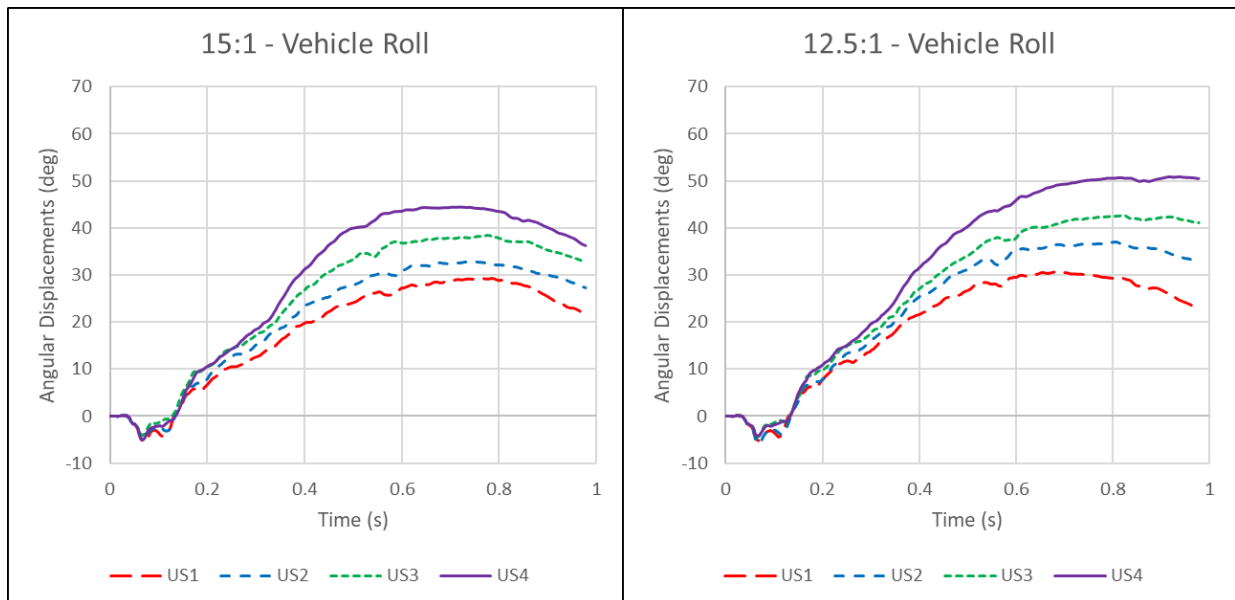


Figure 80. Euler Roll Angular Displacement – 15:1 (Left); 12.5:1 (Right)

For each impact location, the peak roll angle remained below the maximum threshold defined by MASH 2016. At each impact location, the magnitude of the roll increased when the flare rate was increased from 15:1 to 12.5:1, and the magnitude also increased as the impact

location moved upstream. All roll angles were decreasing in magnitude at the end of the simulations, which indicated that the vehicle models were stabilizing. Thus, no vehicle exhibited rollover. The US3 and US4 locations at the 12.5:1 flare rate exhibited the greatest probability of rollover due to the large magnitudes of roll angle and the relatively constant roll angle during the last 0.2 seconds of the simulation. The pitch angles did not approach the maximum threshold of ± 75 degrees, with peak pitch values of approximately 10 degrees.

It is likely that the behavior of the impacting tire has a significant effect on the stability of the vehicle during impacts with the flared transition. In the CIP study simulations, the detachment of the impacting right-front tire enabled the vehicle to continue to roll towards the barrier. If the wheel did not detach or remained within the wheel well after exiting the installation, it would likely reduce the magnitude of the vehicle roll.

The overlap between the right-front impacting tire and the rigid buttress was measured relative to the traveled way. During the 2270P CIP study simulations, suspension failure was modeled and the wheel was detached but still remained within the wheel well at the time of tire-buttress overlap measurement. As shown in Figure 81, the peak overlap occurred at the US2 impact location for the 15:1 flare rate and at the US3 impact location for the 12.5:1 flare rate. However, the wheel was engaged by the thrie-beam guardrail and did not contact the upstream face of the buttress at the evaluated impact locations.

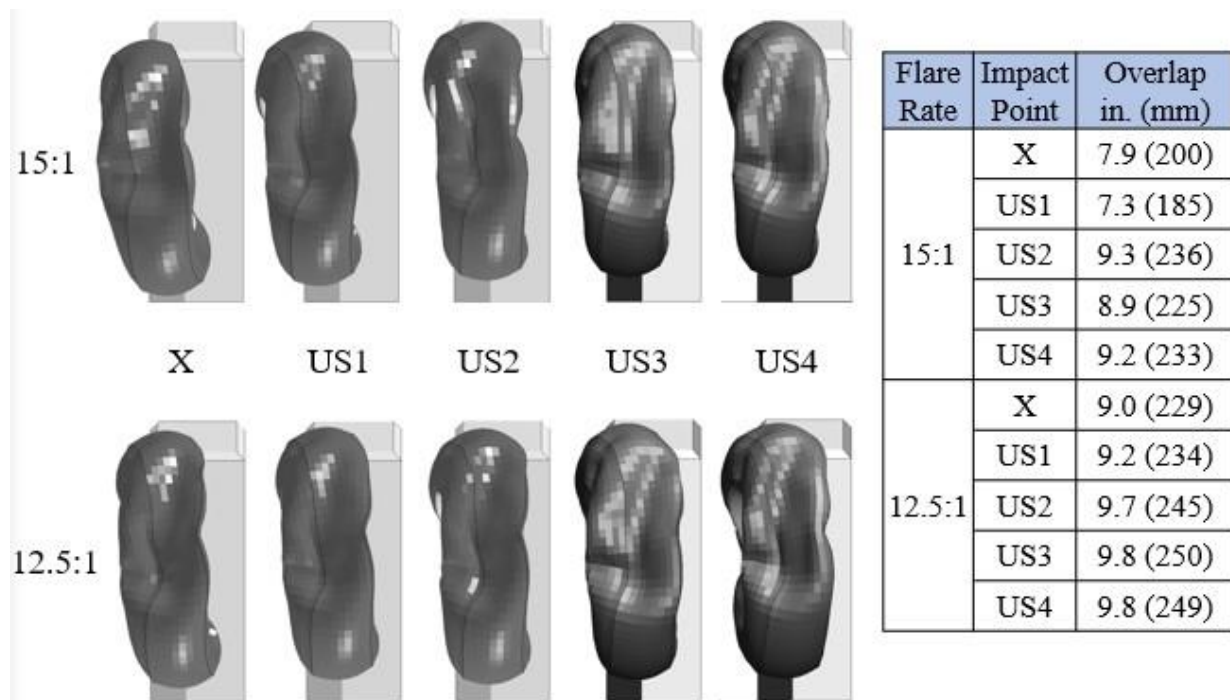


Figure 81. Tire-Buttress Overlap

The US2 impact location for the 15:1 flared installation exhibited the peak tire-buttress overlap and a post no. 20 deflection that was only 0.2 in. (5 mm) lower than the peak post no. 20 deflection, which occurred at the US4 impact location. Additionally, the US2 impact location exhibited only slightly reduced magnitudes of longitudinal occupant risk values and a greater

propensity for roll when compared to the US1 impact location, at which the largest longitudinal occupant risk values were recorded. Accordingly, the US2 impact location was identified as the CIP for the 15:1 flared installation over the US1 impact location, as it exhibited a greater propensity for snag on the rigid buttress and greater roll, along with significant longitudinal occupant risk values.

The maximum value of the measured longitudinal ORA for the 12.5:1 flare occurred at the US2 location. The US2 impact location exhibited the second highest post no. 20 deflection and a tire-buttress overlap that was only 0.2 in. (5 mm) lower than the peak tire-buttress overlap. Additionally, the US2 location exhibited the peak yaw angle at the end of the simulation. Thus, the US2 impact location was identified as the CIP for the 12.5:1 flared installation because it exhibited the peak longitudinal ORA, peak vehicle yaw, and significant propensity for vehicle snag on the rigid buttress.

Based on the evaluated criteria, CIP's for the critical flare rates were selected. As shown in Figure 82, the recommended CIP occurred at the US2 location for the 15:1 installation, which corresponded to 93 in. (2,362 mm) upstream from the rigid buttress, measured tangent to the guardrail. The recommended CIP at the US2 location for the 12.5:1 installation is shown in Figure 83, which is located 92 in. (2,337 mm) upstream from the rigid buttress. Simulated impacts at the US2 impact locations exhibited high occupant risk values and showed greater potential for interactions with the rigid concrete buttress when compared to the other evaluated impact locations, resulting in their selection as the 2270P CIP's for the flared AGT installations.

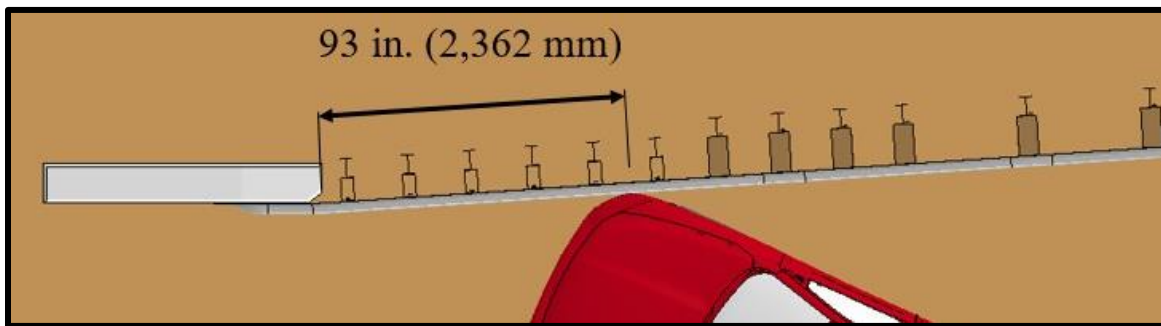


Figure 82. 15:1 2270P CIP Location

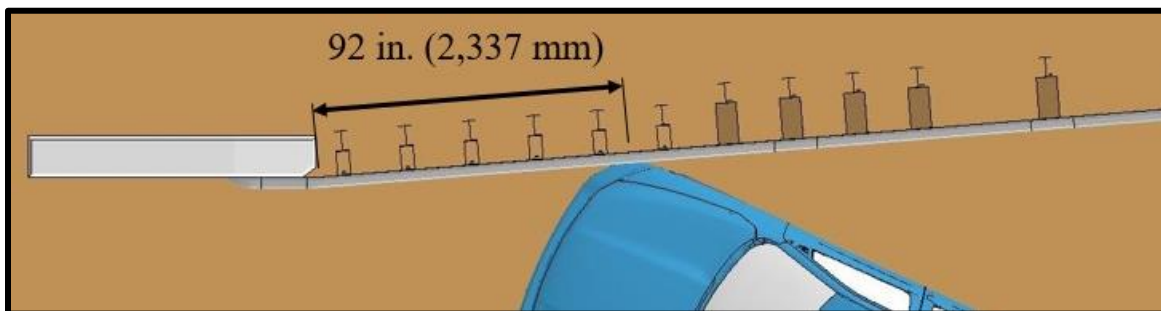


Figure 83. 12.5:1 2270P CIP Location

6.4.2 1100C CIP Study

A model of a 2010 Toyota Yaris, originally developed by the National Crash Analysis Center at the George Washington University [26], was used to evaluate the downstream end of the flared AGT installations. Five impact points with the 1100C vehicle model were evaluated for the 15:1 installation and the 12.5:1 installation to identify the CIP location that would result in the highest likelihood of test failure. Suspension failure with the small car was not modeled.

The evaluated impact points were shifted approximately 26 in. (660 mm) downstream from the 2270P impact locations on the 15:1 and 12.5:1 flared AGT installations. The longitudinal shift of the impact locations closer to the buttress was performed based on the previous CIP recommendations for small car AGT testing [13]. The impact points were spaced at approximately 9-in. (229-mm) intervals, as shown in Figure 84 and summarized in Table 29. Due to numerical instabilities with the 1100C small car model, multiple simulations required the impact point to be shifted 1 in. (25 mm) upstream for the simulation to run to completion. Thus, for several cases, the 9-in. (229-mm) interval was either reduced or extended by 1 in. (25 mm).

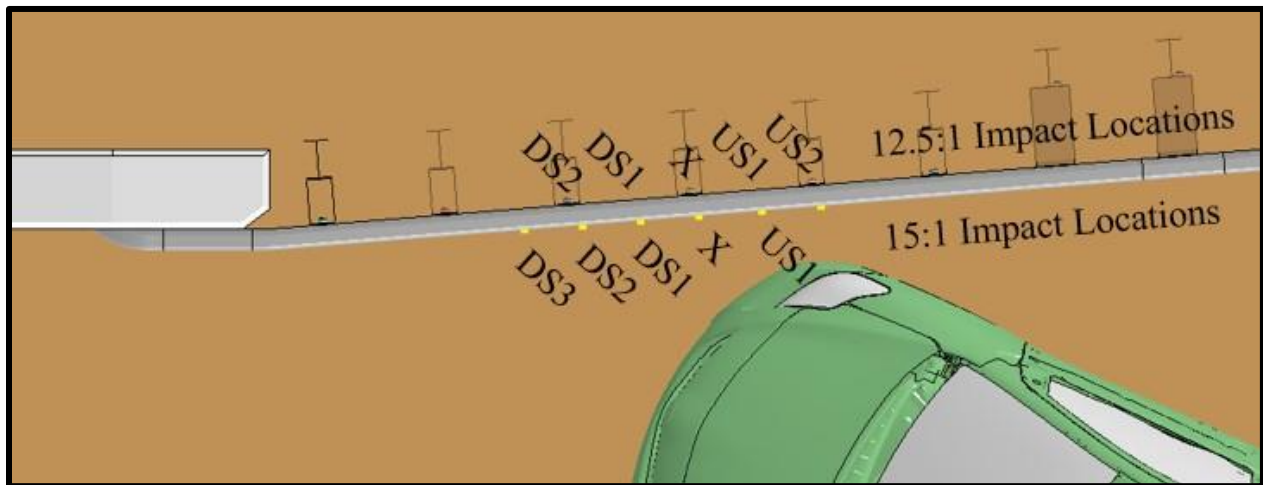


Figure 84. 1100C CIP Impact Point Locations

Table 29. Summary of 1100C CIP Study Impact Locations

Impact Location* in. (mm)	DS3	DS2	DS1	X	US1	US2
15:1	41 (1,041)	50** (1,270)	58 (1,473)	68** (1,727)	77 (1,956)	-
12.5:1	-	48 (1,219)	57 (1,448)	66 (1,676)	75 (1,905)	84 (2,134)

*Impact location measured upstream from buttress tangent to flared guardrail

**Impact location shifted 1 in. (25 mm) upstream to resolve model instability

To select a CIP for each of the studied flare rates, three main parameters were considered: occupant risk, system deflection immediately upstream of the buttress, and vehicle angular displacements. The parameters were selected to gauge the propensity for vehicle snag on the

upstream end of the rigid buttress and vehicle rollover, as well as to quantify the severity of the impact to the vehicle’s occupants.

The 1100C Yaris vehicle model impacted each of the flared AGT installations at a speed of 62.1 mph (100 km/h). The effective impact angles with respect to the guardrail system were 28.8 degrees with the 15:1 flared installation and 29.6 degrees with the installation installed with a 12.5:1 flare. Summaries of the results for the 15:1 and 12.5:1 flared CIP studies are contained in Tables 30 and 31, respectively, and sequential images are presented in Appendix E.

Analysis of the simulation results shows that the small car satisfied the MASH 2016 evaluation criteria during all simulated impacts with both the 15:1 and the 12.5:1 flared installations. The longitudinal occupant risk values for each impact location plotted versus the shift in impact location are shown in Figures 85 and 86 for the 15:1 and 12.5:1 flared AGTs, respectively.

Table 30. Summary of 1100C 15:1 Flared AGT CIP Study

Impact Location US from Buttress Tangent to Rail in. (mm)		41 (1,041)	50 (1,270)	58 (1,473)	68 (1,727)	77 (1,956)	MASH 2016 Limits
Evaluation Criteria		DS3	DS2	DS1	X	US1	
OIV ft/s (m/s)	Longitudinal	-34.2 (-10.4)	-33.9 (-10.3)	-32.8 (-10.0)	-33.2 (-10.1)	-31.7 (-9.7)	±40 (12.2)
	Lateral	31.6 (9.6)	32.3 (9.8)	33.7 (10.3)	33.9 (10.3)	34.2 (10.4)	±40 (12.2)
ORA g’s	Longitudinal	-8.3	-8.6	-13.9	-8.8	-12.7	±20.49
	Lateral	5.2	5.6	7.7	5.2	4.7	±20.49
Maximum Angular Displacement degrees	Roll	8.5	9.0	8.6	7.4	8.6	±75
	Pitch	14.9	14.2	13.7	13.5	12.3	±75
	Yaw	80.9	86.8	90.6	90.7	80.9	not required
Maximum Dynamic Deflection in. (mm)		1.7 (43)	2.2 (55)	2.6 (65)	3.5 (88)	3.7 (93)	N/A

Table 31. Summary of 1100C 12.5:1 Flared AGT CIP Study

Impact Location US from Buttress Tangent to Rail in. (mm)		48 (1,219)	57 (1,448)	66 (1,676)	75 (1,905)	84 (2,134)	MASH 2016 Limits
Evaluation Criteria		DS2	DS1	X	US1	US2	
OIV ft/s (m/s)	Longitudinal	-35.3 (-10.8)	-33.7 (-10.3)	-34.4 (-10.5)	-33.7 (-10.3)	-33.1 (-10.1)	±40 (12.2)
	Lateral	31.8 (9.7)	33.7 (10.3)	34.4 (10.5)	34.7 (10.6)	33.8 (10.3)	±40 (12.2)
ORA g's	Longitudinal	-6.4	-14.6	-10.1	-10.5	-13.5	±20.49
	Lateral	5.4	6.8	5.9	4.5	6.1	±20.49
Maximum Angular Displacement degrees	Roll	9.3	9.1	8.5	8.6	9.4	±75
	Pitch	15.5	15.0	13.4	13.1	12.2	±75
	Yaw	84.1	90.2	93.8	88.1	81.3	not required
Maximum Dynamic Deflection in. (mm)		2.1 (54)	2.5 (63)	3.7 (93)	3.9 (100)	4.2 (106)	N/A

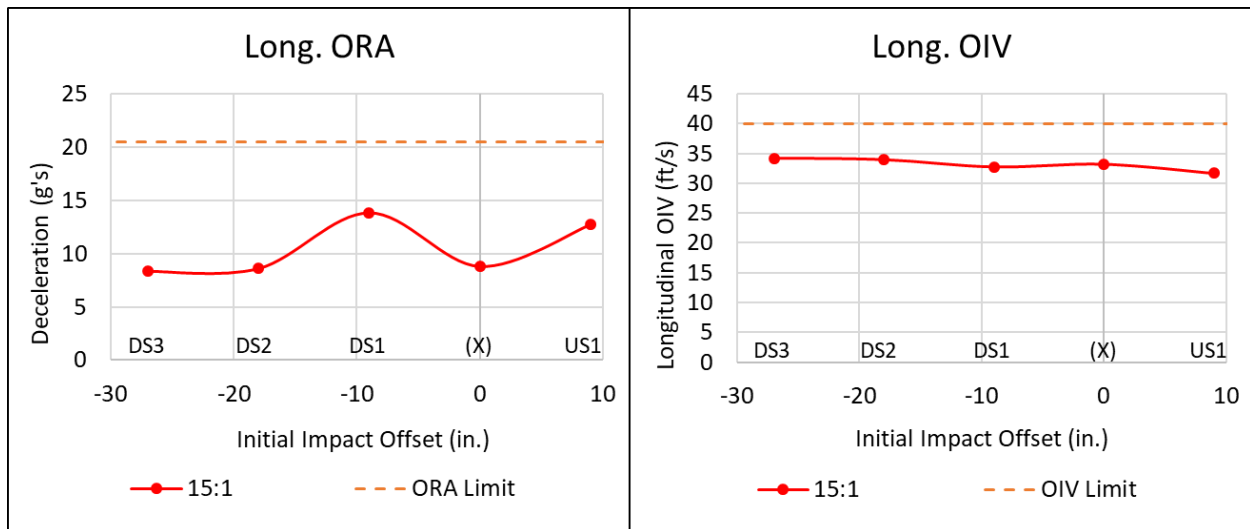


Figure 85. 15:1 1100C CIP Study Longitudinal Occupant Risk

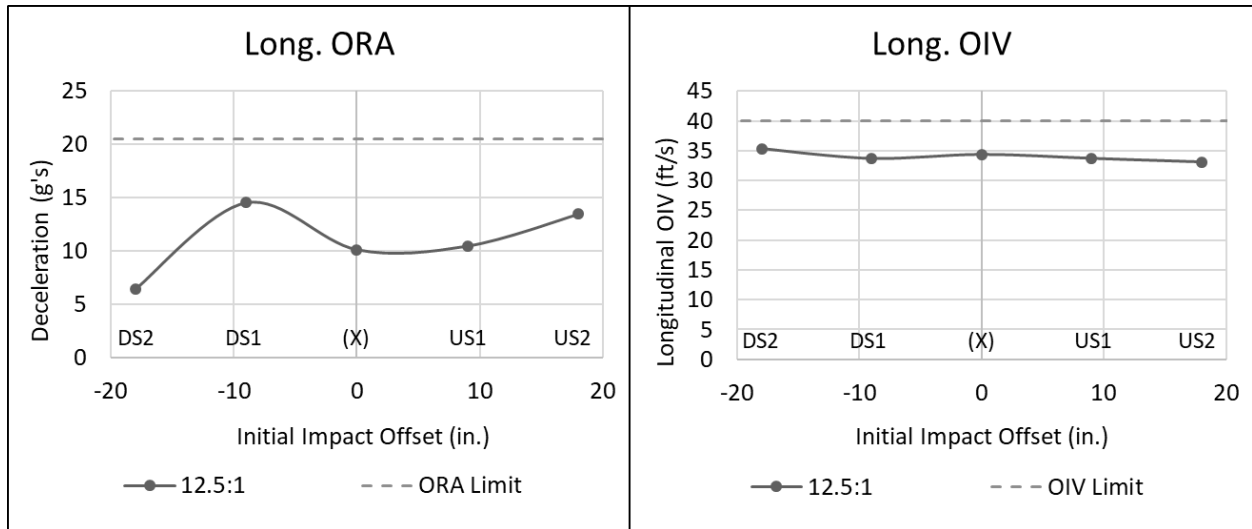


Figure 86. 12.5:1 1100C CIP Study Longitudinal Occupant Risk

The lateral overlap of the impacting tire across the upstream face of the standardized concrete buttress was measured with respect to the tangent roadway to gauge the propensity for wheel snag. As shown in Figure 87, the measured tire-buttress overlap generally decreased as the impact location moved upstream. However, the right-front impacting tire contacted the guardrail posts during all simulated impacts except for the DS3 impact location on the 15:1 flared installation. Additionally, the right-front impacting tire contacted the upstream face of the rigid buttress at each impact location and exhibited the potential for vehicle snag.

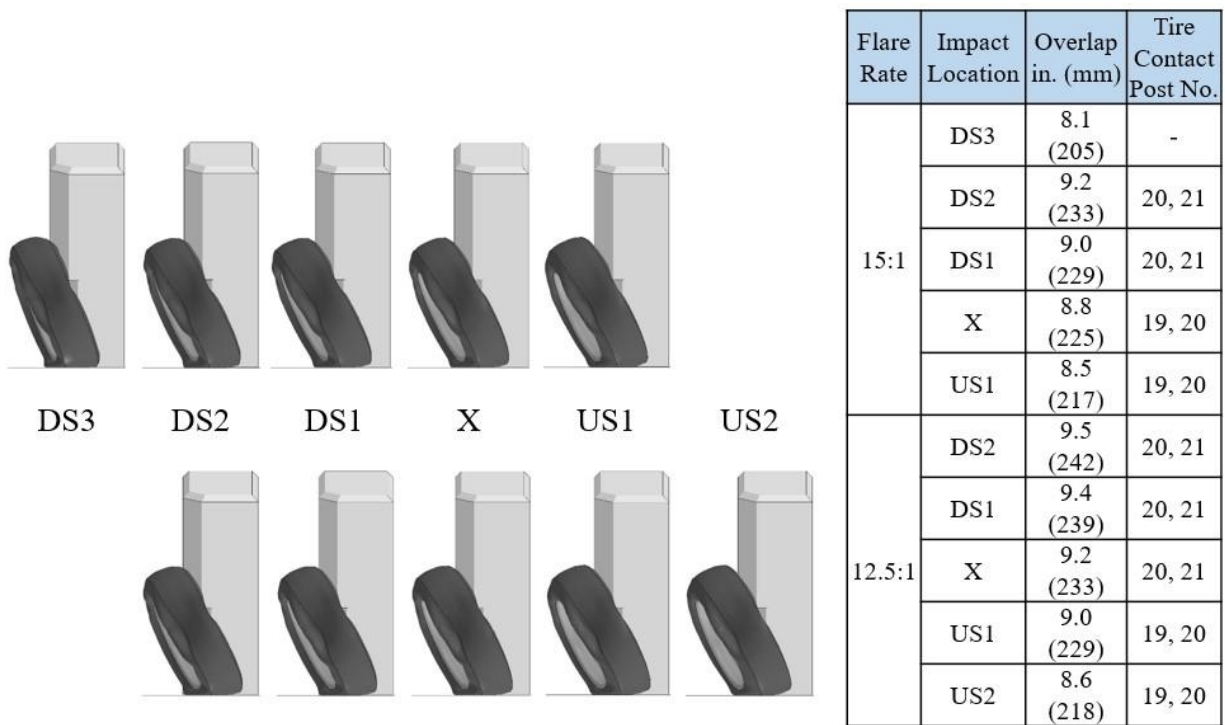


Figure 87. 1100C Right-Front Tire-Buttress Overlap

In addition to the tire-buttress overlap, the peak deflection of post no. 20 was measured. Large deflections of posts immediately upstream of the buttress would expose the rigid concrete buttress and result in a greater propensity for vehicle snag and larger pocketing angles when compared to small deflections of the posts upstream from the buttress. The peak dynamic deflections of post no. 20 for both the 15:1 and 12.5:1 flared installations are shown in Table 32.

Table 32. 1100C Simulation Post No. 20 Deflections

Flare Rate	Impact Location, in. (mm)					
	DS3	DS2	DS1	X	US1	US2
15:1	1.7 (43)	2.2 (55)	2.4 (61)	2.5 (63)	2.3 (57)	-
12.5:1	-	2.1 (54)	2.5 (63)	2.8 (71)	2.6 (66)	2.5 (64)

The peak post no. 20 deflections exhibited a relatively small variation in magnitude as the impact point was shifted upstream when compared to the post no. 20 deflection measurements for the 2270P vehicle model. For both flared installations, the farthest downstream impact location resulted in the smallest deflection of post no. 20. The largest deflections of post no. 20 occurred at the X location for the 15:1 and 12.5:1 flared installations.

Vehicle stability was evaluated by measuring the roll, pitch, and yaw of the vehicle during the impact event. According to the criteria outlined in MASH 2016, maximum roll and pitch values should not exceed ± 75 degrees. The peak roll angular displacement occurred at the DS2 impact location for the 15:1 and at the US2 impact location for the 12.5:1 flared installations, with magnitudes of 9.0 degrees and 9.4 degrees, respectively. Peak pitch angular displacements occurred at the DS3 location for the 15:1 and at the DS2 impact location for the 12.5:1 flared installations, with magnitudes of 14.9 degrees and 15.5 degrees respectively. Thus, no simulation approached the ± 75 degree limit established in MASH 2016. However, the maximum yaw angular displacements reached values of 90.7 degrees and 93.8 degrees at the X impact location for the 15:1 and 12.5:1 installations, respectively.

Based on the evaluated criteria, CIPs for the critical flare rates were selected for the 15:1 and 12.5:1 installations, as shown in Figures 88 and 89. For both installations, the recommended CIP was at the DS1 impact location. Measured tangent to the guardrail, this impact location was 58 in. (1,473 mm) upstream from the rigid buttress for the 15:1 installation and 57 in. (1,448 mm) upstream from the rigid buttress for the 12.5:1 installation. For the 15:1 installation, the DS1 impact location exhibited the peak lateral and longitudinal ORA values, and the second largest peak roll and yaw values. The post no. 20 deflection and tire-buttress overlap were just 0.1 in. (2 mm) and 0.2 in. (4 mm) lower than the peak measured parameters, respectively. For the 12.5:1 flared installation, the DS1 impact location exhibited the peak longitudinal and lateral ORA and the second largest peak pitch and yaw. The post no. 20 deflection and tire-buttress overlap were just 0.3 in. (8 mm) and 0.1 in. (3 mm) lower than the peak measured parameters, respectively.

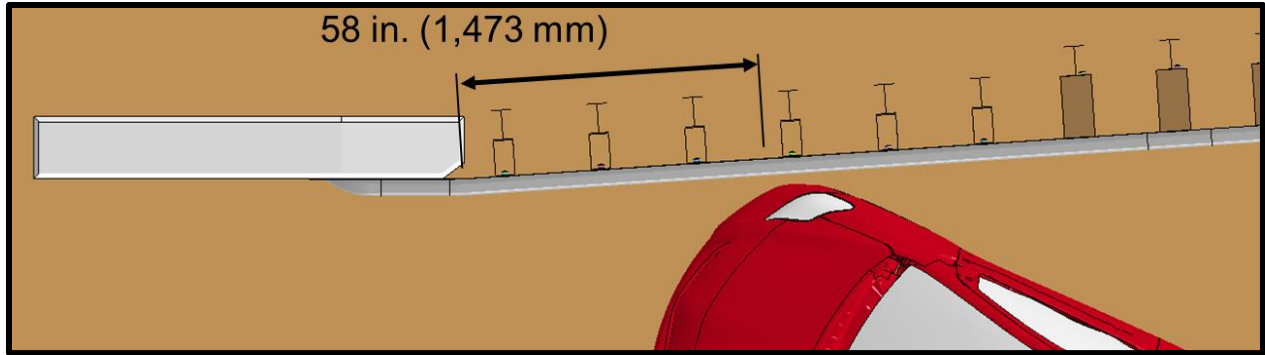


Figure 88. 15:1 1100C CIP Location (DS1)

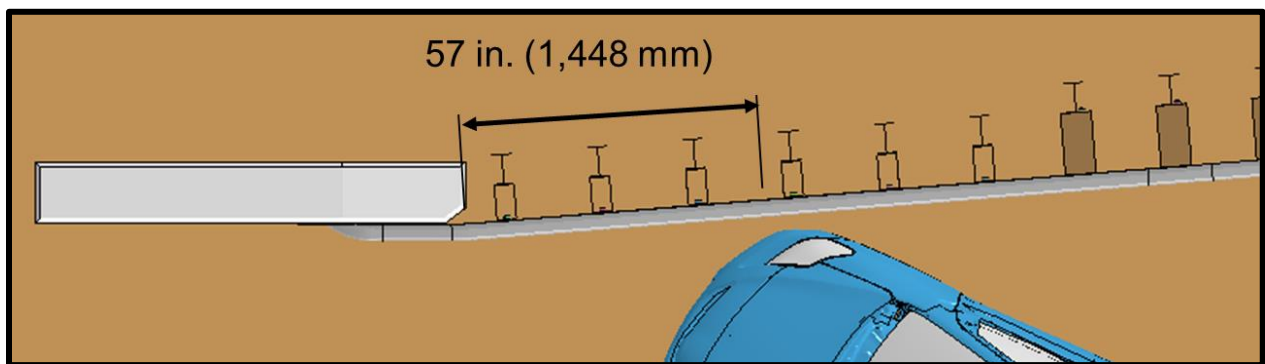


Figure 89. 12.5:1 1100C CIP Location (DS1)

6.4.3 Critical Flare CIP Comparison

The data from the CIP locations for the 15:1 and 12.5:1 flared installations and the tangent installation were directly compared to assess the differences in installation performance at the two critical flare rates. Impact severity, occupant risk criteria, angular displacements, tire-buttress overlap, and exit criteria were compared, in addition to the flared installation LONs.

The changes in velocity in both the longitudinal and lateral directions were plotted for each of the AGT installations. As shown in Figure 90, the tangent AGT installation exhibited the lowest magnitude longitudinal change in velocity for both the 1100C and 2270P vehicles. Additionally, for both the 2270P and 1100C vehicles, the steeper 12.5:1 flare rate resulted in larger magnitude longitudinal changes in velocity when compared to the 15:1 flare rate.

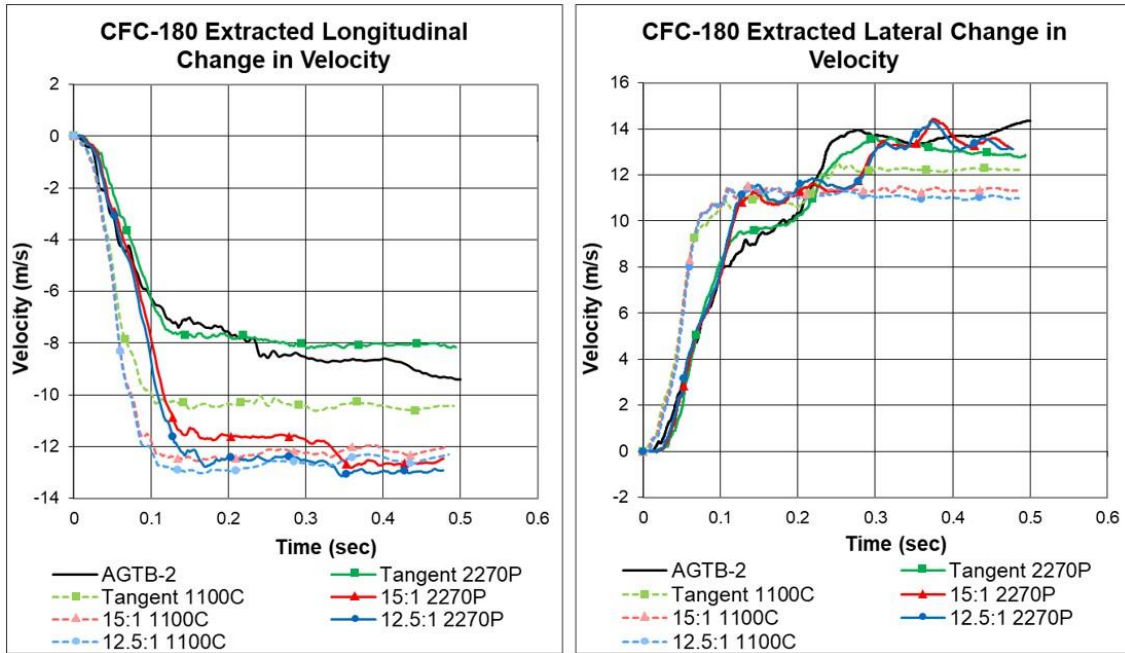


Figure 90. Comparison of Change in Velocity

To evaluate the propensity of the vehicle to snag on the rigid buttress, the overlap between the impacting right-front tire and the upstream face of the buttress was measured. As shown in Figure 91, the tire-buttress overlap was significantly larger for both flared installations when compared to the tangent installation, and the tire-buttress overlap became larger as the flare rate was increased from 15:1 to 12.5:1.

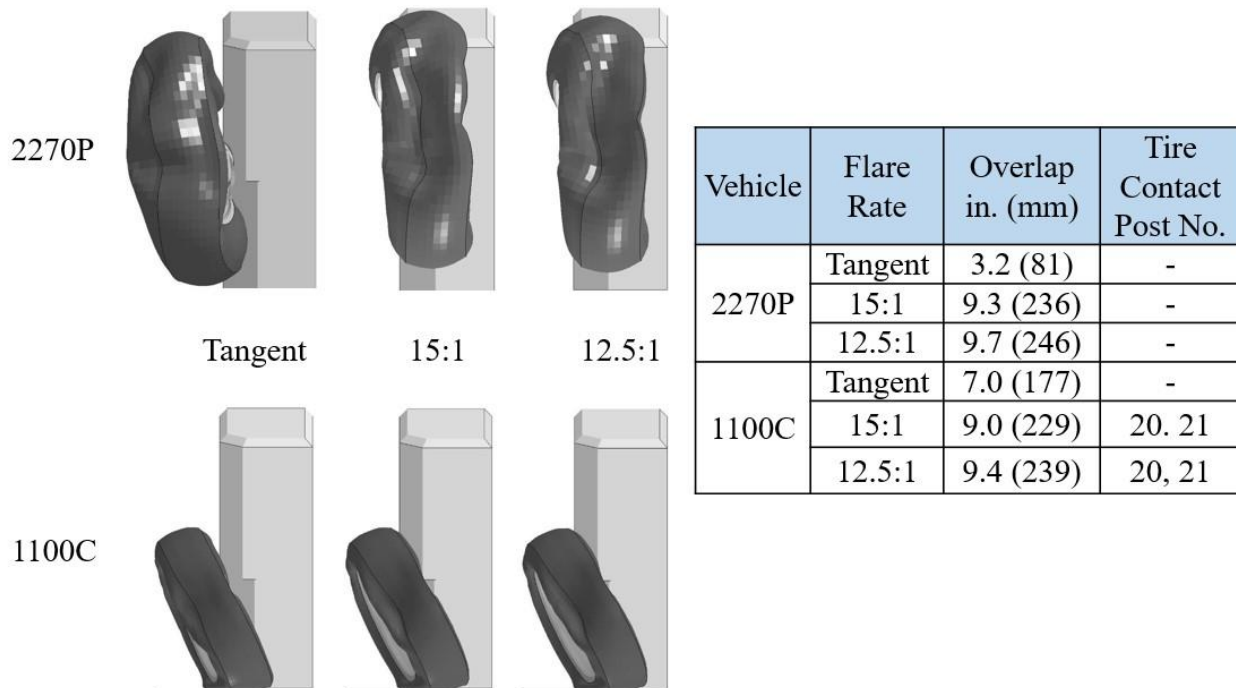


Figure 91. Tire-Buttress Overlap Comparison

The vehicle orientation and change in velocity at exit were recorded for each simulation. The change in velocity at exit was calculated by subtracting the vehicle’s exit velocity from the impact velocity. As shown in Table 33, the change in velocity at exit increased in value as the flare rate was increased. For the 2270P vehicle, the exit angle also increased as the flare rate was increased. The 1100C vehicle did not exhibit the same trend, as the 12.5:1 exit angle was 1.4 degrees smaller than the 15:1 exit angle.

The vehicle orientation at exit is shown in Figure 92. Note, exit was recorded at the time of last contact. Thus, the 2270P vehicle extends over the top of the buttress at exit due to vehicle roll, but it is not in contact with the barrier. Additionally, the validated tangent model overpredicted the magnitude of the vehicle exit angle. Thus, the flared AGT simulation exit angles may be greater than what would occur in the full-scale crash test.

Table 33. Exit Conditions

Test Vehicle	Flare Rate	Exit Angle degrees	Change in Velocity at Exit mph (km/h)
2270P	Tangent	14.1	18.0 (29.0)
	15:1	25.4	28.1 (45.3)
	12.5:1	29.6	29.0 (46.8)
1100C	Tangent	24.7	23.7 (38.1)
	15:1	36.3	27.7 (44.6)
	12.5:1	34.9	28.4 (45.7)

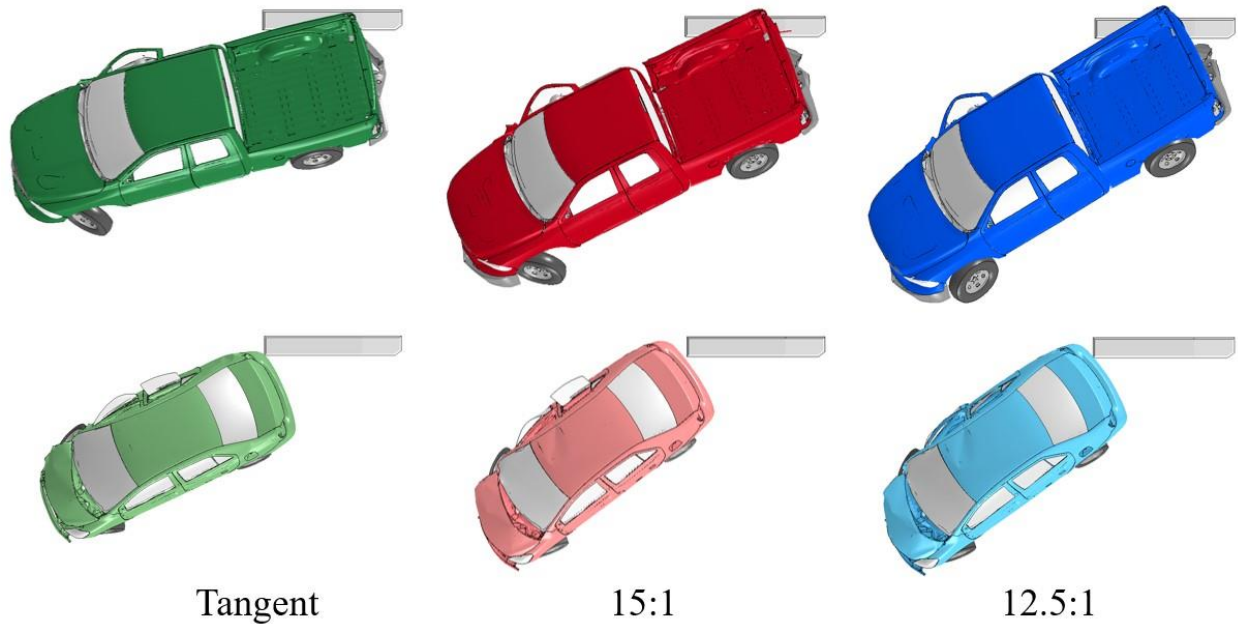


Figure 92. Vehicle Orientation at Exit: Tangent, 15:1, 12.5:1

The exit box criterion was also evaluated to gauge the propensity for the vehicle to re-enter the traveled way after exiting the AGT installation. The vehicle trajectory and exit box after impacts with the tangent and flared installations for the 2270P and 1100C vehicles are shown in Figures 93 and 94, respectively. The left-front tire of the 2270P vehicle crossed the lower boundary of the exit box during impacts with both the 15:1 and 12.5:1 flared installations. During the impact with the 12.5:1 flared installation, the 2270P vehicle exhibited greater yaw angles and the left-front tire crossed the lower exit box boundary earlier when compared to the 2270P vehicle trajectory during the 15:1 flared installation simulation.

All four of the 1100C vehicle tires crossed the downstream boundary of the exit box during the simulated impacts with the 15:1 and the 12.5:1 flared installations. However, the 1100C vehicles exhibited significant yaw and were approximately perpendicular to the traveled way as they crossed the downstream boundary of the exit box. Both the 2270P and 1100C vehicles satisfied the exit box criteria during simulated impacts with the tangent installation. Note that the tangent simulations were not re-run with extended simulation run times and therefore did not fully pass through the exit box.

Although the 2270P's left-front tire crossed the lower boundary during impact with the flared installations, the vehicle's trajectory satisfied the exit box criterion, both with the 2270P and 1100C vehicles. However, due to the greater yaw angle of the 2270P vehicle, the 12.5:1 flare rate was determined to be more critical than the 15:1 flare rate for vehicle reentry into the traveled way.

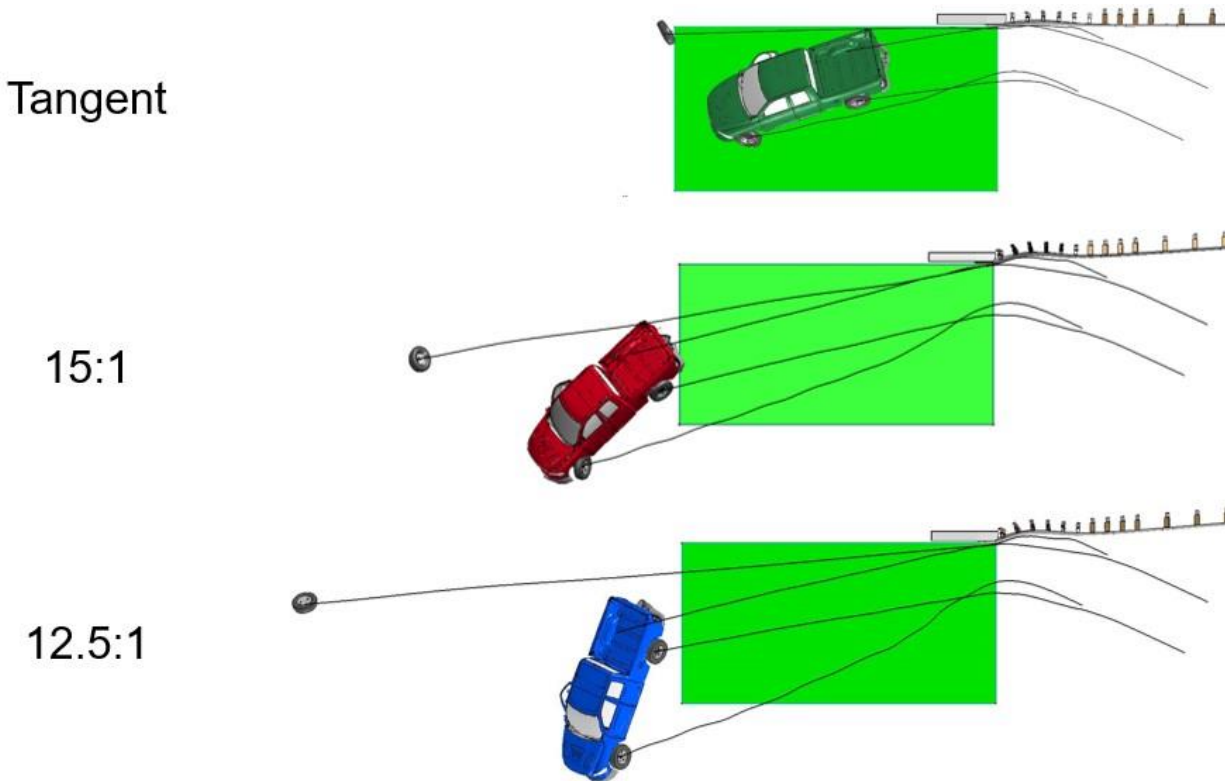


Figure 93. 2270P Vehicle Trajectory and Exit Box

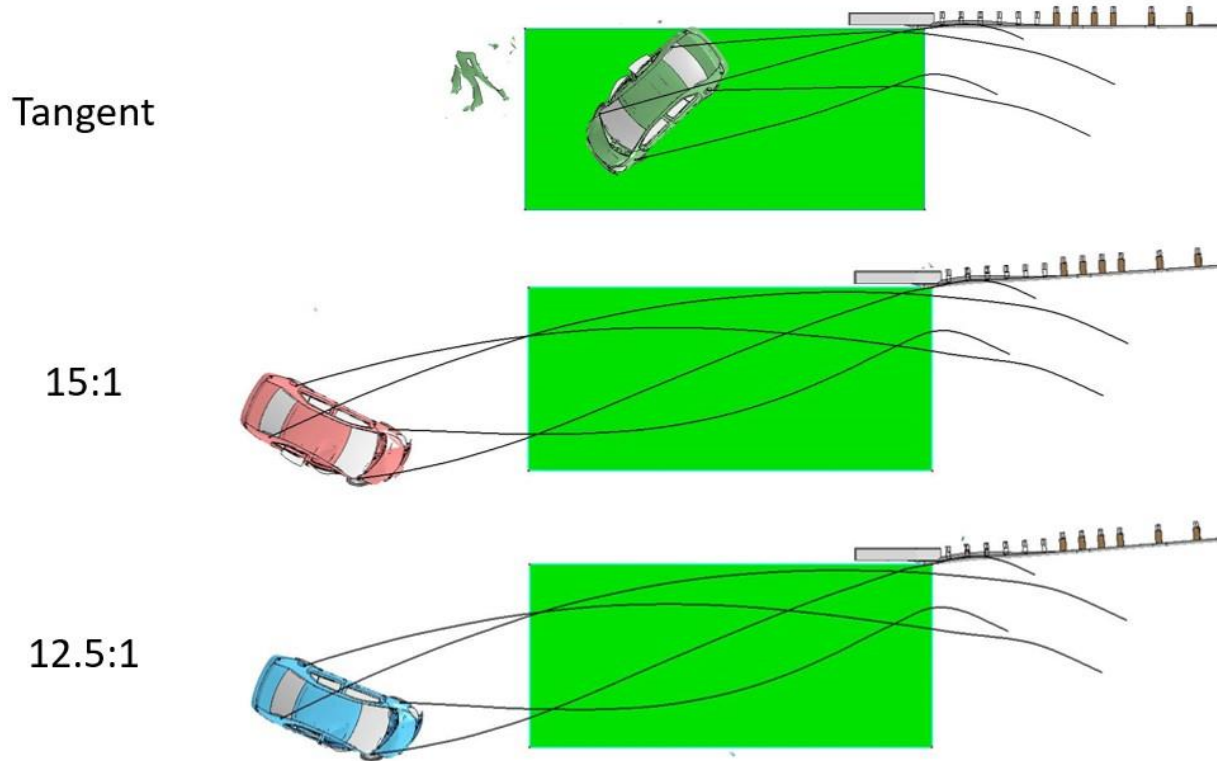


Figure 94. 1100C Vehicle Trajectory and Exit Box

Of the two critical flare rates, the more aggressive 12.5:1 flare rate exhibited larger magnitude occupant risk values than the 15:1 flare rate. Impact severity, longitudinal ORA, vehicle angular displacements, exit angle for the 2270P vehicle, tire-buttress overlap, and changes in velocity were all larger magnitude for the 12.5:1 flared installation than the 15:1 flared installation. When examining the estimated LON for each of the flared installations, the 12.5:1 flare rate reduced the LON 10 ft (3 m) more than the 15:1 flare rate. A summary of the compared parameters is contained in Table 34.

Table 34. Summary of 12.5:1 vs. 15:1 Flared AGT Evaluation Criteria

Evaluation Criteria		2270P			1100C		
		Tangent	15:1	12.5:1	Tangent	15:1	12.5:1
Impact US from Buttress in. (mm)		89 (2,261)	93 (2,362)	92 (2,337)	63 (1,600)	58 (1,473)	57 (1,448)
Impact Severity, kip-ft (kJ)		115 (156)	150 (203)	157 (213)	56 (76)	73 (99)	76 (103)
OIV ft/s (m/s)	Longitudinal	-21.0 (-6.4)	-26.0 (-7.9)	-27.8 (-8.5)	-27.3 (-8.3)	-32.8 (-10.0)	-33.7 (-10.3)
	Lateral	27.1 (8.3)	25.2 (7.7)	25.4 (7.7)	31.8 (9.7)	33.7 (10.3)	33.7 (10.3)
ORA g's	Longitudinal	-6.4	-13.9	-16.0	-11.0	-13.9	-14.6
	Lateral	8.2	14.8	14.9	7.6	7.7	6.8
Maximum Angular Displacement degrees	Roll	26.5	27.2	30.3	6.8	8.6	9.1
	Pitch	7.2	8.8	9.9	12.9	13.7	15.0
	Yaw	42.7	54.1	62.1	67.3	90.6	90.2
Tire-Buttress Overlap in. (mm)		3.2 (81)	9.3 (236)	9.7 (246)	7.0 (177)	9.0 (229)	9.4 (239)
Exit Angles, degrees		14.1	25.4	29.6	24.7	36.3	34.9
LON ft (m)		220 (67.1)	127 (38.7)	117 (35.7)	220 (67.1)	127 (38.7)	117 (35.7)

7 SUMMARY, CONCLUSIONS, AND RECOMMENDATIONS

The objective of this research study was to identify the critical flare rate for flaring AGTs away from the primary roadway. Installing an AGT with a flared configuration results in reduced LON as well as a greater clear zone in front of the barrier, which reduces both installation cost and accident frequency. This research determined the maximum allowable flare rate that could safely be applied to 31-in. (787-mm) tall three-beam AGTs without concrete curbs that utilize MGS upstream of the transition. The Phase I research consisted of a literature review, development and validation of a tangent AGT LS-DYNA model, LS-DYNA simulation of multiple flared AGT models, and the determination of the critical flare rate and CIPs for full-scale testing.

The previous AGT testing outlined in the literature review demonstrated how slight alterations to an AGT can change the outcome of full-scale tests. Post embedment depth, buttress geometry, or the addition/removal of a curb can be attributed to the difference between a successful and unsuccessful full-scale test.

From the literature review, the Iowa Transition installation and the Standardized Transition Buttress installation were identified as critical AGT designs due to the large dynamic deflections exhibited during full-scale testing and the small size of the guardrail posts when compared to other AGT installations (W6x9 in the Iowa Transition and W6x8.5 in the Standardized Transition Buttress) [1, 8]. Both factors are critical to the crashworthiness of AGT installations due to the greater propensity for vehicle pocketing and snag.

Ultimately, the Standardized Transition Buttress AGT in test no. AGTB-2 was identified as the critical AGT design for evaluating the flared AGT. In addition to implementing the critical design components of the Iowa Transition, the test no. AGTB-2 installation incorporated the standardized transition buttress, which included chamfers that would likely reduce vehicle and tire snag during impacts with the flared AGT.

A LON analysis was performed to quantify the LON reduction for five different flare rates which ranged from 25:1 to 10:1. The flared AGT configurations resulted in significant LON reductions that ranged from 67.2 ft (20.5 m) with the 25:1 flare rate to 115.2 ft (35.1 m) with the 10:1 flare rate, when compared to the LON required for the tangent installation. Additionally, the flared AGT configurations resulted in greater lateral offsets of the guardrail.

A baseline computer simulation model of the tangent Standardized Transition Buttress installation, which was identified as the critical AGT design, was developed and validated with test no. AGTB-2 crash test data in accordance with the procedures for V&V of computer simulations used for roadside safety applications, outlined in NCHRP Report W179 [21]. The validated tangent AGT model was modified to model flared AGT installations at each of the studied flare rates.

The 15:1 and 12.5:1 flare rates were identified as the maximum critical flare rates. The study was conducted using both the 2007 Chevrolet Silverado and 2018 Dodge Ram vehicle models. Evaluated parameters included occupant risk, tire-buttress overlap, and system deflections. The two critical flare rates exhibited the largest reductions in system LON while maintaining the safety performance criteria outlined in MASH 2016. Further research was conducted on both the 15:1 and 12.5:1 flare rates with the 2270P and 1100C vehicles to identify

the CIPs which would produce the largest propensity for snag on the rigid buttress and the greatest likelihood of test failure.

Nine impact locations spaced at 9-in. (229-mm) intervals were simulated with the 2270P vehicle and five impact locations spaced at 9-in. (229-mm) intervals were simulated with the 1100C vehicle for each of the two critical flare rates. Criteria including system deflections, tire-buttress overlap, vehicle angular displacements, and occupant risk values were evaluated. CIPs were selected based on the evaluated parameters for both the 2270P and 1100C vehicles at the 15:1 and 12.5:1 flare rates.

At the evaluated CIP locations, the more aggressive 12.5:1 flare rate exhibited larger magnitude occupant risk values than the 15:1 flare rate. Impact severity, longitudinal ORA, vehicle angular displacements, exit angle for the 2270P vehicle, tire-buttress overlap, and changes in velocity were all larger magnitude for the 12.5:1 flared installation than the 15:1 flared installation. When examining the estimated LON for each of the flared installations, the 12.5:1 flare rate only offered an additional 10-ft (3-m) reduction beyond the reduction offered by the 15:1 flare rate. Based on the evaluation criteria in the simulations, the 15:1 flare rate installation would have a greater potential to pass the MASH 2016 safety performance criteria.

Based on the data presented herein and with feedback from sponsors, the 15:1 flare rate was selected as the critical flare rate for full-scale testing. The 15:1 flared AGT exhibited reduced occupant risk criteria and improved vehicle stability over the 12.5:1 flared AGT and offered a comparable reduction in LON that was only 10 ft (3 m) longer than the LON of the more aggressive 12.5:1 flare rate.

It is recommended that the 15:1 flare rate AGT with a flare starting at the upstream end of the thrie-beam terminal connector is full-scale crash tested to MASH 2016 TL-3, which requires two full-scale crash tests to evaluate the performance of longitudinal barrier systems: MASH 2016 test designation no. 3-20 with the 1100C small car and MASH 2016 test designation no. 3-21 with the 2270P pickup truck. However, there may be up to two CIPs for AGT tests: near the downstream end to maximize snagging on the buttress, and near the upstream end to maximize pocketing and snag at the W-to-thrie transition element.

CIPs were identified at the downstream end of the 15:1 flared installation, which correspond to 93 in. (2,362 mm) and 58 in. (1,473 mm) upstream from the upstream face of the rigid buttress, measured tangent to the guardrail, for MASH 2016 test designation nos. 3-21 and 3-20 with the 2270P pickup truck and 1100C small car, respectively. These impact locations will evaluate the flared transition for vehicle snag on the concrete buttress. An additional CIP will be identified in the Phase II study for MASH 2016 test designation no. 3-20 at the upstream end of the transition to maximize snagging and pocketing at the W-to-thrie transition element.

Future research could include evaluating alternate flared AGT configurations. Alternate AGT configurations, including those that incorporate alternate transition heights (i.e., 34-in. (864-mm) AGT buttress [13]), concrete curbs, alternate rigid buttress shapes, and hybrid flare rates were not within the scope of this Phase I effort. As noted previously, AGTs have been shown to be sensitive to changes in components within the transition region. Thus, further evaluation could be conducted on alternate flared AGT configurations upon successful completion of the full-scale crash testing matrix for the proposed configuration.

8 REFERENCES

1. Rosenbaugh, S.K., Faller, R.K., Asselin, N., and Hartwell, J.A., *Development of a Standardized Buttress for Approach Guardrail Transitions*, Report No. TRP-03-369-20, Midwest Roadside Safety Facility, University of Nebraska-Lincoln, Lincoln, Nebraska, November 10, 2020.
2. Stolle, C.S., Polivka, K.A., Reid, J.D., Faller, R.K., Sicking, D.L., Bielenberg, R.W., and Rohde, J.R., *Evaluation of Critical Flare Rates for the Midwest Guardrail System (MGS)*, Report No. TRP-03-191-08, Midwest Roadside Safety Facility, University of Nebraska-Lincoln, Lincoln, Nebraska, July 15, 2008.
3. Ross, H.E., Sicking, D.L., Zimmer, R.A., and Michie, J.D., *Recommended Procedures for the Safety Performance Evaluation of Highway Features*, National Cooperative Highway Research Program (NCHRP) Report 350, Transportation Research Board, Washington, D.C., 1993
4. *Manual for Assessing Safety Hardware (MASH), Second Edition*, American Association of State Highway and Transportation Officials (AASHTO), Washington, D.C., 2016.
5. *LS-DYNA Keyword User's Manual, Volume 1 R10.1* Livermore Software Technology Company (LSTC), Livermore, California, 2017.
6. *Manual for Assessing Safety Hardware (MASH)*, American Association of State Highway and Transportation Officials (AASHTO), Washington, D.C., 2009.
7. Michie, J.D., *Recommended Procedures for the Safety Performance Evaluation of Highway Appurtenances*, National Cooperative Highway Research Program (NCHRP) Report 230, Transportation Research Board, Washington, D.C., March 1981.
8. Polivka, K.A., Faller, R.K., Sicking, D.L., Rohde, J.R., Bielenberg, R.W., Reid, J.D., and Coon, B.A., *Performance Evaluation of the Guardrail to Concrete Barrier Transition – Update to NCHRP 350 Test No. 3-21 with 28" C.G. Height (2214T-1)*, Report No. TRP-03-175-06, Midwest Roadside Safety Facility, University of Nebraska-Lincoln, Lincoln, Nebraska, October 12, 2006.
9. Arrington, D.R., Bligh, R.P., and Menges, W.L., *MASH Test 3-21 on TL-3 Thrie Beam Transition Without Curb*, Report No. FHWA/TX-13/9-1002-12-3, Texas A&M Transportation Institute, College Station, Texas, July 2013.
10. Bligh, R.P., Arrington, D.R., and Menges, W.L., *Development of a MASH TL-2 Guardrail-to-Bridge Rail Transition Compatible with 31-Inch Guardrail*, Report No. FHWA/TX-12/9-1002-8, Texas A&M Transportation Institute, College Station, Texas, December 2011.
11. Bullard, D.L., Bligh, R.P., and Menges, W.L., *Appendix G: MASH TL-3 Testing and Evaluation of the W-Beam Transition*, TTI-RF Project 476460-1-3, Texas A&M Transportation Institute, College Station, Texas, March 2010.

12. Jewell, J., Clark, N., and Peter, R., *Compliance Crash Testing of a Nested Thrie Beam Transition Barrier*, Report No. FHWA/CA/TL-2001/09, California Department of Transportation, Sacramento, California, May 2002.
13. Rosenbaugh, S.K., Fallet, W.G., Faller, R.K., Bielenberg, R.W., and Schmidt, J.D., *34-in. Tall Thrie Beam Transition to Concrete Buttress*, Report No. TRP-03-367-19, Midwest Roadside Safety Facility, University of Nebraska-Lincoln, Lincoln, Nebraska, March 27, 2019.
14. Rosenbaugh, S.K., Lechtenberg, K.A., Faller, R.K., Sicking, D.L., Bielenberg, R.W., and Reid, J.D., *Development of the MGS Approach Guardrail Transition Using Standardized Steel Posts*, Report No. TRP-03-210-10, Midwest Roadside Safety Facility, University of Nebraska-Lincoln, Lincoln, Nebraska, December 21, 2010.
15. Winkelbauer, B.J., Putjenter, J.G., Rosenbaugh, S.K., Lechtenberg, K.A., Bielenberg, R.W., Faller, R.K., and Reid, J.D., *Dynamic Evaluation of MGS Stiffness Transition with Curb*, Report No. TRP-03-291-14, Midwest Roadside Safety Facility, University of Nebraska-Lincoln, Lincoln, Nebraska, June 30, 2014.
16. Williams, W.F., Bligh, R.P., and Menges, W.L., *MASH TL-3 Testing and Evaluation of the TXDOT T131RC Bridge Rail Transition*, Report No. FHWA/TX-13/9-1002-12-4, Texas A&M Transportation Institute, College Station, Texas, March 2013.
17. Bligh, R.P., Ross, H.E., and Bullard, L., *Crash Testing Florida DOT Standard Guardrail Transition Section at Connection to Bridge Traffic Rail Wing Post*, Test No. 0385-1, Texas A&M Transportation Institute, College Station, Texas, 1989.
18. Dobrovolny, C.S., Menges, W.L., and Kuhn, D.L., *Full-Scale MASH Crash Testing of Stacked W-Beam Transition for 31-inch Guardrail*, Test Report No. 604581-1, Texas A&M Transportation Institute, College Station, Texas, May 11, 2016.
19. Abu-Odeh, A.Y., McCaskey, K., Bligh, R.P., Menges, W.L., and Kuhn, D.L., *Crash Test and MASH TL-3 Evaluation of the TxDOT Short Radius Guardrail*, Report No. FHWA/TX-15/0-6711-1, Texas A&M Transportation Institute, College Station, Texas, March 2015.
20. *Roadside Design Guide*, American Association of State Highway and Transportation Officials (AASHTO), Issue 4, Washington, D.C., 2011.
21. Ray, M.H., Plaxico, C.A., and Anghileri, M., *Procedures for Verification and Validation of Computer Simulations Used for Roadside Safety Applications*, NCHRP Web-Only Report 179, NCHRP Project No. 22-24, March 2010.
22. Bickhaus, R.F., Rasmussen, J.D., and Reid, J.D., *Development and Validation of a Thrie-Beam AGT LS-DYNA Model*, Report No. TRP-03-441-22, Midwest Roadside Safety Facility, University of Nebraska-Lincoln, Lincoln, NE, December 20, 2021.

23. *Vehicle Modeling*, National Crash Analysis Center, George Washington University, Washington, D.C. Retrieved from: <http://www.ncac.gwu.edu/research/reports.html>, August 20, 2014.
24. Dhafer, M., *Update on New MASH Pickup Truck Model*, Center for Collision Safety and Analysis, TRB 98th Annual Meeting (2019) Roadside Safety Design Computational Mechanics Subcommittee, AFB20(1), Washington, D.C., January 14, 2019, Obtained on February 12, 2019.
25. Eller, C.M., Polivka, K.A., Faller, R.K., Sicking, D.S., Rohde, J.R., Reid, J.D., Bielenberg, B.W., and Allison, E.M., *Development of the Midwest Guardrail System (MGS) W-Beam to Thrie Beam Transition Element*, Report No. TRP-03-167-07, Midwest Roadside Safety Facility, University of Nebraska-Lincoln, Lincoln, NE, November 26, 2007.
26. National Crash Analysis Center, *2010 Toyota Yaris FE Model*, Retrieved from <http://www.ncac.gwu.edu/vml/archive/ncac/vehicle/yaris-vlm.pdf>, Accessed June 1, 2013.

9 APPENDICES

Appendix A. AGT LS-DYNA Model Parts

Table A-1. Summary of AGT Model Parts and LS-DYNA Parameters

Part Number	Part Name	Element Type (*SECTION)	Element Formulation	Thickness	Material Type	Material Formulation (*MAT)
4700	post-1	Solid	Fully Integrated S/R (2)	-	Wood	Plastic Kinematic
4708	post-1-hole	Solid	Fully Integrated Quadratic 8 Node Element (3)	-	-	Isotropic Elastic Failure
4701	p1-bolt-head-nulls	Shell	Belytschko-Tsay (2)	1	-	Null
4702	p1-bolt-solids	Solid	Constant Stress (1)	-	Steel	Rigid
4703	p1-washer	Solid	Constant Stress (1)	-	Steel	Rigid
4704	p1-tube	Shell	Belytschko-Tsay (2)	2.38125	Steel	Rigid
4705	p1-tube-bolt	Solid	Constant Stress (1)	-	Steel	Rigid
4706	p1-tube-washers	Solid	Constant Stress (1)	-	Steel	Rigid
4707	p1-tube-yoke-holes	Shell	Belytschko-Tsay (2)	2.38125	-	Rigid
4710	post-2	Solid	Fully Integrated S/R (2)	-	Wood	Plastic Kinematic
4718	post-2-hole	Solid	Fully Integrated Quadratic 8 Node Element (3)	-	-	Isotropic Elastic Failure
4711	p2-bolt-head-nulls	Shell	Belytschko-Tsay (2)	1	-	Null
4712	p2-bolt-solids	Solid	Constant Stress (1)	-	Steel	Rigid
4713	p2-washer	Solid	Constant Stress (1)	-	Steel	Rigid
4714	p2-tube	Shell	Belytschko-Tsay (2)	2.38125	Steel	Rigid
4715	p2-tube-bolt	Solid	Constant Stress (1)	-	Steel	Rigid
4716	p2-tube-washers	Solid	Constant Stress (1)	-	Steel	Rigid
4717	p2-tube-yoke-holes	Shell	Belytschko-Tsay (2)	2.38125	-	Rigid
4721	ac_bearing-plate	Solid	Constant Stress (1)	-	Steel	Rigid
4722	ac-swage-fitting-and-stud-1	Solid	Constant Stress (1)	-	Steel	Rigid
4723	ac-washer-1	Solid	Constant Stress (1)	-	Steel	Rigid
4724	ac-nut-1	Solid	Constant Stress (1)	-	Steel	Rigid
4725	ac-post-sleeve-1	Solid	Constant Stress (1)	-	Steel	Rigid
4726	ac-end-plate	Solid	Constant Stress (1)	-	Steel	Rigid
4727	ac-swage-fitting-and-stud-2	Solid	Constant Stress (1)	-	Steel	Rigid
4728	ac-washer-2	Solid	Constant Stress (1)	-	Steel	Rigid
4729	ac-nut-2	Solid	Constant Stress (1)	-	Steel	Rigid
4730	anchor-bracket	Solid	Constant Stress (1)	-	Steel	Rigid
4731	ab-washers-nut-side	Solid	Constant Stress (1)	-	Steel	Rigid
4732	ab-washers-head-side	Solid	Constant Stress (1)	-	Steel	Rigid
4733	ab-bolts	Solid	Constant Stress (1)	-	Steel	Rigid
4740	ground-line-strut	Shell	Belytschko-Tsay (2)	5	Steel	Piecewise Linear Plasticity
4720	anchor-cable	Beam	Hughes-Liu (1)	-	6x19 .75 in. Wire Rope	Piecewise Linear Plasticity
4761	soil-top	Solid	-	-	Soil	Drucker Prager
4762	soil-bottom	Solid	-	-	Soil	Drucker Prager
4763	soil-nulls	Shell	Belytschko-Tsay (2)	1	-	Null

Table A-2. Summary of AGT Model Parts and LS-DYNA Parameters, Cont.

Part Number	Part Name	Element Type (*SECTION)	Element Formulation	Thickness	Material Type	Material Formulation (*MAT)
4764	soil-crate	Shell	Belytschko-Tsay (2)	1	-	Rigid
1001	buttress--front	Shell	Belytschko-Tsay (2)	2	Concrete	Rigid
1002	buttress-side	Shell	Belytschko-Tsay (2)	2	Concrete	Rigid
1003	buttress-top	Shell	Belytschko-Tsay (2)	2	Concrete	Rigid
1004	buttress-back	Shell	Belytschko-Tsay (2)	2	Concrete	Rigid
4100	post-bolt-springs-w	Discrete	DRO=Translational Spring/Damper (0)	-	Steel	Spring Nonlinear Elastic
4101	post-bolt-springs-thrie	Discrete	DRO=Translational Spring/Damper (0)	-	Steel	Spring Nonlinear Elastic
4102	post-bolt-springs-tran	Discrete	DRO=Translational Spring/Damper (0)	-	Steel	Spring Nonlinear Elastic
4203-4221	bolt-p3 - bolt-p21	Solid	Fully Integrated S/R (2)	-	Steel	Rigid
4303-4321	nut-p3 - nut-p21	Solid	Fully Integrated S/R (2)	-	Steel	Rigid
4151	post-bolt-springs-thrie-b	Discrete	DRO=Translational Spring/Damper (0)	-	Steel	Spring Nonlinear Elastic
4152	post-bolt-springs-tran-b	Discrete	DRO=Translational Spring/Damper (0)	-	Steel	Spring Nonlinear Elastic
4261-4271	bolt-p11b - bolt-p21b	Solid	Fully Integrated S/R (2)	-	Steel	Rigid
4361-4371	nut-p11b - nut-p21b	Solid	Fully Integrated S/R (2)	-	Steel	Rigid
4001	posts-w-flange	Shell	Fully Integrated Shell Element (16)	4.953	Steel (A36)	Piecewise Linear Plasticity
4002	posts-w-web	Shell	Fully Integrated Shell Element (16)	4.318	Steel (A36)	Piecewise Linear Plasticity
4003	posts-w-blockouts	Solid	Fully Integrated S/R (2)	-	Wood	Elastic
4011	posts-thrie-flange	Shell	Fully Integrated Shell Element (16)	4.953	Steel (A36)	Piecewise Linear Plasticity
4012	posts-thrie-web	Shell	Fully Integrated Shell Element (16)	4.318	Steel (A36)	Piecewise Linear Plasticity
4013	posts-thrie-blockouts	Solid	Fully Integrated S/R (2)	-	Wood	Elastic
4021	posts-tran-flange	Shell	Fully Integrated Shell Element (16)	4.953	Steel (A36)	Piecewise Linear Plasticity
4022	posts-tran-web	Shell	Fully Integrated Shell Element (16)	4.318	Steel (A36)	Piecewise Linear Plasticity
4400	soil-parallel-w	Discrete	DRO=Translational Spring/Damper (0)	-	Equivalent Soil	Spring General Nonlinear
4401	soil-perpentic-w	Discrete	DRO=Translational Spring/Damper (0)	-	Equivalent Soil	Spring General Nonlinear
4402	soil-parallel-thrie	Discrete	DRO=Translational Spring/Damper (0)	-	Equivalent Soil	Spring General Nonlinear
4403	soil-perpentic-thrie	Discrete	DRO=Translational Spring/Damper (0)	-	Equivalent Soil	Spring General Nonlinear
4404	soil-parallel-tran	Discrete	DRO=Translational Spring/Damper (0)	-	Equivalent Soil	Spring General Nonlinear
4405	soil-perpentic-tran	Discrete	DRO=Translational Spring/Damper (0)	-	Equivalent Soil	Spring General Nonlinear
4410	soil-masses-w	Shell	Belytschko-Tsay (2)	0.5	-	Rigid
4412	soil-masses-thrie	Shell	Belytschko-Tsay (2)	0.5	-	Rigid
4414	soil-masses-tran	Shell	Belytschko-Tsay (2)	0.5	-	Rigid
4503-4521	tube-3 - tube-21	Shell	Belytschko-Tsay (2)	0.5	-	Rigid
4023	tran-blockouts-steel	Shell	Fully Integrated Shell Element (16)	4.7625	Steel	Piecewise Linear Plasticity
4040-4051	bo-hole-p16-rr-upr - bo-hole-p21-rr-lwr	Shell	Fully Integrated Shell Element (16)	4.7625	-	Rigid
4060-4071	bo-hole-p16-frt-upr - bo-hole-p21-frt-lwr	Shell	Fully Integrated Shell Element (16)	4.7625	-	Rigid
2001	wbeam-1-25ft	Shell	Fully Integrated Shell Element (16)	2.67	Steel	Piecewise Linear Plasticity
2002	wbeam-1-holes	Shell	Fully Integrated Shell Element (16)	2.67	-	Piecewise Linear Plasticity
2003	wbeam-1-holes-ab-rigid	Shell	Fully Integrated Shell Element (16)	2.67	-	Rigid
2004	wbeam-1-holes-nulls	Shell	Fully Integrated Shell Element (16)	2.67	-	Null

Table A-3. Summary of AGT Model Parts and LS-DYNA Parameters, Cont.

Part Number	Part Name	Element Type (*SECTION)	Element Formulation	Thickness	Material Type	Material Formulation (*MAT)
2005	wbeam-2-12.5ft	Shell	Fully Integrated Shell Element (16)	2.67	Steel	Piecewise Linear Plasticity
2006	wbeam-3-12.5ft	Shell	Fully Integrated Shell Element (16)	2.67	Steel	Piecewise Linear Plasticity
2007	wbeam-mid-holes	Shell	Fully Integrated Shell Element (16)	2.67	-	Piecewise Linear Plasticity
2011	w2t-rail	Shell	Fully Integrated Shell Element (16)	3.43	Steel	Piecewise Linear Plasticity
2012	w2t-rail-holes	Shell	Fully Integrated Shell Element (16)	3.43	-	Piecewise Linear Plasticity
2015	thrie-1	Shell	Fully Integrated Shell Element (16)	2.67	Steel	Piecewise Linear Plasticity
2016	thrie-1-holes	Shell	Fully Integrated Shell Element (16)	2.67	-	Piecewise Linear Plasticity
2017	thrie-2	Shell	Fully Integrated Shell Element (16)	5.34	Steel	Piecewise Linear Plasticity
2018	thrie-2-holes	Shell	Fully Integrated Shell Element (16)	5.34	-	Piecewise Linear Plasticity
2021	thrie-end-shoe	Shell	Fully Integrated Shell Element (16)	3.43	Steel	Piecewise Linear Plasticity
2022	thrie-end-shoe-holes	Shell	Fully Integrated Shell Element (16)	3.43	-	Rigid

Appendix B. V&V of Silverado and Tangent AGT Simulation

A MASH 2270P Pickup Truck
(Report 350 or MASH08 or EN1317 Vehicle Type)

Striking a 31-in. tall Approach Guardrail Transition
(roadside hardware type and name)

Report Date: 4/10/2019

Type of Report (check one)

- Verification (known numerical solution compared to new numerical solution) or
 Validation (full-scale crash test compared to a numerical solution).

General Information	Known Solution	Analysis Solution
Performing Organization	MwRSF	MwRSF
Test/Run Number:	AGTB-2	agt-v3r-v15-single-thrie
Vehicle:	2010 Dodge Ram 1500 Quad Cab	2007 Chevrolet Silverado
Reference:		
Impact Conditions		
Vehicle Mass:	2267 kg	2270 kg
Speed:	100.8 km/h	100.8 km/h
Angle:	25.4	25.0
Impact Point:	152 mm US CL P17	152 mm US CL P17

Composite Validation/Verification Score

List the Report 350/MASH08 or EN1317 Test Number	
Part I	Did all solution verification criteria in Table E-1 pass?
Part II	Do all the time history evaluation scores from Table E-2 result in a satisfactory comparison (i.e., the comparison passes the criterion)? If all the values in Table E-2 did not pass, did the weighted procedure shown in Table E-3 result in an acceptable comparison. If all the criteria in Table E-2 pass, enter "yes." If all the criteria in Table E-2 did not pass but Table E-3 resulted in a passing score, enter "yes."
Part III	All the criteria in Table E-4 (Test-PIRT) passed?
	Are the results of Steps I through III all affirmative (i.e., YES)? If all three steps result in a "YES" answer, the comparison can be considered validated or verified. If one of the steps results in a negative response, the result cannot be considered validated or verified.

The analysis solution (check one) is is NOT verified/validated against the known solution.

PART I: BASIC INFORMATION

These forms may be used for validation or verification of roadside hardware crash tests. If the known solution is a full-scale crash test (i.e., physical experiment) which is being compared to a numerical solution (e.g., LSDYNA analysis) then the procedure is a validation exercise. If the known solution is a numerical solution (e.g., a prior finite element model using a different program or earlier version of the software) then the procedure is a verification exercise. This form can also be used to verify the repeatability of crash tests by comparing two full-scale crash test experiments. Provide the following basic information for the validation/verification comparison:

1. What type of roadside hardware is being evaluated (check one)?
 Longitudinal barrier or transition
 Terminal or crash cushion
 Breakaway support or work zone traffic control device
 Truck-mounted attenuator
 Other hardware: _____

2. What test guidelines were used to perform the full-scale crash test (check one)?
 NCHRP Report 350
 MASH08
 EN1317
 Other: MASH 2016

3. Indicate the test level and number being evaluated (fill in the blank). 3-21

4. Indicate the vehicle type appropriate for the test level and number indicated in item 3 according to the testing guidelines indicated in item 2.

NCHRP Report 350/MASH08

- | | | |
|---------------------------------|---|---------------------------------------|
| <input type="checkbox"/> 700C | <input type="checkbox"/> 820C | <input type="checkbox"/> 1100C |
| <input type="checkbox"/> 2000P | <input checked="" type="checkbox"/> 2270P | <input type="checkbox"/> Other: _____ |
| <input type="checkbox"/> 8000S | <input type="checkbox"/> 10000S | |
| <input type="checkbox"/> 36000V | | |
| <input type="checkbox"/> 36000T | | |

EN1317

- | | | |
|---|---|---|
| <input type="checkbox"/> Car (900 kg) | <input type="checkbox"/> Car (1300 kg) | <input type="checkbox"/> Car (1500 kg) |
| <input type="checkbox"/> Rigid HGV (10 ton) | <input type="checkbox"/> Rigid HGV (16 ton) | <input type="checkbox"/> Rigid HGV (30 ton) |
| <input type="checkbox"/> Bus (13 ton) | <input type="checkbox"/> Articulated HGV (38 ton) | <input type="checkbox"/> Other: _____ |

PART II: ANALYSIS SOLUTION VERIFICATION

Using the results of the analysis solution, fill in the values for Table E-1. These values are indications of whether the analysis solution produced a numerically stable result and do not necessarily mean that the result is a good comparison to the known solution. The purpose of this table is to ensure that the numerical solution produces results that are numerically stable and conform to the conservation laws (e.g., energy, mass and momentum).

Table E-1. Analysis Solution Verification Table

Verification Evaluation Criteria	Change (%)	Pass?
<i>Total energy</i> of the analysis solution (i.e., kinetic, potential, contact, etc.) must not vary more than 10 percent from the beginning of the run to the end of the run.	1.2%	Yes
<i>Hourglass Energy</i> of the analysis solution at the end of the run is less than <i>five percent</i> of the total <i>initial energy</i> at the <i>beginning</i> of the run.	11.36%	No
<i>Hourglass Energy</i> of the analysis solution at the end of the run is less than <i>ten percent</i> of the total <i>internal energy</i> at the <i>end</i> of the run.	54.69%	No
The part/material with the highest amount of hourglass energy at the end of the run is less than ten percent of the total internal energy of the part/material at the end of the run. (Part id=2000682, hg=40200, internal energy at end of run=302)	13,311%	No
Mass added to the total model is less than five percent of the total model mass at the beginning of the run.	0.07%	Yes
The part/material with the most mass added had less than 10 percent of its initial mass added. (Part id=4023: tran-blockouts-steel, Initial Mass=48.285 kg, Mass Added=9.64 kg)	19.96%	No
The moving parts/materials in the model have less than five percent of mass added to the initial moving mass of the model.	0.19%	Yes
There are no shooting nodes in the solution?	No	Yes
There are no solid elements with negative volumes?	No	Yes

If all the analysis solution verification criteria are scored as passing, the analysis solution can be verified or validated against the known solution. If any criterion in Table E-1 does not pass one of the verification criterion listed in Table E-1, the analysis solution cannot be used to verify or validate the known solution. If there are exceptions that the analyst thinks are relevant these should be footnoted in the table and explained below the table.

The Analysis Solution (check one) passes does NOT pass all the criteria in Table E1-1

with without exceptions as noted.

PART III: TIME HISTORY EVALUATION TABLE

Using the RSVVP computer program ('Single channel' option), compute the Sprague-Geers MPC metrics and ANOVA metrics using time-history data from the known and analysis solutions for a time period starting at the beginning of the contact and ending at the loss of contact. Both the Sprague-Geers and ANOVA metrics must be calculated based on the original units the data was collected in (e.g., if accelerations were measured in the experiment with accelerometers then the comparison should be between accelerations. If rate gyros were used in the experiment, the comparison should be between rotation rates). If all six data channels are not available for both the known and analysis solutions, enter "N/A" in the column corresponding to the missing data. Enter the values obtained from the RSVVP program in Table E-2 and indicate if the comparison was acceptable or not by entering a "yes" or "no" in the "Agree?" column. Attach a graph of each channel for which the metrics have been compared at the end of the report.

Enter the filter, synchronization method and shift/drift options used in RSVVP to perform the comparison so that it is clear to the reviewer what options were used. Normally, SAE J211 filter class 180 is used to compare vehicle kinematics in full-scale crash tests. Either synchronization option in RSVVP is acceptable and both should result in a similar start point. The shift and drift options should generally only be used for the experimental curve since shift and drift are characteristics of sensors. For example, the zero point for an accelerometer sometimes "drifts" as the accelerometer sits out in the open environment of the crash test pad whereas there is no sensor to "drift" or "shift" in a numerical solution.

In order for the analysis solution to be considered in agreement with the known solution (i.e., verified or validated), all the criteria scored in Table E-2 must pass. If all the channels in Table E-2 do not pass, fill out Table E-3, the multi-channel weighted procedure.

If one or more channels do not satisfy the criteria in Table E-2, the multi-channel weighting option may be used. Using the RSVVP computer program ('Multiple channel' option), compute the Sprague-Geers MPC metrics and ANOVA metrics using all the time histories data from the known and analysis solutions for a time period starting at the beginning of the contact and ending at the loss of contact. If all six data channels are not available for both the known and analysis solutions, enter "N/A" in the column corresponding to the missing data.

For some types of roadside hardware impacts, some of the channels are not as important as others. An example might be a breakaway sign support test where the lateral (i.e., Y) and vertical (i.e., Z) accelerations are insignificant to the dynamics of the crash event. The weighting procedure provides a way to weight the most important channels more highly than less important channels. The procedure used is based on the area under the curve, therefore, the weighing scheme will weight channels with large areas more highly than those with smaller areas. In general, using the "Area (II)" method is acceptable although if the complete inertial properties of the vehicle are available the "inertial" method may be used. Enter the values obtained from the RSVVP program in Table E-3 and indicate if the comparison was acceptable or not by entering a "yes" or "no" in the "Agree?" column.

In order for the analysis solution to be considered in agreement with the known solution (i.e., verified or validated), all the criteria scored in Table E-3 must pass.

Table E-2. Roadside Safety Validation Metrics Rating Table – Time History Comparisons (single channel option – CFC-60)

Evaluation Criteria							Time interval [_ 0 sec; 0.5 sec_]					
RSVVP Curve Preprocessing Options										M	P	Pass?
	Filter Option	Sync. Option	Shift		Drift		M	P	Pass?			
			True Curve	Test Curve	True Curve	Test Curve						
O Sprague-Geers Metrics List all the data channels being compared. Calculate the M and P metrics using RSVVP and enter the results. Values less than or equal to 40 are acceptable.												
X acceleration	CFC 60	N	N	N	N	N	20.7	31.6	Yes			
Y acceleration	CFC 60	N	N	N	N	N	6.4	25.7	Yes			
Z acceleration	CFC 60	N	N	N	N	N	27.1	48.5	No			
Roll rate	CFC 60	N	N	N	N	N	0.9	36.2	Yes			
Pitch rate	CFC 60	N	N	N	N	N	11	47.5	No			
Yaw rate	CFC 60	N	N	N	N	N	20	11.2	Yes			
P ANOVA Metrics List all the data channels being compared. Calculate the ANOVA metrics using RSVVP and enter the results. Both of the following criteria must be met: <ul style="list-style-type: none"> The mean residual error must be less than five percent of the peak acceleration ($\bar{e} \leq 0.05 \cdot a_{Peak}$) and The standard deviation of the residuals must be less than 35 percent of the peak acceleration ($\sigma \leq 0.35 \cdot a_{Peak}$) 							Mean Residual	Standard Deviation of Residuals	Pass?			
X acceleration/Peak										-0.48	21.61	Yes
Y acceleration/Peak										1.84	26.53	Yes
Z acceleration/Peak										-2.31	33.5	Yes
Roll rate										1.24	7.1	Yes
Pitch rate										0.24	9.34	Yes
Yaw rate										0.93	11.37	Yes

The Analysis Solution (check one) passes does NOT pass all the criteria in Table E-2 (single-channel time history comparison). If the Analysis Solution does NOT pass, perform the analysis in Table E-3 (multi-channel time history comparison).

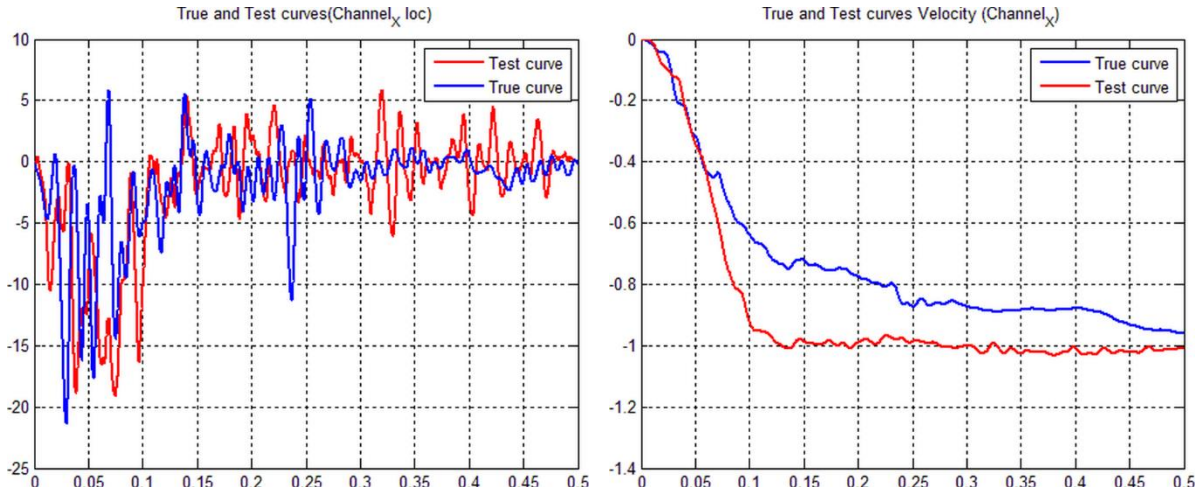


Figure 1. X-Channel (left) acceleration-time history data used to compute metrics, and (right) integration of acceleration-time history data

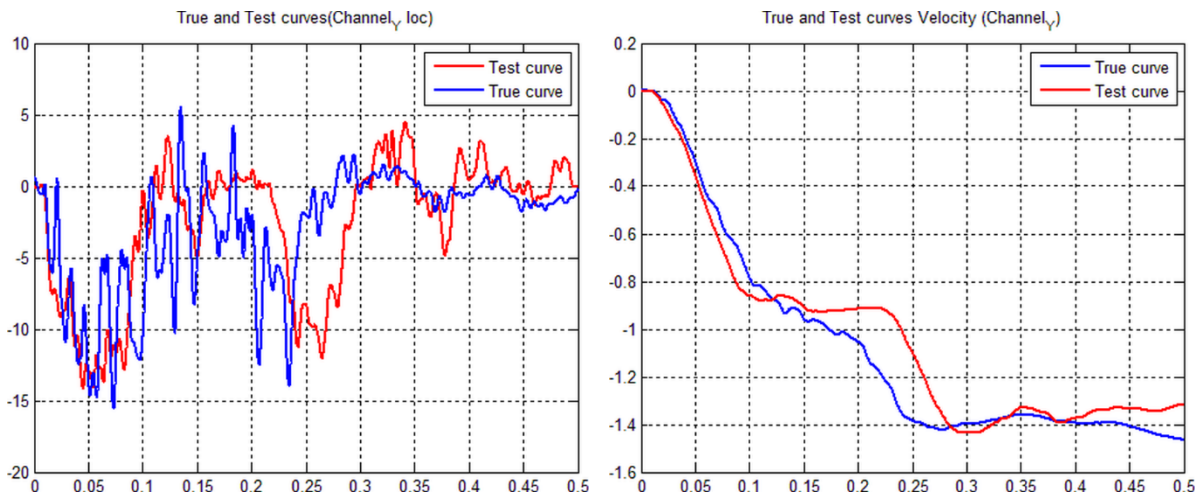


Figure 2. Y-Channel (left) acceleration-time history data used to compute metrics, and (right) integration of acceleration-time history data

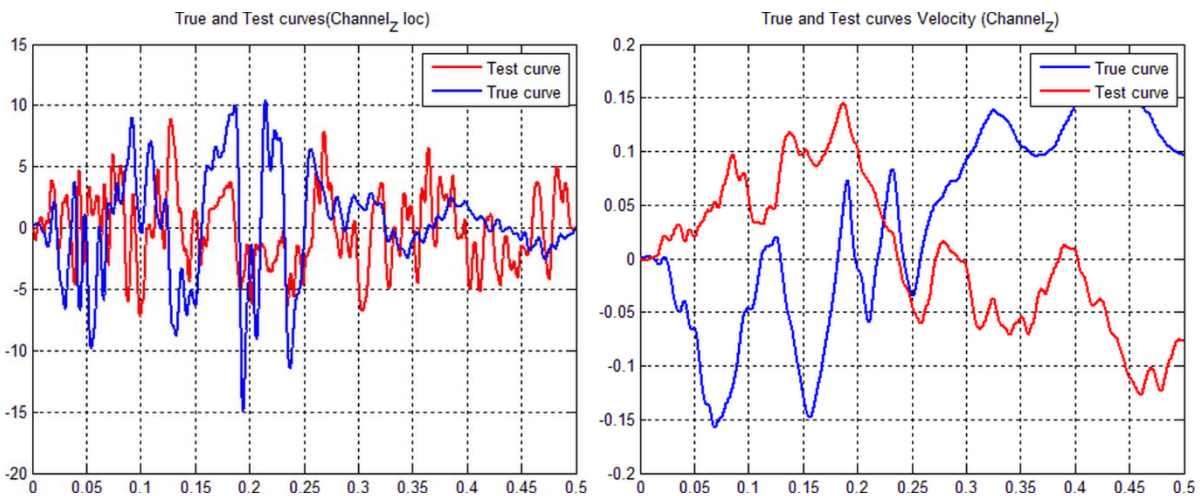


Figure 3. Z-Channel (left) acceleration-time history data used to compute metrics, and (right) integration of acceleration-time history data

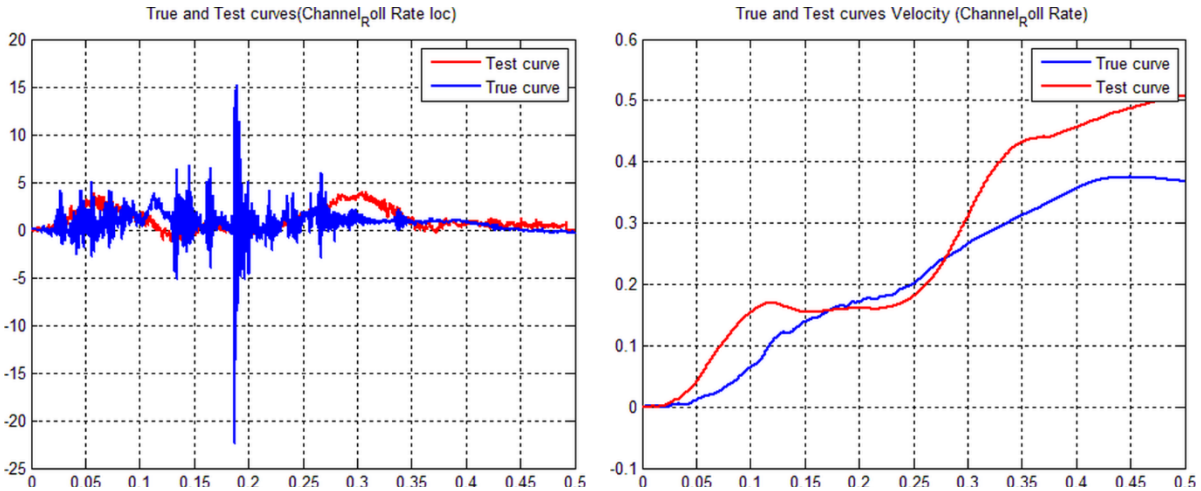


Figure 4. Roll Channel (left) angular rate-time history data used to compute metrics, and (right) integration of angular rate-time history data

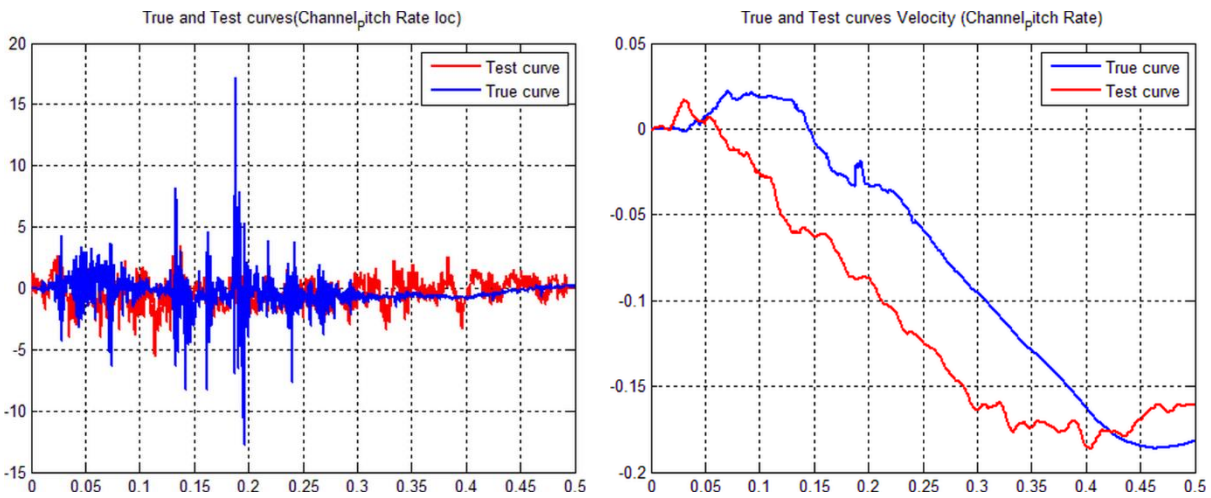


Figure 5. Pitch Channel (left) angular rate-time history data used to compute metrics, and (right) integration of angular rate-time history data

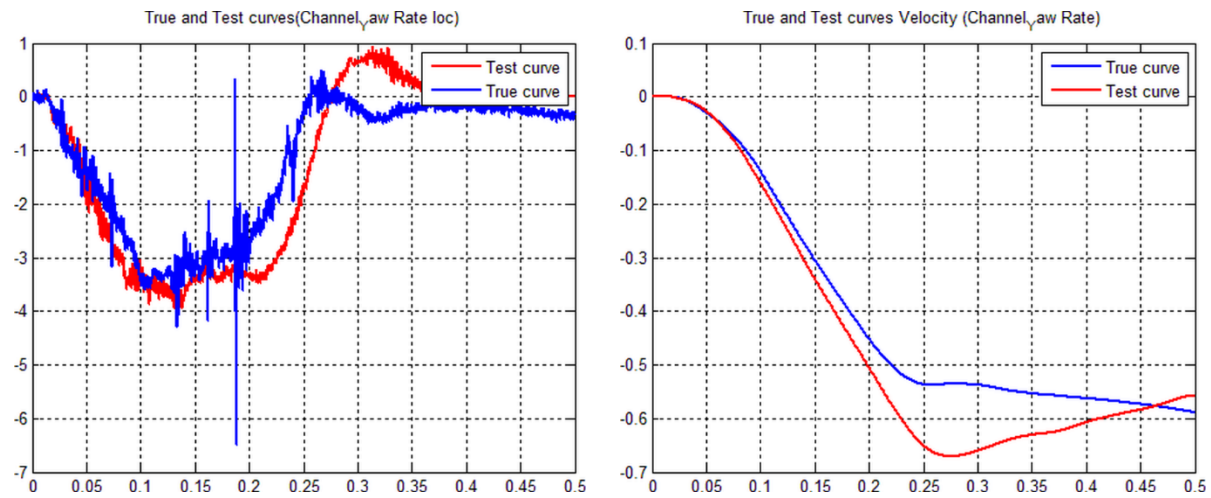


Figure 6. Yaw Channel (left) angular rate-time history data used to compute metrics, and (right) integration of angular rate-time history data

Table E-3. Roadside Safety Validation Metrics Rating Table – Time History Comparisons (multi-channel option – CFC-60)

Evaluation Criteria (time interval [_ 0 sec; 0.5 sec_])																	
Channels (Select which were used)																	
<input checked="" type="checkbox"/> X Acceleration	<input checked="" type="checkbox"/> Y Acceleration	<input checked="" type="checkbox"/> Z Acceleration															
<input checked="" type="checkbox"/> Roll rate	<input checked="" type="checkbox"/> Pitch rate	<input checked="" type="checkbox"/> Yaw rate															
Multi-Channel Weights <input checked="" type="checkbox"/> Area II method <input type="checkbox"/> Inertial method	X Channel: Y Channel: Z Channel: Yaw Channel: Roll Channel: Pitch Channel:	<table border="1"> <caption>Channel Weights Data</caption> <thead> <tr> <th>Channel</th> <th>Weight</th> </tr> </thead> <tbody> <tr> <td>X acc</td> <td>0.19</td> </tr> <tr> <td>Y acc</td> <td>0.29</td> </tr> <tr> <td>Z acc</td> <td>0.02</td> </tr> <tr> <td>Yaw</td> <td>0.26</td> </tr> <tr> <td>Roll</td> <td>0.16</td> </tr> <tr> <td>Pitch</td> <td>0.08</td> </tr> </tbody> </table>		Channel	Weight	X acc	0.19	Y acc	0.29	Z acc	0.02	Yaw	0.26	Roll	0.16	Pitch	0.08
Channel	Weight																
X acc	0.19																
Y acc	0.29																
Z acc	0.02																
Yaw	0.26																
Roll	0.16																
Pitch	0.08																
O	Sprague-Geer Metrics Values less or equal to 40 are acceptable.	M	P	Pass?													
		12.5	27	Yes													
P	ANOVA Metrics Both of the following criteria must be met: <ul style="list-style-type: none"> The mean residual error must be less than five percent of the peak acceleration $(\bar{e} \leq 0.05 \cdot a_{Peak})$ The standard deviation of the residuals must be less than 35 percent of the peak acceleration $(\sigma \leq 0.35 \cdot a_{Peak})$ 	Mean Residual	Standard Deviation of Residuals	Pass?													
		0.9	17.3	Yes													

The Analysis Solution (check one) passes does NOT pass all the criteria in Table E-3.

Table E-2. Roadside Safety Validation Metrics Rating Table – Time History Comparisons (single channel option – CFC-180)

Evaluation Criteria							Time interval [_ 0 sec; 0.5 sec_]					
O	Sprague-Geers Metrics List all the data channels being compared. Calculate the M and P metrics using RSVVP and enter the results. Values less than or equal to 40 are acceptable.						M	P	Pass?			
	RSVVP Curve Preprocessing Options											
		Filter Option	Sync. Option	Shift		Drift						
				True Curve	Test Curve	True Curve				Test Curve		
	X acceleration	CFC 180	N	N	N	N				29.9	36	Yes
	Y acceleration	CFC 180	N	N	N	N				3.1	28.7	Yes
	Z acceleration	CFC 180	N	N	N	N				1	50.4	No
	Roll rate	CFC 180	N	N	N	N				0.9	36.2	Yes
Pitch rate	CFC 180	N	N	N	N	11	47.5	No				
Yaw rate	CFC 180	N	N	N	N	20	11.2	Yes				
P	ANOVA Metrics List all the data channels being compared. Calculate the ANOVA metrics using RSVVP and enter the results. Both of the following criteria must be met: <ul style="list-style-type: none"> The mean residual error must be less than five percent of the peak acceleration ($\bar{e} \leq 0.05 \cdot a_{Peak}$) and The standard deviation of the residuals must be less than 35 percent of the peak acceleration ($\sigma \leq 0.35 \cdot a_{Peak}$) 						Mean Residual	Standard Deviation of Residuals	Pass?			
	X acceleration/Peak									-0.43	23.44	Yes
	Y acceleration/Peak									1.49	25.23	Yes
	Z acceleration/Peak									-1.67	31.54	Yes
	Roll rate									1.24	7.1	Yes
	Pitch rate									0.24	9.34	Yes
	Yaw rate									0.93	11.37	Yes

The Analysis Solution (check one) passes does NOT pass all the criteria in Table E-2 (single-channel time history comparison). If the Analysis Solution does NOT pass, perform the analysis in Table E-3 (multi-channel time history comparison).

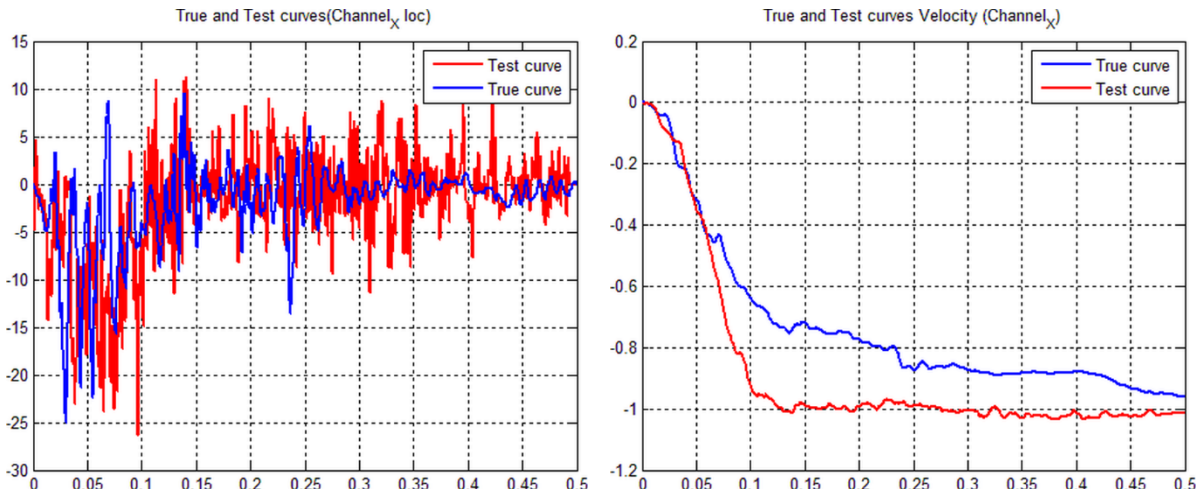


Figure 7. X-Channel (left) acceleration-time history data used to compute metrics, and (right) integration of acceleration-time history data

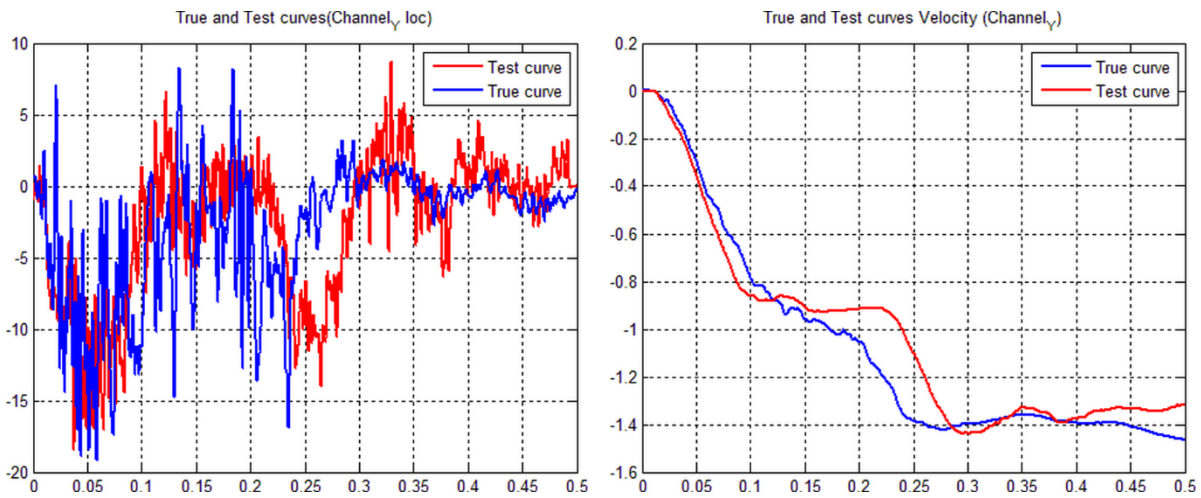


Figure 8. Y-Channel (left) acceleration-time history data used to compute metrics, and (right) integration of acceleration-time history data

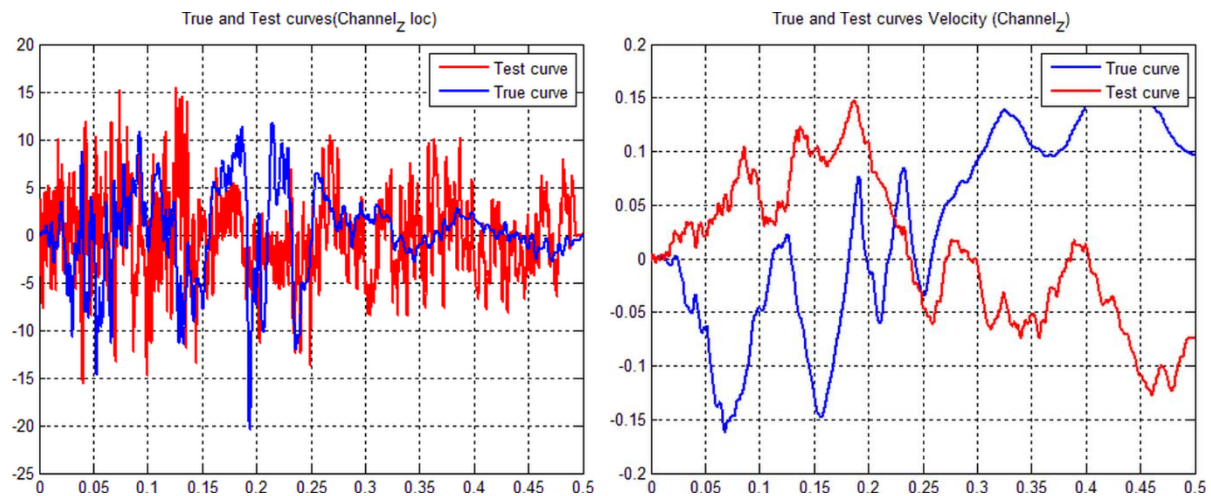


Figure 9. Z-Channel (left) acceleration-time history data used to compute metrics, and (right) integration of acceleration-time history data

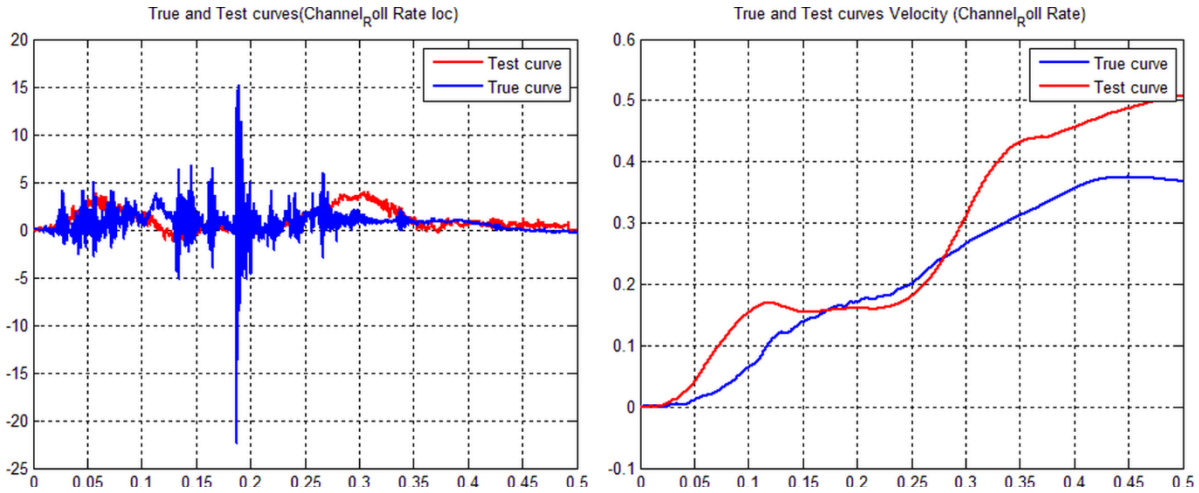


Figure 10. Roll Channel (left) angular rate-time history data used to compute metrics, and (right) integration of angular rate-time history data

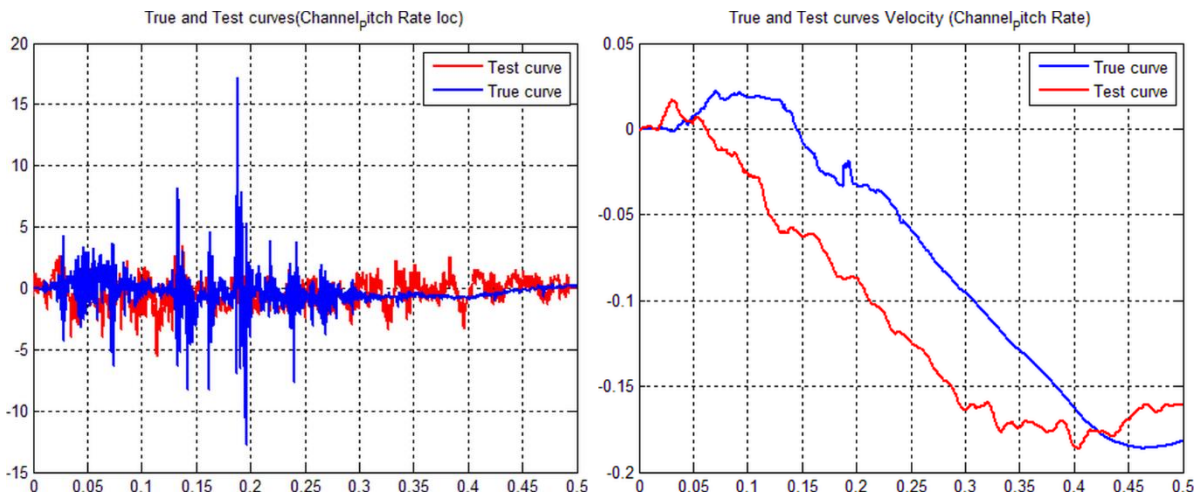


Figure 11. Pitch Channel (left) angular rate-time history data used to compute metrics, and (right) integration of angular rate-time history data

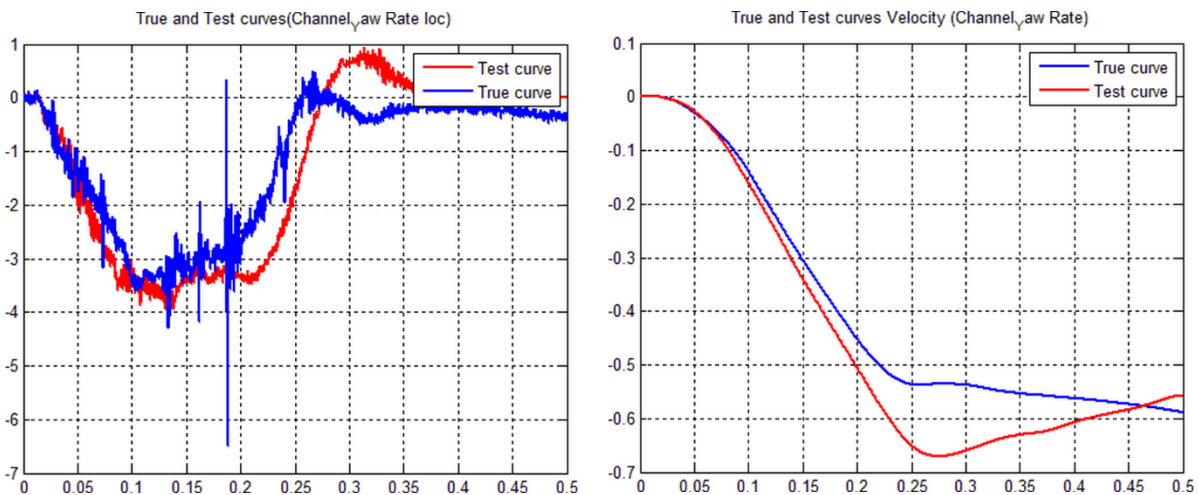


Figure 12. Yaw Channel (left) angular rate-time history data used to compute metrics, and (right) integration of angular rate-time history data

Table E-3. Roadside Safety Validation Metrics Rating Table – Time History Comparisons (multi-channel option – CFC-180)

Evaluation Criteria (time interval [0 sec; 0.5 sec])																	
Channels (Select which were used)																	
<input checked="" type="checkbox"/> X Acceleration	<input checked="" type="checkbox"/> Y Acceleration	<input checked="" type="checkbox"/> Z Acceleration															
<input checked="" type="checkbox"/> Roll rate	<input checked="" type="checkbox"/> Pitch rate	<input checked="" type="checkbox"/> Yaw rate															
Multi-Channel Weights <input checked="" type="checkbox"/> Area II method <input type="checkbox"/> Inertial method	X Channel: Y Channel: Z Channel: Yaw Channel: Roll Channel: Pitch Channel:	<table border="1"> <caption>Channel Weights</caption> <thead> <tr> <th>Channel</th> <th>Weight</th> </tr> </thead> <tbody> <tr> <td>X acc</td> <td>0.19</td> </tr> <tr> <td>Y acc</td> <td>0.29</td> </tr> <tr> <td>Z acc</td> <td>0.00</td> </tr> <tr> <td>Yaw</td> <td>0.26</td> </tr> <tr> <td>Roll</td> <td>0.16</td> </tr> <tr> <td>Pitch</td> <td>0.08</td> </tr> </tbody> </table>		Channel	Weight	X acc	0.19	Y acc	0.29	Z acc	0.00	Yaw	0.26	Roll	0.16	Pitch	0.08
Channel	Weight																
X acc	0.19																
Y acc	0.29																
Z acc	0.00																
Yaw	0.26																
Roll	0.16																
Pitch	0.08																
O	Sprague-Geer Metrics Values less or equal to 40 are acceptable.	M	P	Pass?													
		12.8	28.7	Yes													
P	ANOVA Metrics Both of the following criteria must be met: <ul style="list-style-type: none"> The mean residual error must be less than five percent of the peak acceleration $(\bar{e} \leq 0.05 \cdot a_{Peak})$ The standard deviation of the residuals must be less than 35 percent of the peak acceleration $(\sigma \leq 0.35 \cdot a_{Peak})$ 	Mean Residual	Standard Deviation of Residuals	Pass?													
		0.8	17.2	Yes													

The Analysis Solution (check one) passes does NOT pass all the criteria in Table E-3.

PART IV: PHENOMENA IMPORTANCE RANKING TABLE

Table E-4 is similar to the evaluation tables in Report 350 and MASH. For the Report 350 or MASH test number identified in Part I (e.g., test 3-10, 5-12, etc.), circle all the evaluation criteria applicable to that test in Table E-4. The tests that apply to each criterion are listed in the far right column without the test level designator. For example, if a Report 350 test 3-11 is being compared (i.e., a pickup truck striking a barrier at 25 degrees and 100 km/hr), circle all the criteria in the second column where the number “11” appears in the far right column. Some of the Report 350 evaluation criteria have been removed (i.e., J and K) since they are not generally useful in assessing the comparison between the known and analysis solutions.

Table E-4. Evaluation Criteria Test Applicability Table

Evaluation Factors	Evaluation Criteria	Applicable Tests								
Structural Adequacy	A Test article should contain and redirect the vehicle; the vehicle should not penetrate, under-ride, or override the installation although controlled lateral deflection of the test article is acceptable.	10, 11, 12, 20, 21, 22, 35, 36, 37, 38								
	B The test article should readily activate in a predictable manner by breaking away, fracturing or yielding.	60, 61, 70, 71, 80, 81								
	C Acceptable test article performance may be by redirection, controlled penetration or controlled stopping of the vehicle.	30, 31,, 32, 33, 34, 39, 40, 41, 42, 43, 44, 50, 51, 52, 53								
Occupant Risk	D Detached elements, fragments or other debris from the test article should not penetrate or show potential for penetrating the occupant compartment, or present an undue hazard to other traffic, pedestrians or personnel in a work zone.	All								
	E Detached elements, fragments or other debris from the test article, or vehicular damage should not block the driver's vision or otherwise cause the driver to lose control of the vehicle. (Answer Yes or No)	70, 71								
	F The vehicle should remain upright during and after the collision although moderate roll, pitching and yawing are acceptable.	All except those listed in criterion G								
	G It is preferable, although not essential, that the vehicle remain upright during and after collision.	12, 22 (for test level 1 – 30, 31, 32, 33, 34, 35, 36, 37, 38, 39, 40, 41, 42, 43, 44)								
	H	Occupant impact velocities should satisfy the following:								
		Occupant Impact Velocity Limits (m/s)								
		<table border="1" data-bbox="412 1073 1057 1209"> <thead> <tr> <th data-bbox="412 1073 626 1104">Component</th> <th data-bbox="626 1073 841 1104">Preferred</th> <th data-bbox="841 1073 1057 1104">Maximum</th> </tr> </thead> <tbody> <tr> <td data-bbox="412 1104 626 1167">Longitudinal and Lateral</td> <td data-bbox="626 1104 841 1167">9</td> <td data-bbox="841 1104 1057 1167">12</td> </tr> <tr> <td data-bbox="412 1167 626 1209">Longitudinal</td> <td data-bbox="626 1167 841 1209">3</td> <td data-bbox="841 1167 1057 1209">5</td> </tr> </tbody> </table>	Component	Preferred	Maximum	Longitudinal and Lateral	9	12	Longitudinal	3
Component	Preferred	Maximum								
Longitudinal and Lateral	9	12								
Longitudinal	3	5								
I	Occupant ridedown accelerations should satisfy the following:									
	Occupant Ridedown Acceleration Limits (g's)									
	<table border="1" data-bbox="412 1283 1057 1377"> <thead> <tr> <th data-bbox="412 1283 626 1314">Component</th> <th data-bbox="626 1283 841 1314">Preferred</th> <th data-bbox="841 1283 1057 1314">Maximum</th> </tr> </thead> <tbody> <tr> <td data-bbox="412 1314 626 1377">Longitudinal and Lateral</td> <td data-bbox="626 1314 841 1377">15</td> <td data-bbox="841 1314 1057 1377">20</td> </tr> </tbody> </table>	Component	Preferred	Maximum	Longitudinal and Lateral	15	20	10, 20, 30,31, 32, 33, 34, 36, 40, 41, 42, 43, 50, 51, 52, 53, 60, 61, 70, 71, 80, 81		
Component	Preferred	Maximum								
Longitudinal and Lateral	15	20								
Vehicle Trajectory	L The occupant impact velocity in the longitudinal direction should not exceed 40 ft/sec and the occupant ride-down acceleration in the longitudinal direction should not exceed 20 G's.	11,21, 35, 37, 38, 39								
	M The exit angle from the test article preferable should be less than 60 percent of test impact angle, measured at the time of vehicle loss of contact with test device.	10, 11, 12, 20, 21, 22, 35, 36, 37, 38, 39								
	N Vehicle trajectory behind the test article is acceptable.	30, 31, 32, 33, 34, 39, 42, 43, 44, 60, 61, 70, 71, 80, 81								

Complete Table E-5 according to the results of the known solution (e.g., crash test) and the numerical solution (e.g., simulation). Consistent with Report 350 and MASH, Task E-5 has three parts: the structural adequacy phenomena listed in Table E-5a, the occupant risk phenomena listed in Table E-5b and the vehicle trajectory criteria listed in Table E-5c. If the result of the analysis solution agrees with the known solution, mark the “agree” column “yes.” For example, if the vehicle in both the known and analysis solutions rolls over and, therefore, fails criterion F1, the known and the analysis columns for criterion F1 would be evaluated as “no.” Even though both failed the criteria, they agree with each other so the “agree” column is marked as “yes.” Any criterion that is not applicable to the test being evaluated (i.e., not circled in Table E-4) should be indicated by entering “NA” in the “agree?” column for that row.

Many of the Report 350 evaluation criteria have been subdivided into more specific phenomenon. For example, criterion A is divided into eight sub-criteria, A1 through A8, that provide more specific and quantifiable phenomena for evaluation. Some of the values are simple yes or no questions while other request numerical values. For the numerical phenomena, the analyst should enter the value for the known and analysis result and then calculate the relative difference. Relative difference is always the absolute value of the difference of the known and analysis solutions divided by the known solution. Enter the value in the “relative difference” column. If the relative difference is less than 20 percent, enter “yes” in the “agree?” column.

Sometimes, when the values are very small, the relative difference might be large while the absolute difference is very small. For example, the longitudinal occupant ride down acceleration (i.e., criterion L2) in a test might be 3 g’s and in the corresponding analysis might be 4 g’s. The relative difference is 33 percent but the absolute difference is only 1 g and the result for both is well below the 20 g limit. Clearly, the analysis solution in this case is a good match to the experiment and the relative difference is large only because the values are small. The absolute difference, therefore, should also be entered into the “Difference” column in Table E-5.

The experimental and analysis result can be considered to agree as long as either the relative difference or the absolute difference is less than the acceptance limit listed in the criterion. Generally, relative differences of less than 20 percent are acceptable and the absolute difference limits were generally chosen to represent 20 percent of the acceptance limit in Report 350 or MASH. For example, Report 350 limits occupant ride-down accelerations to those less than 20 g’s so 20 percent of 20 g’s is 4 g’s. As shown for criterion L2 in Table E-5, the relative acceptance limit is 20 percent and the absolute acceptance limit is 4 g’s.

If a numerical model was not created to represent the phenomenon, a value of “NM” (i.e., not modeled) should be entered in the appropriate column of Table E-5. If the known solution for that phenomenon number is “no” then a “NM” value in the “test result” column can be considered to agree. For example, if the material model for the rail element did not include the possibility of failure, “NM” should be entered for phenomenon number T in Table E-5. If the known solution does not indicate rail rupture or failure (i.e., phenomenon T = “no”), then the known and analysis solutions agree and a “yes” can be entered in the “agree?” column. On the other hand, if the known solution shows that a rail rupture did occur resulting in a phenomenon T entry of “yes” for the known solution, the known and analysis solutions do not agree and “no” should be entered in the “agree?” column. Analysts should seriously consider refining their model to incorporate any phenomena that appears in the known solution and is shown in Table E-5.

All the criteria identified in Table E-4 are expected to agree but if one does not and, in the opinion of the analyst, is not considered important to the overall evaluation for this particular comparison, then a footnote should be provided with a justification for why this particular criteria can be ignored for this particular comparison.

Table E-5(a). Roadside Safety Phenomena Importance Ranking Table (Structural Adequacy)

		Evaluation Criteria	Known Result	Analysis Result	Difference Relative/ Absolute	Agree?
Structural Adequacy	A1	Test article should contain and redirect the vehicle; the vehicle should not penetrate, under-ride, or override the installation although controlled lateral deflection of the test article is acceptable. (Answer Yes or No)	Yes	Yes	X	Yes
	A2	Maximum dynamic deflection: - Relative difference is less than 20 percent or - Absolute difference is less than 0.15 m	0.136 m	0.126 m	7.35% 0.01 m	Yes
	A3	Length of vehicle-barrier contact: - Relative difference is less than 20 percent or - Absolute difference is less than 2 m	4.04 m	3.07 m	24.01% 0.97 m	Yes
	A4	Number of broken or significantly bent posts is less than 20 percent. (Posts that deflected greater than 1 in.)	7	6	14.29% 1 post	Yes
	A5	Did the rail element rupture or tear (Answer Yes or No)	No	No	X	Yes
	A6	Were there failures of connector elements (Answer Yes or No).	No	No	X	Yes
	A7	Was there significant snagging between the vehicle wheels and barrier elements (Answer Yes or No).	No	No	X	Yes
	A8	Was there significant snagging between vehicle body components and barrier elements (Answer Yes or No).	Yes	Yes	X	Yes

Table E-5(b). Roadside Safety Phenomena Importance Ranking Table (Occupant Risk)

Evaluation Criteria		Known Result	Analysis Result	Difference Relative/ Absolute	Agree?		
Occupant Risk	D	Detached elements, fragments or other debris from the test article should not penetrate or show potential for penetrating the occupant compartment, or present an undue hazard to other traffic, pedestrians or personnel in a work zone. (Answer Yes or No)	Yes	Yes		Yes	
	F1	The vehicle should remain upright during and after the collision although moderate roll, pitching and yawing are acceptable. (Answer Yes or No)	Yes	Yes		Yes	
	F	F2	Maximum roll of the vehicle: - Relative difference is less than 20 percent or - Absolute difference is less than 5 degrees.	21.25°	29.11°	37.0% 7.86°	No
		F3	Maximum pitch of the vehicle is: - Relative difference is less than 20 percent or - Absolute difference is less than 5 degrees.	6.30°	6.12°	2.9% 0.18°	Yes
		F4	Maximum yaw of the vehicle is: - Relative difference is less than 20 percent or - Absolute difference is less than 5 degrees.	39.58°	39.38°	0.5% 0.20°	Yes
			Occupant impact velocities: - Relative difference is less than 20 percent or - Absolute difference is less than 2 m/s.				
	L1	• Longitudinal OIV (m/s)	-6.18	-8.03	29.9% 1.85 m/s	Yes	
		• Lateral OIV (m/s)	7.50	8.13	8.4% 0.63 m/s	Yes	
		• THIV (m/s)	9.43 m/s	NA	-	NA	
	L2		Occupant accelerations: - Relative difference is less than 20 percent or - Absolute difference is less than 4 g's.				
		• Longitudinal ORA	-7.06 g	-12.10 g	71.4% 5.04 g	No	
		• Lateral ORA	10.40 g	11.00 g	5.8% 0.60 g	Yes	
		• PHD	12.53 g	NA	-	NA	
		• ASI	1.37	NA	-	NA	

Table E-5(c). Roadside Safety Phenomena Importance Ranking Table (Vehicle Trajectory)

Evaluation Criteria			Known Result	Analysis Result	Difference Relative/Absolute	Agree?	
Vehicle Trajectory	M	M1	The exit angle from the test article preferable should be less than 60 percent of test impact angle, measured at the time of vehicle loss of contact with test device.	Yes	Yes	X	Yes
		M2	Exit angle at loss of contact: - Relative difference is less than 20 percent or - Absolute difference is less than 5 degrees.	8.99°	13.99°	55.6% 5.0°	No
		M3	Exit velocity at loss of contact: - Relative difference is less than 20 percent or - Absolute difference is less than 5 degrees.	69.98 km/h	64.92 km/h	7.2% 5.06 km/h	Yes
		M4	One or more vehicle tires failed or de-beaded during the collision event (Answer Yes or No).	Yes	NM	X	No

The Analysis Solution (check one) passes does NOT pass all the criteria in Tables E-5a through E-5c with exceptions as noted without exceptions .

Appendix C. V&V of Ram and Tangent AGT Simulation

A MASH 2270P Pickup Truck
(Report 350 or MASH08 or EN1317 Vehicle Type)

Striking a 31-in. tall Approach Guardrail Transition
(roadside hardware type and name)

Report Date: 6/16/2020

Type of Report (check one)

- Verification (known numerical solution compared to new numerical solution) or
 Validation (full-scale crash test compared to a numerical solution).

General Information	Known Solution	Analysis Solution
Performing Organization	MwRSF	MwRSF
Test/Run Number:	AGTB-2	agt-v18--Ram-v2
Vehicle:	2010 Dodge Ram 1500 Quad Cab	2018 Dodge Ram
Reference:		
Impact Conditions		
Vehicle Mass:	2267 kg	2270 kg
Speed:	100.8 km/h	100.8 km/h
Angle:	25.4 degrees	25 degrees
Impact Point:	152 mm US CL P17	153 mm US CL P17

Composite Validation/Verification Score

List the Report 350/MASH08 or EN1317 Test Number	
Part I	Did all solution verification criteria in Table E-1 pass?
Part II	Do all the time history evaluation scores from Table E-2 result in a satisfactory comparison (i.e., the comparison passes the criterion)? If all the values in Table E-2 did not pass, did the weighted procedure shown in Table E-3 result in an acceptable comparison. If all the criteria in Table E-2 pass, enter "yes." If all the criteria in Table E-2 did not pass but Table E-3 resulted in a passing score, enter "yes."
Part III	All the criteria in Table E-4 (Test-PIRT) passed?
	Are the results of Steps I through III all affirmative (i.e., YES)? If all three steps result in a "YES" answer, the comparison can be considered validated or verified. If one of the steps results in a negative response, the result cannot be considered validated or verified.

The analysis solution (check one) is is NOT verified/validated against the known solution.

PART I: BASIC INFORMATION

These forms may be used for validation or verification of roadside hardware crash tests. If the known solution is a full-scale crash test (i.e., physical experiment) which is being compared to a numerical solution (e.g., LSDYNA analysis) then the procedure is a validation exercise. If the known solution is a numerical solution (e.g., a prior finite element model using a different program or earlier version of the software) then the procedure is a verification exercise. This form can also be used to verify the repeatability of crash tests by comparing two full-scale crash test experiments. Provide the following basic information for the validation/verification comparison:

5. What type of roadside hardware is being evaluated (check one)?

- Longitudinal barrier or transition
 Terminal or crash cushion
 Breakaway support or work zone traffic control device
 Truck-mounted attenuator
 Other hardware: _____

6. What test guidelines were used to perform the full-scale crash test (check one)?

- NCHRP Report 350
 MASH08
 EN1317
 Other: _____ MASH 2016 _____

7. Indicate the test level and number being evaluated (fill in the blank). _____ 3-21 _____

8. Indicate the vehicle type appropriate for the test level and number indicated in item 3 according to the testing guidelines indicated in item 2.

NCHRP Report 350/MASH08

- | | | |
|---------------------------------|---|---------------------------------------|
| <input type="checkbox"/> 700C | <input type="checkbox"/> 820C | <input type="checkbox"/> 1100C |
| <input type="checkbox"/> 2000P | <input checked="" type="checkbox"/> 2270P | <input type="checkbox"/> Other: _____ |
| <input type="checkbox"/> 8000S | <input type="checkbox"/> 10000S | |
| <input type="checkbox"/> 36000V | | |
| <input type="checkbox"/> 36000T | | |

EN1317

- | | | |
|---|---|---|
| <input type="checkbox"/> Car (900 kg) | <input type="checkbox"/> Car (1300 kg) | <input type="checkbox"/> Car (1500 kg) |
| <input type="checkbox"/> Rigid HGV (10 ton) | <input type="checkbox"/> Rigid HGV (16 ton) | <input type="checkbox"/> Rigid HGV (30 ton) |
| <input type="checkbox"/> Bus (13 ton) | <input type="checkbox"/> Articulated HGV (38 ton) | <input type="checkbox"/> Other: _____ |

PART II: ANALYSIS SOLUTION VERIFICATION

Using the results of the analysis solution, fill in the values for Table E-1. These values are indications of whether the analysis solution produced a numerically stable result and do not necessarily mean that the result is a good comparison to the known solution. The purpose of this table is to ensure that the numerical solution produces results that are numerically stable and conform to the conservation laws (e.g., energy, mass and momentum).

Table E-1. Analysis Solution Verification Table

Verification Evaluation Criteria	Change (%)	Pass?
<i>Total energy</i> of the analysis solution (i.e., kinetic, potential, contact, etc.) must not vary more than 10 percent from the beginning of the run to the end of the run.	0.42%	Yes
<i>Hourglass Energy</i> of the analysis solution at the end of the run is less than <i>five percent</i> of the total <i>initial energy</i> at the <i>beginning</i> of the run.	2.36%	Yes
<i>Hourglass Energy</i> of the analysis solution at the end of the run is less than <i>ten percent</i> of the total <i>internal energy</i> at the <i>end</i> of the run.	9.70%	Yes
The part/material with the highest amount of hourglass energy at the end of the run is less than ten percent of the total internal energy of the part/material at the end of the run. (Part id=32000440, hg=3,480, Internal energy at end of run=12,700)	27.40%*	No
Mass added to the total model is less than five percent of the total model mass at the beginning of the run.	0.05%	Yes
The part/material with the most mass added had less than 10 percent of its initial mass added. (Part id=40004023, Added mass=6.88, Initial mass=48.29)	14.25%**	No
The moving parts/materials in the model have less than five percent of mass added to the initial moving mass of the model.	0.09%	Yes
There are no shooting nodes in the solution?	No	Yes
There are no solid elements with negative volumes?	No	Yes

*Largest hourglass energy part is vehicle’s outer right-front rim, resolvable with increased computation

**Steel transition blockouts have most added mass, resolvable with increased computation

If all the analysis solution verification criteria are scored as passing, the analysis solution can be verified or validated against the known solution. If any criterion in Table E-1 does not pass one of the verification criterion listed in Table E-1, the analysis solution cannot be used to verify or validate the known solution. If there are exceptions that the analyst thinks are relevant these should be footnoted in the table and explained below the table.

The Analysis Solution (check one) passes does NOT pass all the criteria in Table E1-1
with without exceptions as noted.

PART III: TIME HISTORY EVALUATION TABLE

Using the RSVVP computer program ('Single channel' option), compute the Sprague-Geers MPC metrics and ANOVA metrics using time-history data from the known and analysis solutions for a time period starting at the beginning of the contact and ending at the loss of contact. Both the Sprague-Geers and ANOVA metrics must be calculated based on the original units the data was collected in (e.g., if accelerations were measured in the experiment with accelerometers then the comparison should be between accelerations. If rate gyros were used in the experiment, the comparison should be between rotation rates). If all six data channels are not available for both the known and analysis solutions, enter "N/A" in the column corresponding to the missing data. Enter the values obtained from the RSVVP program in Table E-2 and indicate if the comparison was acceptable or not by entering a "yes" or "no" in the "Agree?" column. Attach a graph of each channel for which the metrics have been compared at the end of the report.

Enter the filter, synchronization method and shift/drift options used in RSVVP to perform the comparison so that it is clear to the reviewer what options were used. Normally, SAE J211 filter class 180 is used to compare vehicle kinematics in full-scale crash tests. Either synchronization option in RSVVP is acceptable and both should result in a similar start point. The shift and drift options should generally only be used for the experimental curve since shift and drift are characteristics of sensors. For example, the zero point for an accelerometer sometimes "drifts" as the accelerometer sits out in the open environment of the crash test pad whereas there is no sensor to "drift" or "shift" in a numerical solution.

In order for the analysis solution to be considered in agreement with the known solution (i.e., verified or validated), all the criteria scored in Table E-2 must pass. If all the channels in Table E-2 do not pass, fill out Table E-3, the multi-channel weighted procedure.

If one or more channels do not satisfy the criteria in Table E-2, the multi-channel weighting option may be used. Using the RSVVP computer program ('Multiple channel' option), compute the Sprague-Geers MPC metrics and ANOVA metrics using all the time histories data from the known and analysis solutions for a time period starting at the beginning of the contact and ending at the loss of contact. If all six data channels are not available for both the known and analysis solutions, enter "N/A" in the column corresponding to the missing data.

For some types of roadside hardware impacts, some of the channels are not as important as others. An example might be a breakaway sign support test where the lateral (i.e., Y) and vertical (i.e., Z) accelerations are insignificant to the dynamics of the crash event. The weighting procedure provides a way to weight the most important channels more highly than less important channels. The procedure used is based on the area under the curve, therefore, the weighing scheme will weight channels with large areas more highly than those with smaller areas. In general, using the "Area (II)" method is acceptable although if the complete inertial properties of the vehicle are available the "inertial" method may be used. Enter the values obtained from the RSVVP program in Table E-3 and indicate if the comparison was acceptable or not by entering a "yes" or "no" in the "Agree?" column.

In order for the analysis solution to be considered in agreement with the known solution (i.e., verified or validated), all the criteria scored in Table E-3 must pass.

Table E-2. Roadside Safety Validation Metrics Rating Table – Time History Comparisons (single channel option – CFC60)

Evaluation Criteria							Time interval [0.0 sec; 0.49 sec]					
O	Sprague-Geers Metrics List all the data channels being compared. Calculate the M and P metrics using RSVVP and enter the results. Values less than or equal to 40 are acceptable.						M	P	Pass?			
	RSVVP Curve Preprocessing Options											
		Filter Option	Sync. Option	Shift		Drift						
				True Curve	Test Curve	True Curve				Test Curve		
	X acceleration	CFC60	N	N	N	N				13.2	29.9	Yes
	Y acceleration	CFC60	N	N	N	N				2.3	20.5	Yes
	Z acceleration	CFC60	N	N	N	N				1.7	56.6	No
	Roll rate	CFC60	N	N	N	N				4.5	34.3	Yes
	Pitch rate	CFC60	N	N	N	N				31.0	43.4	No
	Yaw rate	CFC60	N	N	N	N				16.0	7.2	Yes
P	ANOVA Metrics List all the data channels being compared. Calculate the ANOVA metrics using RSVVP and enter the results. Both of the following criteria must be met: <ul style="list-style-type: none"> The mean residual error must be less than five percent of the peak acceleration ($\bar{e} \leq 0.05 \cdot a_{Peak}$) and The standard deviation of the residuals must be less than 35 percent of the peak acceleration ($\sigma \leq 0.35 \cdot a_{Peak}$) 						Mean Residual	Standard Deviation of Residuals	Pass?			
	X acceleration/Peak									1.02	17.40	Yes
	Y acceleration/Peak									2.03	21.05	Yes
	Z acceleration/Peak									-3.00	42.93	No
	Roll rate									0.77	6.69	Yes
	Pitch rate									-0.12	10.79	Yes
	Yaw rate									-3.36	6.93	Yes

The Analysis Solution (check one) passes does NOT pass all the criteria in Table E-2 (single-channel time history comparison). If the Analysis Solution does NOT pass, perform the analysis in Table E-3 (multi-channel time history comparison).

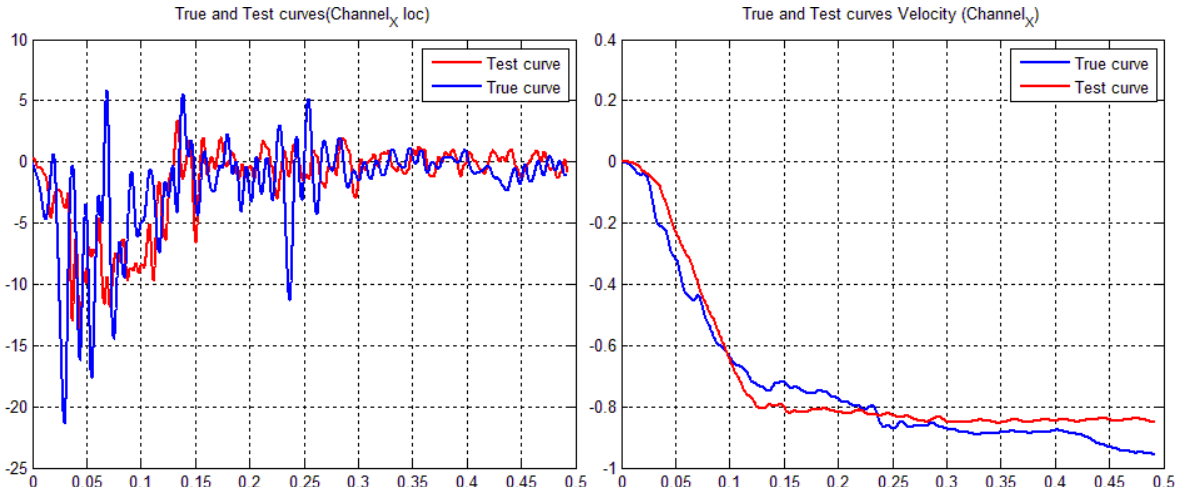


Figure 1. X-Channel (left) acceleration-time history data used to compute metrics, and (right) integration of acceleration-time history data

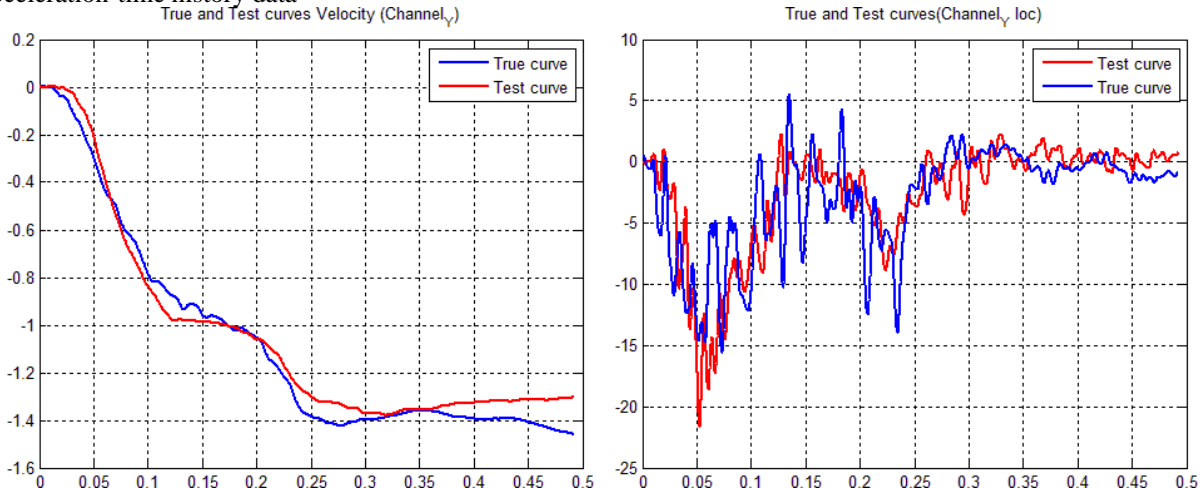


Figure 2. Y-Channel (left) acceleration-time history data used to compute metrics, and (right) integration of acceleration-time history data

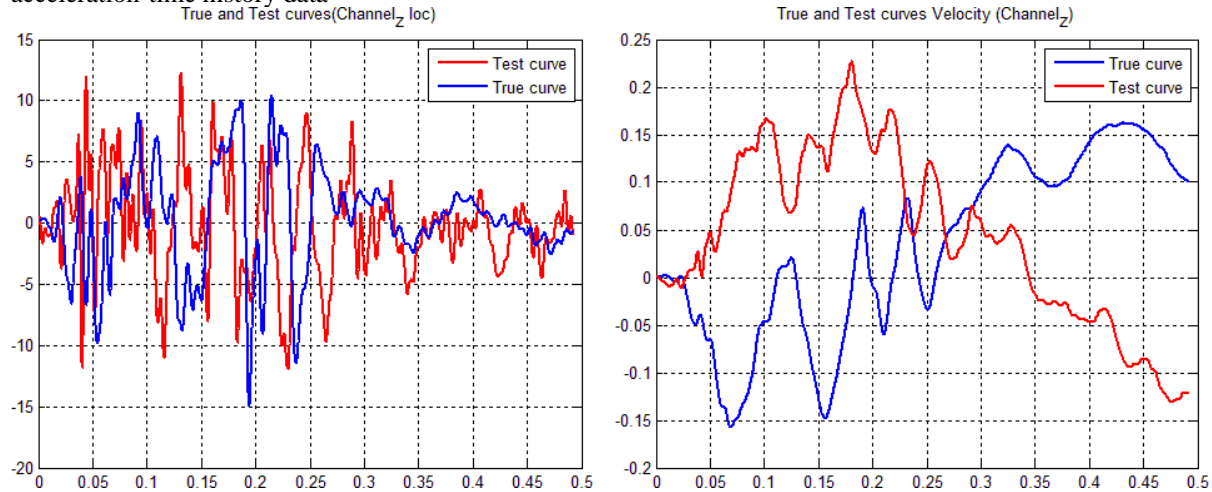


Figure 3. Z-Channel (left) acceleration-time history data used to compute metrics, and (right) integration of acceleration-time history data

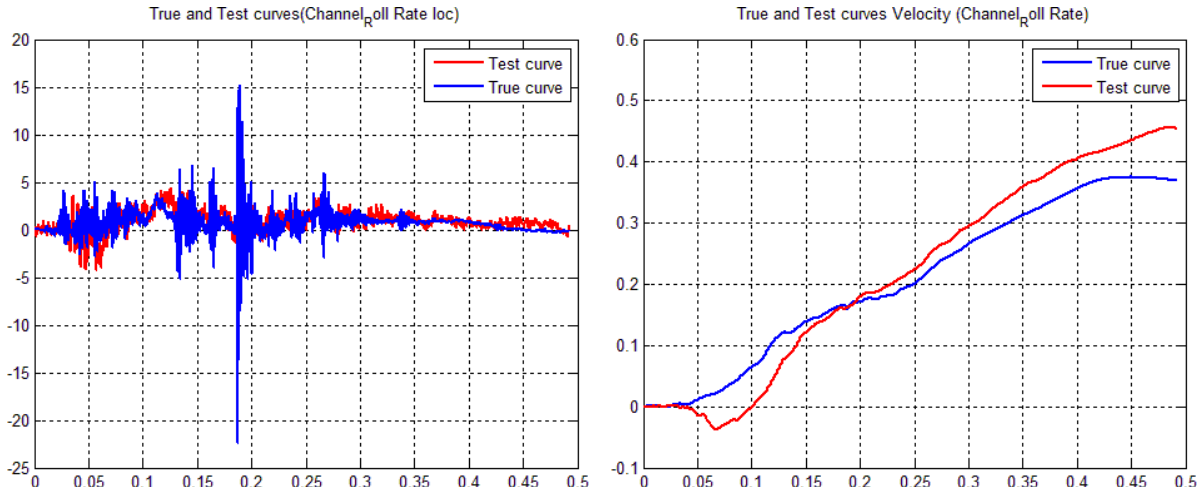


Figure 4. Roll Channel (left) angular rate-time history data used to compute metrics, and (right) integration of angular rate-time history data

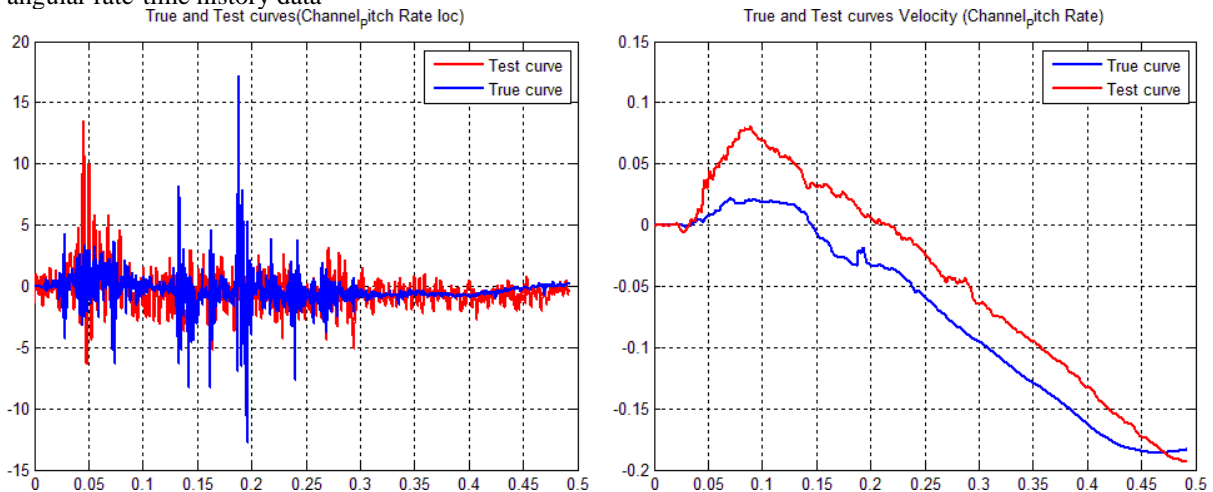


Figure 5. Pitch Channel (left) angular rate-time history data used to compute metrics, and (right) integration of angular rate-time history data

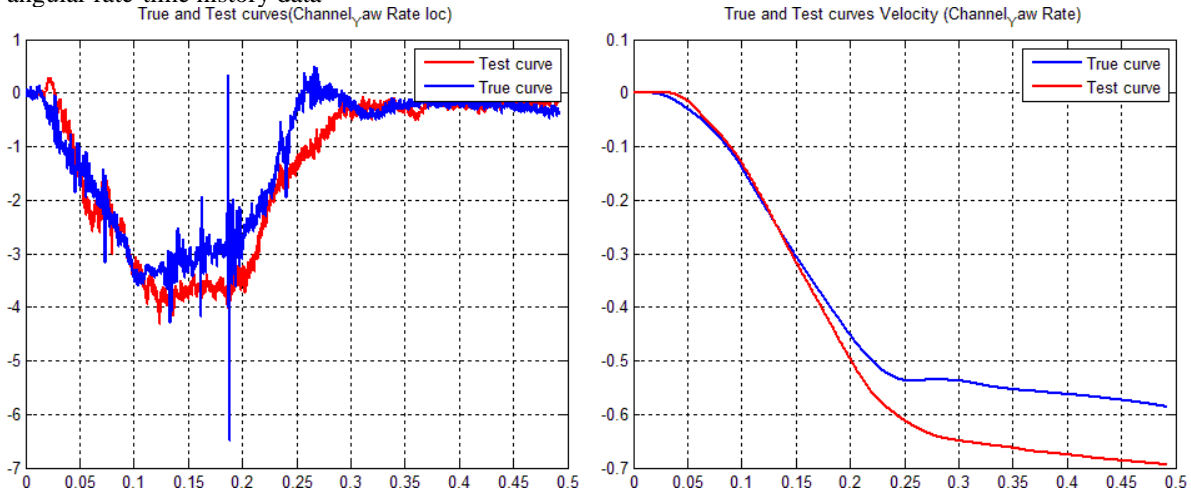


Figure 6. Yaw Channel (left) angular rate-time history data used to compute metrics, and (right) integration of angular rate-time history data

Table E-3. Roadside Safety Validation Metrics Rating Table – Time History Comparisons (multi-channel option CFC60)

Evaluation Criteria (time interval [0.0 sec; 0.49 sec])																	
Channels (Select which were used)																	
<input checked="" type="checkbox"/> X Acceleration	<input checked="" type="checkbox"/> Y Acceleration	<input checked="" type="checkbox"/> Z Acceleration															
<input checked="" type="checkbox"/> Roll rate	<input checked="" type="checkbox"/> Pitch rate	<input checked="" type="checkbox"/> Yaw rate															
Multi-Channel Weights <input checked="" type="checkbox"/> Area II method <input type="checkbox"/> Inertial method		X Channel: Y Channel: Z Channel: Yaw Channel: Roll Channel: ____ Pitch Channel:	<table border="1"> <caption>Weighting factors</caption> <thead> <tr> <th>Channel</th> <th>Weighting Factor</th> </tr> </thead> <tbody> <tr> <td>X acc</td> <td>0.19</td> </tr> <tr> <td>Y acc</td> <td>0.29</td> </tr> <tr> <td>Z acc</td> <td>0.02</td> </tr> <tr> <td>Yaw</td> <td>0.26</td> </tr> <tr> <td>Roll</td> <td>0.16</td> </tr> <tr> <td>Pitch</td> <td>0.08</td> </tr> </tbody> </table>	Channel	Weighting Factor	X acc	0.19	Y acc	0.29	Z acc	0.02	Yaw	0.26	Roll	0.16	Pitch	0.08
Channel	Weighting Factor																
X acc	0.19																
Y acc	0.29																
Z acc	0.02																
Yaw	0.26																
Roll	0.16																
Pitch	0.08																
O	Sprague-Geer Metrics Values less or equal to 40 are acceptable.	M	P	Pass?													
		10.6	23.7	Yes													
P	ANOVA Metrics Both of the following criteria must be met: <ul style="list-style-type: none"> The mean residual error must be less than five percent of the peak acceleration $(\bar{e} \leq 0.05 \cdot a_{Peak})$ The standard deviation of the residuals must be less than 35 percent of the peak acceleration $(\sigma \leq 0.35 \cdot a_{Peak})$ 	Mean Residual	Standard Deviation of Residuals	Pass?													
		0.0	14.0	Yes													

The Analysis Solution (check one) passes does NOT pass all the criteria in Table E-3.

Table E-2. Roadside Safety Validation Metrics Rating Table – Time History Comparisons (single channel option – CFC180)

Evaluation Criteria							Time interval [0.0 sec; 0.49 sec]		
O	Sprague-Geers Metrics List all the data channels being compared. Calculate the M and P metrics using RSVVP and enter the results. Values less than or equal to 40 are acceptable.								
	RSVVP Curve Preprocessing Options						M	P	Pass?
	Filter Option	Sync. Option	Shift		Drift				
True Curve			Test Curve	True Curve	Test Curve				
X acceleration	CFC180	N	N	N	N	N	8.7	32.9	Yes
Y acceleration	CFC180	N	N	N	N	N	2.1	25.4	Yes
Z acceleration	CFC180	N	N	N	N	N	54.9	54.8	No
Roll rate	CFC180	N	N	N	N	N	4.5	34.3	Yes
Pitch rate	CFC180	N	N	N	N	N	31.0	43.4	No
Yaw rate	CFC180	N	N	N	N	N	16.0	7.2	Yes
P	ANOVA Metrics List all the data channels being compared. Calculate the ANOVA metrics using RSVVP and enter the results. Both of the following criteria must be met: <ul style="list-style-type: none"> The mean residual error must be less than five percent of the peak acceleration ($\bar{e} \leq 0.05 \cdot a_{Peak}$) and The standard deviation of the residuals must be less than 35 percent of the peak acceleration ($\sigma \leq 0.35 \cdot a_{Peak}$) 						Mean Residual	Standard Deviation of Residuals	Pass?
X acceleration/Peak	0.88	17.78	Yes						
Y acceleration/Peak	1.64	22.57	Yes						
Z acceleration/Peak	-2.17	43.67	No						
Roll rate	0.77	6.69	Yes						
Pitch rate	-0.12	10.79	Yes						
Yaw rate	-3.36	6.93	Yes						

The Analysis Solution (check one) passes does NOT pass all the criteria in Table E-2 (single-channel time history comparison). If the Analysis Solution does NOT pass, perform the analysis in Table E-3 (multi-channel time history comparison).

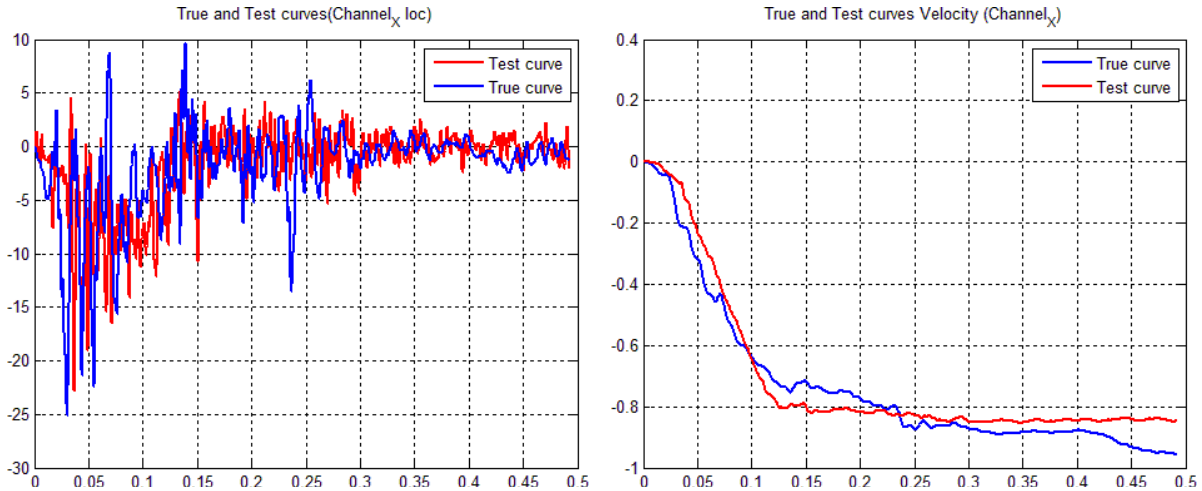


Figure 7. X-Channel (left) acceleration-time history data used to compute metrics, and (right) integration of acceleration-time history data

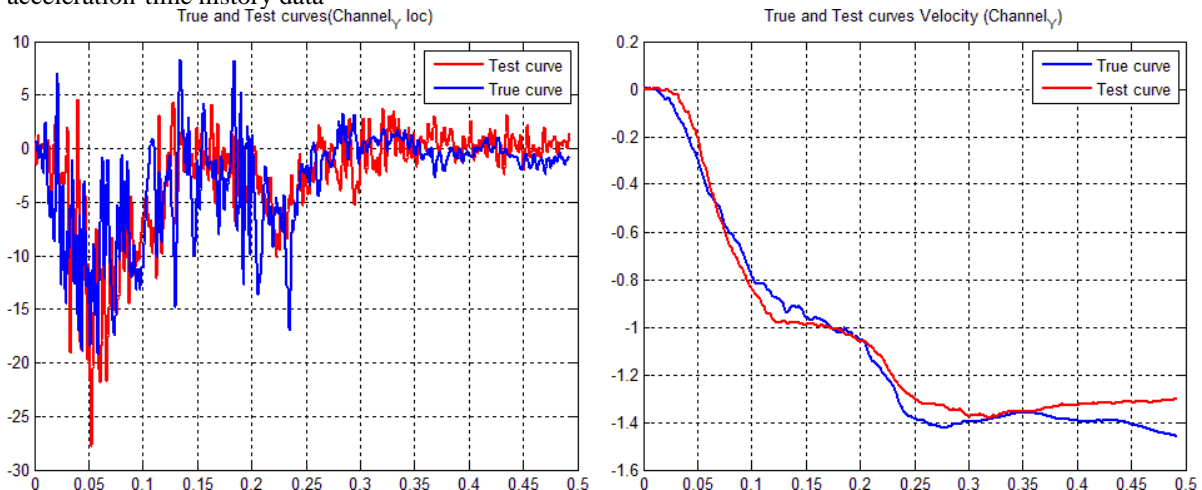


Figure 8. Y-Channel (left) acceleration-time history data used to compute metrics, and (right) integration of acceleration-time history data

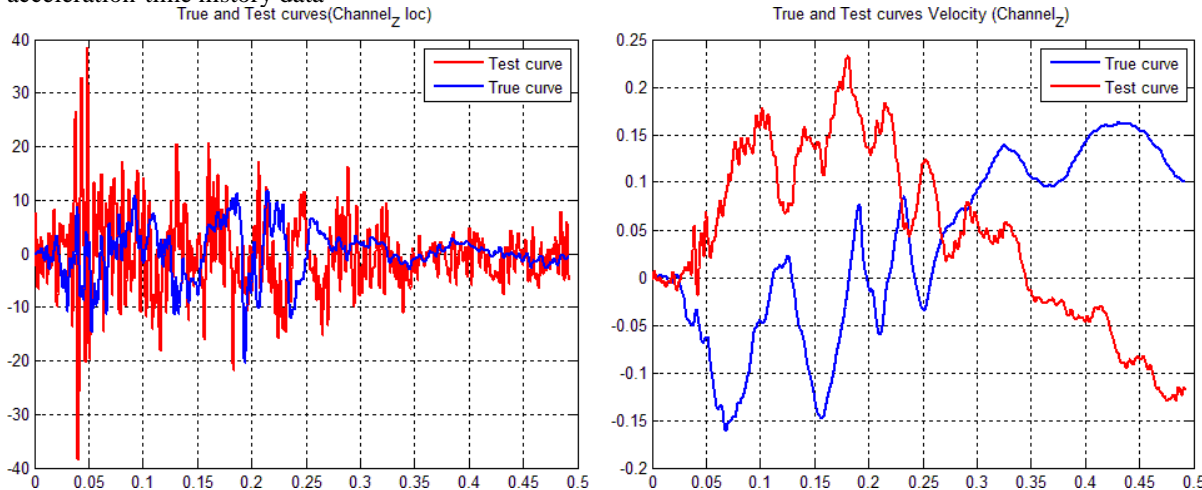


Figure 9. Z-Channel (left) acceleration-time history data used to compute metrics, and (right) integration of acceleration-time history data

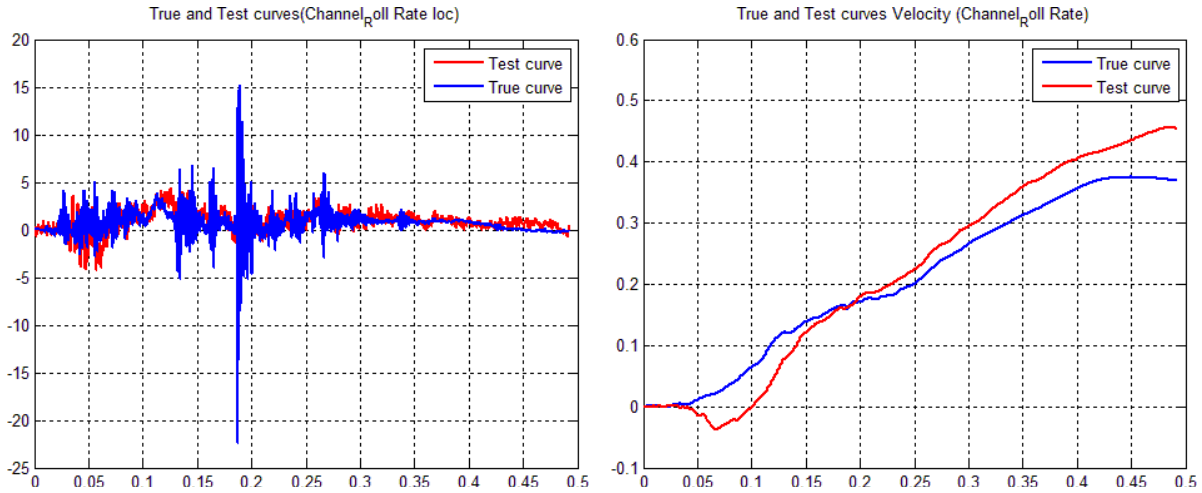


Figure 10. Roll Channel (left) angular rate-time history data used to compute metrics, and (right) integration of angular rate-time history data

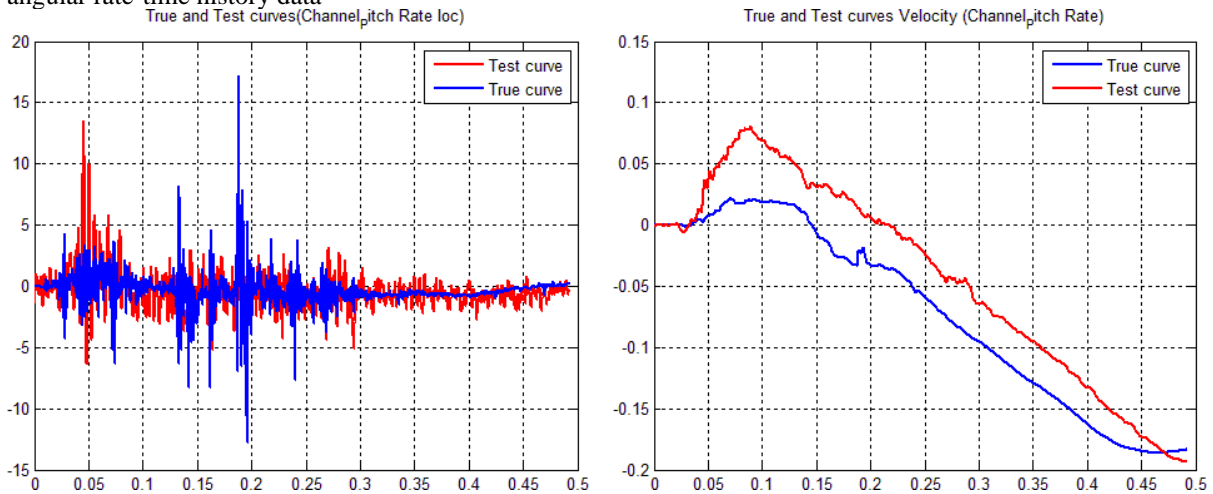


Figure 11. Pitch Channel (left) angular rate-time history data used to compute metrics, and (right) integration of angular rate-time history data

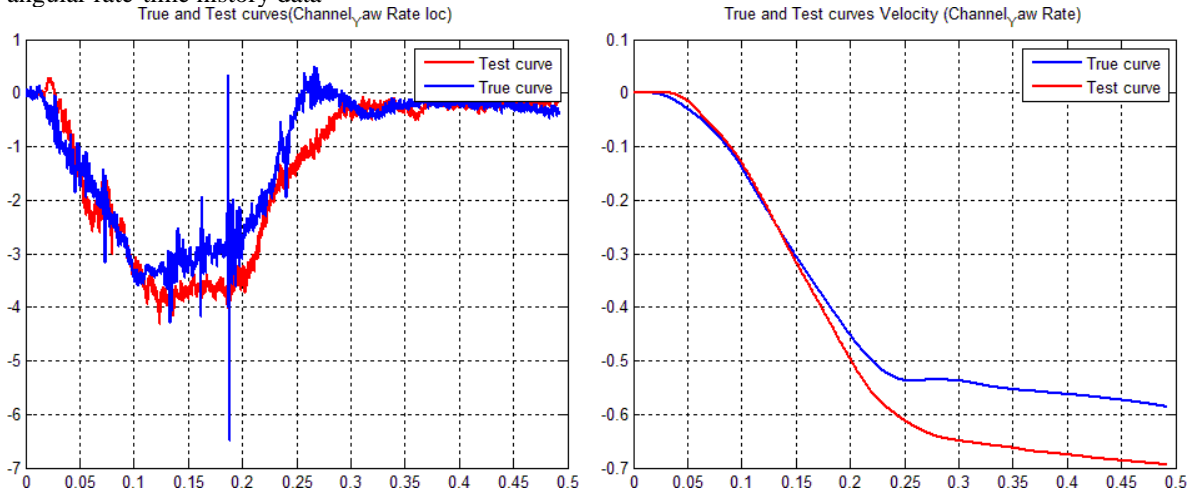


Figure 12. Yaw Channel (left) angular rate-time history data used to compute metrics, and (right) integration of angular rate-time history data

Table E-3. Roadside Safety Validation Metrics Rating Table – Time History Comparisons (multi-channel option)

Evaluation Criteria (time interval [0.0 sec; 0.49 sec])																	
Channels (Select which were used)																	
<input checked="" type="checkbox"/> X Acceleration	<input checked="" type="checkbox"/> Y Acceleration	<input checked="" type="checkbox"/> Z Acceleration															
<input checked="" type="checkbox"/> Roll rate	<input checked="" type="checkbox"/> Pitch rate	<input checked="" type="checkbox"/> Yaw rate															
Multi-Channel Weights <input checked="" type="checkbox"/> Area II method <input type="checkbox"/> Inertial method		X Channel: Y Channel: Z Channel: Yaw Channel: Roll Channel: ____ Pitch Channel:	<table border="1"> <caption>Weighting factors</caption> <thead> <tr> <th>Channel</th> <th>Weighting Factor</th> </tr> </thead> <tbody> <tr> <td>X acc</td> <td>0.19</td> </tr> <tr> <td>Y acc</td> <td>0.29</td> </tr> <tr> <td>Z acc</td> <td>0.02</td> </tr> <tr> <td>Yaw</td> <td>0.26</td> </tr> <tr> <td>Roll</td> <td>0.16</td> </tr> <tr> <td>Pitch</td> <td>0.08</td> </tr> </tbody> </table>	Channel	Weighting Factor	X acc	0.19	Y acc	0.29	Z acc	0.02	Yaw	0.26	Roll	0.16	Pitch	0.08
Channel	Weighting Factor																
X acc	0.19																
Y acc	0.29																
Z acc	0.02																
Yaw	0.26																
Roll	0.16																
Pitch	0.08																
O	Sprague-Geer Metrics Values less or equal to 40 are acceptable.		<table border="1"> <thead> <tr> <th>M</th> <th>P</th> <th>Pass?</th> </tr> </thead> <tbody> <tr> <td>10.7</td> <td>25.6</td> <td>Yes</td> </tr> </tbody> </table>	M	P	Pass?	10.7	25.6	Yes								
	M	P	Pass?														
10.7	25.6	Yes															
P	ANOVA Metrics Both of the following criteria must be met: <ul style="list-style-type: none"> The mean residual error must be less than five percent of the peak acceleration $(\bar{e} \leq 0.05 \cdot a_{Peak})$ The standard deviation of the residuals must be less than 35 percent of the peak acceleration ($\sigma \leq 0.35 \cdot a_{Peak}$) 		<table border="1"> <thead> <tr> <th>Mean Residual</th> <th>Standard Deviation of Residuals</th> <th>Pass?</th> </tr> </thead> <tbody> <tr> <td>-0.2</td> <td>14.5</td> <td>Yes</td> </tr> </tbody> </table>	Mean Residual	Standard Deviation of Residuals	Pass?	-0.2	14.5	Yes								
	Mean Residual	Standard Deviation of Residuals	Pass?														
-0.2	14.5	Yes															

The Analysis Solution (check one) passes does NOT pass all the criteria in Table E-3.

PART IV: PHENOMENA IMPORTANCE RANKING TABLE

Table E-4 is similar to the evaluation tables in Report 350 and MASH. For the Report 350 or MASH test number identified in Part I (e.g., test 3-10, 5-12, etc.), circle all the evaluation criteria applicable to that test in Table E-4. The tests that apply to each criterion are listed in the far right column without the test level designator. For example, if a Report 350 test 3-11 is being compared (i.e., a pickup truck striking a barrier at 25 degrees and 100 km/hr), circle all the criteria in the second column where the number “11” appears in the far right column. Some of the Report 350 evaluation criteria have been removed (i.e., J and K) since they are not generally useful in assessing the comparison between the known and analysis solutions.

Table E-4. Evaluation Criteria Test Applicability Table

Evaluation Factors	Evaluation Criteria	Applicable Tests								
Structural Adequacy	A Test article should contain and redirect the vehicle; the vehicle should not penetrate, under-ride, or override the installation although controlled lateral deflection of the test article is acceptable.	10, 11, 12, 20, 21, 22, 35, 36, 37, 38								
	B The test article should readily activate in a predictable manner by breaking away, fracturing or yielding.	60, 61, 70, 71, 80, 81								
	C Acceptable test article performance may be by redirection, controlled penetration or controlled stopping of the vehicle.	30, 31,, 32, 33, 34, 39, 40, 41, 42, 43, 44, 50, 51, 52, 53								
Occupant Risk	D Detached elements, fragments or other debris from the test article should not penetrate or show potential for penetrating the occupant compartment, or present an undue hazard to other traffic, pedestrians or personnel in a work zone.	All								
	E Detached elements, fragments or other debris from the test article, or vehicular damage should not block the driver's vision or otherwise cause the driver to lose control of the vehicle. (Answer Yes or No)	70, 71								
	F The vehicle should remain upright during and after the collision although moderate roll, pitching and yawing are acceptable.	All except those listed in criterion G								
	G It is preferable, although not essential, that the vehicle remain upright during and after collision.	12, 22 (for test level 1 - 30, 31, 32, 33, 34, 35, 36, 37, 38, 39, 40, 41, 42, 43, 44)								
	Occupant impact velocities should satisfy the following:									
	Occupant Impact Velocity Limits (m/s)									
	H	<table border="1" data-bbox="613 1066 1161 1213"> <thead> <tr> <th data-bbox="613 1066 719 1108">Component</th> <th data-bbox="719 1066 829 1108">Preferred</th> <th data-bbox="829 1066 1161 1108">Maximum</th> </tr> </thead> <tbody> <tr> <td data-bbox="613 1108 719 1171">Longitudinal and Lateral</td> <td data-bbox="719 1108 829 1171">9</td> <td data-bbox="829 1108 1161 1171">12</td> </tr> <tr> <td data-bbox="613 1171 719 1213">Longitudinal</td> <td data-bbox="719 1171 829 1213">3</td> <td data-bbox="829 1171 1161 1213">5</td> </tr> </tbody> </table>	Component	Preferred	Maximum	Longitudinal and Lateral	9	12	Longitudinal	3
Component	Preferred	Maximum								
Longitudinal and Lateral	9	12								
Longitudinal	3	5								
10, 20, 30,31, 32, 33, 34, 36, 40, 41, 42, 43, 50, 51, 52, 53, 80, 81	60, 61, 70, 71									
	Occupant ridedown accelerations should satisfy the following:									
	Occupant Ridedown Acceleration Limits (g's)									
	I	<table border="1" data-bbox="613 1276 1161 1381"> <thead> <tr> <th data-bbox="613 1276 719 1318">Component</th> <th data-bbox="719 1276 829 1318">Preferred</th> <th data-bbox="829 1276 1161 1318">Maximum</th> </tr> </thead> <tbody> <tr> <td data-bbox="613 1318 719 1381">Longitudinal and Lateral</td> <td data-bbox="719 1318 829 1381">15</td> <td data-bbox="829 1318 1161 1381">20</td> </tr> </tbody> </table>	Component	Preferred	Maximum	Longitudinal and Lateral	15	20		
Component	Preferred	Maximum								
Longitudinal and Lateral	15	20								
10, 20, 30,31, 32, 33, 34, 36, 40, 41, 42, 43, 50, 51, 52, 53, 60, 61, 70, 71, 80, 81										
Vehicle Trajectory	L The occupant impact velocity in the longitudinal direction should not exceed 40 ft/sec and the occupant ride-down acceleration in the longitudinal direction should not exceed 20 G's.	11,21, 35, 37, 38, 39								
	M The exit angle from the test article preferable should be less than 60 percent of test impact angle, measured at the time of vehicle loss of contact with test device.	10, 11, 12, 20, 21, 22, 35, 36, 37, 38, 39								
	N Vehicle trajectory behind the test article is acceptable.	30, 31, 32, 33, 34, 39, 42, 43, 44, 60, 61, 70, 71, 80, 81								

Complete Table E-5 according to the results of the known solution (e.g., crash test) and the numerical solution (e.g., simulation). Consistent with Report 350 and MASH, Task E-5 has three parts: the structural adequacy phenomena listed in Table E-5a, the occupant risk phenomena listed in Table E-5b and the vehicle trajectory criteria listed in Table E-5c. If the result of the analysis solution agrees with the known solution, mark the “agree” column “yes.” For example, if the vehicle in both the known and analysis solutions rolls over and, therefore, fails criterion F1, the known and the analysis columns for criterion F1 would be evaluated as “no.” Even though both failed the criteria, they agree with each other so the “agree” column is marked as “yes.” Any criterion that is not applicable to the test being evaluated (i.e., not circled in Table E-4) should be indicated by entering “NA” in the “agree?” column for that row.

Many of the Report 350 evaluation criteria have been subdivided into more specific phenomenon. For example, criterion A is divided into eight sub-criteria, A1 through A8, that provide more specific and quantifiable phenomena for evaluation. Some of the values are simple yes or no questions while other request numerical values. For the numerical phenomena, the analyst should enter the value for the known and analysis result and then calculate the relative difference. Relative difference is always the absolute value of the difference of the known and analysis solutions divided by the known solution. Enter the value in the “relative difference” column. If the relative difference is less than 20 percent, enter “yes” in the “agree?” column.

Sometimes, when the values are very small, the relative difference might be large while the absolute difference is very small. For example, the longitudinal occupant ride down acceleration (i.e., criterion L2) in a test might be 3 g’s and in the corresponding analysis might be 4 g’s. The relative difference is 33 percent but the absolute difference is only 1 g and the result for both is well below the 20 g limit. Clearly, the analysis solution in this case is a good match to the experiment and the relative difference is large only because the values are small. The absolute difference, therefore, should also be entered into the “Difference” column in Table E-5.

The experimental and analysis result can be considered to agree as long as either the relative difference or the absolute difference is less than the acceptance limit listed in the criterion. Generally, relative differences of less than 20 percent are acceptable and the absolute difference limits were generally chosen to represent 20 percent of the acceptance limit in Report 350 or MASH. For example, Report 350 limits occupant ride-down accelerations to those less than 20 g’s so 20 percent of 20 g’s is 4 g’s. As shown for criterion L2 in Table E-5, the relative acceptance limit is 20 percent and the absolute acceptance limit is 4 g’s.

If a numerical model was not created to represent the phenomenon, a value of “NM” (i.e., not modeled) should be entered in the appropriate column of Table E-5. If the known solution for that phenomenon number is “no” then a “NM” value in the “test result” column can be considered to agree. For example, if the material model for the rail element did not include the possibility of failure, “NM” should be entered for phenomenon number T in Table E-5. If the known solution does not indicate rail rupture or failure (i.e., phenomenon T = “no”), then the known and analysis solutions agree and a “yes” can be entered in the “agree?” column. On the other hand, if the known solution shows that a rail rupture did occur resulting in a phenomenon T entry of “yes” for the known solution, the known and analysis solutions do not agree and “no” should be entered in the “agree?” column. Analysts should seriously consider refining their model to incorporate any phenomena that appears in the known solution and is shown in Table E-5.

All the criteria identified in Table E-4 are expected to agree but if one does not and, in the opinion of the analyst, is not considered important to the overall evaluation for this particular comparison, then a footnote should be provided with a justification for why this particular criteria can be ignored for this particular comparison.

Table E-5(a). Roadside Safety Phenomena Importance Ranking Table (Structural Adequacy)

		Evaluation Criteria	Known Result	Analysis Result	Difference Relative/ Absolute	Agree?
Structural Adequacy	A1	Test article should contain and redirect the vehicle; the vehicle should not penetrate, under-ride, or override the installation although controlled lateral deflection of the test article is acceptable. (Answer Yes or No)	Yes	Yes	X	Yes
	A2	Maximum dynamic deflection: - Relative difference is less than 20 percent or - Absolute difference is less than 0.15 m	0.136 m	0.109 m	19.85% 0.03 m	Yes
	A3	Length of vehicle-barrier contact: - Relative difference is less than 20 percent or - Absolute difference is less than 2 m	4.04 m	3.17 m	21.53% 0.87 m	Yes
	A4	Number of broken or significantly bent posts is less than 20 percent. (Posts with deflections > 1 in. (25.4 mm))	7	5	28.57% 2 posts	No*
	A5	Did the rail element rupture or tear (Answer Yes or No)	No	No	X	Yes
	A6	Were there failures of connector elements (Answer Yes or No).	No	No	X	Yes
	A7	Was there significant snagging between the vehicle wheels and barrier elements (Answer Yes or No).	No	No	X	Yes
	A8	Was there significant snagging between vehicle body components and barrier elements (Answer Yes or No).	No	No	X	Yes

* Soil strength is dependent on post spacing in full-scale test and acts independently in simulation.

Table E-5(b). Roadside Safety Phenomena Importance Ranking Table (Occupant Risk)

Evaluation Criteria		Known Result	Analysis Result	Difference Relative/ Absolute	Agree?		
Occupant Risk	D	Detached elements, fragments or other debris from the test article should not penetrate or show potential for penetrating the occupant compartment, or present an undue hazard to other traffic, pedestrians or personnel in a work zone. (Answer Yes or No)	Yes	Yes		Yes	
	F1	The vehicle should remain upright during and after the collision although moderate roll, pitching and yawing are acceptable. (Answer Yes or No)	Yes	Yes		Yes	
	F	F2	Maximum roll of the vehicle (t=350ms): - Relative difference is less than 20 percent or - Absolute difference is less than 5 degrees.	17.51	18.97	8.34% 1.46 degrees	Yes
		F3	Maximum pitch of the vehicle is (t=350ms): - Relative difference is less than 20 percent or - Absolute difference is less than 5 degrees.	3.67	1.76	52.04% 1.91 degrees	Yes
		F4	Maximum yaw of the vehicle is (t=350ms): - Relative difference is less than 20 percent or - Absolute difference is less than 5 degrees.	33.12	39.44	19.08% 6.32 degrees	Yes
			Occupant impact velocities: - Relative difference is less than 20 percent or - Absolute difference is less than 2 m/s.				
	L1	• Longitudinal OIV (m/s)	-6.18	-6.35	2.75% 0.17 m/s	Yes	
		• Lateral OIV (m/s)	7.50	8.24	9.87% 0.74 m/s	Yes	
		• THIV (m/s)	9.43 m/s	NA	-	NA	
	L2		Occupant accelerations: - Relative difference is less than 20 percent or - Absolute difference is less than 4 g's.				
		• Longitudinal ORA	-7.06	-7.75	9.77% 0.69 g's	Yes	
		• Lateral ORA	10.40	8.13	21.83% 2.27 g's	Yes	
		• PHD	12.53	NA	-	NA	
		• ASI	1.37	NA	-	NA	

Table E-5(c). Roadside Safety Phenomena Importance Ranking Table (Vehicle Trajectory)

Evaluation Criteria			Known Result	Analysis Result	Difference Relative/ Absolute	Agree?	
Vehicle Trajectory	M	M1	The exit angle from the test article preferable should be less than 60 percent of test impact angle, measured at the time of vehicle loss of contact with test device.	Yes	Yes	X	Yes
		M2	Exit angle at loss of contact: - Relative difference is less than 20 percent or - Absolute difference is less than 5 degrees.	8.99	14.07	56.51% 5.08 degrees	No*
		M3	Exit velocity at loss of contact: - Relative difference is less than 20 percent or - Absolute difference is less than 5 degrees.	69.98	71.01	1.47% 1.03 km/h	Yes
		M4	One or more vehicle tires failed or de-beaded during the collision event (Answer Yes or No).	Yes	Yes	X	Yes

* In the simulation, the detached tire remained in the wheel well and did not exit under the vehicle as in the full-scale test resulting in an exit angle discrepancy.

The Analysis Solution (check one) passes does NOT pass all the criteria in Tables E-5a through E-5c with exceptions as noted without exceptions .

Appendix D. 2270P CIP Study Simulation Sequential Images



Figure D-1. 15:1 DS4 Simulation (Left) vs. 15:1 DS3 Simulation (Right) Sequential Images



Figure D-2. 15:1 DS2 Simulation (Left) vs. 15:1 DS1 Simulation (Right) Sequential Images



Figure D-3. 15:1 X Simulation (Left) vs. 15:1 US1 Simulation (Right) Sequential Images

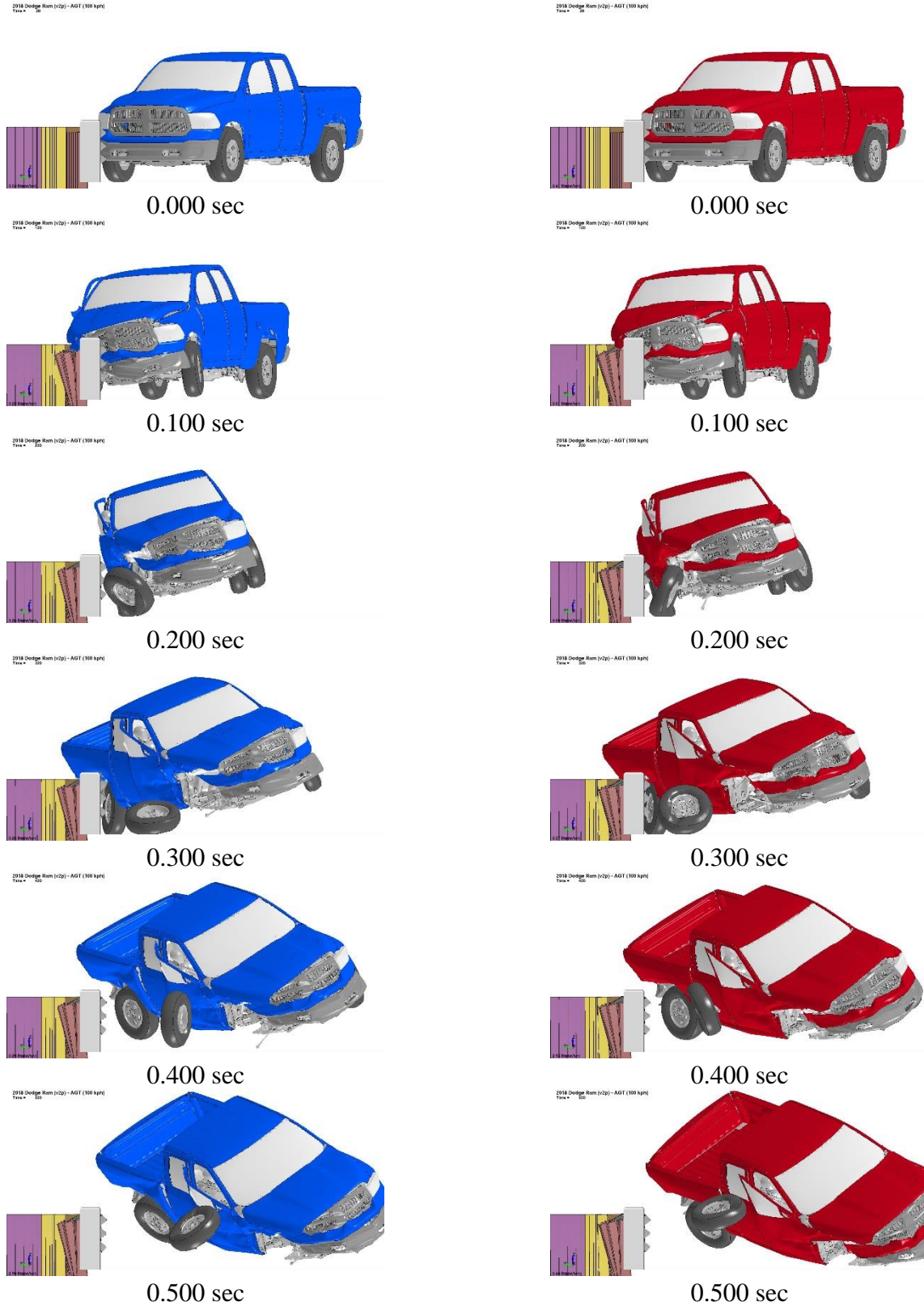


Figure D-4. 15:1 US2 Simulation (Left) vs. 15:1 US3 Simulation (Right) Sequential Images

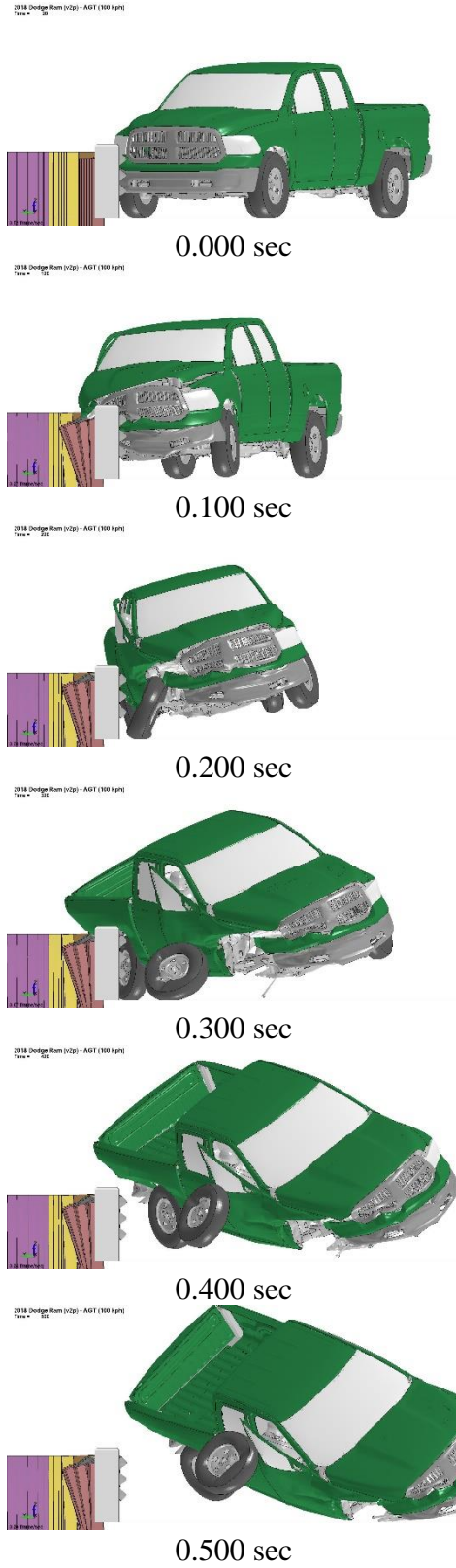


Figure D-5. 15:1 US4 Simulation Sequential Images



Figure D-6. 12.5:1 DS4 Simulation (Left) vs. 12.5:1 DS3 Simulation (Right) Sequential Images



Figure D-7. 12.5:1 DS2 Simulation (Left) vs. 12.5:1 DS1 Simulation (Right) Sequential Images

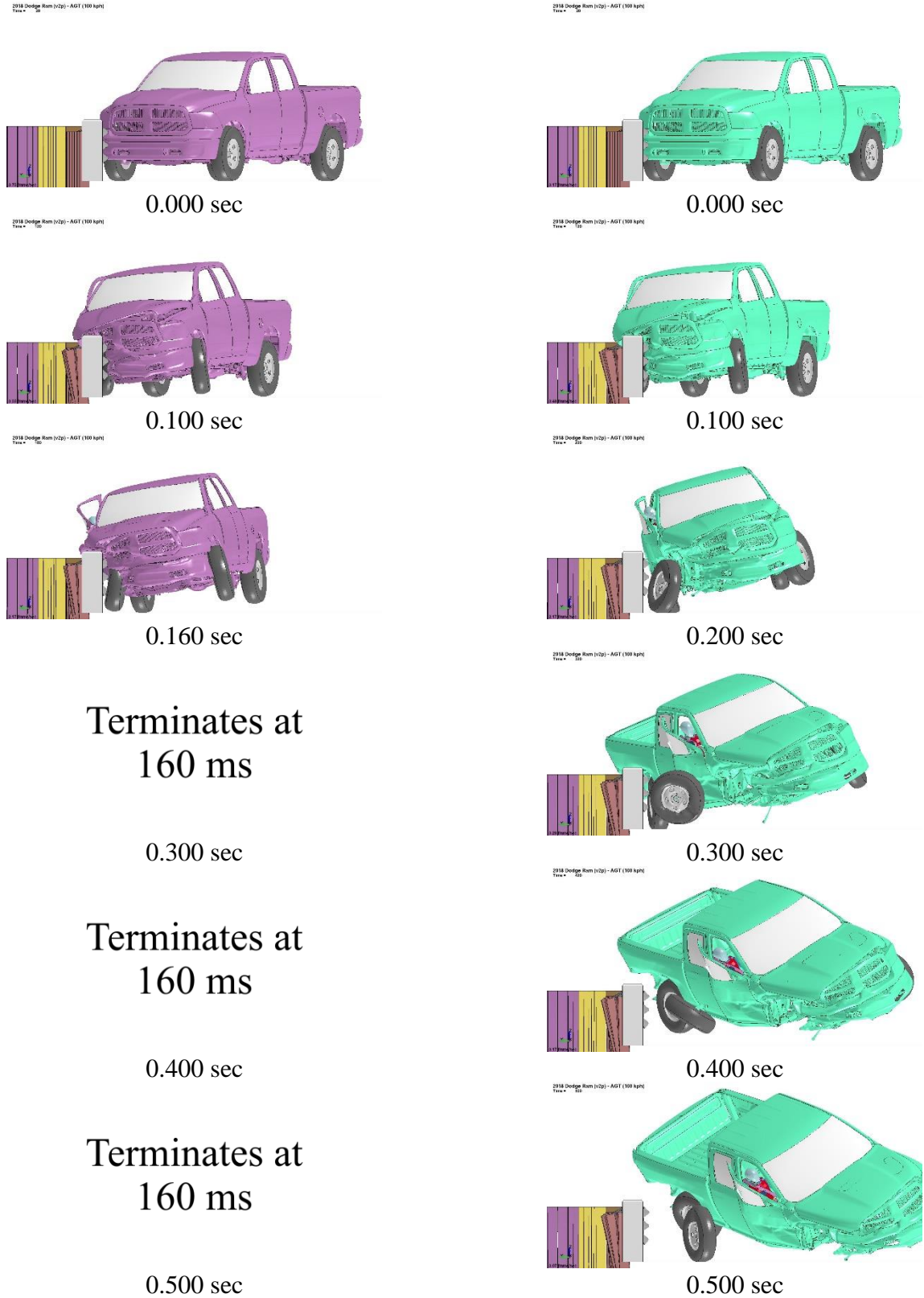


Figure D-8. 12.5:1 X Simulation (Left) vs. 12.5:1 US1 Simulation (Right) Sequential Images

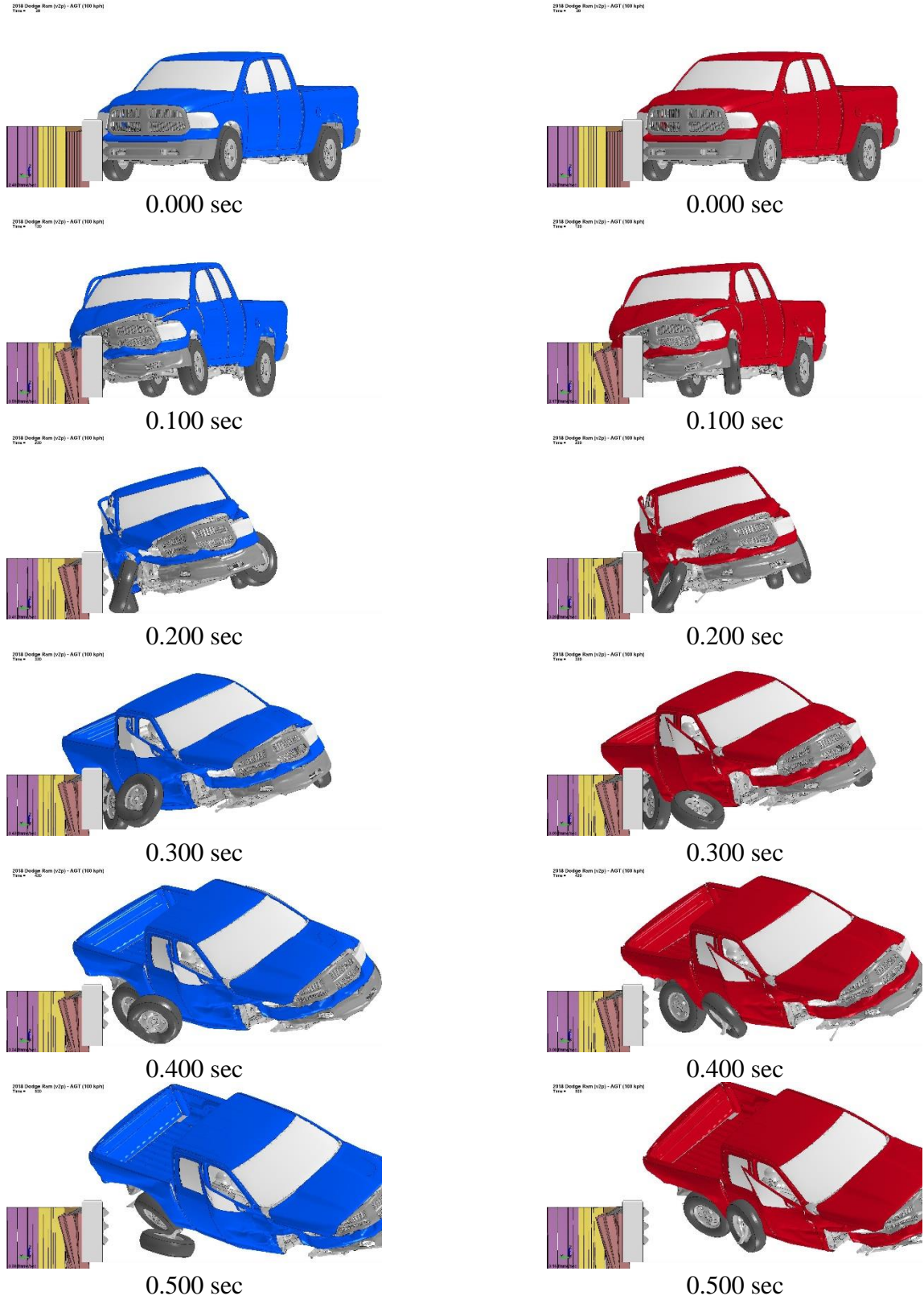


Figure D-9. 12.5:1 US2 Simulation (Left) vs. 12.5:1 US3 Simulation (Right) Sequential Images

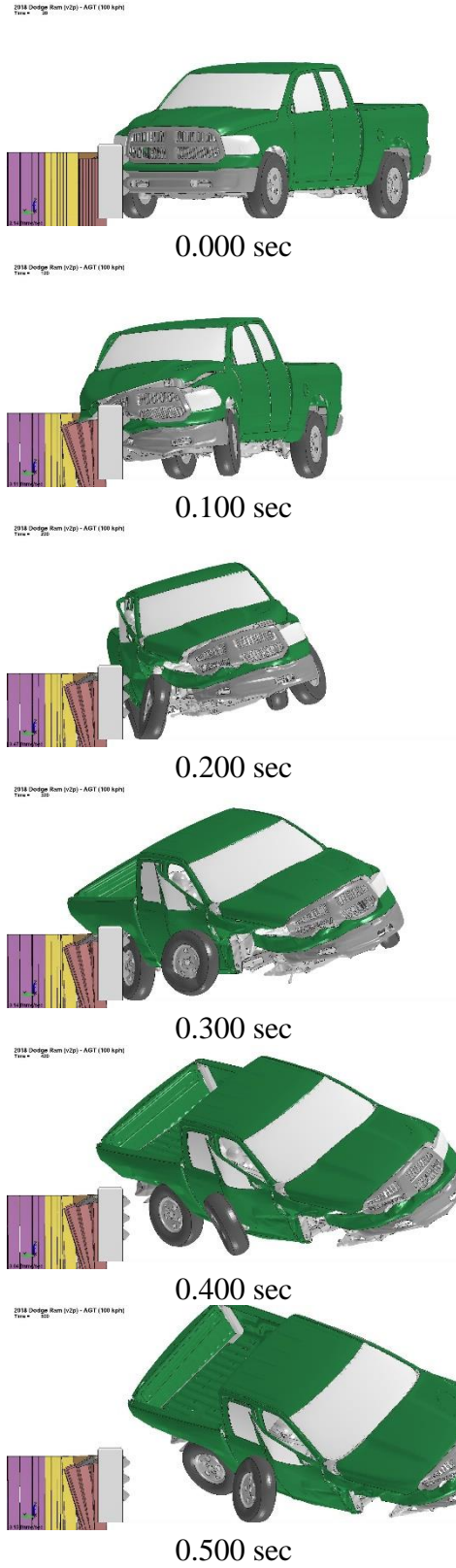


Figure D-10. 12.5:1 US4 Simulation Sequential Images

Appendix E. 1100C CIP Study Simulation Sequential Images

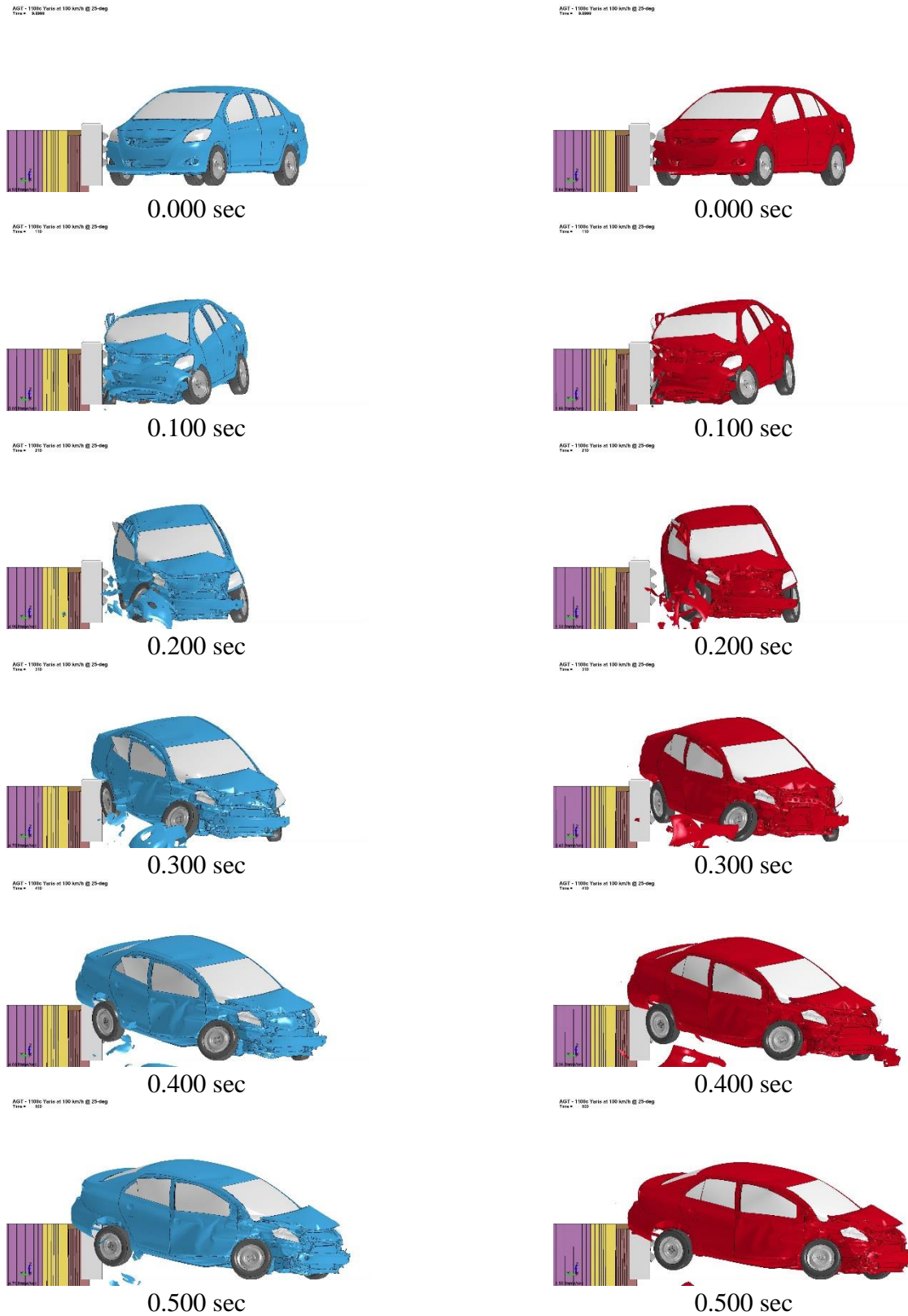


Figure E-1. 15:1 DS3 Simulation (Left) vs. 15:1 DS2 Simulation (Right) Sequential Images



Figure E-2. 15:1 DS1 Simulation (Left) vs. 15:1 X Simulation (Right) Sequential Images

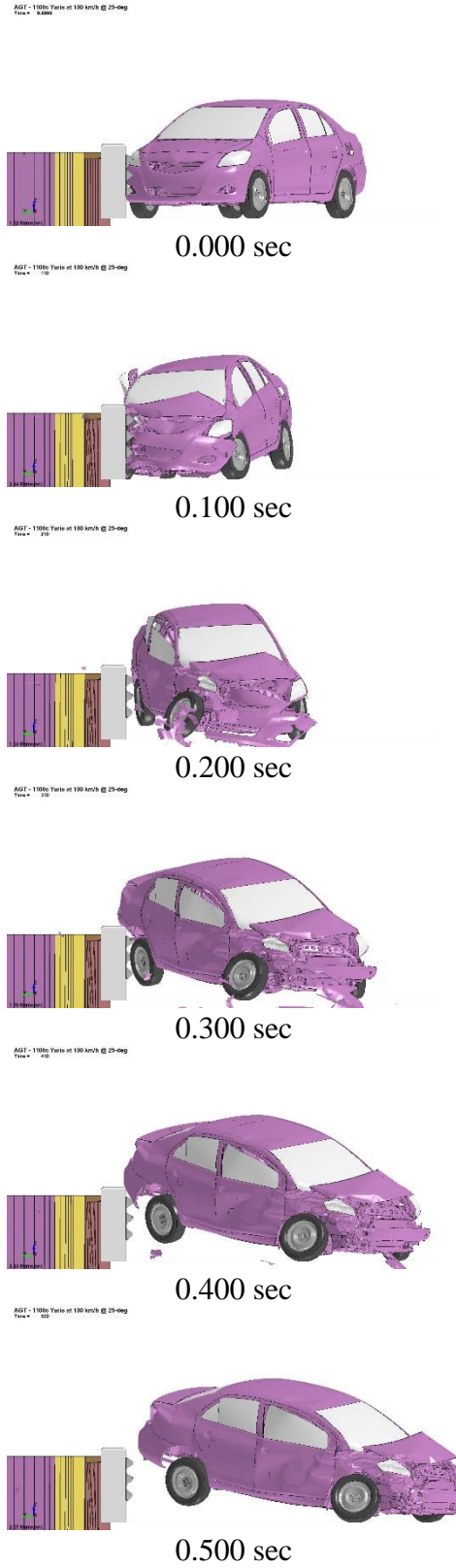


Figure E-3. 15:1 US1 Simulation Sequential Images

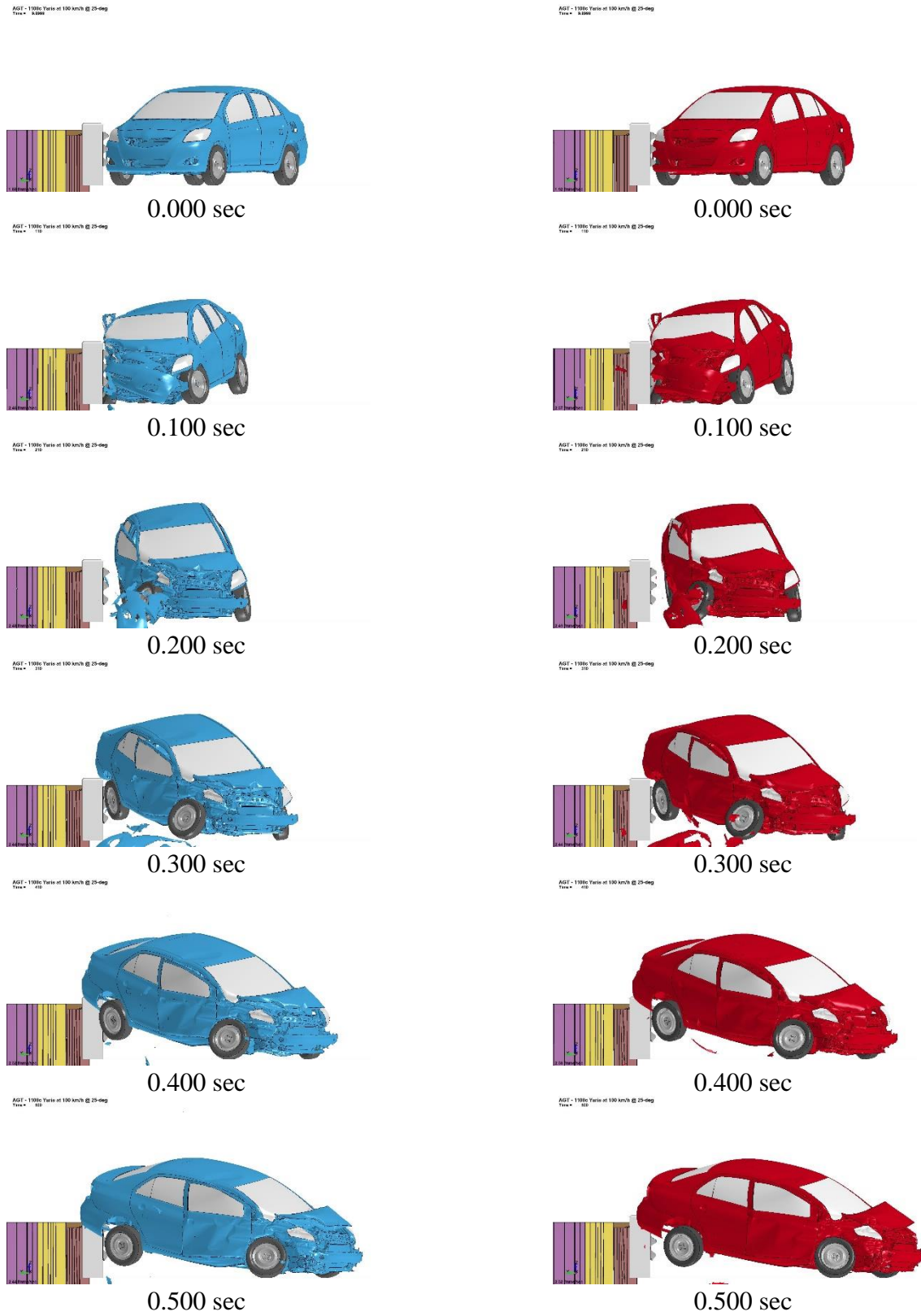


Figure E-4. 12.5:1 DS2 Simulation (Left) vs. 12.5:1 DS1 Simulation (Right) Sequential Images



Figure E-5. 12.5:1 X Simulation (Left) vs. 12.5:1 US1 Simulation (Right) Sequential Images

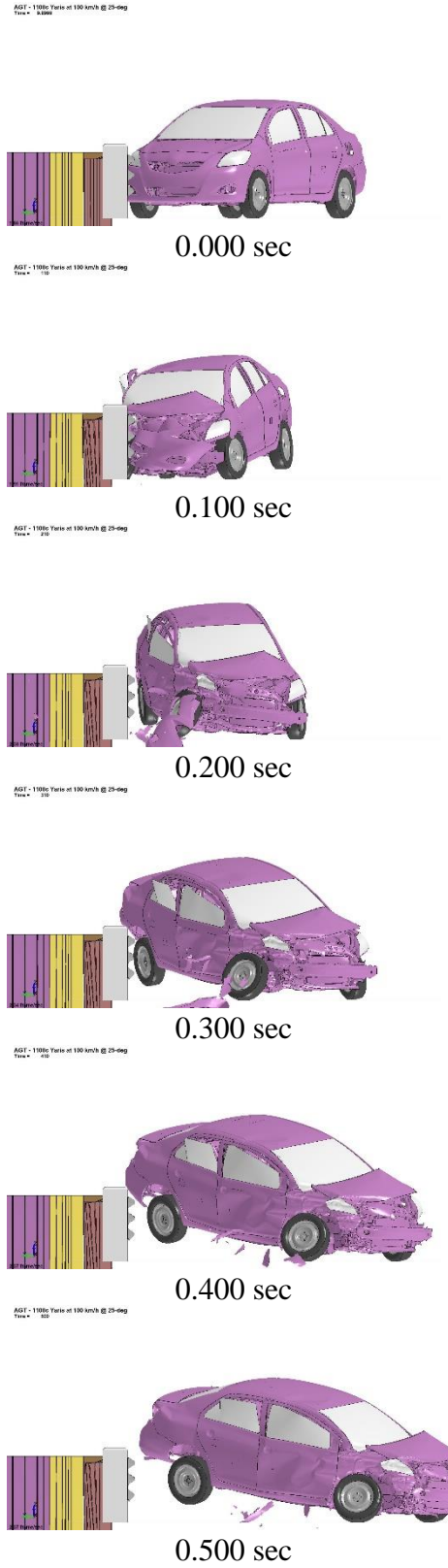


Figure E-6. 12.5:1 US2 Simulation Sequential Images

END OF DOCUMENT